Electronic Supporting Information

Oxidative C-N Fusion of Pyridinyl-Substituted Porphyrins

Mathieu Berthelot,[a] Guillaume Hoffmann,[a] Asmae Bousfiha,[a] Julie Echaubard,[a] Julien Roger,[a] Hélène Cattey,[a] Anthony Romieu,[a,b] Dominique Lucas,[a] Paul Fleurat-Lessard[a] and Charles H. Devillers*,[a]

[a] Institut de Chimie Moléculaire de l'Université de Bourgogne, UMR6302, CNRS, Université Bourgogne Franche-Comté, F-21000 Dijon, France

[b] Institut Universitaire de France, 103, Boulevard Saint-Michel, 75005 Paris, France

E-mail: charles.devillers@u-bourgogne.fr

Table of Contents

General Comments

Unless otherwise noted, all reactions were carried out without protection from air. CH_2Cl_2 was distilled over P_2O_5 under argon or dried over alumina cartridges using a solvent purification system PureSolv PS-MD-5 model from Innovative Technology and kept under argon. MeCN and DMF were dried over alumina cartridges using a solvent purification system PureSolv PS-MD-5 model from Innovative Technology and kept under argon. All other solvents used for reactions were obtained from commercial suppliers and used as received. 5,15-Bis(*p*-tolyl)porphyrin (DTP, **5**) was synthesized according to known procedures.[1] TLC were carried out on Merck DC Kieselgel 60 F-254 aluminium sheets. The spots were directly visualized or through illumination with UV lamp (λ = 254/365 nm). Column chromatography purifications were performed manually on silica gel (SiO_2, 40-63 µm) from Sigma-Aldrich (technical grade). Aluminium oxide (Al_2O_3, aluminium oxide 90 standardized for column chromatographic adsorption analysis acc. to Brockmann) was provided by Merck. C_{18}-SiO_2 used for reversed-phase purification by flash-column chromatography was provided by Sigma-Aldrich (20-22% loading, 40-75 µm, 60 Å pore size). The HPLC-gradient grade acetonitrile (CH_3CN) was obtained from Biosolve or Carlo Erba. Formic acid (FA, grade "eluent additive for LC-MS") was provided by Sigma Aldrich. Aq. mobile-phases for HPLC were prepared using water purified with a PURELAB Ultra system from ELGA (purified to 18.2 MΩcm).

Instruments and methods

Lyophilization steps were performed with a Christ Alpha 2–4 LD plus. ^{1}H-, ^{13}C-, ^{19}F- and ^{31}P-NMR spectra were recorded either on a Bruker Avance 300, on a Bruker Avance 500 or on a Bruker Avance 600 III HD spectrometer. Chemical shifts are expressed in parts per million (ppm) from the residual non-deuterated solvent signal.[2] J values are expressed in Hz. Spectra were calibrated to TMS on the basis of the relative chemical shift of the residual non-deuterated solvent signal as an internal standard. HPLC-MS analyses were performed on a Thermo-Dionex Ultimate 3000 instrument (pump + auto- sampler) equipped with a diode array detector (Thermo-Dionex DAD 3000-RS) and a MSQ Plus single quadrupole mass spectrometer (LRMS analyses through ESI). Purification by semi-preparative HPLC was performed on a Thermo-Dionex Ultimate 3000 instrument equipped with a RS Variable Detector (four distinct wavelengths). High-resolution mass spectra (HRMS) were recorded either on a Thermo LTQ Orbitrap XL apparatus equipped with an ESI source or on a Bruker UltraflexII LRF 2000 MALDI-TOF mass spectrometer (matrix: dithranol). UV-visible absorption spectra were recorded on a VARIAN Cary 50 UV-Visible spectrophotometer using quartz cells.

High-performance liquid chromatography separations

Two chromatographic systems were used for the analytical experiments (HPLC-MS) or the purification (semi-preparative HPLC) respectively:
System A: RP-HPLC-MS (Phenomenex Kinetex C_{18} column, 2.6 µm, 2.1 × 50 mm) with CH_3CN (+ 0.1% FA) and 0.1% aq. FA (pH 2.7) as eluents [linear gradient from 5% to 100% (5 min) of CH_3CN followed by isochratic at 100% (1.5 min)] at a flow rate of 0.5 mL/min. UV-visible detection was achieved at 220, 260, 430 and 600 nm (+ diode array detection in the range 220-750 nm). ESI-MS detection in the positive/negative mode ("full scan", 150-1750 a.m.u., data type: centroid, needle voltage: 3.5 kV, detector voltage: 1100 V, probe temperature: 350 °C, cone voltage: 75 V and scan time: 1 s). System B: semi-preparative RP-HPLC (SiliCycle SiliaChrom C_{18} column, 10 µm, 20 × 250 mm) with CH_3CN and 0.1% aq. FA (pH

2.7) as eluents [5% CH_3CN (5 min), followed by a gradient of 5% to 30% CH_3CN (12.5 min), then 30% to 100% CH_3CN (56 min)] at a flow rate of 20.0 mL/min. Quadruple UV-vis detection was achieved at 220, 260, 430 and 600 nm.

Synthesis and characterization

5,15-Bis(*p*-tolyl)-10-phenylporphyrin (4)

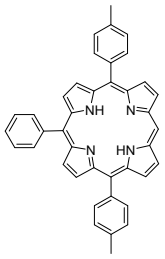

Chemical Formula: $C_{40}H_{30}N_4$
Exact Mass: 566.2470
Molecular Weight: 566.7080

4

4 was synthesized as reported in reference [3]. A 500 mL Schlenk flask containing 5,15-bis(*p*-tolyl)porphyrin **5** (1.003 g, 2.05 mmol, 1.0 eq.) was heated at 100 °C under high vacuum for 30 min. After cooling to room temperature, dry THF (270 mL) was introduced to the Schlenk flask under argon. The solution was cooled to 0 °C (ice bath) and 1.88 M phenyllithium solution in Bu_2O (6.6 mL, 12.41 mmol, 6.0 eq.) was added. The resulting reaction mixture was stirred at 0 °C for 15 min., then at room temperature for 15 min. An argon degassed solution containing 50 mL of THF and 10 mL of deionized water was added dropwise to the mixture under argon and the resulting green solution was stirred at room temperature for further 10 min. DDQ (1.858 g, 8.19 mmol, 4.0 eq.) was then introduced to the Schlenk flask and the mixture was stirred at room temperature without protection from air for one hour. The resulting purple solution was directly filtered on Al_2O_3 pad (h = 7 cm, $Ø$ = 4 cm) and it was eluted with CH_2Cl_2. The purple solid obtained after removing the solvent was precipitated in MeOH. The precipitate was washed with MeOH and dried at 120 °C under vacuum for 1 h giving **4** in 90% yield (1.063 g, 1.88 mmol). Characterization data (^{1}H and ^{13}C{^{1}H} NMR, UV-Vis., HRMS) were in agreement with those published in reference [3].

5-Bromo-10,20-bis(*p*-tolyl)-15-phenylporphyrin (7)[4]

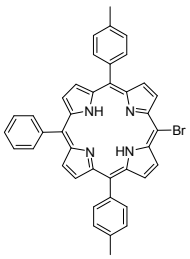

Chemical Formula: $C_{40}H_{29}BrN_4$
Exact Mass: 644.1576
Molecular Weight: 645.6040

7

A solution of **4** (970 mg, 1.68 mmol, 1.0 eq.) in $CHCl_3$ (230 mL) with pyridine (0.28 mL, 3.469 mmol, 2.07 eq.) was cooled to 0 °C. NBS (366 mg, 2.054 mmol, 1.22 eq.) was added and the resulting reaction mixture was stirred at 0 °C for 40 min., monitoring the progress of the reaction by TLC (SiO_2, CH_2Cl_2/*n*-heptane (7:3, v/v)). Acetone (30 mL) was then added, then the solvent was removed by rotary evaporation. The crude product was recrystallized in a CH_2Cl_2/MeOH mixture. The precipitate was washed with MeOH and dried at 120 °C under vacuum for 45 min. giving **7** in 95% yield (1.077 g, 1.67 mmol). Characterization data (^{1}H and ^{13}C{^{1}H} NMR, UV-Vis., HRMS) were in agreement with those published in reference [4].

5-(Pyridin-2-ylthio)-10,20-bis(*p*-tolyl)-15-phenylporphyrin (11)

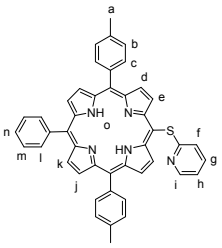

Chemical Formula: $C_{45}H_{33}N_5S$
Exact Mass: 675.2457
Molecular Weight: 675.8540

11

7 (525 mg, 0.77 mmol) was dissolved in dry DMF (48 mL) with 2-mercaptopyridine (121 mg, 1.09 mmol, 1.4 eq.) and Cs_2CO_3 (504 mg, 1.55 mmol, 2.0 eq.). The solution was degassed by bubbling argon for 30 min then stirred at 100 °C for 85 min, monitoring the progress of the reaction by TLC (SiO_2, CH_2Cl_2). The solvent was evaporated and the crude product was purified by column chromatography (SiO_2, CH_2Cl_2). Two fractions were collected. The first one contained traces of **7** whereas the second one contained **11**. After evaporation of the solvent, **11**

was then recrystallized in a CH_2Cl_2/MeOH mixture. The resulting precipitate was washed with MeOH to give **11** in 78% yield (409 mg, 0.61 mmol). ^{1}H NMR ($CDCl_3$, 300 MHz, 295 K): δ (ppm) 9.87 (d, $^3J_{H-H}$ = 4.9 Hz, 2H), 8.92 (d, $^3J_{H-H}$ = 4.9 Hz, 2H), 8.83 (s, 4H), 8.52 (ddd, $^3J_{H-H}$ = 4.8 Hz, $^4J_{H-H}$ = 2.0 Hz, $^4J_{H-H}$ = 0.9 Hz, 1H), 8.20 (dd, $^3J_{H-H}$ = 7.5 Hz, $^4J_{H-H}$ = 1.8 Hz, 2H), 8.08 (d, $^3J_{H-H}$ = 7.9 Hz, 4H), 7.77 (m, 3H), 7.56 (d, $^3J_{H-H}$ = 7.7 Hz, 4H), 6.92 (td, $^3J_{H-H}$ = 7.7, $^4J_{H-H}$ = 2.0 Hz, 1H), 6.84 (ddd, $^3J_{H-H}$ = 7.4 Hz, $^3J_{H-H}$ = 4.8 Hz, $^4J_{H-H}$ = 1.2 Hz, 1H), 5.95 (dt, $^3J_{H-H}$ = 8.1, $^4J_{H-H}$ = 1.1 Hz, 1H), 2.71 (s, 6H), -2.59 (s, 2H); ^{13}C{^{1}H} NMR ($CDCl_3$, 126 MHz, 300 K) : δ (ppm) 166.0, 149.1, 142.0, 138.9, 137.8, 136.8, 134.6, 134.6, 128.1, 127.6, 126.9, 122.8, 121.7, 121.3, 119.3, 104.0, 53.6, 21.7; R_f 0.81 (SiO_2, CH_2Cl_2); λ_{max} (CH_2Cl_2) / nm (log ε): 423 (5.66), 520 (4.34), 555 (4.02), 594 (3.86), 648 (3.66); HRMS (ESI+) : *m*/*z* cald for $C_{45}H_{33}N_5S$ $[M + H]^+$ 676.2529, found 676.2536.

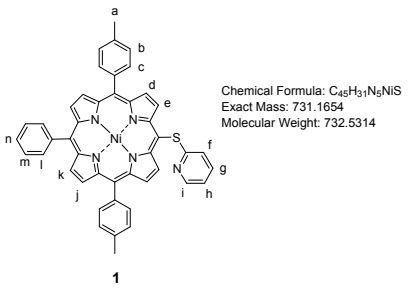

5-(Pyridin-2-ylthio)-10,20-bis(*p*-tolyl)-15-phenylporphyrinato]nickel(II) (1)

A solution of **11** (201 mg, 0.30 mmol, 1.0 eq.) and $Ni(OAc)_2.4H_2O$ (149 mg, 0.60 mmol, 2.0 eq.) in DMF (15 mL) was degassed by bubbling argon for 30 min. The solution was then stirred at 160 °C for 70 min, monitoring the progress of the reaction by TLC (SiO_2, CH_2Cl_2). The reaction mixture was allowed to cool to room temperature and then deionized water (30 mL) was added. The resulting precipitate was washed with deionized water and dried at 120 °C under vacuum for 3 h to give **1** in 84 % yield (187 mg, 0.20 mmol). ^{1}H NMR ($CDCl_3$, 300 MHz, 295 K): δ (ppm) 9.64 (d, $^3J_{H-H}$ = 5.0 Hz, 2H), 8.74 (d, $^3J_{H-H}$ = 5.0 Hz, 2H), 8.65 (s, 4H), 8.37 (ddd, $^3J_{H-H}$ = 4.9 Hz, $^4J_{H-H}$ = 2.0 Hz, $^4J_{H-H}$ = 0.9 Hz, 1H), 7.92 (dd, $^3J_{H-H}$ = 7.4 Hz, $^4J_{H-H}$ = 2.0 Hz, 2H), 7.79 (d, $^3J_{H-H}$ = 7.9 Hz, 4H), 7.62 (s, 3H), 7.70 (d, $^3J_{H-H}$ = 7.6 Hz, 4H), 6.85 (ddd, $^3J_{H-H}$ = 8.1 Hz, $^3J_{H-H}$ = 7.4 Hz, $^4J_{H-H}$ = 1.9 Hz, 1H), 6.74 (ddd, $^3J_{H-H}$ = 7.4 Hz, $^3J_{H-H}$ = 4.8 Hz, $^4J_{H-H}$ = 1.1 Hz, 1H), 5.70 (dt, $^3J_{H-H}$ = 8.1 Hz, $^4J_{H-H}$ = 1.0 Hz, 1H), 2.57 (s, 6H); ^{13}C{^{1}H} NMR ($CDCl_3$, 126 MHz, 300 K): δ (ppm) 164.8, 149.0, 147.1, 143.6, 143.4, 142.4, 140.7, 137.8, 137.6, 136.8, 134.0, 133.7, 132.8, 132.5, 132.4, 128.0, 127.8, 127.1, 121.4, 121.0, 119.8, 119.4, 103.7, 21.6; R_f 0.67 (SiO_2, CH_2Cl_2); λ_{max} (CH_2Cl_2) / nm (log ε): 419 (5.22), 534 (4.08), 566 (3.75); HRMS (ESI+): *m*/z cald for $C_{45}H_{31}N_5NiS$ $[M]^+$ 731.1648 found 731.1682, $[M+H]^+$ 732.1726, found 732.1747.

Fused 5-(pyridin-2-ylthio)-10,20-bis(*p*-tolyl)-15-phenylporphyrinato]nickel(II) (1^+,PF_6^-)

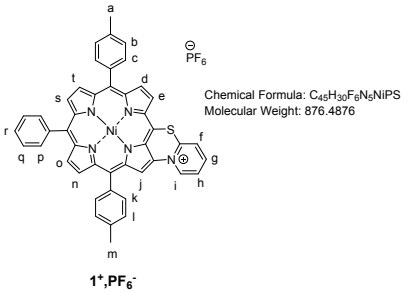

Nickel(II) porphyrin **1** (50 mg, 68.4 µmol, 1.0 eq.) and PIFA (29.3 mg, 68.1 µmol, 1.0 eq.) were introduced in a dry 25 mL round bottom flask. Dry CH_2Cl_2 (12 mL) was added and the mixture was stirred at room temperature for 3.5 h, monitoring the progress of the reaction by TLC (SiO_2, CH_2Cl_2). At that time, an additional amount of PIFA (5.9 mg, 13.7 µmol, 0.2 eq.) was added. After 1 h, the solvent was evaporated. The crude product which bears the CF_3COO^- counter-anion as attested by ^{19}F NMR analysis, was eluted with CH_3CN through an anion-exchange resin (AMBERLIT™ IRA96 resin) previously saturated with PF_6^- anions. The solvent was then removed under vacuum and the product was purified by column chromatography (SiO_2, $CHCl_3$/MeOH (9:1, v/v)). The first fraction contained traces of an unknown impurity whereas the second one contained the desired product **1^+,PF_6^-**. This latter was recrystallized in

CH_2Cl_2/*n*-hexane. The precipitate was filtered under vacuum, washed with *n*-hexane and dried at 150 °C under high vacuum for 1 h to give (**1**$^+$,**PF**$_6^-$) in 98% yield (59 mg,67.3 µmol). ^{1}H NMR (CD_3COCD_3, 500 MHz, 298 K): δ (ppm) 9.31 (d, $^3J_{H-H}$ = 6.0 Hz, 1H), 8.88 (s, 1H), 8.80 (d, $^3J_{H-H}$ = 5.0 Hz, 1H), 8.77 (d, $^3J_{H-H}$ = 4.9 Hz, 1H), 8.74 (d, $^3J_{H-H}$ = 5.0 Hz, 1H), 8.67 (d, $^3J_{H-H}$ = 4.9 Hz, 1H), 8.32 (d, $^3J_{H-H}$ = 4.8 Hz, 1H), 8.12 (t, $^3J_{H-H}$ = 7.8 Hz, 1H), 8.07 (d, $^3J_{H-H}$ = 6.8 Hz, 2H), 8.05 (doublet masked under doublet at 8.07 ppm, 1H), 7.91 – 7.86 (m, 1H), 7.83 (t, $^3J_{H-H}$ =7.3 Hz, 2H), 7.69 (d, $^3J_{H-H}$ = 5.4 Hz, 1H), 7.67 (d, $^3J_{H-H}$ = 7.5 Hz, 2H), 7.60 (d, $^3J_{H-H}$ = 7.4 Hz, 2H), 7.57 (d, $^3J_{H-H}$ = 7.3 Hz, 2H), 7.50 (d, $^3J_{H-H}$ = 7.4 Hz, 2H), 7.45 (d, $^3J_{H-H}$ = 8.2 Hz, 2H), 2.71 (s, 3H), 2.67 (s, 3H); ^{13}C{^{1}H} NMR (CD_3COCD_3, 126 MHz, 300 K): δ (ppm) 145.7, 145.5, 144.4, 144.2, 143.2,141.7, 140.6, 139.8, 139.3, 139.2, 138.8, 137.0, 136.9, 135.6, 135.3, 135.0, 134.8, 134.6, 134.5, 134.2, 134.1, 129.4, 129.3, 128.9, 128.3, 126.9, 126.3, 124.5, 124.3, 121.9, 120.7, 120.5, 116.3, 21.6, 21.5; ^{19}F NMR (CD_3COCD_3, 470 MHz, 300 K): δ (ppm) -72.40 (d, $^3J_{F-P}$ = 708.2 Hz); ^{31}P NMR (CD_3COCD_3, 202 MHz, 298 K): δ (ppm) -144.25 (hpt); R_f 0.32 (SiO_2, $CHCl_3$/MeOH, 9:1, v/v); λ_{max} (CH_2Cl_2) / nm (log ε): 419 (5.30), 549 (4.26); HRMS (ESI+): *m*/*z* cald for $C_{45}H_{30}N_5NiS^+$ [M - PF_6]$^+$ 730.1570, found 730.1580.

5-bromo-10,20-bis(*p*-tolyl)porphyrin (8)[5]

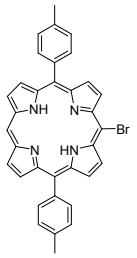

Chemical Formula: $C_{34}H_{25}BrN_4$
Exact Mass: 568.1263
Molecular Weight: 569.5060

8

A solution of **5** (1.000 g, 2.04 mmol) in $CHCl_3$ (640 mL) was cooled to 5 °C. NBS (290 mg, 1.63 mmol, 0.8 eq.) was then added and the reaction mixture was stirred at 5 °C for 20 minutes, monitoring the progress of the reaction by TLC (SiO_2, CH_2Cl_2, *n*-heptane (7:3, v/v)). Acetone (50 mL) was added and the solvent was evaporated. The crude mixture was precipitated in a CH_2Cl_2/MeOH mixture and filtrated under vacuum. The solid was washed with cold MeOH and dried at 150 °C under vacuum for 45 min to give 1.071 g of a mixture of **8** (60%), **9** (12%) and **5** (28%). We did not manage to separate **8** from **9** and **5** on this gram scale reaction due to their poor solubility. That is why the following S_NAr reaction was directly performed with this mixture.

^{1}H NMR of **8** ($CDCl_3$, 300 MHz, 295.1 K): δ (ppm) 10.30 (s, 1H), 9.39 (d, $^3J_{H-H}$ = 4.6 Hz, 2H), 9.11 (d, $^3J_{H-H}$ = 4.6 Hz, 2H), 8.99 (d, $^3J_{H-H}$ = 2.4 Hz, 2H), 8.98 (d, $^3J_{H-H}$ = 2.6 Hz, 2H),), 8.10 (d, $^3J_{H-H}$ = 7.9 Hz, 4H), 7.60 (d, $^3J_{H-H}$ = 7.9 Hz, 4H), 2.73 (s, 6H), -2.99 (s, 2H).

^{1}H NMR of **9** ($CDCl_3$, 300 MHz, 295 K): δ (ppm) 9.61 (d, $^3J_{H-H}$ = 4.9 Hz, 4H), 8.86 (d, $^3J_{H-H}$ = 4.9 Hz, 4H), 8.04 (d, $^3J_{H-H}$ = 7.9 Hz, 4H), 7.55 (d, $^3J_{H-H}$ = 7.9 Hz, 4H), 2.73 (s, 6H), -3.10 (s, 2H).

^{1}H NMR of **5** ($CDCl_3$, 300 MHz, 295 K): δ (ppm 10.16 (s, 2H), 9.74 (d, $^3J_{H-H}$ = 4.8 Hz, 4H), 9.28 (d, $^3J_{H-H}$ = 4.7 Hz, 4H), 8.17 (d, $^3J_{H-H}$ = 8.0 Hz, 4H) 7.62 (d, $^3J_{H-H}$ = 8.0 Hz, 4H), 2.74 (s, 6H), -2.72 (s, 2H); R_f 0.55 (**5**), 0.73 (**8**), 0.82 (**9**) (SiO_2, CH_2Cl_2/*n*-heptane, (7:3, v/v)).

5-(Pyridin-2-ylthio)-10,20-bis(*p*-tolyl)porphyrin (12)

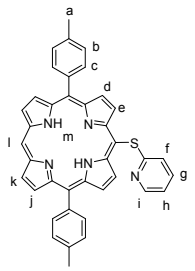

Chemical Formula: $C_{39}H_{29}N_5S$
Exact Mass: 599.2144
Molecular Weight: 599.7560

12

The previous mixture of **8** (60%), **9** (12%) and **5** (28%) (500 mg, 0.754 mmol of Br function) was dissolved in dry DMF (20 mL) with 2-mercaptopyridine (119.0 mg, 1.07 mmol, 1.4 eq. per Br function) and Cs_2CO_3 (495 mg, 1.52 mmol, 2.0 eq. per Br function). The solution was degassed by bubbling argon for 10 minutes then stirred at 100 °C for 6.25 h, monitoring the progress of the reaction by TLC (SiO_2, CH_2Cl_2/*n*-heptane (7:3, v/v)). The solvent was evaporated and the crude product was purified by column chromatography

(SiO_2, CH_2Cl_2). Three fractions were collected containing a mixture of non-brominated (**5**) and brominated porphyrins (**8-9**) (Fraction A1), a mixture of **12** and traces of **13**, **5**, **8** and **9** (Fraction A2) and a mixture of disubstituted (**13**) and traces of **5**, **8** and **9** (Fraction A3). Fraction A2 was then purified again by column chromatography (SiO_2, CH_2Cl_2). Three new fractions were obtained containing **5**, **8** and **9** (Fraction B1), **12** (Fraction B2) and disubstituted porphyrin **13** (Fraction B3). Fraction (B2) was evaporated and then recrystallized in a CH_2Cl_2/MeOH mixture. The solid was washed with MeOH and dried at 150 °C under vacuum for 90 min to give **12** in 61 % yield (197.6 mg, 3.29×10^{-1} mmol). ^{1}H NMR ($CDCl_3$, 500 MHz, 298 K): δ (ppm) 10.26 (s, 1H), 9.95 (d, $^3J_{H-H}$ = 4.8 Hz, 2H), 9.33 (d, $^3J_{H-H}$ = 4.5 Hz, 2H), 9.00 (dd, $^3J_{H-H}$ = 10.1, $^3J_{H-H}$ = 4.7 Hz, 4H), 8.51 (ddd, $^3J_{H-H}$ = 4.9, $^4J_{H-H}$ = 2.0, $^4J_{H-H}$ = 0.9 Hz, 1H), 8.11 (d, $^3J_{H-H}$ = 7.9 Hz, 4H), 7.59 (d, $^3J_{H-H}$ = 7.9 Hz, 4H), 6.89 (ddd, $^3J_{H-H}$ = 8.3, $^3J_{H-H}$ = 7.4, $^4J_{H-H}$ = 1.9 Hz, 1H), 6.83 (ddd, $^3J_{H-H}$ = 7.3, $^3J_{H-H}$ = 4.9, 1.1 Hz, $^4J_{H-H}$ = 1H), 5.92 (dt, $^3J_{H-H}$ = 8.3, $^4J_{H-H}$ = 1.1 Hz, 1H), 2.72 (s, 6H), -2.89 (s, 2H); ^{13}C{^{1}H} NMR ($CDCl_3$, 126 MHz, 300 K): δ (ppm) 166.1, 149.1, 138.5, 137.8, 136.9, 134.7, 132.7, 131.7, 127.8, 121.8, 120.7, 119.2, 107.3, 104.7, 77.4, 77.2, 76.9, 21.7; R_f 0.65 (SiO_2, CH_2Cl_2); λ_{max} (CH_2Cl_2) / nm (log ε) : 418 (5.75), 515 (4.43), 548 (3.67), 585 (3.76); HRMS (MALDI-TOF, positive mode): *m/z* cald for $C_{39}H_{29}N_5S$ $[M + H]^+$ 600.2216, found 600.2196.

[5-(Pyridin-2-ylthio)-10,20-bis(*p*-tolyl)porphyrinato]nickel(II) (2)

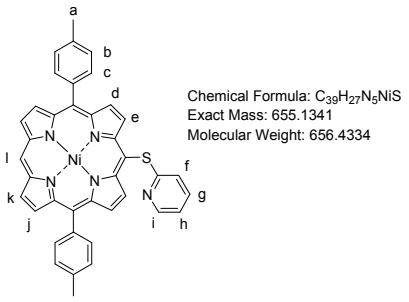

2

A solution of **13** (192 mg, 0.32 mmol, 1.0 eq.) and $Ni(OAc)_2.4H_2O$ (159 mg, 0.64 mmol, 2.0 eq.) in DMF (15 mL) was degassed by bubbling argon for 35 min. The solution was then stirred at 160 °C for 90 min, monitoring the progress of the reaction by TLC (SiO_2, CH_2Cl_2). The mixture was allowed to cool to room temperature and deionized water (20 mL) was added. The crude solid obtained was filtered under vacuum, washed with deionized water and dried at 150 °C under vacuum for 3 hours to give **2** as a red solid in 90% yield (190 mg, 2.89×10^{-1} mmol). ^{1}H NMR ($CDCl_3$, 300 MHz, 295 K): δ (ppm) 9.80 (s, 1H), 9.77 (d, $^3J_{H-H}$ = 5.0 Hz, 2H), 9.10 (d, $^3J_{H-H}$ = 4.8 Hz, 2H), 8.86 (t, $^3J_{H-H}$ = 4.7 Hz, 4H), 8.45 (ddd, $^3J_{H-H}$ = 4.8, $^4J_{H-H}$ = 2.0, $^4J_{H-H}$ = 0.9 Hz, 1H), 7.88 (d, $^3J_{H-H}$ = 7.9 Hz, 4H), 7.49 (d, $^3J_{H-H}$ = 7.9 Hz, 4H), 6.91 (td, $^3J_{H-H}$ = 7.8, $^4J_{H-H}$ = 2.0 Hz, 1H), 6.80 (ddd, $^3J_{H-H}$ = 7.5, $^3J_{H-H}$ = 4.8, $^4J_{H-H}$ = 1.1 Hz, 1H), 5.75 (dt, $^3J_{H-H}$ = 8.2, $^4J_{H-H}$ = 1.0 Hz, 1H), 2.66 (s, 6H); ^{13}C{^{1}H} NMR ($CDCl_3$, 126 MHz, 298 K): δ (ppm) 164.9, 149.0, 146.8, 143.5,142.4, 137.7, 137.6, 136.7, 133.8, 133.8, 132.7, 132.6, 132.4, 127.8, 121.4, 119.4, 119.3, 106.4, 104.2, 21.6; R_f 0.48 (SiO_2, CH_2Cl_2); λ_{max} (CH_2Cl_2) / nm (log ε): 412 (5.14), 527 (4.02), 559 (3.76); HRMS (ESI): *m/z* cald for $C_{39}H_{27}N_5NiS$ $[M + H]^+$ 656.1413, found 656.1432.

Fused [5-(pyridin-2-ylthio)-10,20-bis(*p*-tolyl)porphyrinato]nickel(II) (2^+,PF_6^-)

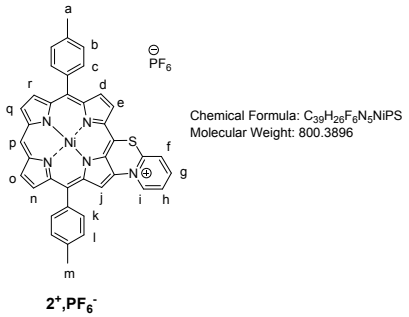

2^+,PF_6^-

Nickel(II) porphyrin **2** (49.6 mg, 75.6 µmol, 1.0 eq.) and PIFA (32.8 mg, 76.3 µmol, 1.0 eq.) were introduced in a dry 25 mL round bottom flask. Dry CH_2Cl_2 (12 mL) was added and the mixture was stirred at room temperature for 3.5 h, monitoring the progress of the reaction by TLC (SiO_2, CH_2Cl_2). At that time, an additional amount of PIFA (6.8 mg,15.8 µmol, 0.2 eq.) was added. The mixture was stirred for one hour before adding again a further amount of PIFA (6.4 mg, 14.9 µmol, 0.2 eq.). After one hour, the solvent was evaporated. The crude product which bears the $CF_3CO_2^-$ counter-anion as attested by ^{19}F NMR analysis, was eluted with CH_3CN through an anion-exchange resin (AMBERLIT^{TM} IRA96 resin) previously

saturated with PF_6^- anions. The solvent was removed and the solid was recrystallized in a CH_2Cl_2/*n*-hexane mixture. The precipitate obtained was washed with *n*-hexane and dried at 150 °C under vacuum for 2 hours providing the fused product **2⁺,PF₆⁻** in 81% yield (48.9 mg, 61.1 µmol). ^{1}H NMR (CD_3COCD_3, 500 MHz, 298 K) δ 9.49 (s, 1H), 8.83 (t, $^3J_{H-H}$ = 5.0 Hz, 2H), 8.78 (d, $^3J_{H-H}$ = 5.7 Hz, 1H), 8.44 (d, $^3J_{H-H}$ = 4.4 Hz, 1H), 8.41 (d, $^3J_{H-H}$ = 4.5 Hz, 1H), 8.21 (s, 1H), 7.94 (d, $^3J_{H-H}$ = 4.1 Hz, 2H), 7.94 (triplet masked under doublet at 7.94 ppm, 1H), 7.53 (t, $^3J_{H-H}$ = 5.8 Hz, 1H), 7.46 (d, $^3J_{H-H}$ = 7.3 Hz, 2H), 7.43 (d, $^3J_{H-H}$ = 7.3 Hz, 2H), 7.41 (d, $^3J_{H-H}$ = 7.3 Hz, 2H), 7.28 (d, $^3J_{H-H}$ = 6.6 Hz, 2H), 7.28 (doublet masked under doublet at 7.28 ppm, 1H) 6.98 (d, $^3J_{H-H}$ = 5.4 Hz, 1H), 2.69 (s, 3H), 2.68 (s, 3H); ^{13}C{^{1}H} NMR ($CDCl_3$, 126 MHz, 298 K): δ (ppm) 145.9, 145.4, 145.3, 143.8, 143.6, 142.7, 141.4, 139.0, 139.0, 139.0, 137.9, 136.9, 136.4, 134.8, 134.7, 134.7, 134.6, 134.5, 134.3, 133.4, 131.5, 129.2, 128.8, 126.0, 125.6, 124.5, 122.6, 120. 9, 119.2, 115.0, 106.3, 102.7, 21.6, 21.5; ^{19}F NMR (CD_3COCD_3, 470 MHz, 300 K): δ (ppm) -72.65 (d, $^2J_{F-P}$ = 707.5 Hz, 6F); ^{31}P NMR (CD_3COCD_3, 202 MHz, 298 K): δ (ppm) -144.24 (hpt); R_f 0.46 (SiO_2, $CHCl_3$/MeOH, (9:1, v/v)); λ_{max} (CH_2Cl_2) / nm (log ε): 413 (5.07), 541 (4.09). HRMS (ESI+): *m/z* cald for $C_{39}H_{26}N_5NiS^+$ $[M - PF_6]^+$ 654.1257, found 654.1266.

[5,15-Bis(*p*-tolyl)porphyrinato]zinc(II) (6)[5]

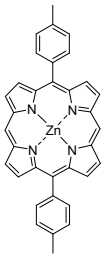

Chemical Formula: $C_{34}H_{24}N_4Zn$
Exact Mass: 552.1292
Molecular Weight: 553.9740

6

A solution of **5** (1.200 g, 2.45 mmol, 1.0 eq.) and $Zn(OAc)_2.2H_2O$ (1.074 g, 4.87 mmol, 2.0 eq.) in a mixture of $CHCl_3$ (156 mL) and MeOH (56 mL) was stirred at 60 °C for 1.5 h, monitoring the progress of the reaction by TLC (SiO_2 CH_2Cl_2/*n*-heptane (7:3, v/v)). The solvent was removed by rotary evaporation and the crude product was recrystallized in CH_2Cl_2/MeOH mixture. The precipitate obtained was washed with MeOH and dried for 90 min at 110 °C to give **6** in 82% yield (1.113 g, 2.01 mmol). Characterization data (^{1}H and ^{13}C{^{1}H} NMR, UV-Vis., HRMS) were in agreement with those published in reference [5].

[5,15-Bis(bromo)-10,20-bis(*p*-tolyl)porphyrinato]zinc(II) (10)[6]

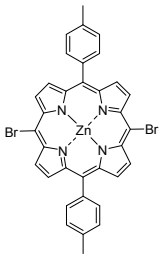

Chemical Formula: $C_{34}H_{22}Br_2N_4Zn$
Exact Mass: 707.9503
Molecular Weight: 711.7660

10

6 (1.111 g, 2.01 mmol, 1.00 eq.) was dissolved in $CHCl_3$ (260 mL). Pyridine (0.65 mL, 8.05 mmol, 4.01 eq.) was introduced to the mixture and the solution was cooled to 2 °C. NBS (731 mg, 4.11 mmol, 2.05 eq.) was then added and the reaction mixture was stirred at 2 °C for 15 min, monitoring the progress of the reaction by TLC (SiO_2, CH_2Cl_2/*n*-heptane (7:3, v/v)). The solvent was removed under vacuum and the product was recrystallized in a CH_2Cl_2/MeOH mixture. The precipitate was washed with MeOH and dried under vacuum at 110 °C for 90 min to give **10** coordinated by 1.26 eq. of pyridine (1.619 g, 1.99 mmol, 99%). Characterization data (^{1}H and ^{13}C{^{1}H} NMR, UV-Vis., HRMS) were in agreement with those published in reference [6].

5,15-Bis(bromo)-10,20-bis(*p*-tolyl)porphyrin (9)

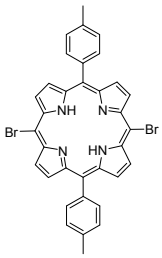

Chemical Formula: $C_{34}H_{24}Br_2N_4$
Exact Mass: 646.0368
Molecular Weight: 648.4020

9

Zinc porphyrin **10** (1.616 g, 2.27 mmol, 1.0 eq.) was dissolved in CH_2Cl_2 (80 mL). TFA (3.2 mL, 41.8 mmol, 18.4 eq.) was added and the reaction mixture was stirred at room temperature for 35 min, monitoring the progress of the reaction by TLC (SiO_2, CH_2Cl_2/*n*-heptane (7:3, v/v)). Deionized water (80 mL) was added and the organic layer was washed one more time

with 80 mL of dionized water. The solvent was removed by rotary evaporation to give **9** which was directly used in the next step.

5,15-Bis(pyridin-2-ylthio)-10,20-bis(*p*-tolyl)porphyrin (13)

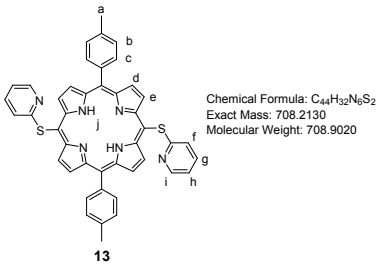

A solution of bromo-porphyrin **9**, 2-mercaptopyridine (748 mg, 6.73 mmol, 2.8 eq.) and Cs_2CO_3 (3.132 g, 9.61 mmol, 4.0 eq.) in dry DMF (60 mL) was degassed by bubbling argon through the solution for 30 min. The mixture was then stirred at 100 °C under argon for 2 h, monitoring the progress of the reaction by TLC (SiO_2, CH_2Cl_2/MeOH (98:2, v/v)). The solvent was removed by rotary evaporation and the crude product was recrystallized in a CH_2Cl_2/MeOH mixture. The precipitate obtained was washed with MeOH and dried at 110 °C for 3 h to give **13** in 60% yield (974 mg, 1.37 mmol). ^{1}H NMR ($CDCl_3$, 500 MHz, 298 K): δ (ppm) 9.88 (d, $^3J_{H-H}$ = 4.8 Hz, 4H), 8.91 (d, $^3J_{H-H}$ = 4.8 Hz, 4H), 8.49 (dd, $^3J_{H-H}$ = 4.5 Hz, $^4J_{H-H}$ = 1.5 Hz, 2H), 8.06 (d, $^3J_{H-H}$ = 8.0 Hz, 4H), 7.56 (d, $^3J_{H-H}$ = 7.6 Hz, 4H), 6.95 (ddd, $^3J_{H-H}$ = 8.2 Hz, $^4J_{H-H}$ = 6.3 Hz, $^4J_{H-H}$ = 2.1 Hz, 2H), 6.85 (ddd, $^3J_{H-H}$ = 6.7 Hz, $^4J_{H-H}$ = 4.4 Hz, $^4J_{H-H}$ = 1.3 Hz, 2H), 6.02 (d, $^3J_{H-H}$ = 8.3 Hz, 2H), 2.71 (s, 6H), -2.63 (s, 2H); ^{13}C{^{1}H} NMR ($CDCl_3$, 126 MHz, 300 K): δ (ppm) 165.6, 149.2, 138.5, 138.0, 136.9, 134.6, 127.7, 121.8, 119.5, 107.1, 21.7; R_f 0.94 (SiO_2, CH_2Cl_2/MeOH, 98/2, v/v).); λ_{max} (CH_2Cl_2) / nm (log ε): 427 (5.24), 524 (4.07), 561 (3.96), 601 (3.74), 656 (4.02); HRMS (ESI+): *m/z* cald for $C_{44}H_{32}N_6S_2$ $[M + H]^+$ 709.2203, found 709.2210.

[5,15-Bis(pyridin-2-ylthio)-10,20-bis(*p*-tolyl)porphyrinato]nickel(II) (3)

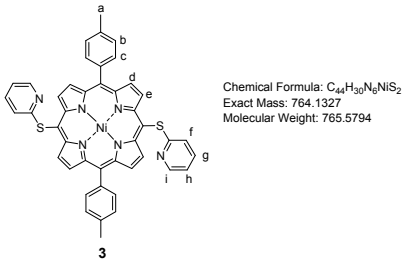

A solution of **13** (175 mg, 2.47×10^{-1} mmol, 1.0 eq.) and $Ni(OAc)_2.4H_2O$ (123 mg, 4.94×10^{-1} mmol, 2.0 eq.) in dry DMF (8.5 mL) was degassed by bubbling argon for 30 min. The solution was then stirred at 160 °C under argon for 4.5 h, monitoring the progress of the reaction by TLC (SiO_2, CH_2Cl_2/*n*-heptane (7:3, v/v)). The solution was allowed to cool to room temperature and deionized water (10 mL) was added. The precipitate was washed with water and dried for 1 h at 150 °C under vacuum to give **3** (with 9% mol. DMF) in 93% yield (168 mg, 1.01 mmol). ^{1}H NMR ($CDCl_3$, 500 MHz, 297 K): δ (ppm) 9.71 (d, $^3J_{H-H}$ = 5.0 Hz, 4H), 8.78 (d, $^3J_{H-H}$ = 5.0 Hz, 4H), 8.42 (d, $^3J_{H-H}$ = 4.5 Hz, 2H), 7.83 (d, $^3J_{H-H}$ = 7.5 Hz, 4H), 7.47 (d, $^3J_{H-H}$ = 7.6 Hz, 4H), 6.98-6.65 (m, 2H), 6.84-6.803 (m, 2H), 5.85 (d, $^3J_{H-H}$ = 8.3 Hz, 2H), 2.64 (s, 6H); ^{13}C{^{1}H} NMR ($CDCl_3$, 126 MHz, 298 K): δ (ppm) 164.3, 149.2, 146.7, 144.0, 138.0, 137.1, 136.8, 134.0, 133.6, 133.1, 127.9, 121.5, 120.2, 119.5, 106.1, 21.6; R_f 0.32 (SiO_2, CH_2Cl_2/MeOH (98:2, v/v); λ_{max} (CH_2Cl_2) / nm (log ε): 424 (5.42), 541 (4.25), 578 (4.18); HRMS (ESI+): *m/z* cald for $C_{34}H_{30}N_6NiS_2$ $[M + H]^+$ 765.1400, found 765.1408.

Fused [5,15-bis(pyridin-2-ylthio)-10,20-bis(*p*-tolyl)porphyrinato]nickel(II) (3^+,PF_6^-)

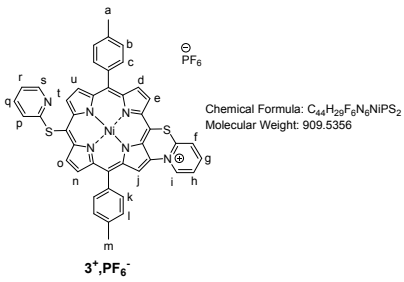

Nickel(II) porphyrin **3** (50.2 mg, 65.6 µmol, 1.0 eq.) and PIFA (28.0 mg, 65.1 µmol, 1.0 eq.) were introduced in a dry 25 mL round-bottom flask. Dry CH_2Cl_2 (12 mL) was added and the mixture was stirred at room temperature for 3.5 h, monitoring the progress of the reaction by TLC (SiO_2, CH_2Cl_2). At that

time, an additional amount of PIFA (5.7 mg, 13.3 µmol, 0.2 eq.) was added. After 1 h, the solvent was evaporated. The crude product which bears the CF_3COO^- counter-anion, as attested by ^{19}F NMR analysis, was eluted with CH_3CN through an anion exchange resin (AMBERLIT™ IRA96 resin) previously saturated with PF_6^- anions. The solvent was then removed under vacuum. The product was purified by column chromatography (SiO_2, $CHCl_3$/MeOH (9:1, v/v)). Two fractions were collected containing traces of impurities (Fraction 1) and (**3⁺,PF₆⁻**) (Fraction 2). Fraction 2 was recrystallized in a CH_2Cl_2/*n*-hexane mixture. The precipitate was washed with *n*-hexane and dried at 150 °C under vacuum for 2 h to give (**3⁺,PF₆⁻**) in 88% yield (52.8 mg, 58 µmol). ^1H NMR (CD_3COCD_3, 500 MHz, 298 K): δ (ppm) 9.85 (d, $^3J_{H-H}$ = 4.77 Hz, 1H), 9.76 (d, $^3J_{H-H}$ = 4.45 Hz, 1H), 9.20 (s, 1H), 8.83 (s, 1H), 8.76 (d, $^3J_{H-H}$ = 4.82 Hz, 1H), 8.71 (d, $^3J_{H-H}$ = 3.90 Hz, 1H), 8.46 (s, 1H), 8.41 (t, $^3J_{H-H}$ = 8.28 Hz, 1H), 8.29 (d, $^3J_{H-H}$ = 4.83 Hz, 1H), 7.95 (d, $^3J_{H-H}$ = 3.45 Hz, 1H), 7.70 (d, $^3J_{H-H}$ = 7.59 Hz, 1H), 7.62 (s, 3H), 7.50 (d, $^3J_{H-H}$ = 6.90, 2H), 7.39 (d, $^3J_{H-H}$ = 6.90 Hz, 2H), 7.33 (s, 3H), 7.02 (td, $^3J_{H-H}$ = 5.17 Hz, $^4J_{H-H}$ = 1.66 Hz, 1H), 2.64 (s, 3H), 2.53 (s, 3H); $^{13}C\{^1H\}$ NMR (CD_3COCD_3, 126 MHz, 298 K): δ (ppm) 161.2, 150.0, 149.4, 149.0, 144.8, 143.3, 142.3, 141.0, 139.1, 138.8, 138.6, 138.2, 137.3, 135.1, 134.9, 134.5, 133.8, 133.7, 132.2, 128.6, 128.3, 127.2, 125.7, 123.3, 122.5, 122.0, 121.7, 120.7, 119.5, 105.4, 21.5, 21.3; R_f 0.29 (SiO_2, $CHCl_3$/MeOH, (9:1, v/v)); λ_{max} (CH_2Cl_2) / nm (log ε): 334 (4.29), 426 (5.14), 555 (4.12), 583 (4.00); HRMS (ESI+): *m/z* cald for $C_{44}H_{30}N_6NiS_2^+$ $[M–PF_6]^+$ 763.1243, found 763.1259.

Doubly-fused [5,15-bis(pyridin-2-ylthio)-10,20-bis(*p*-tolyl)porphyrinato] nickel(II) (*anti*-3²⁺,(PF₆⁻)₂)

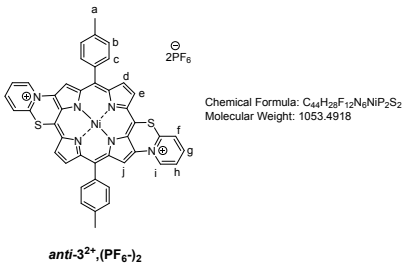

Fused porphyrin **3⁺,PF₆⁻** (50 mg, 55.0 µmol, 1.0 eq.) and PIFA (23.6 mg, 54.9 µmol, 1.0 eq.) were introduced in a dry 25 mL round-bottom flask. The mixture was purged under argon. Dry CH_3CN (3.2 mL) was added and the resulting reaction mixture was stirred at room temperature for 15 h under argon, monitoring the progress of the reaction by TLC (SiO_2, CH_2Cl_2/MeOH (8:2, v/v)). The solvent was then removed by rotary evaporation. Thereafter, the mixture was purified by flash-column chromatography over C_{18}-SiO_2 (21.8 g, step gradient of CH_3CN in 0.1% aq. TFA from 5% to 100%). Two fractions were collected containing ***anti*-3²⁺,(CH₃COO⁻)₂** (Fraction 1) and **3⁺,CH₃COO⁻** (Fraction 2). Fraction 1 which bears the CF_3COO^- counter-anion (from TFA), as attested by ^{19}F NMR analysis, was eluted with CH_3CN through an anion-exchange resin (AMBERLIT™ IRA96 resin) previously saturated with PF_6^- anions. The solvent was then removed by rotary evaporation. This fraction was then recrystallized in a CH_3CN/Et_2O mixture. The precipitate was washed with Et_2O and dried at 130 °C under vacuum for 3 h to give ***anti*-3²⁺,(PF₆⁻)₂** as a green powder in 31% yield (17.8 mg, 16.9 µmol). Others syntheses of this compound were purified by semi-preparative RP-HPLC (system B, t_R = 2.7-3.0 min). The product-containing fractions were lyophilized to give compound ***anti*-3²⁺,(PF₆⁻)₂** as green powder. ^1H NMR (CD_3CN, 500 MHz, 298 K): δ (ppm) 11.03 (s, 2H), 10.52 (s, 2H), 10.26 (s, 2H), 9.85 (d, $^3J_{H-H}$ = 6.5 Hz, 2H), 8.55 (t, $^3J_{H-H}$ = 7.6 Hz, 2H), 8.48 (d, $^3J_{H-H}$ = 8.3 Hz, 2H), 8.16 (t, $^3J_{H-H}$ = 6.6 Hz, 2H), 7.91 (d, $^3J_{H-H}$ = 7.2 Hz, 4H), 7.74 (d, $^3J_{H-H}$ = 6.8 Hz, 4H), 2.79 (s, 6H); $^{13}C\{^1H\}$ NMR (CD_3COCD_3, 126 MHz, 298 K): δ (ppm) 148.8, 145.7, 143.3, 140.2, 136.1, 129.6, 21.62; ^{19}F NMR (CD_3CN, 470 MHz, 298 K): δ (ppm) -72.92 (d, $^3J_{F-P}$ = 706.6 Hz); ^{31}P NMR (CD_3CN, 202 MHz, 298 K): δ (ppm) -142.89 (hept); R_f 0.30 (SiO_2, CH_2Cl_2/MeOH (8:2, v/v)); λ_{max} (CH_3CN) / nm (log ε): 291 (4.44), 321 (4.46), 432 (5.12), 445 (5.10), 561 (4.01),

595 (4.29); HPLC (system A) : t_R = 4.57 min (purity 96.97% at 430 nm); LRMS (ESI+): m/z calcd for $C_{45}H_{30}N_5NiS^+$ $[M - PF_6]^+$ 381.1, found 381.0; HRMS (ESI+): *m/z* cald for $C_{45}H_{30}N_5NiS^+$ $[M - PF_6]^+$ 381.0580 found 381.0580.

Electrochemistry

All manipulations were performed using Schlenk techniques in an atmosphere of dry oxygen-free argon at room temperature (T = 20°C ± 3°C). The supporting electrolyte (tetraethylammonium or tetra-*n*-butylammonium hexafluorophosphate ($TEAPF_6$ or $TBAPF_6$) was degassed under vacuum before use and then dissolved in CH_2Cl_2 (unless otherwise noted) to a concentration of 0.1 mol L^{-1}. The following electrolyte volumes were used for voltammetric analyses and bulk electrolyses:
-anodic compartment: V = 20 mL;
-cathodic compartment: V = 5 mL;
-reference electrode compartment: V = 5 mL.

Voltammetric analyses

Voltammetric analyses were carried out in a standard three-electrode cell, with Biologic SP-300 potentiostat, connected to an interfaced computer that employed EC-Lab (v. 11.10) software. The reference electrode was a saturated calomel electrode (SCE) separated from the analyzed solution by a sintered glass disk filled with the background solution. The auxiliary electrode was a platinum foil separated from the analyzed solution by a sintered glass disk filled with the background solution. For all voltammetric measurements, the working electrode was a platinum electrode (*Ø* = 2 mm). Before each voltammetric analysis, the Pt electrode was polished with a diamond suspension. In these conditions, when operating in CH_2Cl_2 (0.1 M $TBAPF_6$), the formal potential for the ferrocene (+/0) couple was +0.46 V *vs.* SCE.

Bulk electrolyses

Bulk electrolyses were performed in CH_2Cl_2 (0.1 M $TEAPF_6$) (unless otherwise noted) at controlled potential in a cell with three compartments separated with glass frits of medium porosity with a Biologic SP-300 potentiostat, connected to an interfaced computer that employed EC-Lab (v. 11.10) software. Two platinum wire spirals (l = 50 cm, *Ø* = 1 mm for each spiral, $S_{tot} \approx 2\times15 \approx 30$ cm^2) were used as working electrodes, a Pt plate (*ca.* 30 cm^2) was used as the counter electrode and a saturated calomel electrode was used as the reference electrode. TFA (3.5 eq. *vs.* porphyrin) was added in the compartment of the counter electrode to avoid release of chloride anions in the working electrode compartment that might lead to chlorinated products. 2.0 eq. of K_2CO_3 (for neutralization of the released porphyrin *β*-protons) and porphyrins **1-3** were then added in the anodic compartment and a potential corresponding to their first oxidation potential was applied. Electrolyses were followed by TLC analyses and CV analyses and were stopped when the starting porphyrins were consumed.

Fused 5-(pyridin-2-ylthio)-10,20-bis(*p*-tolyl)-15-phenylporphyrinato]nickel(II) (1^+,PF_6^-)
1 (39.7 mg, 54.2 µmol) was electrolyzed at E_{app} = 0.96 V / SCE. After abstraction of 2.8 ± 0.1 F per mol of porphyrin, the organic phase was evaporated, dissolved in 1,2-dichloroethane (DCE) and washed four times (4×100 mL) with hot deionized water (70 °C) to remove the supporting electrolyte. The organic solvent was evaporated and the crude mixture was purified by column chromatography (SiO_2, CH_2Cl_2/MeOH (97:3, v/v, h = 15.5 cm; *Ø* = 3.5 cm). The major brown/red fraction was evaporated and the resulting solid was recrystallized from

CH_2Cl_2/*n*-hexane and dried overnight at 150 °C under vacuum affording **1**$^+$,**PF**$_6^-$ in 71% yield (33.7 mg, 38.4 μmol).

Fused [5-(pyridin-2-ylthio)-10,20-bis(*p*-tolyl)porphyrinato]nickel(II) (2$^+$,PF$_6^-$)
Nickel(II) porphyrin **2** was electrolyzed at E_{app} = 1.04 V / SCE. After abstraction of 2.0 ± 0.1 F per mol of porphyrin, the organic phase was evaporated, dissolved in DCE and washed three times with hot deionized water (70 °C) to remove the supporting electrolyte. The organic solvent was evaporated and the crude mixture was directly recrystallized from CH_2Cl_2/*n*-hexane and dried at 120 °C under vacuum for 2.5 h affording **2**$^+$,**PF**$_6^-$ in 52% yield (28.5 mg, 35.6 μmol).

Fused [5,15-bis(pyridin-2-ylthio)-10,20-bis(*p*-tolyl)porphyrinato]nickel(II) (3$^+$,PF$_6^-$)
Nickel(II) porphyrin **3** (40.2 mg, 52.5 μmol) was electrolyzed at E_{app} = 1.00 V / SCE. After abstraction of 2.1 ± 0.1 F per mol of porphyrin, the organic phase was evaporated, dissolved in DCE and washed four times (4×100 mL) with hot deionized water (70 °C) to remove the supporting electrolyte. The organic solvent was evaporated and the crude mixture was purified by column chromatography (SiO_2, CH_2Cl_2/MeOH (95:5, v/v), *h* = 13 cm; *Ø* = 3 cm). The major brown/red fraction was evaporated and the resulting solid was recrystallized from CH_2Cl_2/*n*-hexane and dried overnight at 150 °C under vacuum affording **3**$^+$,**PF**$_6^-$ in 72% yield (34.7 mg, 3.82×10^{-5} mol).

Doubly-fused [5,15-bis(pyridin-2-ylthio)-10,20-bis(*p*-tolyl)porphyrinato]nickel(II) (*anti*-3^{2+},(PF$_6^-$)$_2$)
Fused porphyrin **3**$^+$,**PF**$_6^-$ (20.0 mg, 22.0 μmol) was electrolyzed at E_{app} = 1.15 V/SCE in CH_3CN (0.1 M $TEAPF_6$). After abstraction of 3.2 ± 0.1 F per mol of porphyrin, ferrocene (8.2 mg, 44.1 μmol, 2.0 eq) was added to the reaction mixture to reduce the possible residual oxidized porphyrin species. The solvent was then removed by rotary evaporation. The crude mixture was directly recrystallized from CH_3CN/deionized water and dried at 150 °C under vacuum for 3 h affording ***anti*-3**$^{2+}$,(**PF**$_6^-$)$_2$ in 23% yield (5.4 mg, 5.12 μmol).

Table S1. Comparison of the yields (%) obtained with chemical/electrochemical oxidation for the fused compounds.

	$1^+,PF_6^-$	$2^+,PF_6^-$	$3^+,PF_6^-$	*anti*-$3^{2+},(PF_6^-)_2$
Chemical oxidation (PIFA)	98	81	88	31
Electrochemical oxidation	71	52	72	23

Voltammetric analyses of 1-3 and $1^+,PF_6^-$, $2^+,PF_6^-$, $3^+,PF_6^-$ and *anti*-$3^{2+},(PF_6^-)_2$

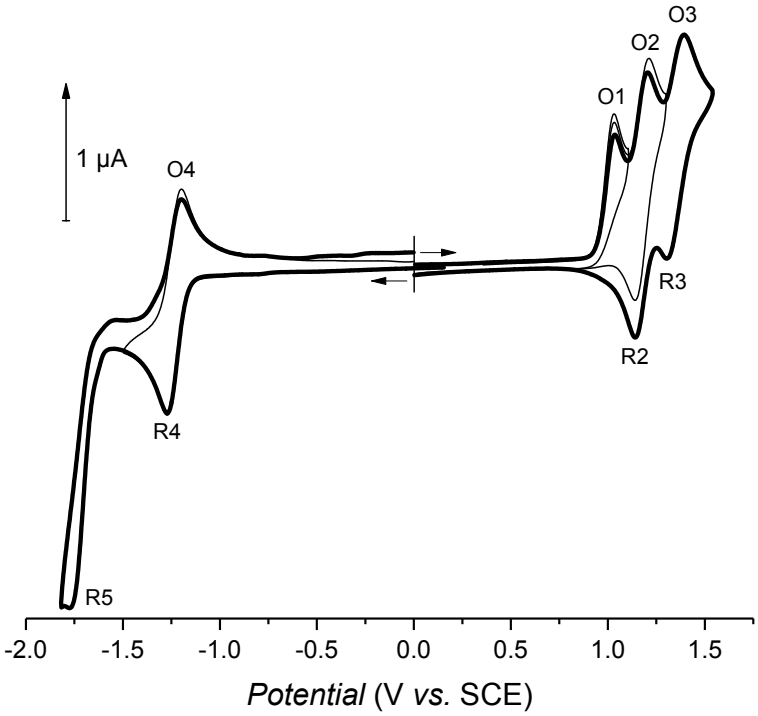

Figure S1. Cyclic voltammetry of a10^{-3} M solution of **1** in CH_2Cl_2 0.1 M $TBAPF_6$, ν = 100 mV.s^{-1}, WE: Pt, Ø = 1 mm.

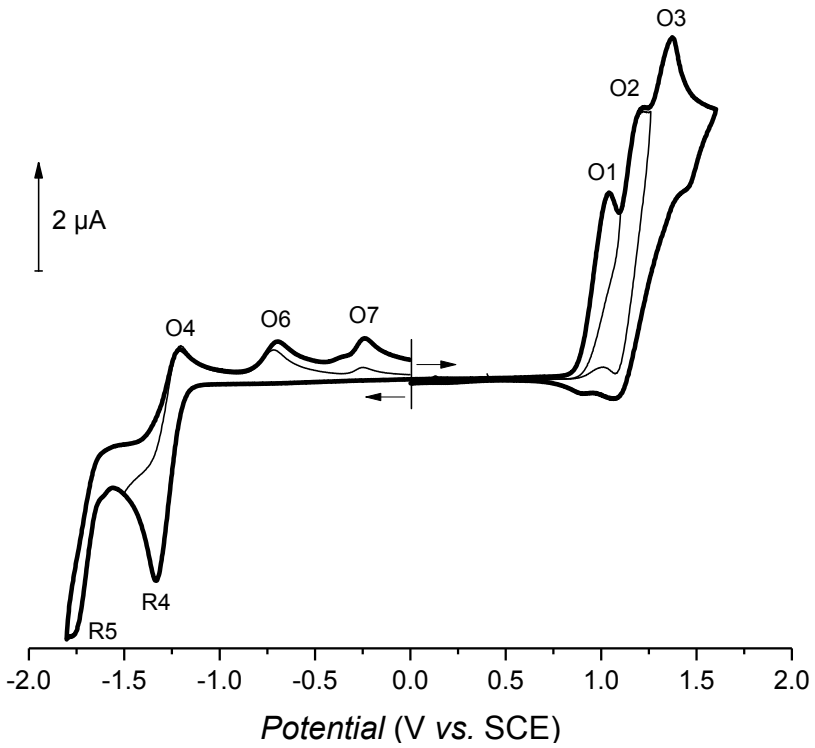

Figure S2. Cyclic voltammetry of a 10^{-3} M solution of **2** in CH_2Cl_2 0.1 M $TBAPF_6$, ν = 100 mV.s^{-1}, WE: Pt, Ø = 1 mm.

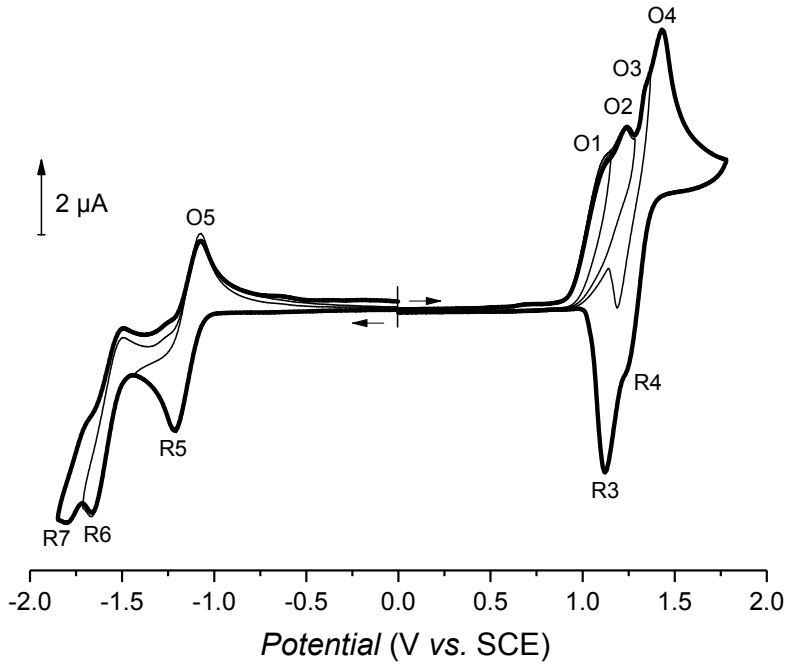

Figure S3. Cyclic voltammetry of a 10^{-3} M solution of **3** in CH_2Cl_2 0.1 M $TBAPF_6$, ν = 100 mV.s^{-1}, WE: Pt, Ø = 1 mm.

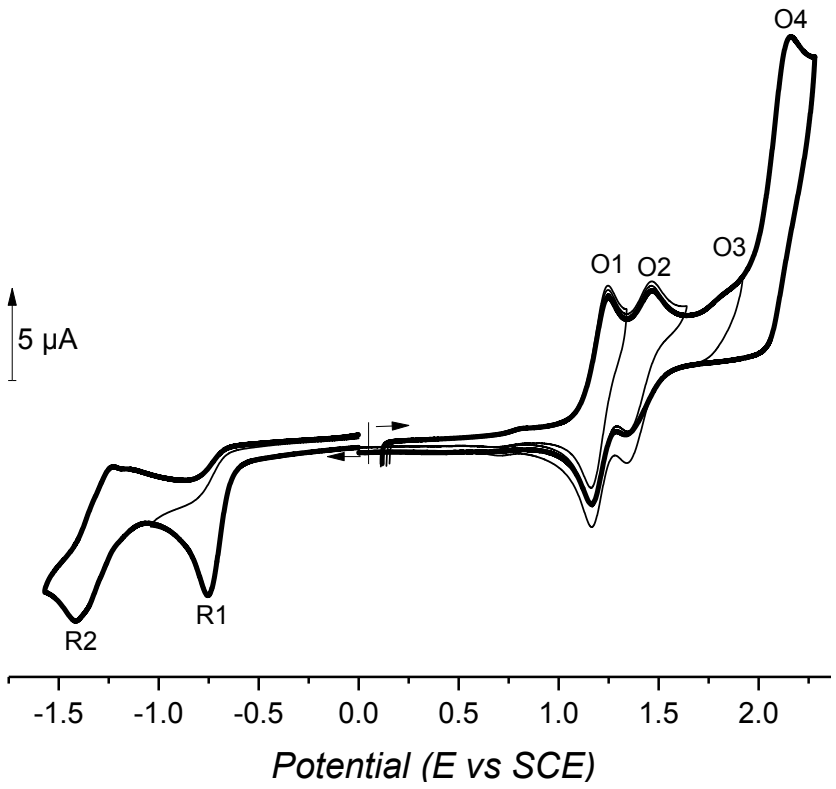

Figure S4. Cyclic voltammetry of a 10^{-3} M solution of $\mathbf{1^+,PF_6^-}$ in CH_2Cl_2 0.1 M $TBAPF_6$, ν = 100 mV.s^{-1}, WE: Pt, Ø = 2 mm.

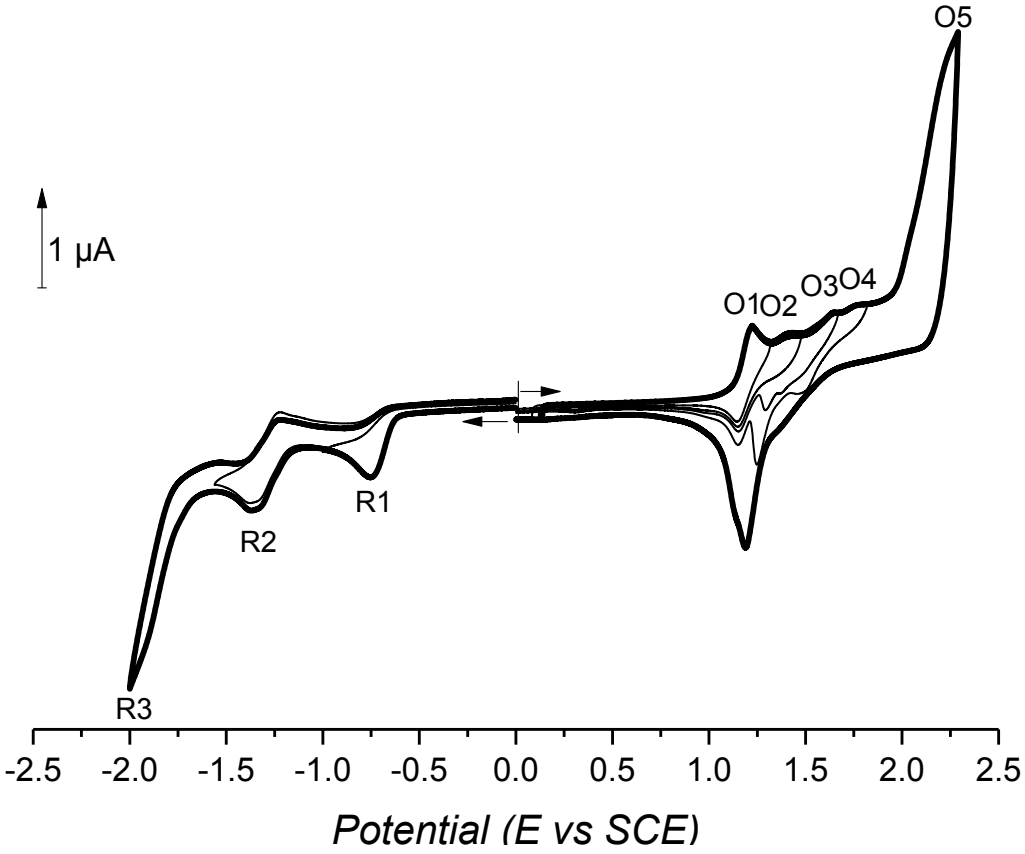

Figure S5. Cyclic voltammetry of a 10^{-3} M solution of $\mathbf{2^+,PF_6^-}$ in CH_2Cl_2 0.1 M $TBAPF_6$, ν = 100 mV.s^{-1}, WE: Pt, Ø = 2 mm.

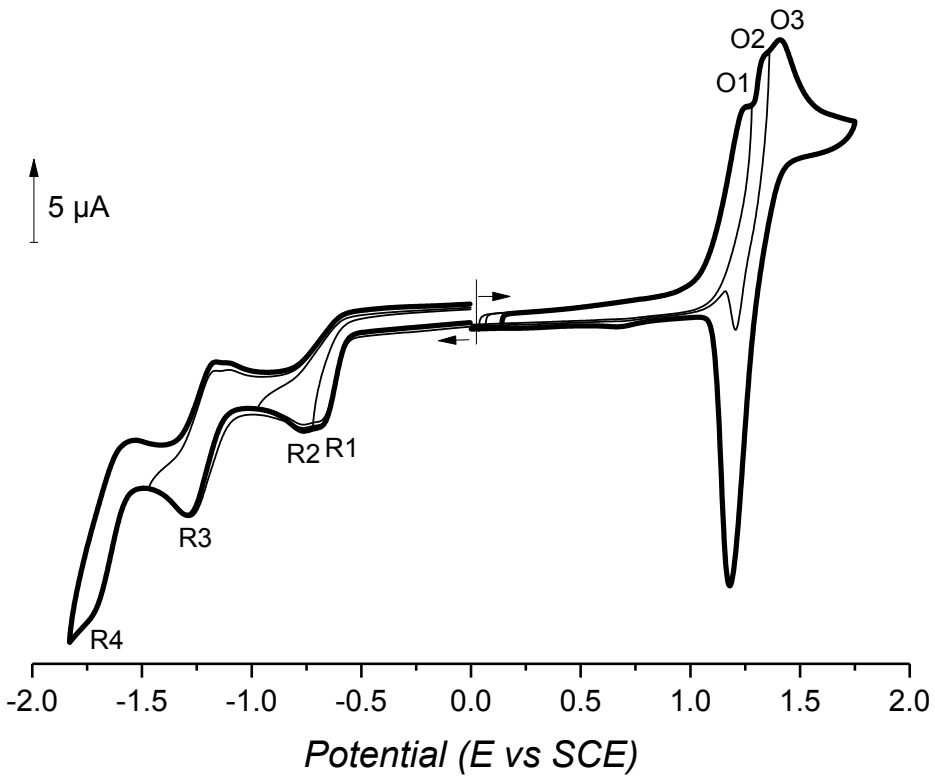

Figure S6. Cyclic voltammetry of a 10^{-3} M solution of $\mathbf{3^{+},PF_6^{-}}$ in CH_2Cl_2 0.1 M $TBAPF_6$, ν = 100 mV.s^{-1}, WE: Pt, Ø = 2 mm.

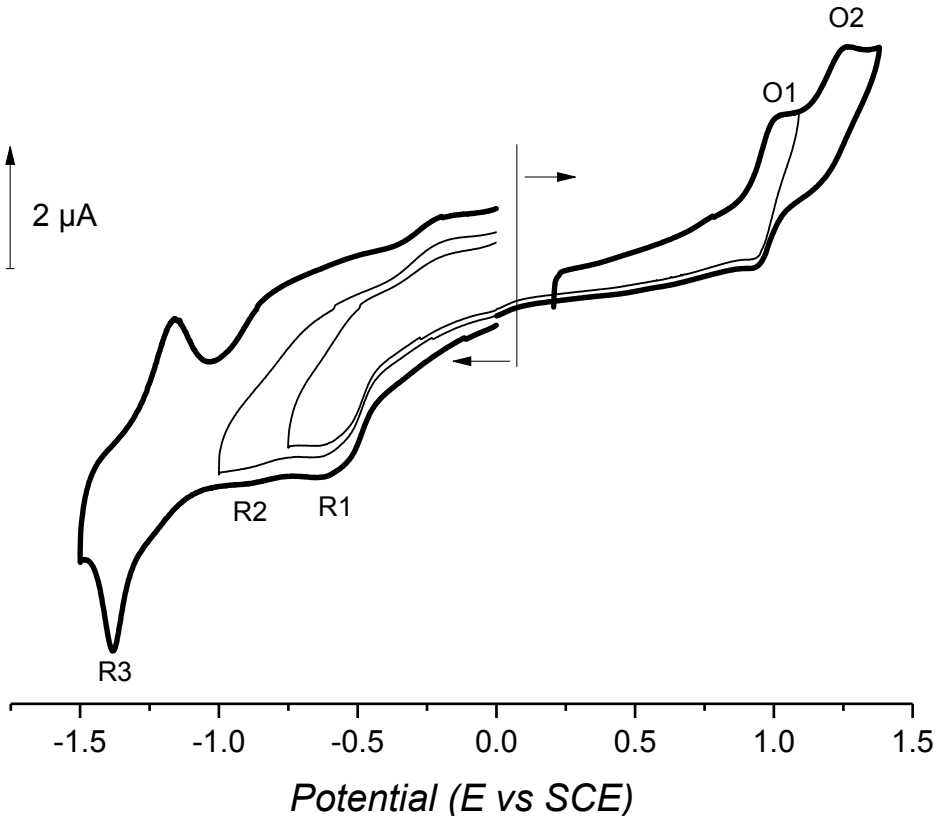

Figure S7. Cyclic voltammetry of a 10^{-3} M solution of ***anti*-$\mathbf{3^{2+},(PF_6^{-})_2}$** in CH_3CN 0.1 M $TBAPF_6$, ν = 100 mV.s^{-1}, WE: Pt, Ø = 2 mm.

NMR, UV-vis. and HRMS spectra of compounds 11-13, 1-3 and 1^{+},PF_6^{-}, 2^{+},PF_6^{-}, 3^{+},PF_6^{-} and *anti*-3^{2+},$(PF_6^{-})_2$

Compound 11

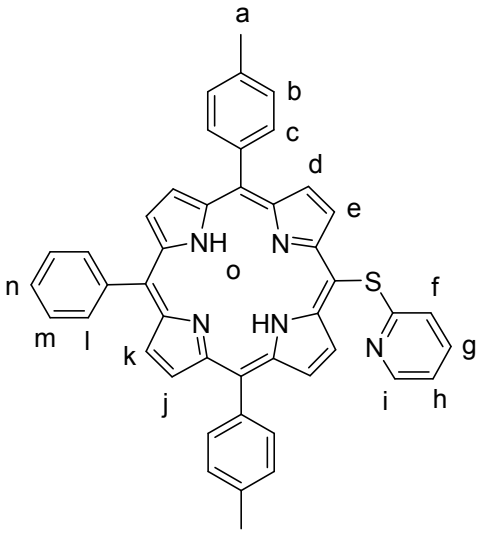

11

Chemical Formula: $C_{45}H_{33}N_5S$
Exact Mass: 675.2457
Molecular Weight: 675.8540

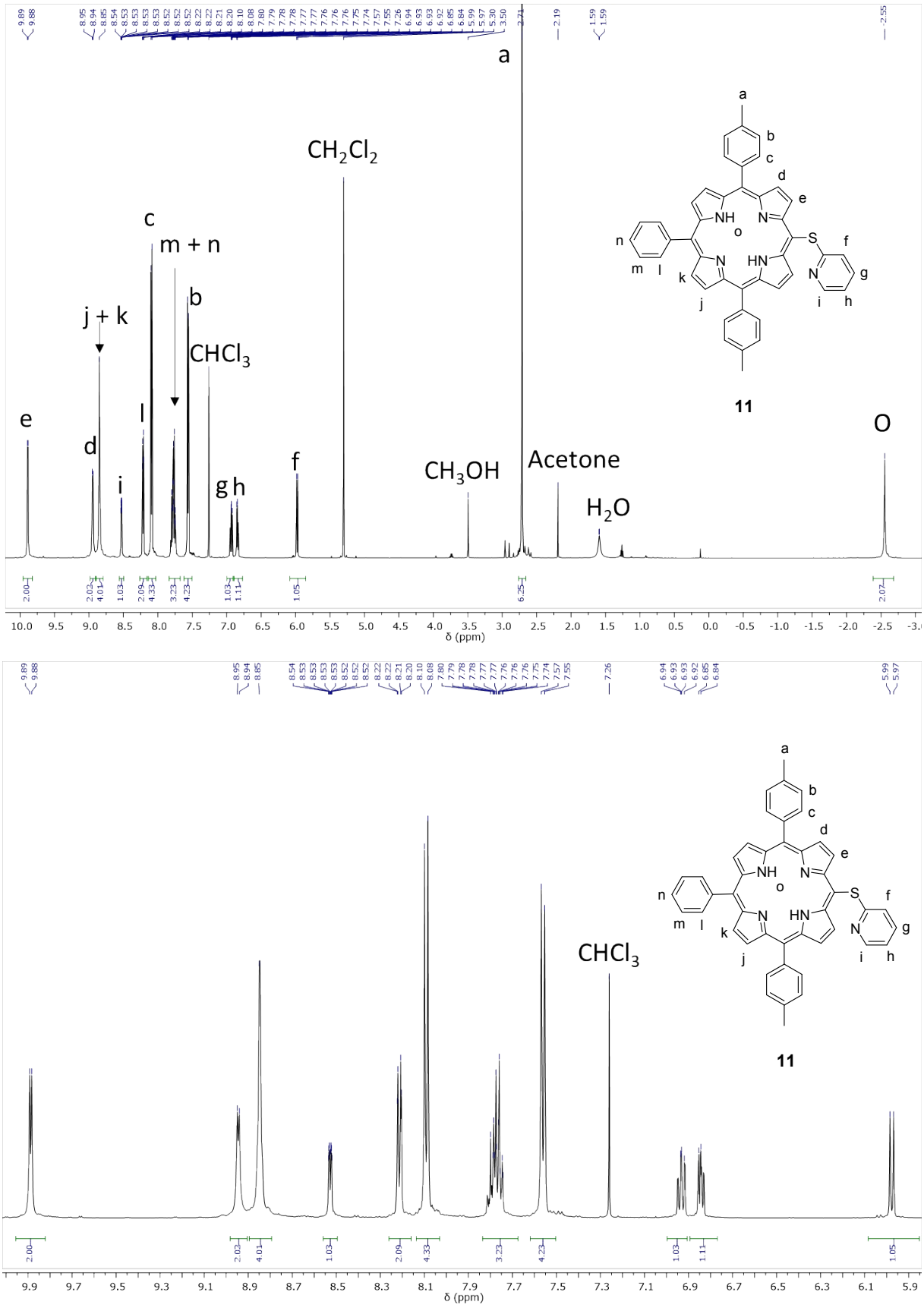

Figure S8. Full range (top) and partial (bottom) ^{1}H NMR spectra of **11** in $CDCl_3$, 300 MHz, 295 K.

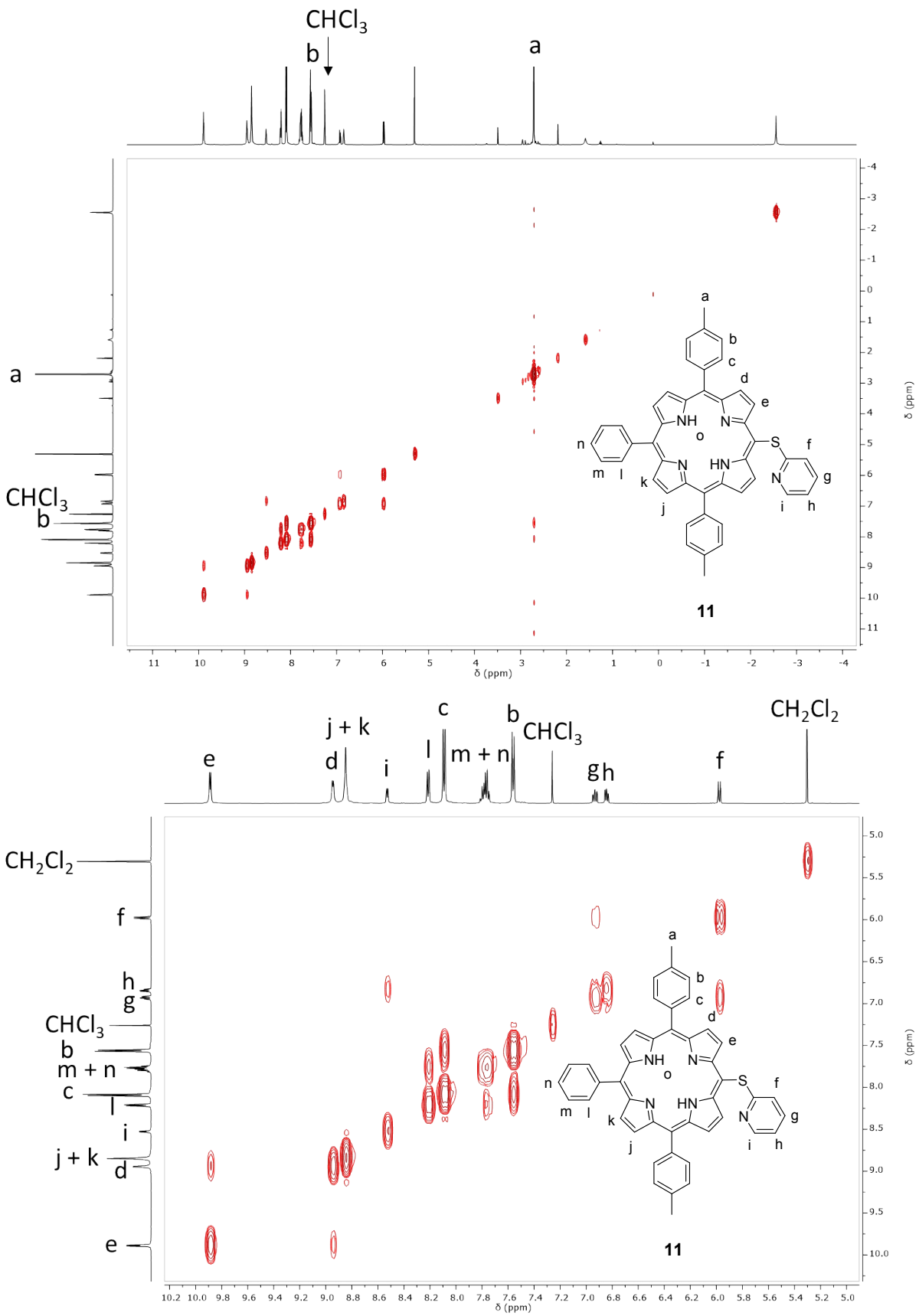

Figure S9. Full range (top) and partial (bottom) ^{1}H-^{1}H COSY NMR spectra of **11** in $CDCl_3$, 500 MHz, 298 K.

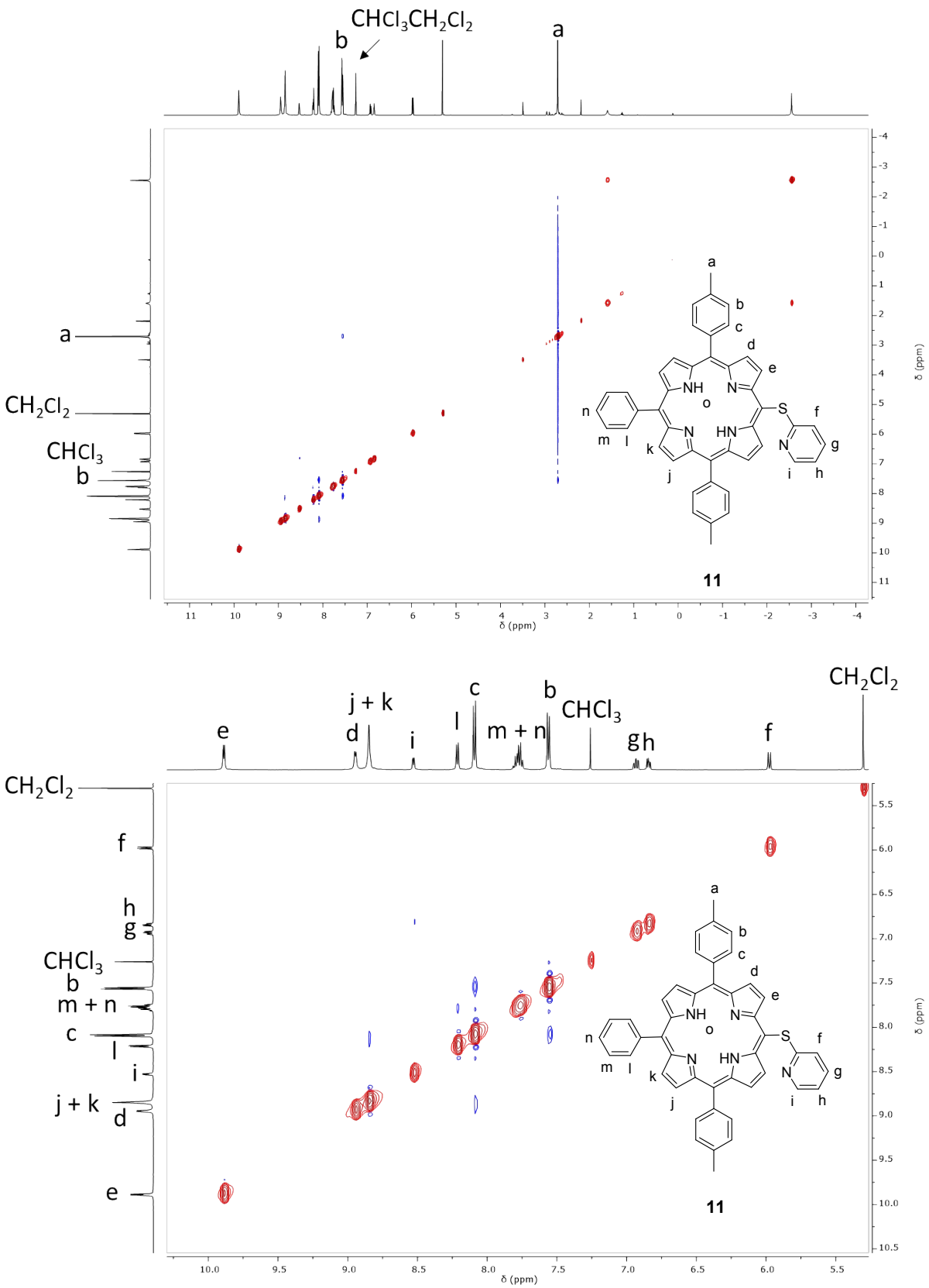

Figure S10. Full range (top) and partial (bottom) ^{1}H-^{1}H NOESY NMR spectra of **11** in $CDCl_3$, 500 MHz, 298 K.

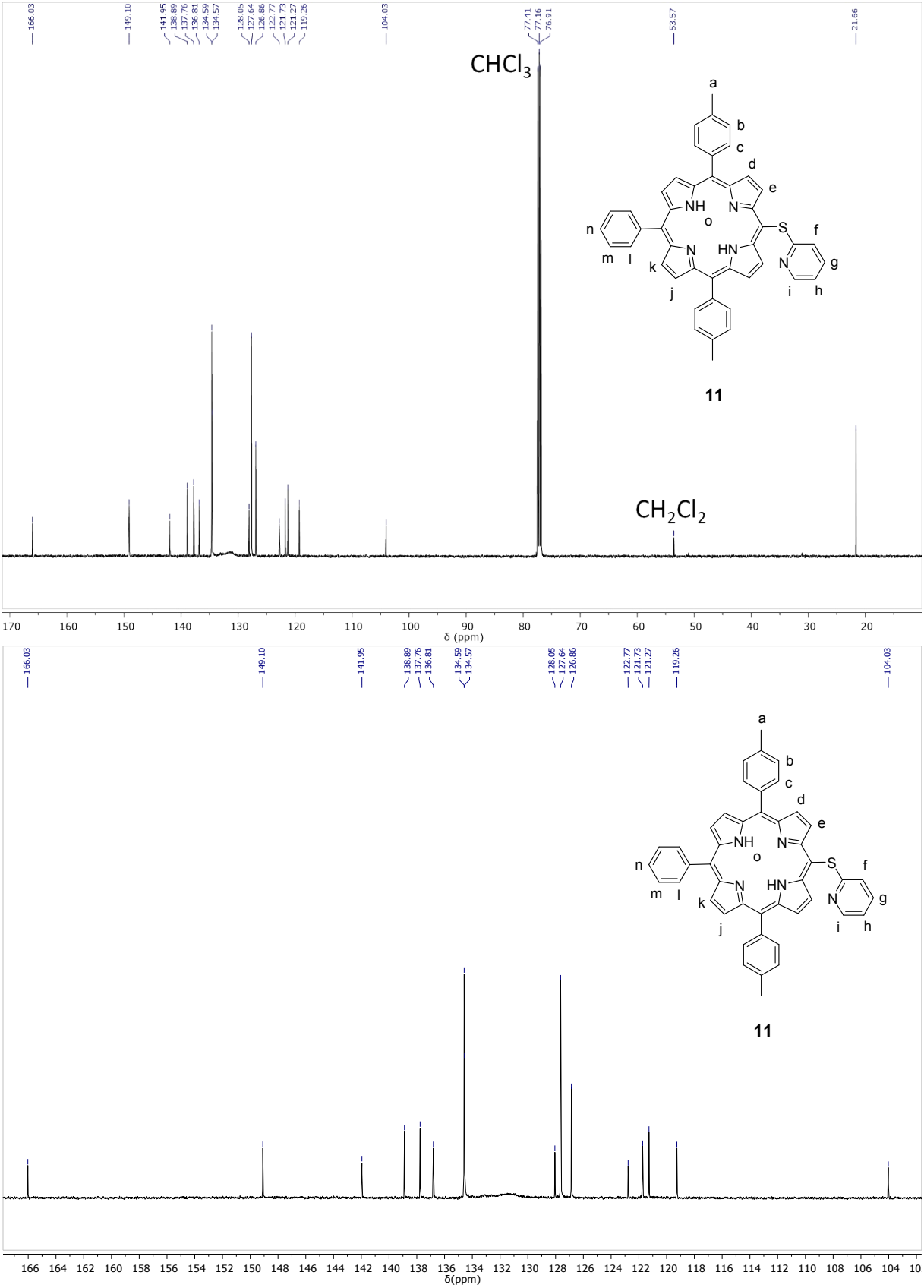

Figure S11. Full range (top) and partial (bottom) $^{13}C\{_1H\}$ NMR spectra of **11** in $CDCl_3$, 126 MHz, 300 K.

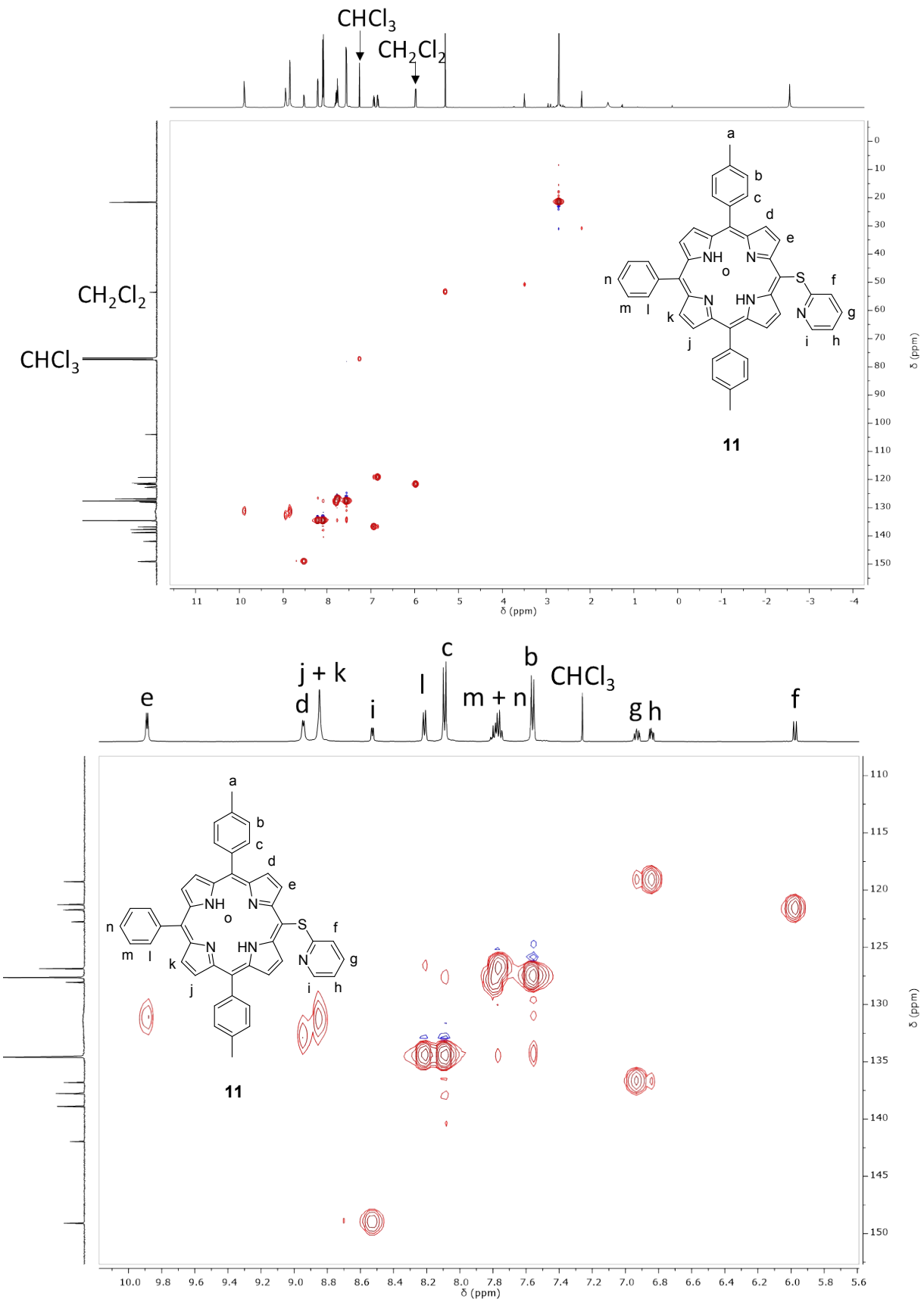

Figure S12. Full range (top) and partial (bottom) ^{1}H-^{13}C HSQC NMR spectra of **11** in $CDCl_3$, 500 MHz, 298 K.

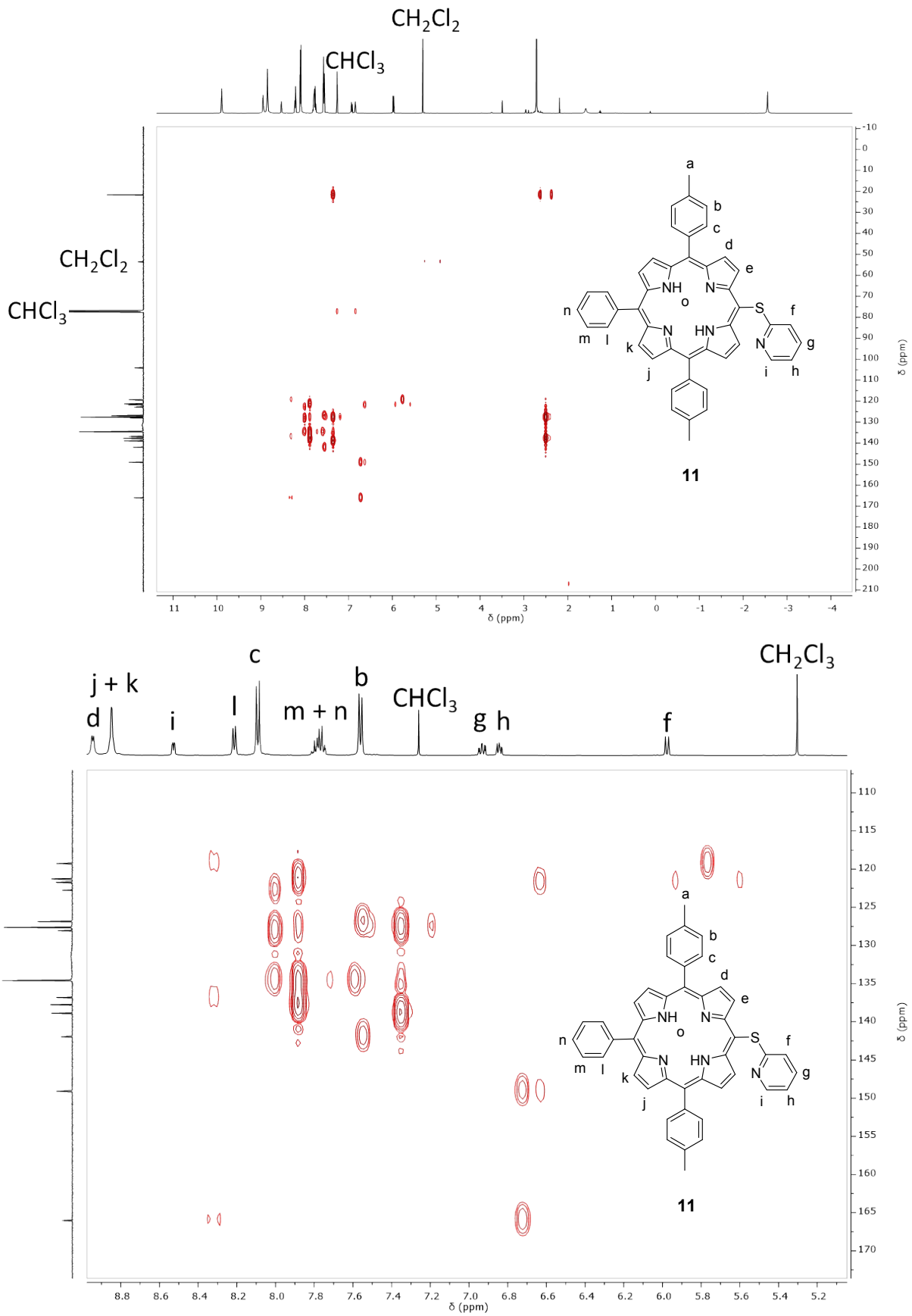

Figure S13. Full range (top) and partial (bottom) ^{1}H-^{13}C HMBC NMR spectra of **11** in $CDCl_3$, 500 MHz, 298 K.

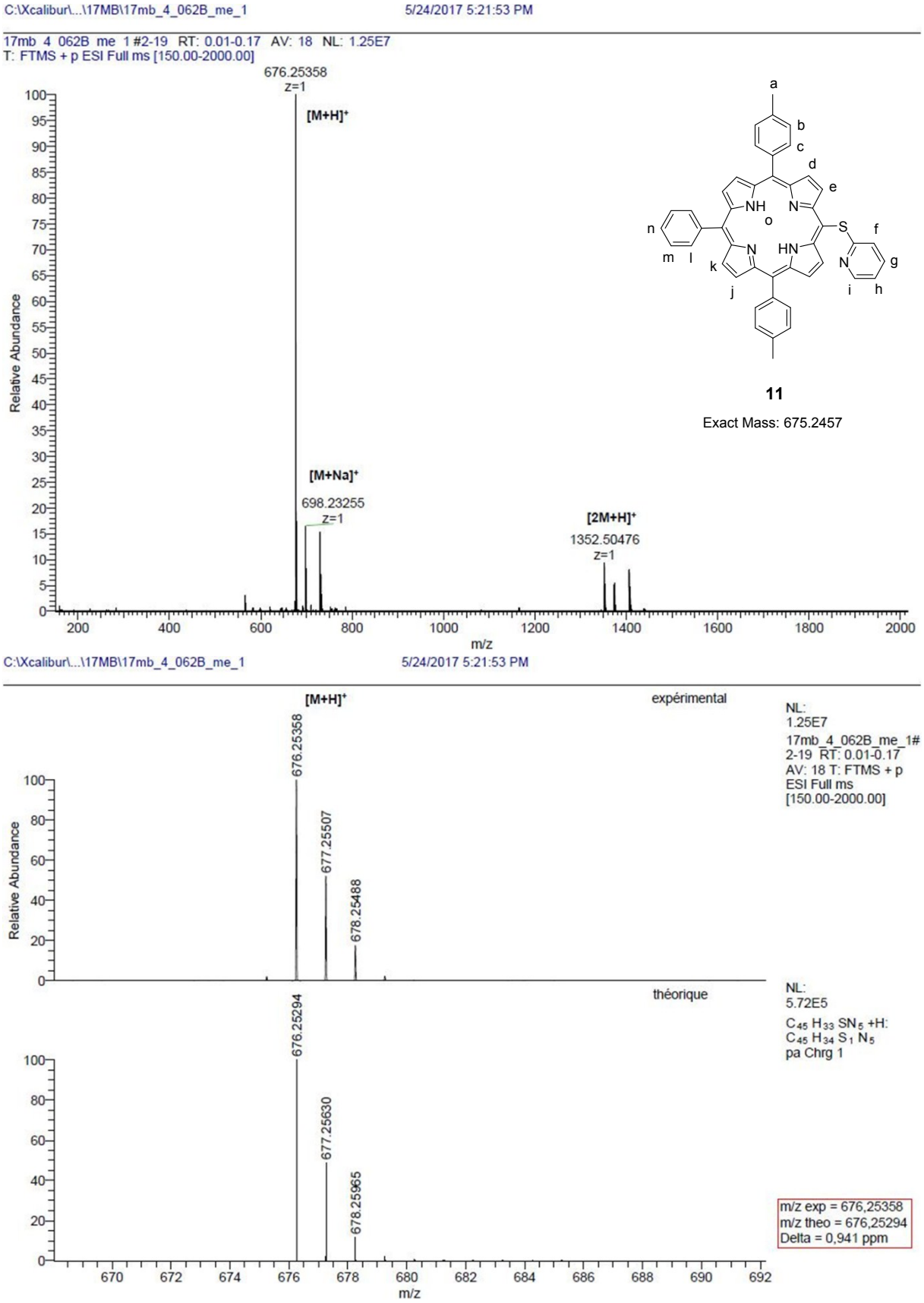

Figure S14. High resolution ESI mass spectrum of **11** and simulation of its isotopic pattern.

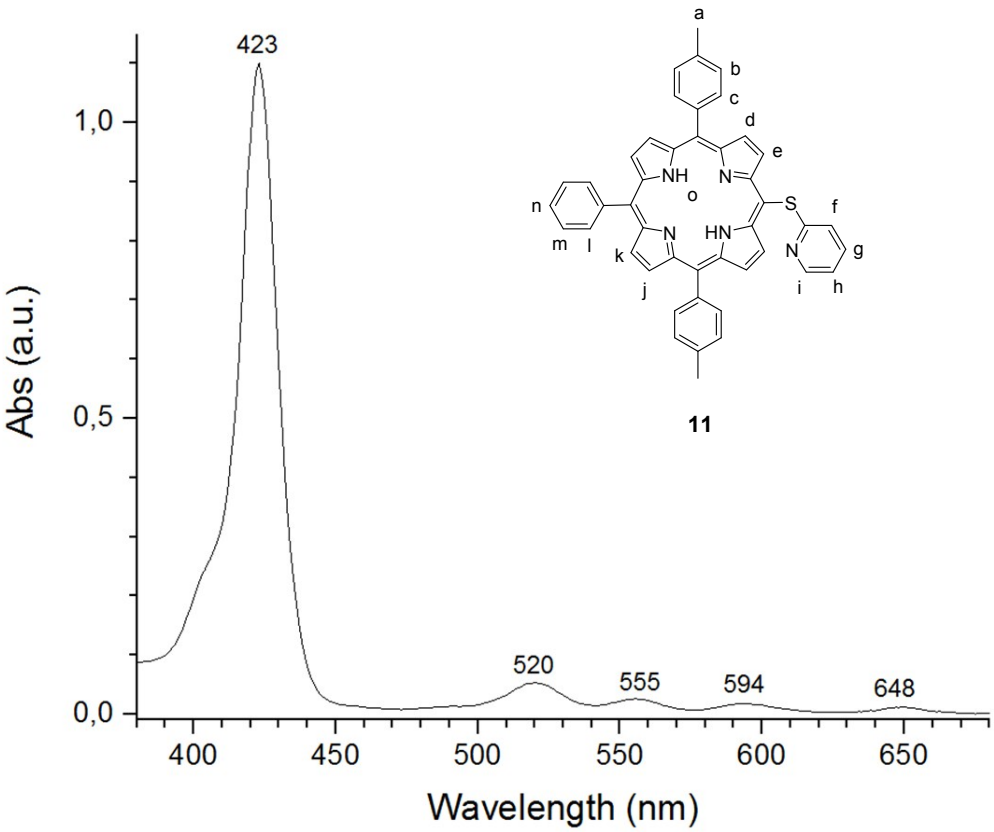

Figure S15. UV-Vis. absorption spectrum of **11** in CH_2Cl_2.

Compound 1

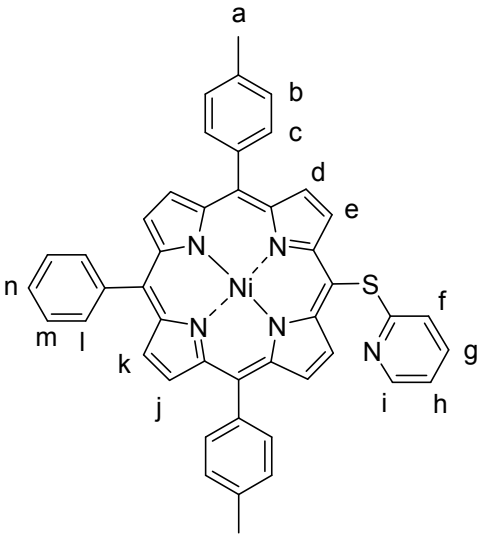

1

Chemical Formula: $C_{45}H_{31}N_5NiS$
Exact Mass: 731.1654
Molecular Weight: 732.5314

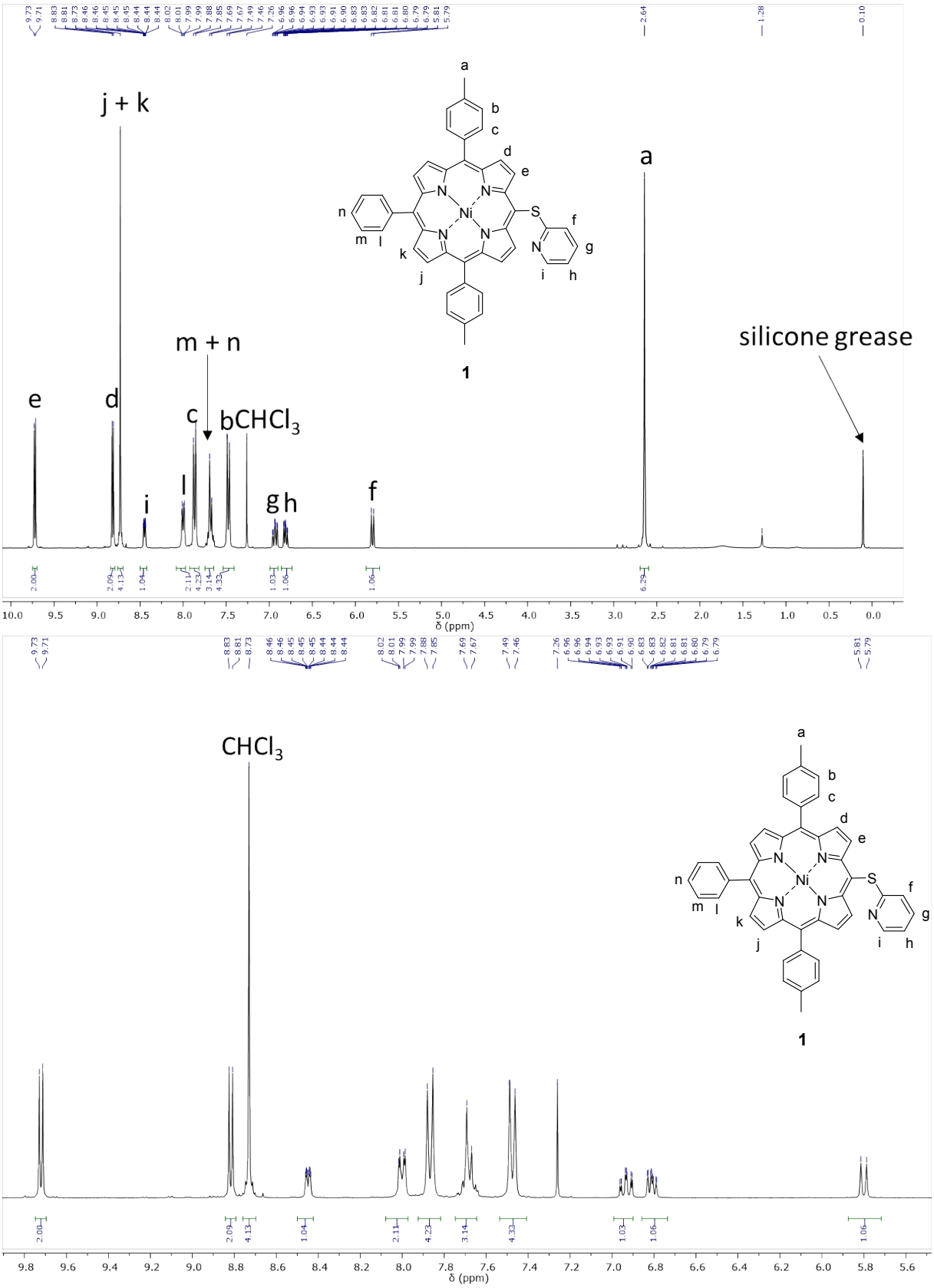

Figure S16. Full range (top) and partial (bottom) ^{1}H NMR spectra of **1** in $CDCl_3$, 300 MHz, 295 K.

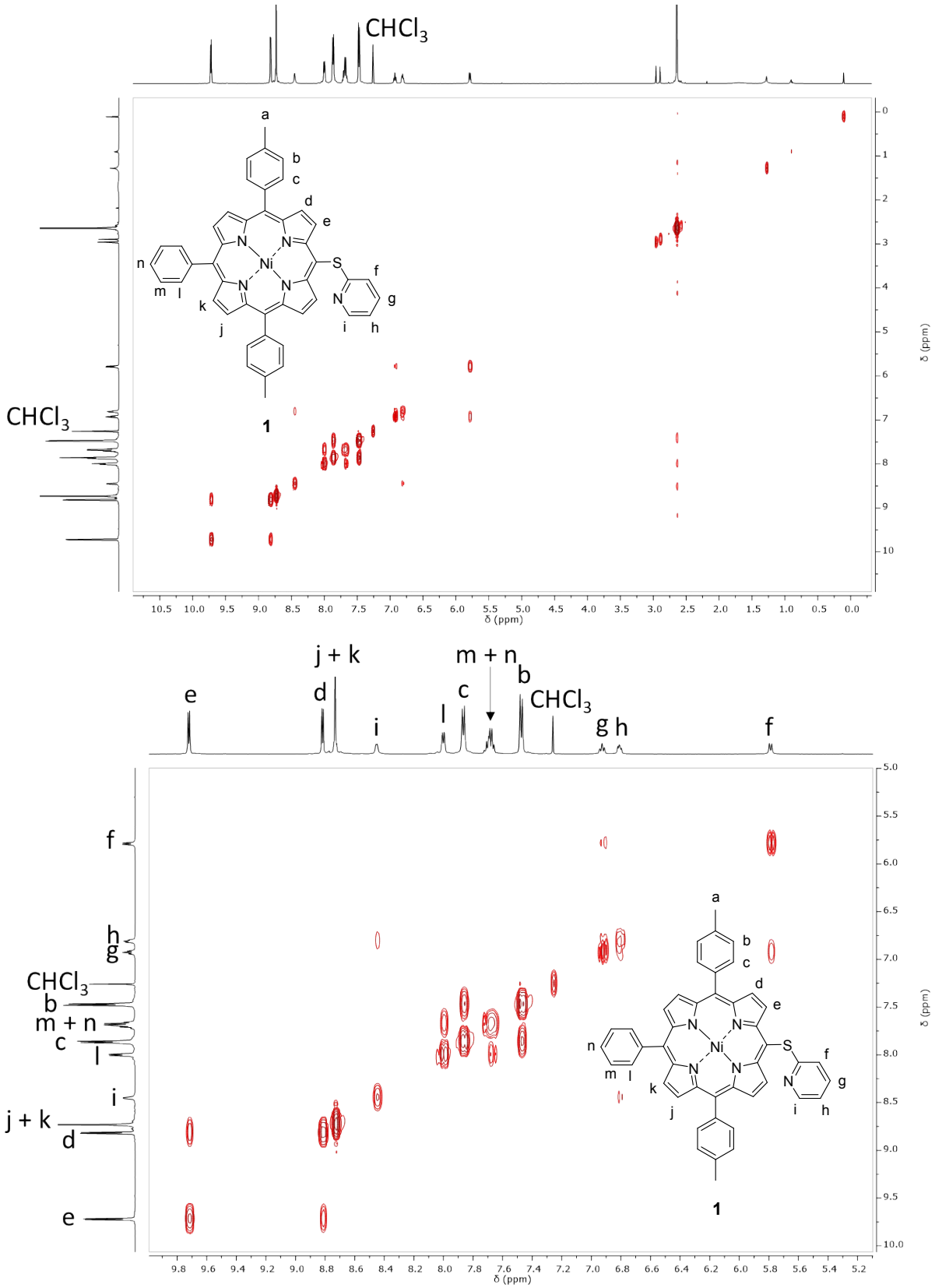

Figure S17. Full range (top) and partial (bottom) ^{1}H-^{1}H COSY NMR spectra of **1** in $CDCl_3$, 500 MHz, 298 K.

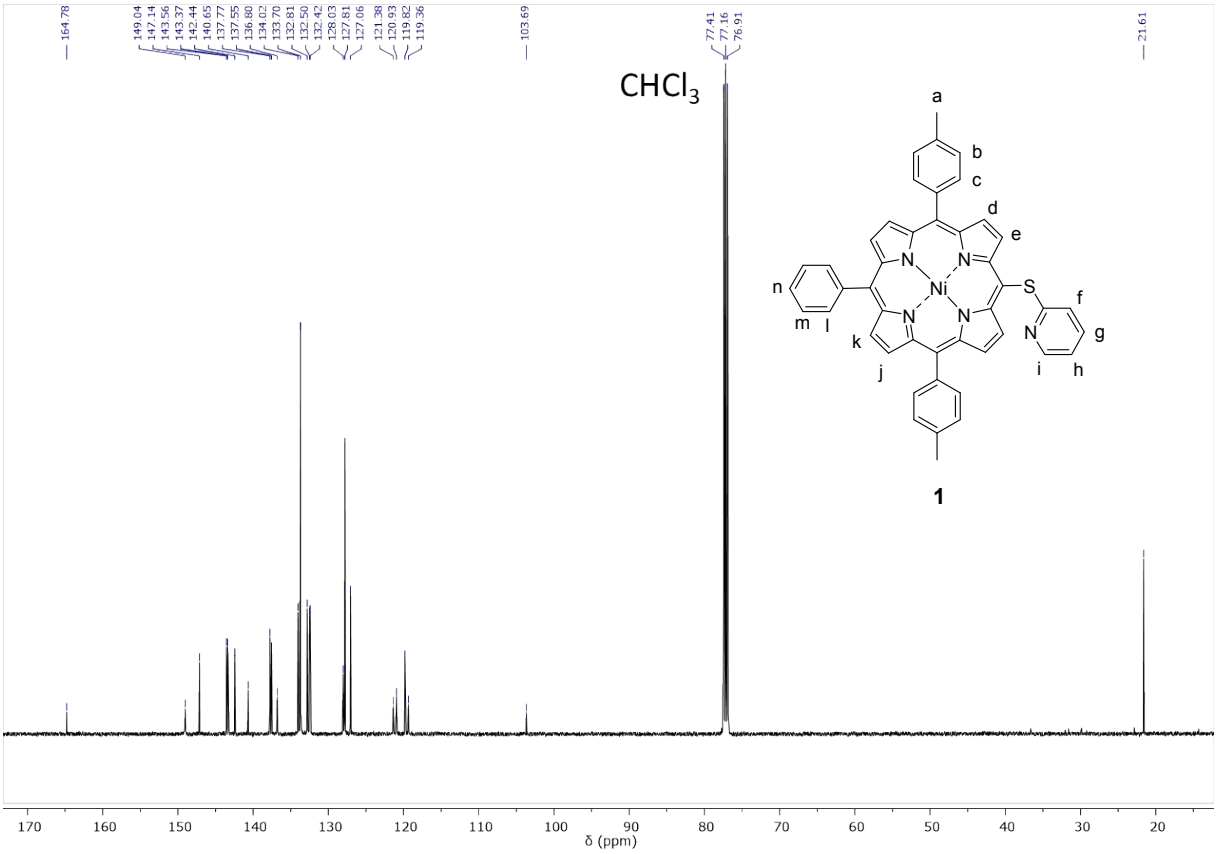

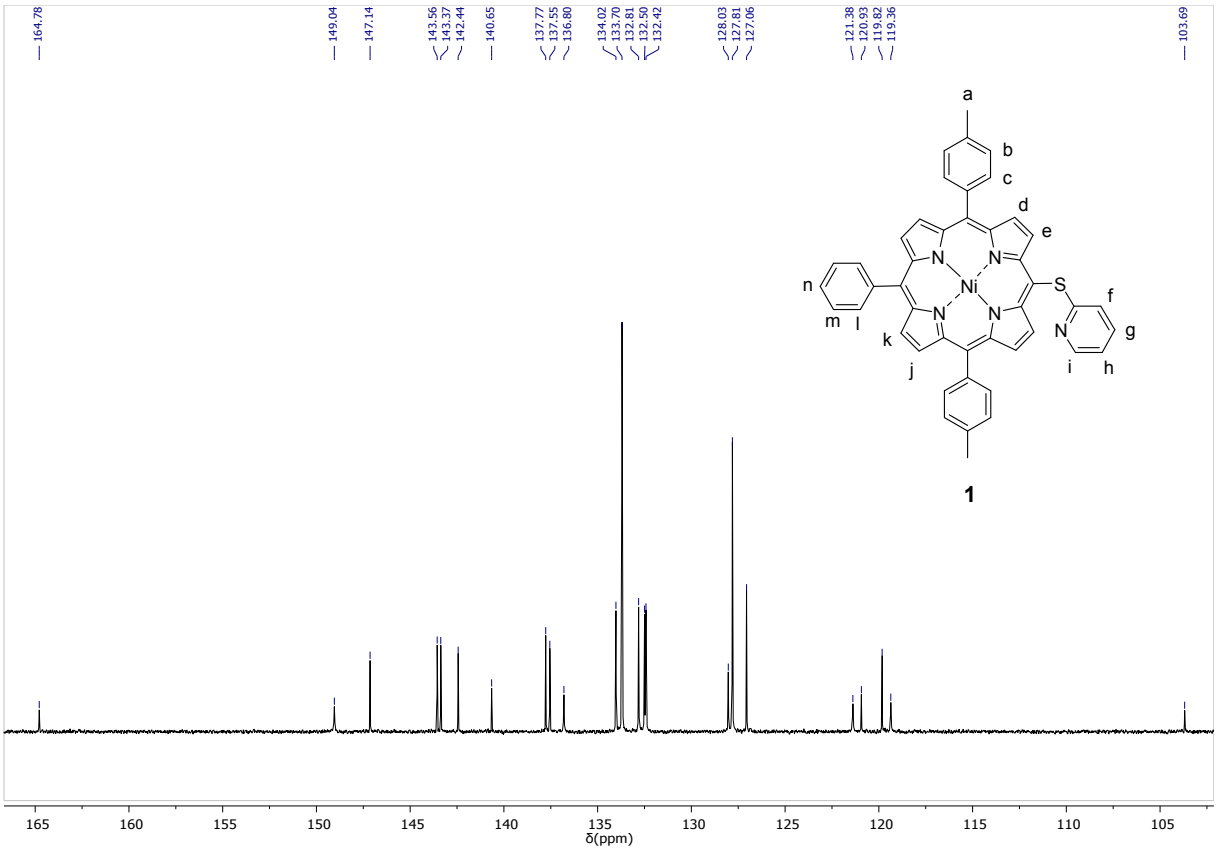

Figure S18. Full range (top) and partial (bottom) $^{13}C\{^{1}H\}$ NMR spectra of **1** in $CDCl_3$, 126 MHz, 300 K.

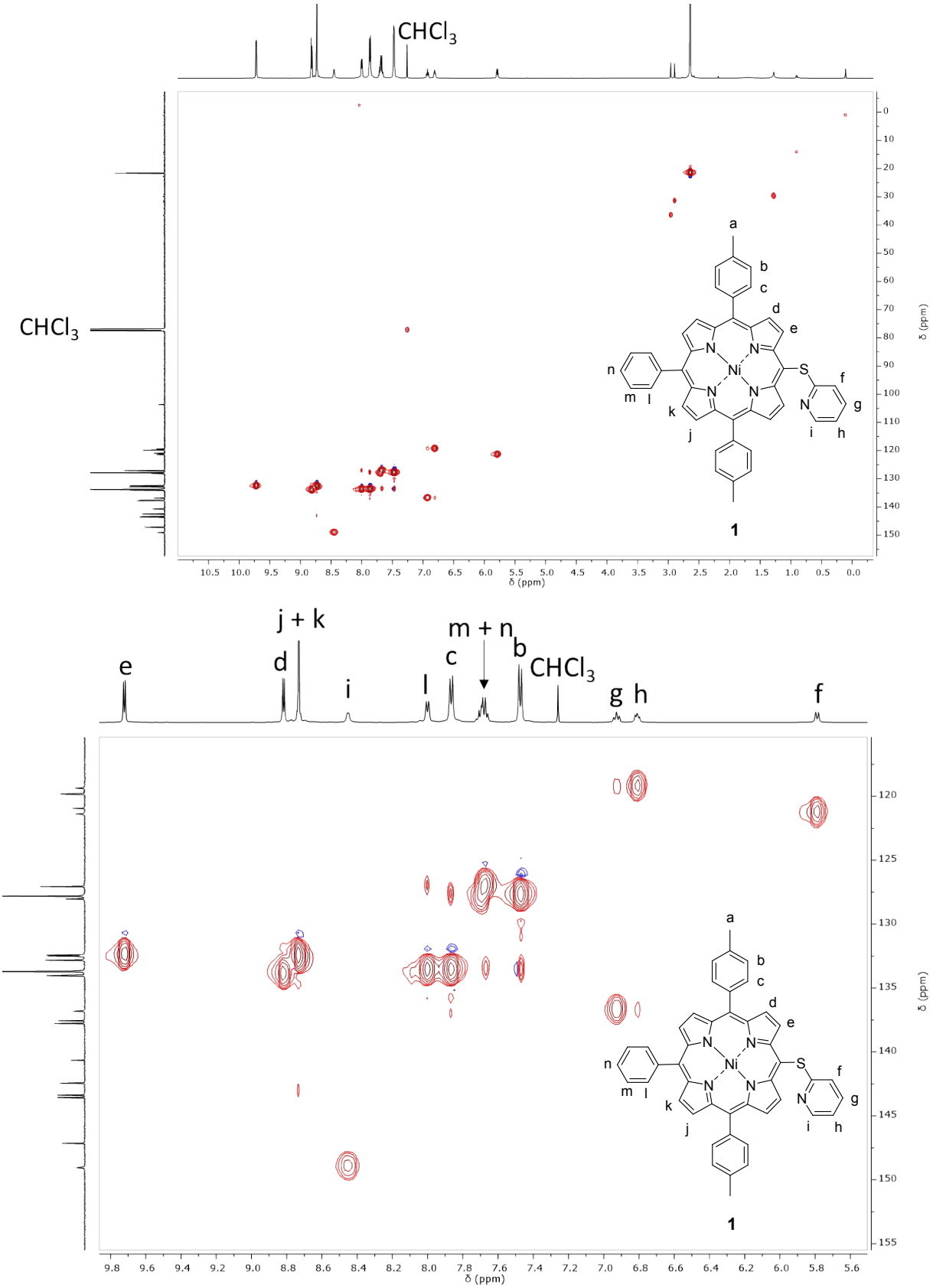

Figure S19. Full range (top) and partial (bottom) ^{1}H-^{13}C HSQC NMR spectra of **1** in $CDCl_3$, 500 MHz, 298 K.

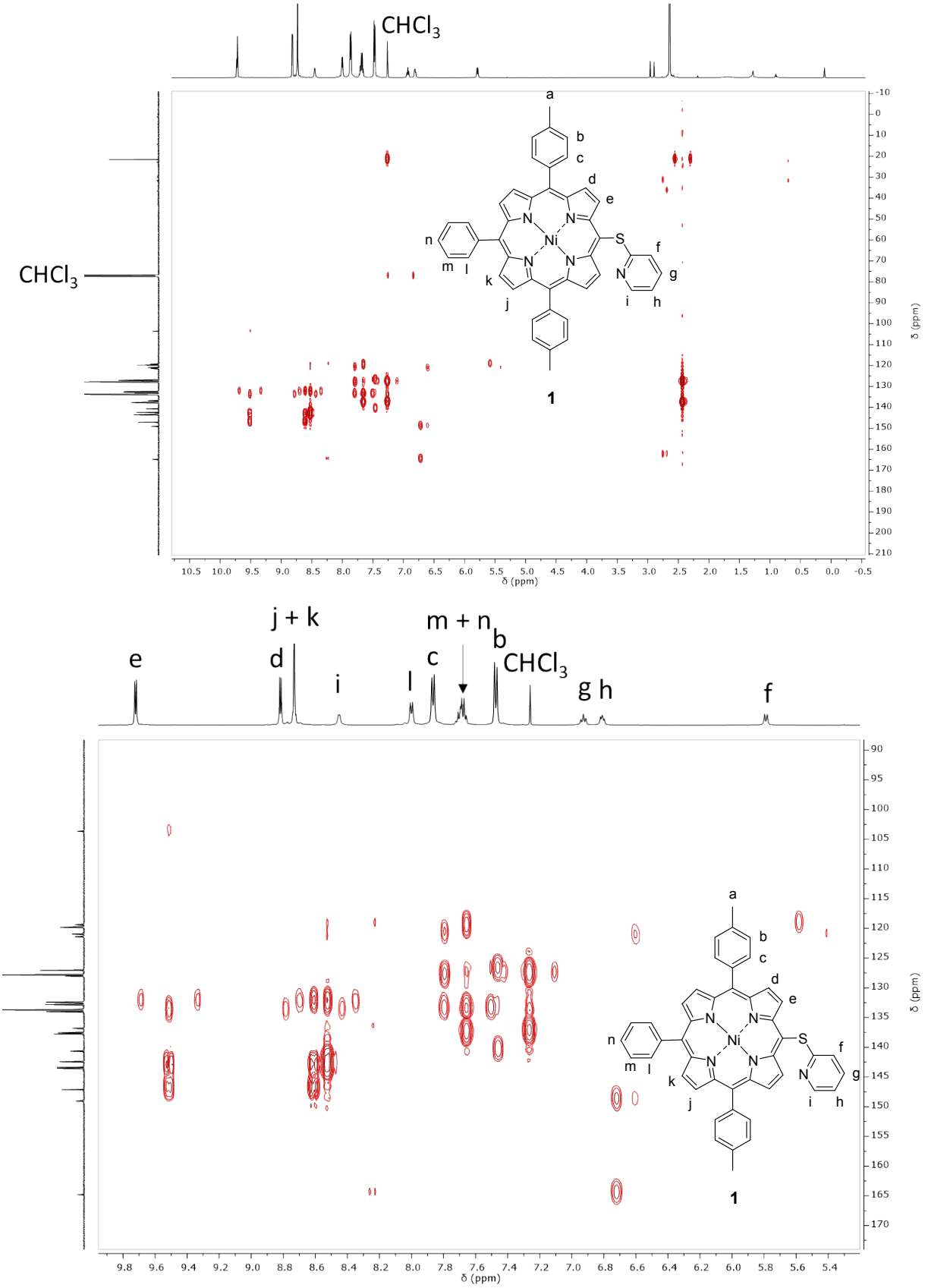

Figure S20. Full range (top) and partial (bottom) ^{1}H-^{13}C HMBC NMR spectra of **1** in $CDCl_3$, 500 MHz, 298 K.

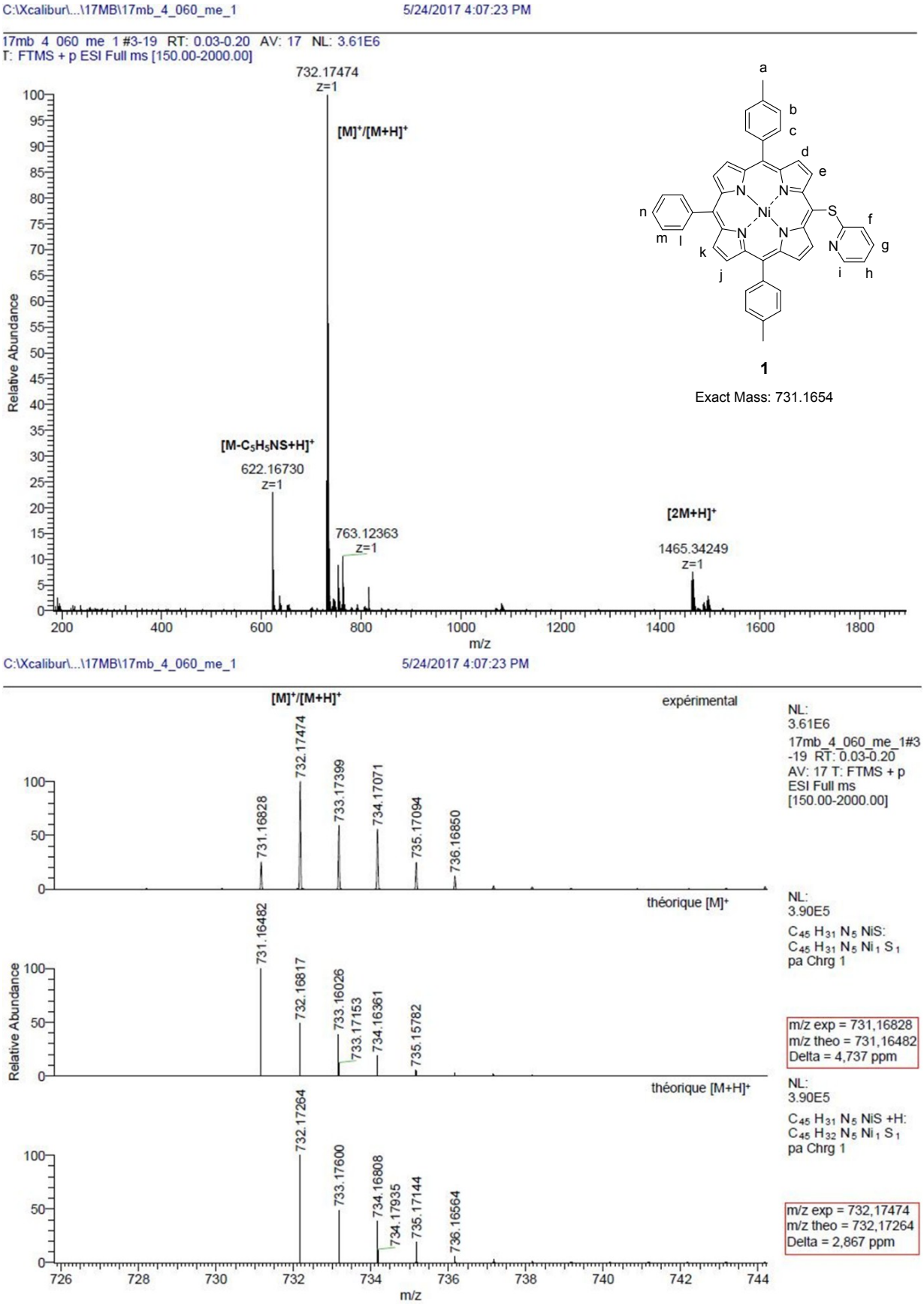

Figure S21. High resolution ESI mass spectrum of **1** and simulation of its isotopic pattern.

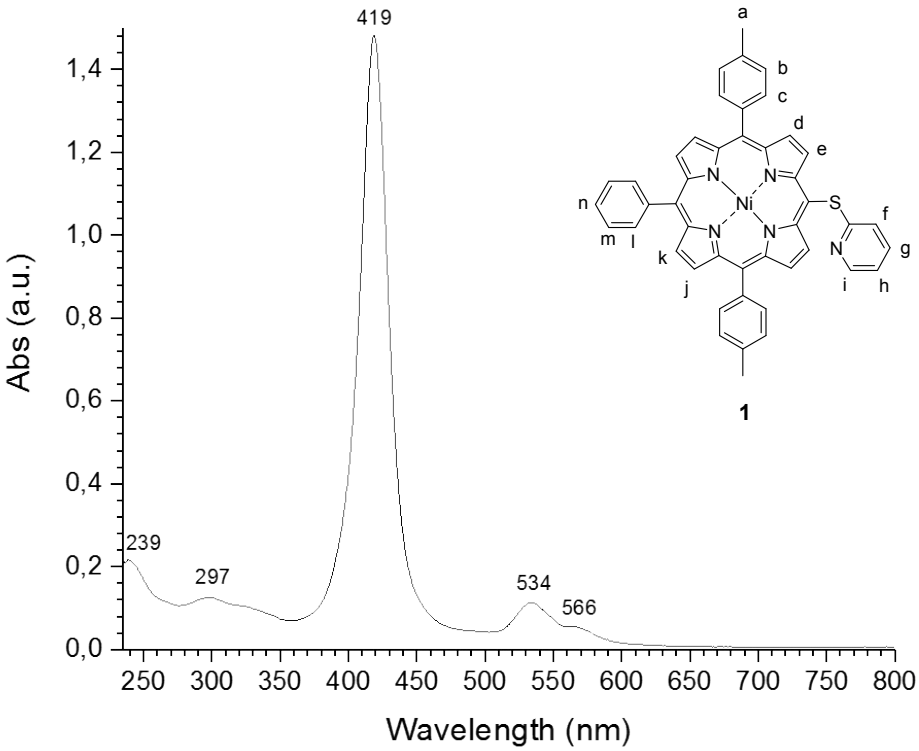

Figure S22. UV-Vis. absorption spectrum of **1** in CH_2Cl_2.

Compound 1^{+},PF_6^{-}

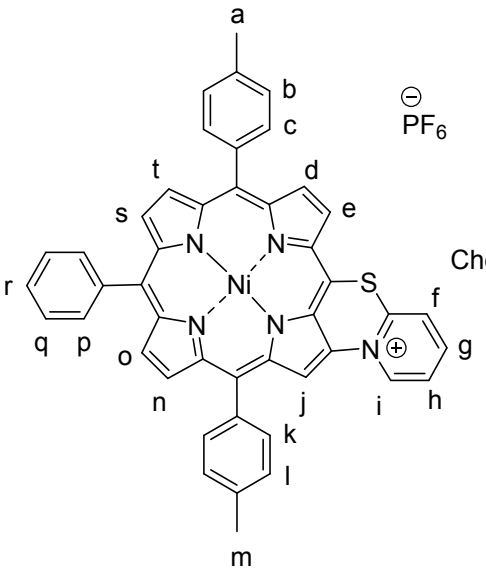

1^{+},PF_6^{-}

Chemical Formula: $C_{45}H_{30}F_6N_5NiPS$
Molecular Weight: 876.4876

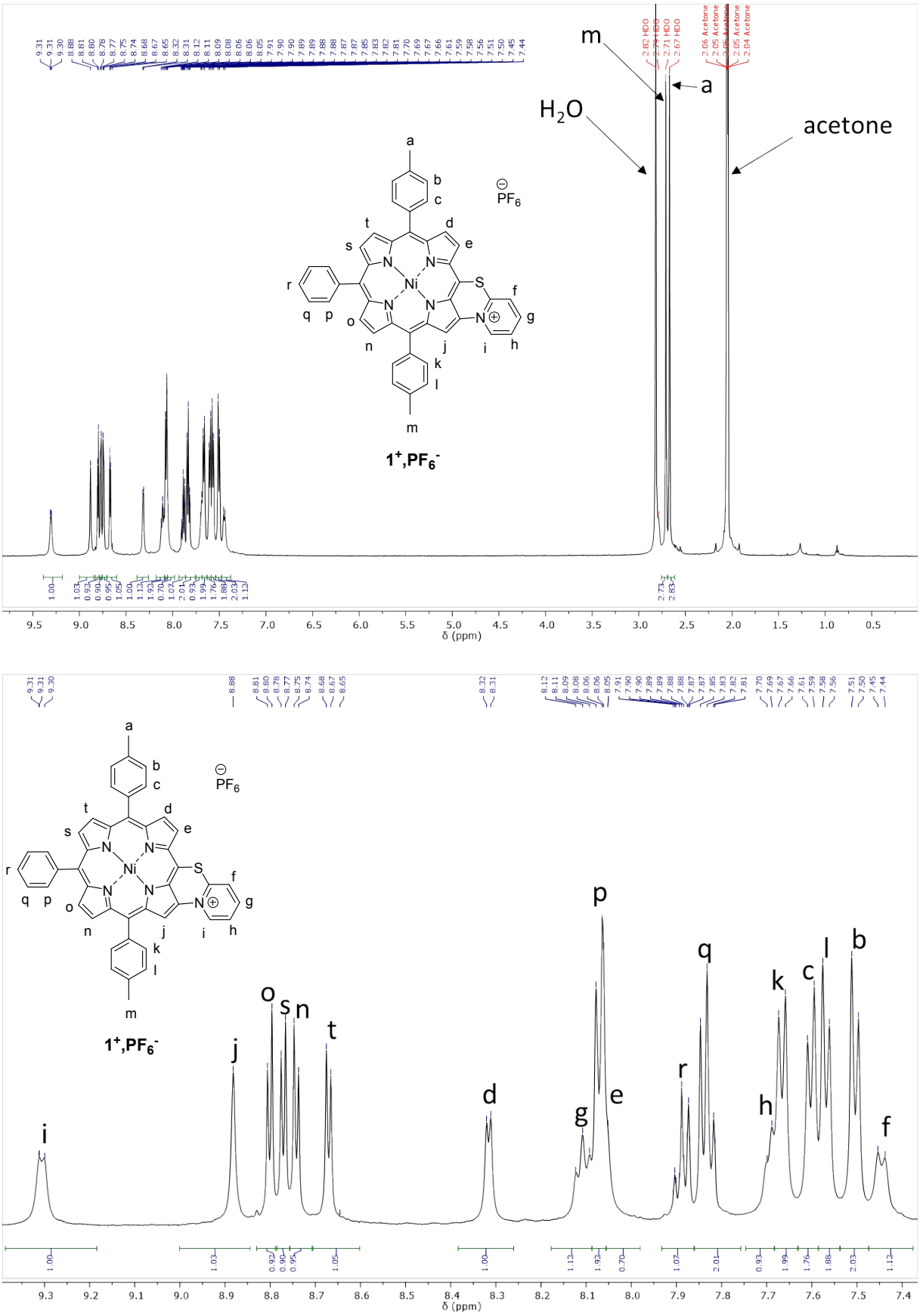

Figure S23. Full range (top) and partial (bottom) ^{1}H NMR spectra of **1**$^{+}$,**PF**$_{6}^{-}$ in CD_3COCD_3, 500 MHz, 298 K.

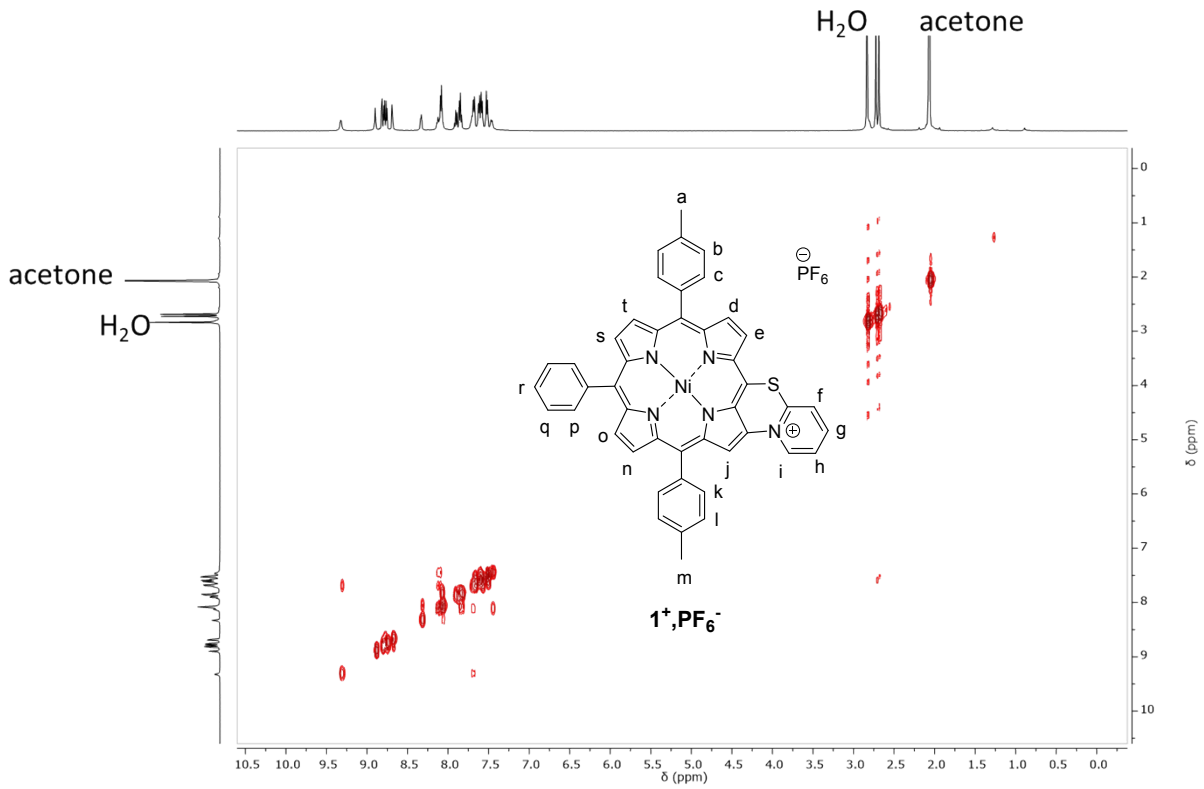

Figure S24. Full range ^{1}H-^{1}H COSY NMR spectrum of **1**$^{+}$**,PF**$_{6}^{-}$ in CD_3COCD_3, 500 MHz, 298 K.

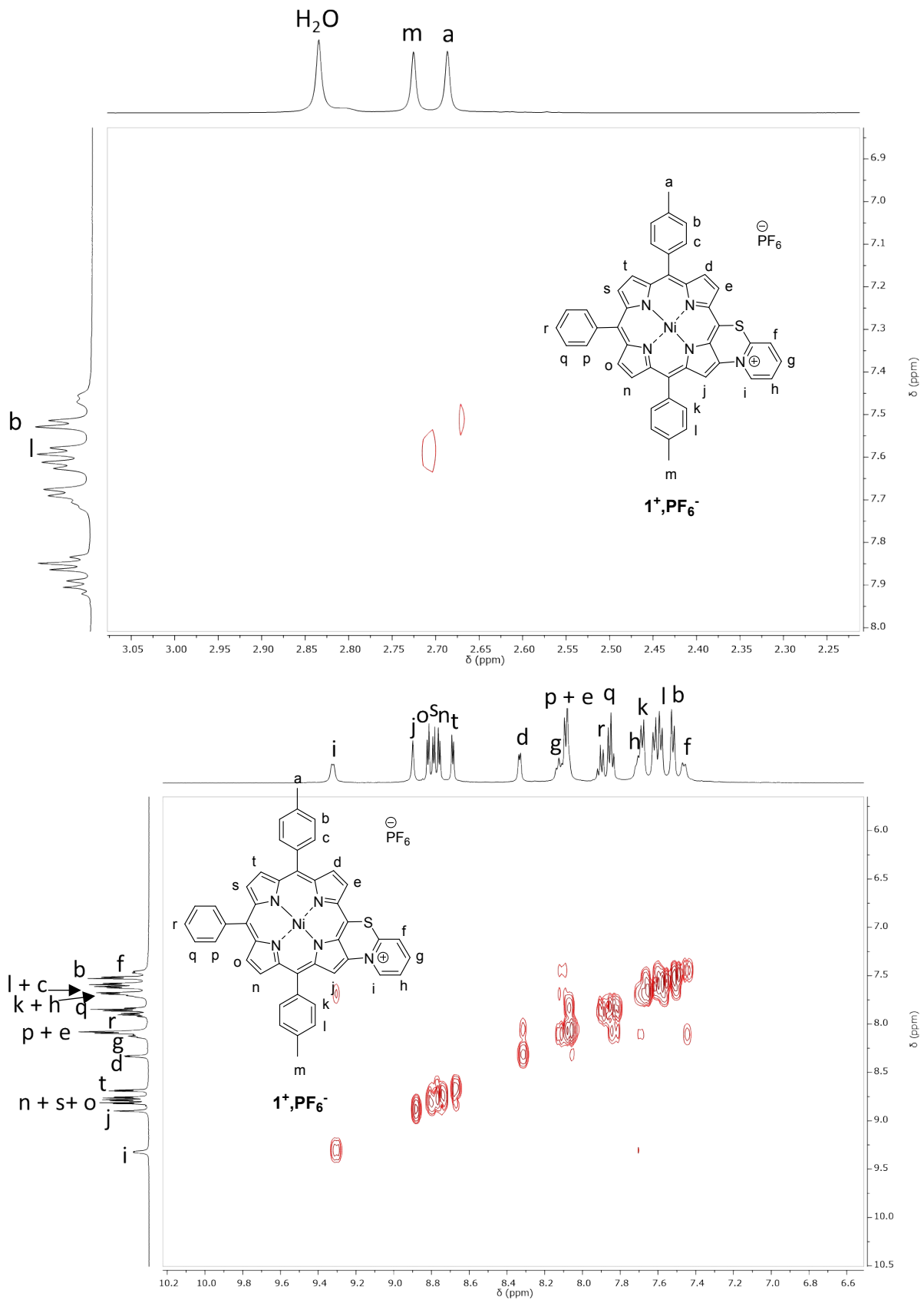

Figure S25. Partial ^{1}H-^{1}H COSY NMR spectra of **1**$^{+}$,**PF**$_{6}^{-}$ in CD_3COCD_3, 500 MHz, 298 K.

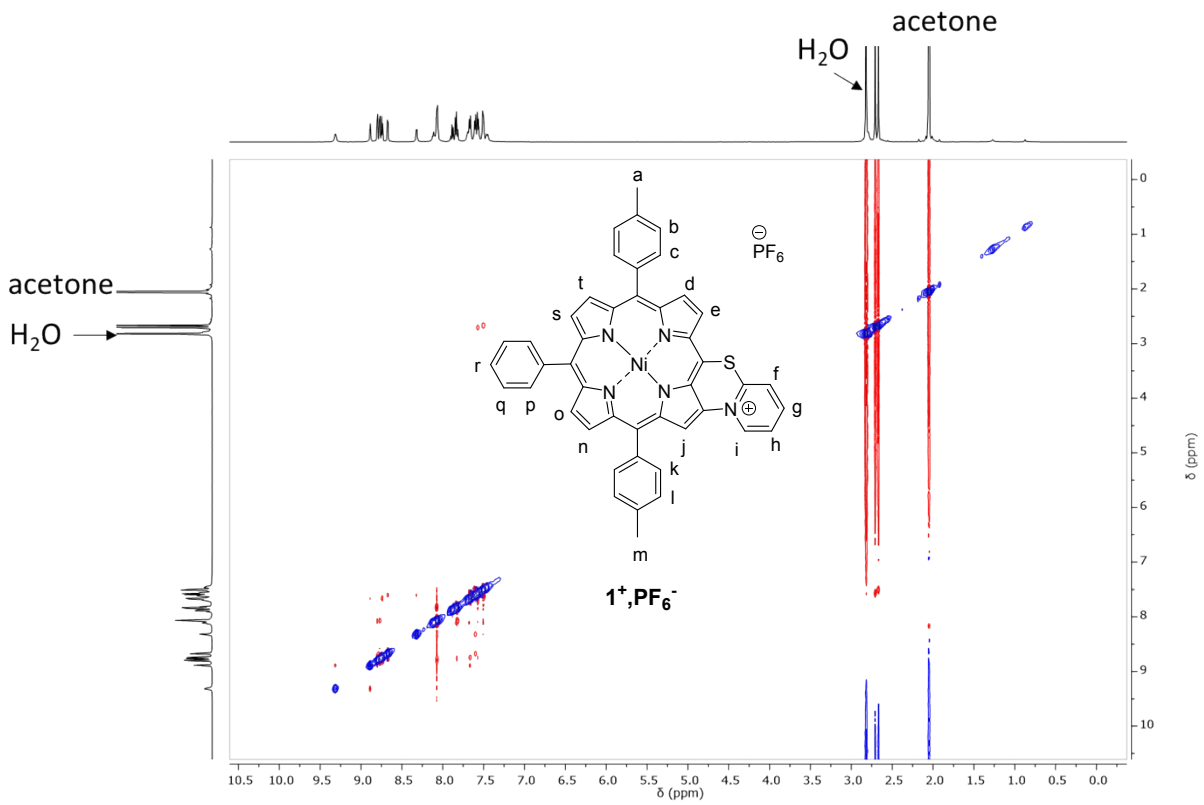

Figure S26. Full range ^{1}H-^{1}H ROESY NMR spectra of **1**$^{+}$,**PF**$_{6}^{-}$ in CD_3COCD_3, 500 MHz, 298 K.

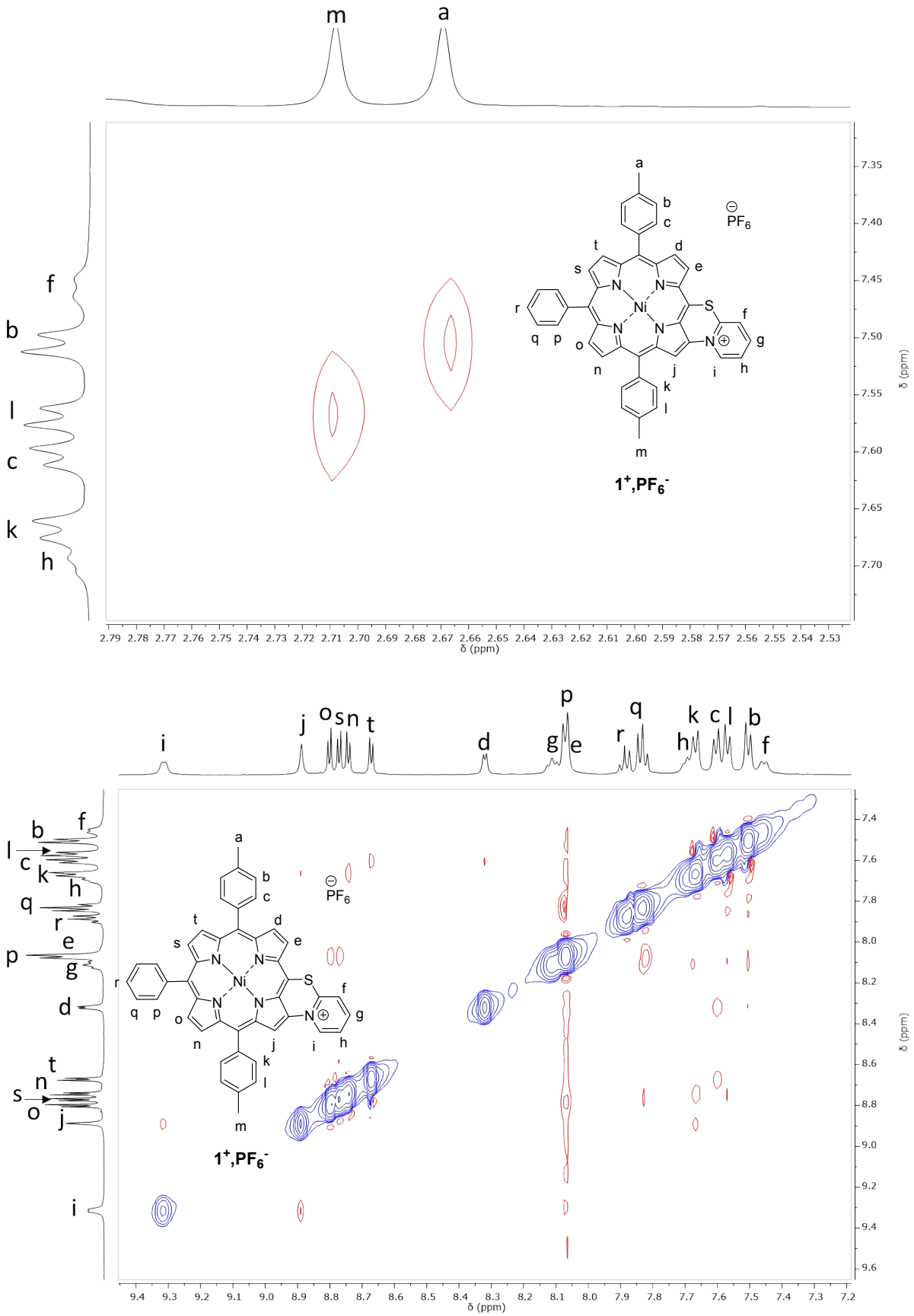

Figure S27. Partial ^{1}H-^{1}H ROESY NMR spectra of **1**$^{+}$,**PF**$_{6}^{-}$ in CD_3COCD_3, 500 MHz, 298 K.

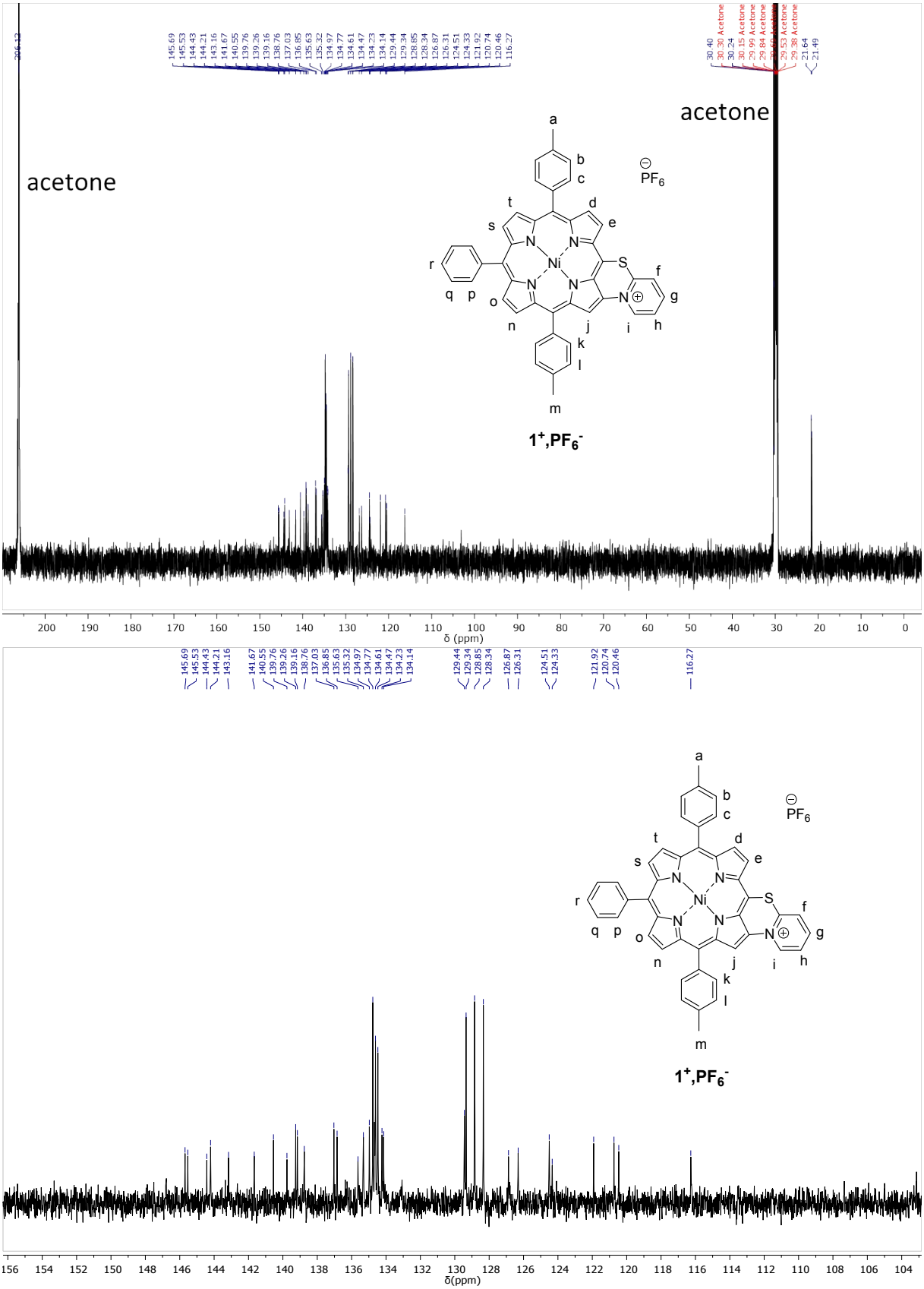

Figure S28. Full range (top) and partial (bottom) $^{13}C\{^{1}H\}$ NMR spectra of **1**$^{+}$,**PF**$_{6}^{-}$ in CD_3COCD_3, 126 MHz, 300 K.

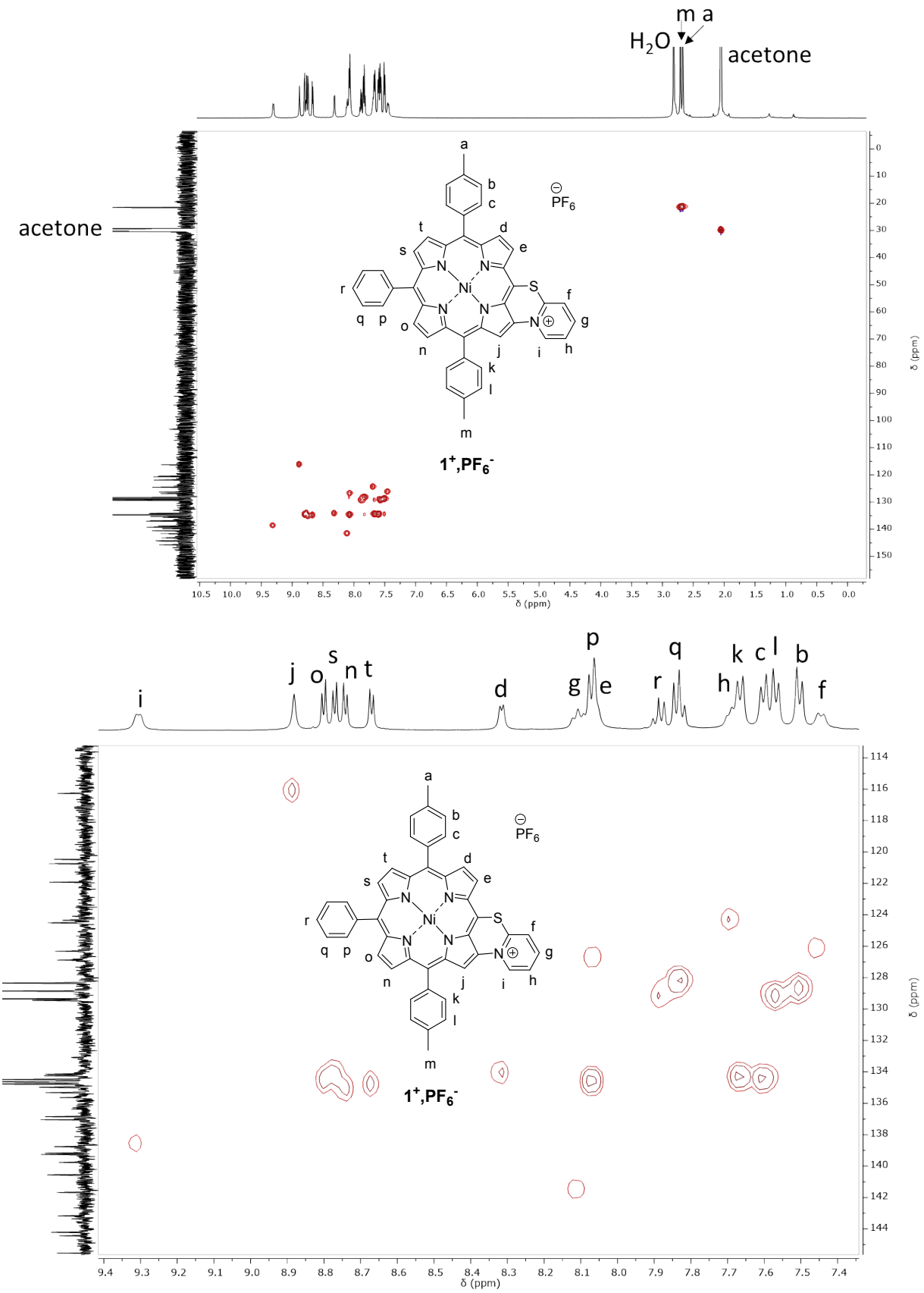

Figure S29. Full range (top) and partial (bottom) ^{1}H-^{13}C HSQC NMR spectra of **1**$^{+}$,**PF**$_{6}^{-}$ in CD_3COCD_3, 500 MHz, 298 K.

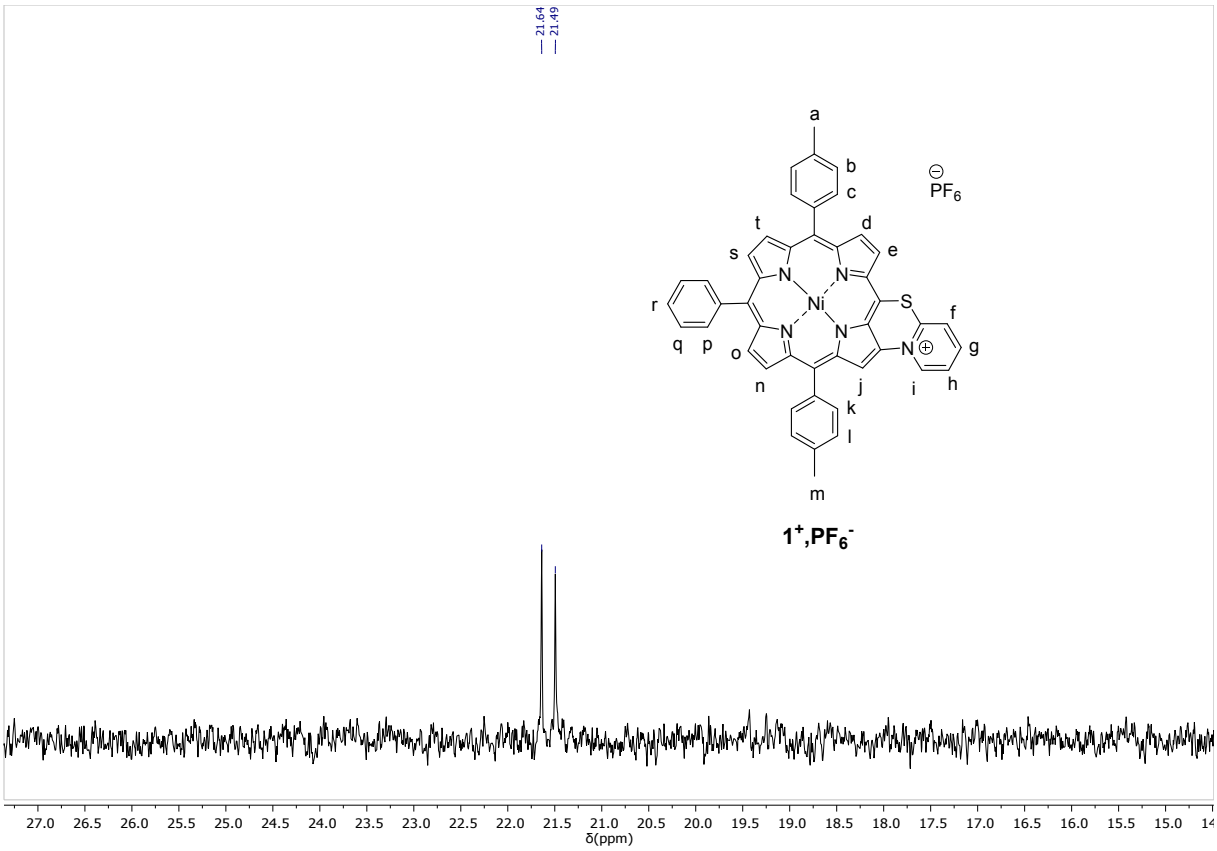

Figure S30. ^{19}F NMR spectrum of $\mathbf{1^+,PF_6^-}$ in CD_3COCD_3, 500 MHz, 300 K.

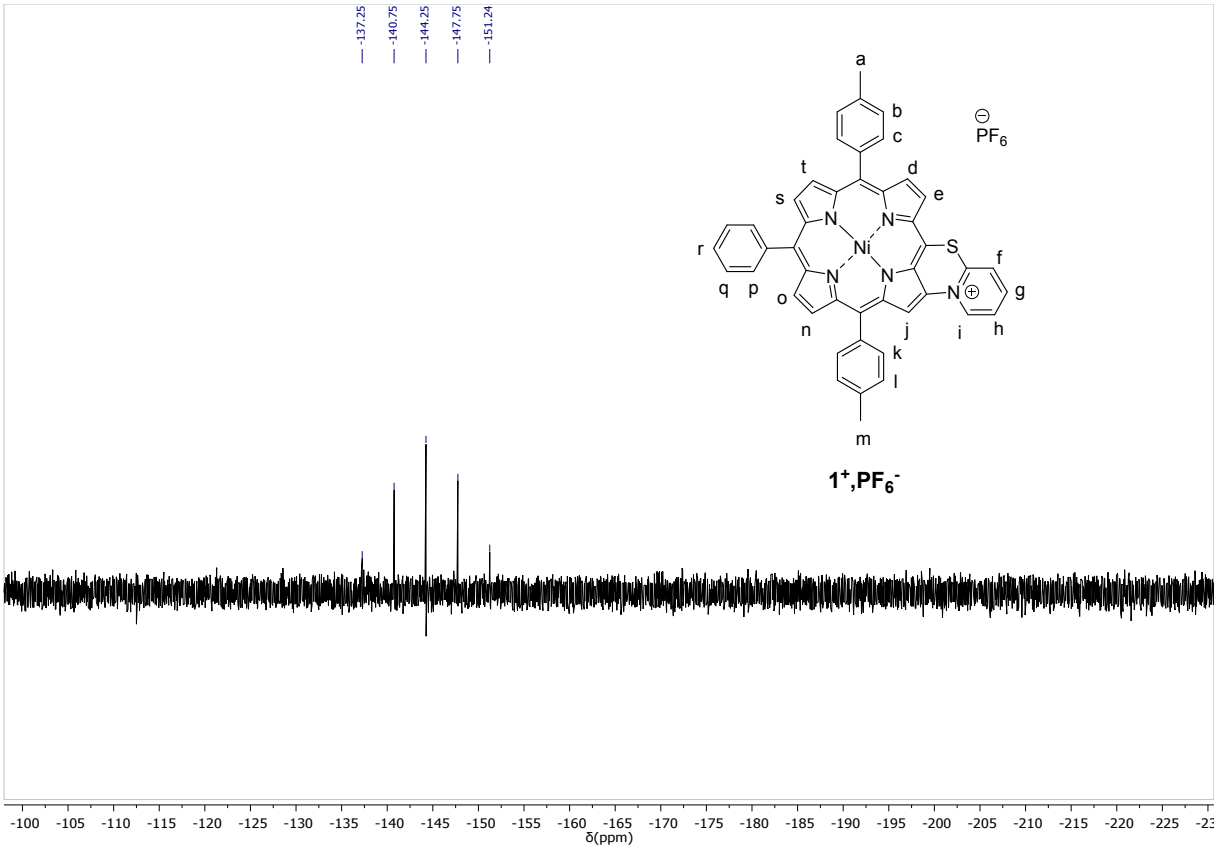

Figure S31. ^{31}P NMR spectrum of $\mathbf{1^+,PF_6^-}$ in CD_3COCD_3, 202 MHz, 298 K.

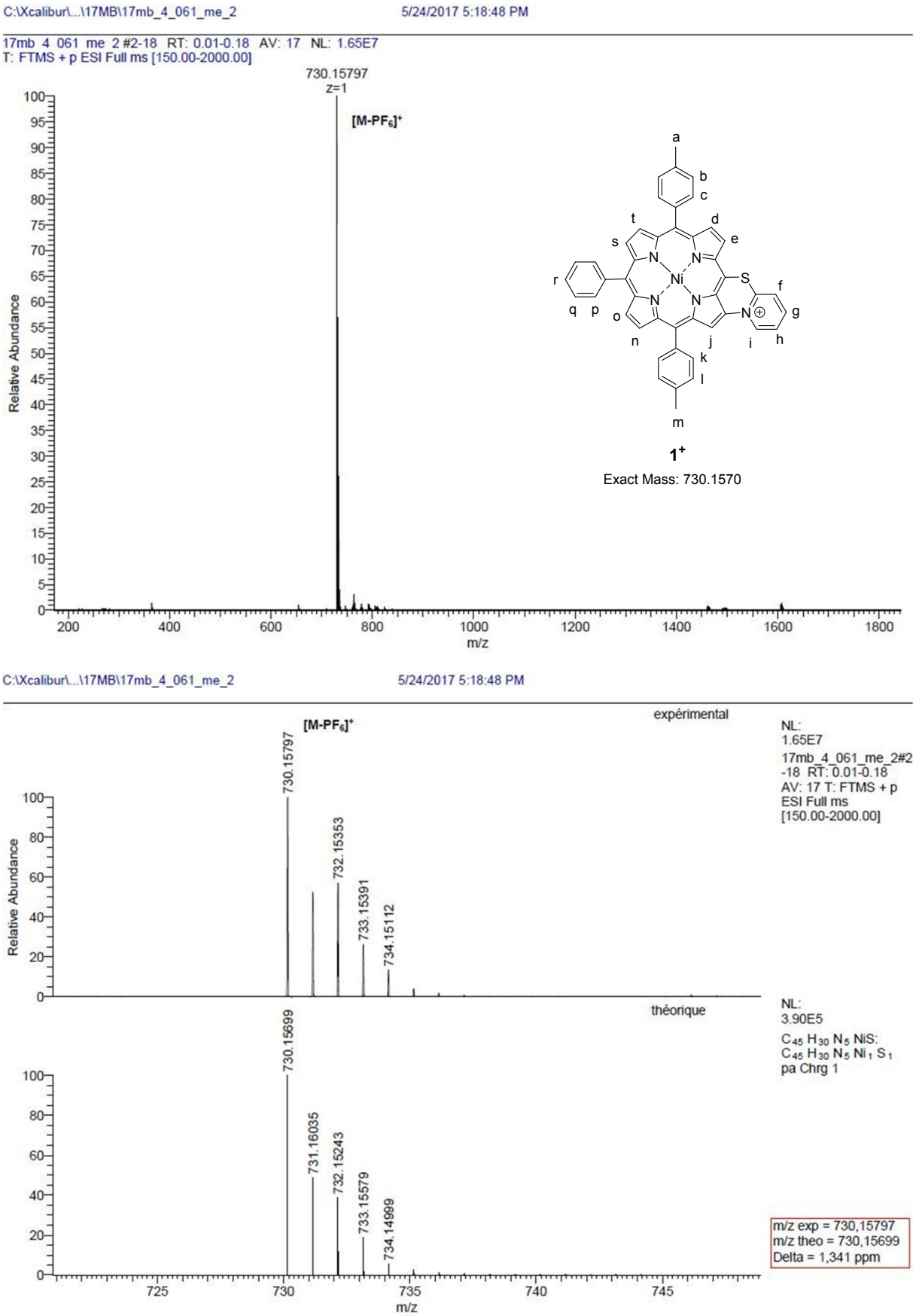

Figure S32. High resolution ESI mass spectrum of $\mathbf{1}^{+}$,$\mathbf{PF_6}^{-}$ and simulation of its isotopic pattern.

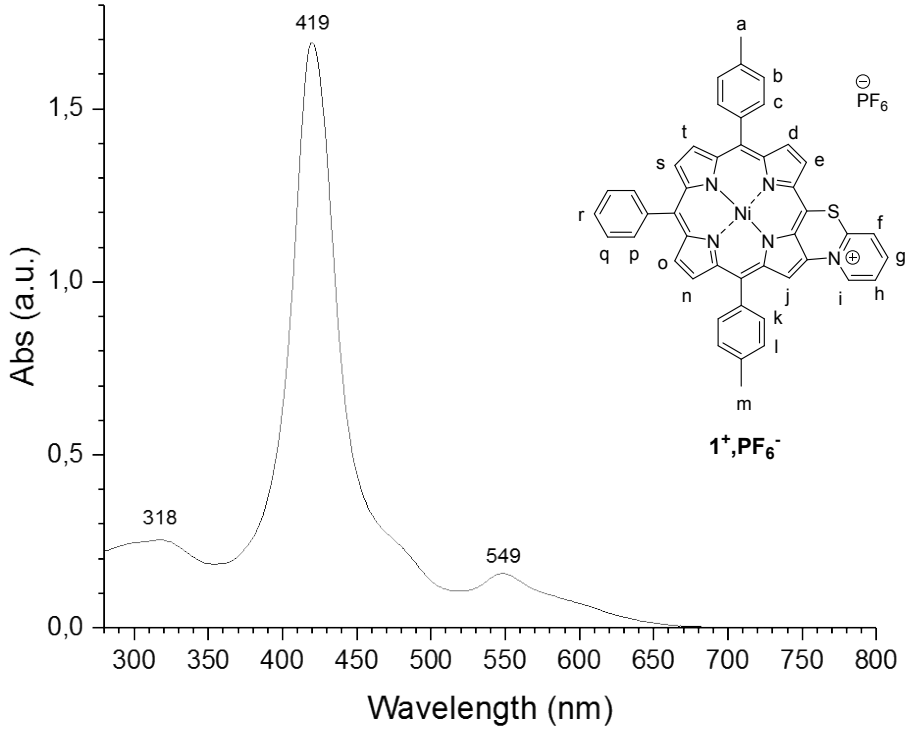

Figure S33. UV-Vis. absorption spectrum of $\mathbf{1^+,PF_6^-}$ in CH_2Cl_2.

Compound 12

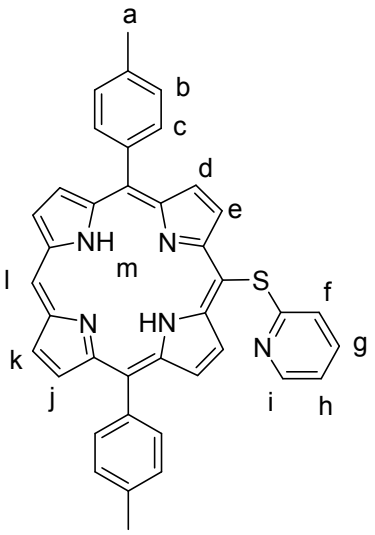

12

Chemical Formula: $C_{39}H_{29}N_5S$
Exact Mass: 599.2144
Molecular Weight: 599.7560

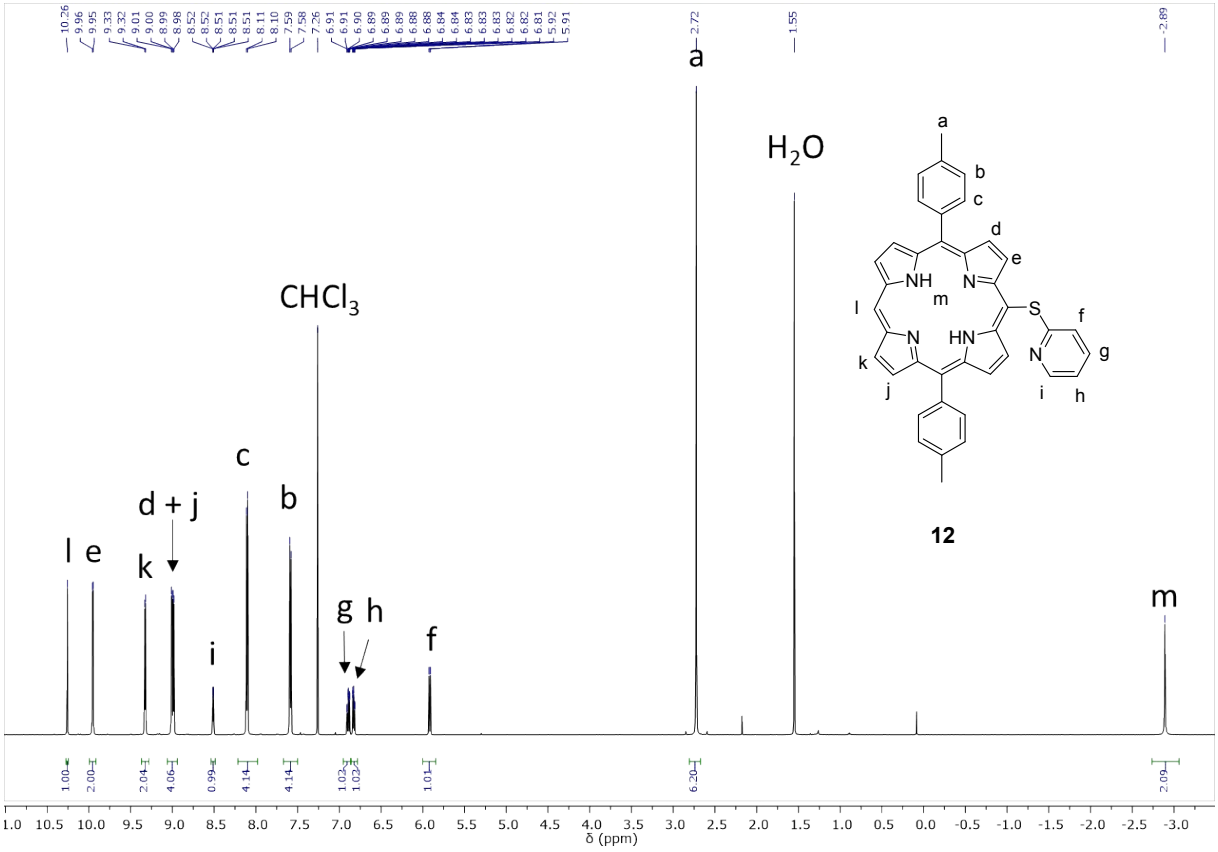

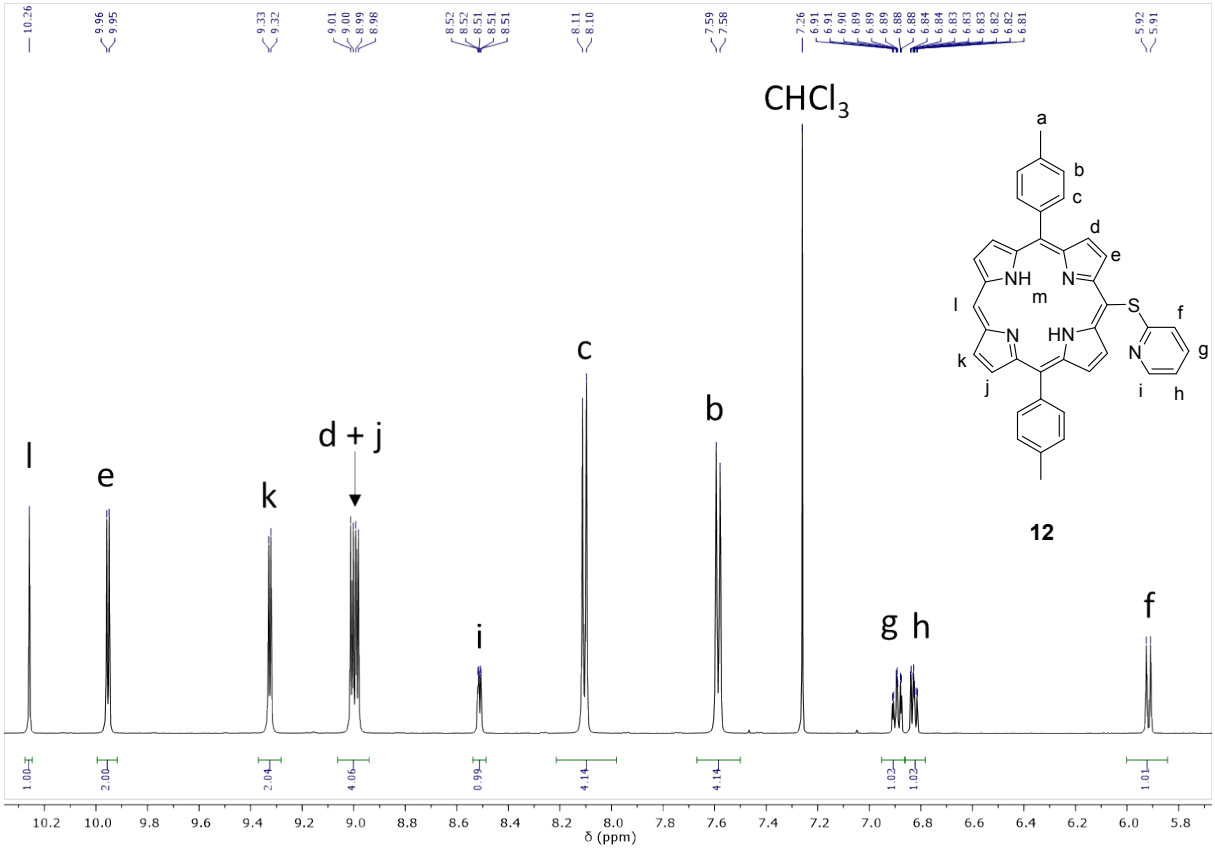

Figure S34. Full range (top) and partial ^{1}H NMR spectra of **12** in $CDCl_3$, 500 MHz, 298 K.

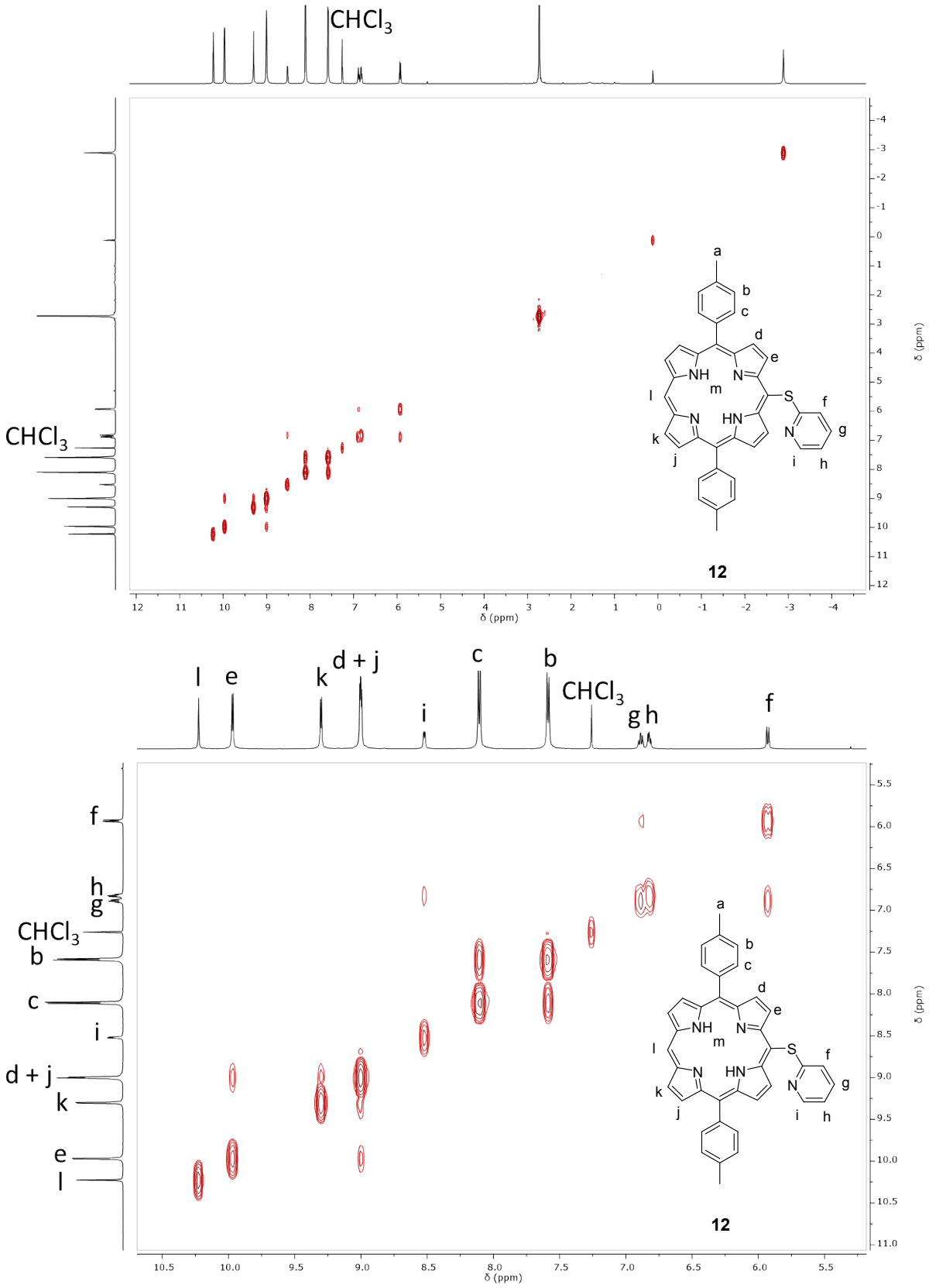

Figure S35. Full range (top) and partial (bottom) ^{1}H-^{1}H COSY NMR spectra of **12** in $CDCl_3$, 500 MHz, 298 K.

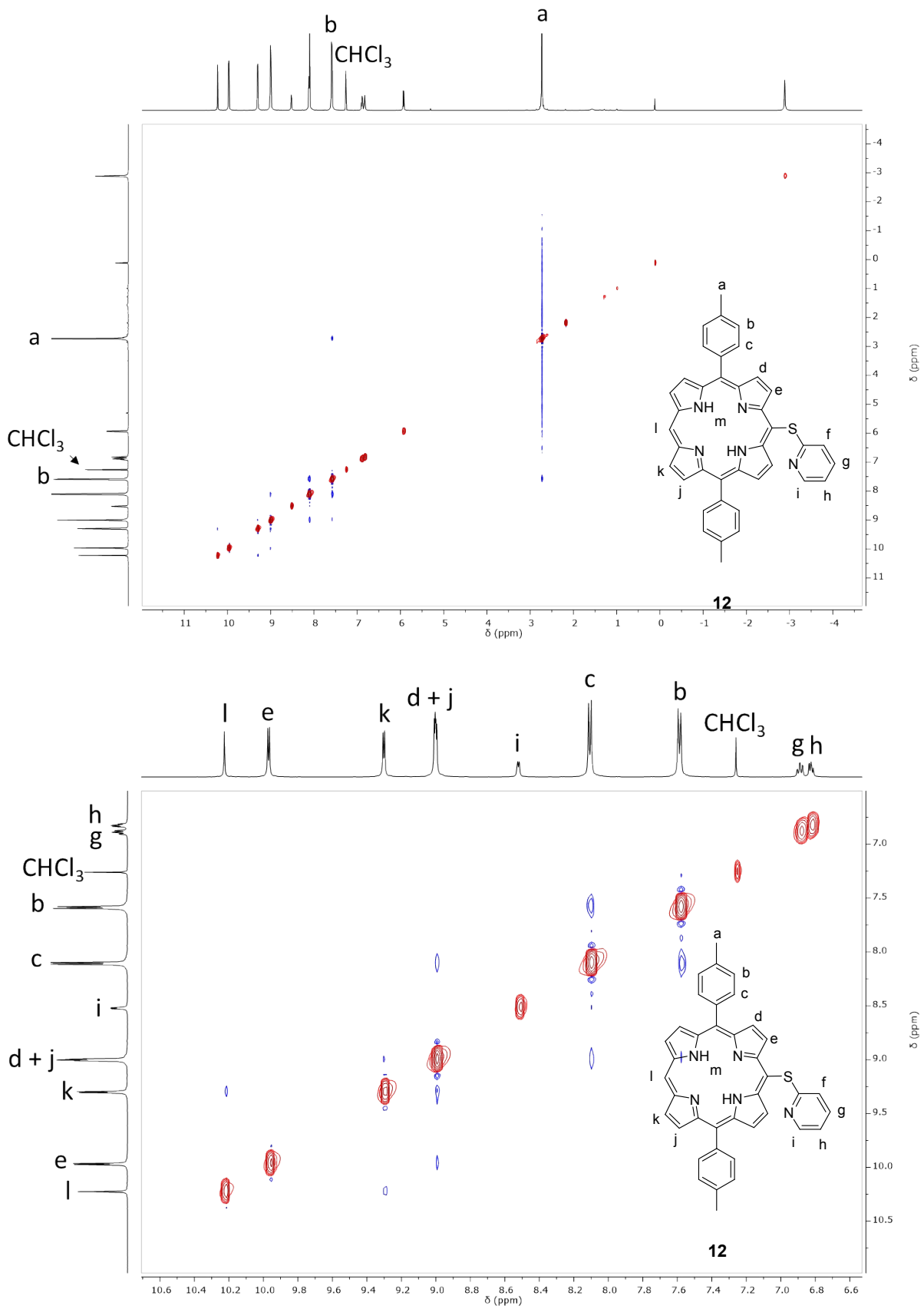

Figure S36.. Full range (top) and partial (bottom) ^{1}H-^{1}H NOESY NMR spectra of **12** in $CDCl_3$, 500 MHz, 298 K.

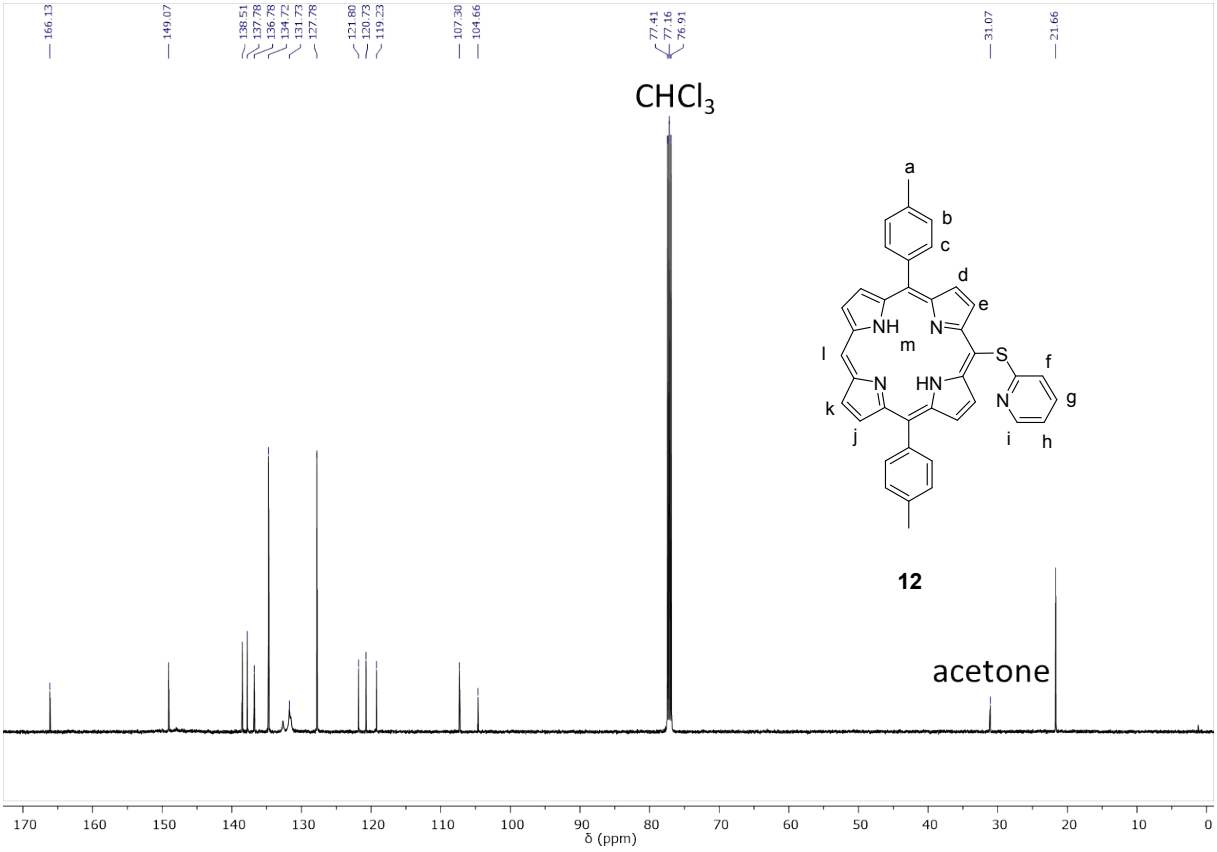

Figure S37. Full range $^{13}C\{^{1}H\}$ NMR spectrum of **12** in $CDCl_3$, 126 MHz, 300 K.

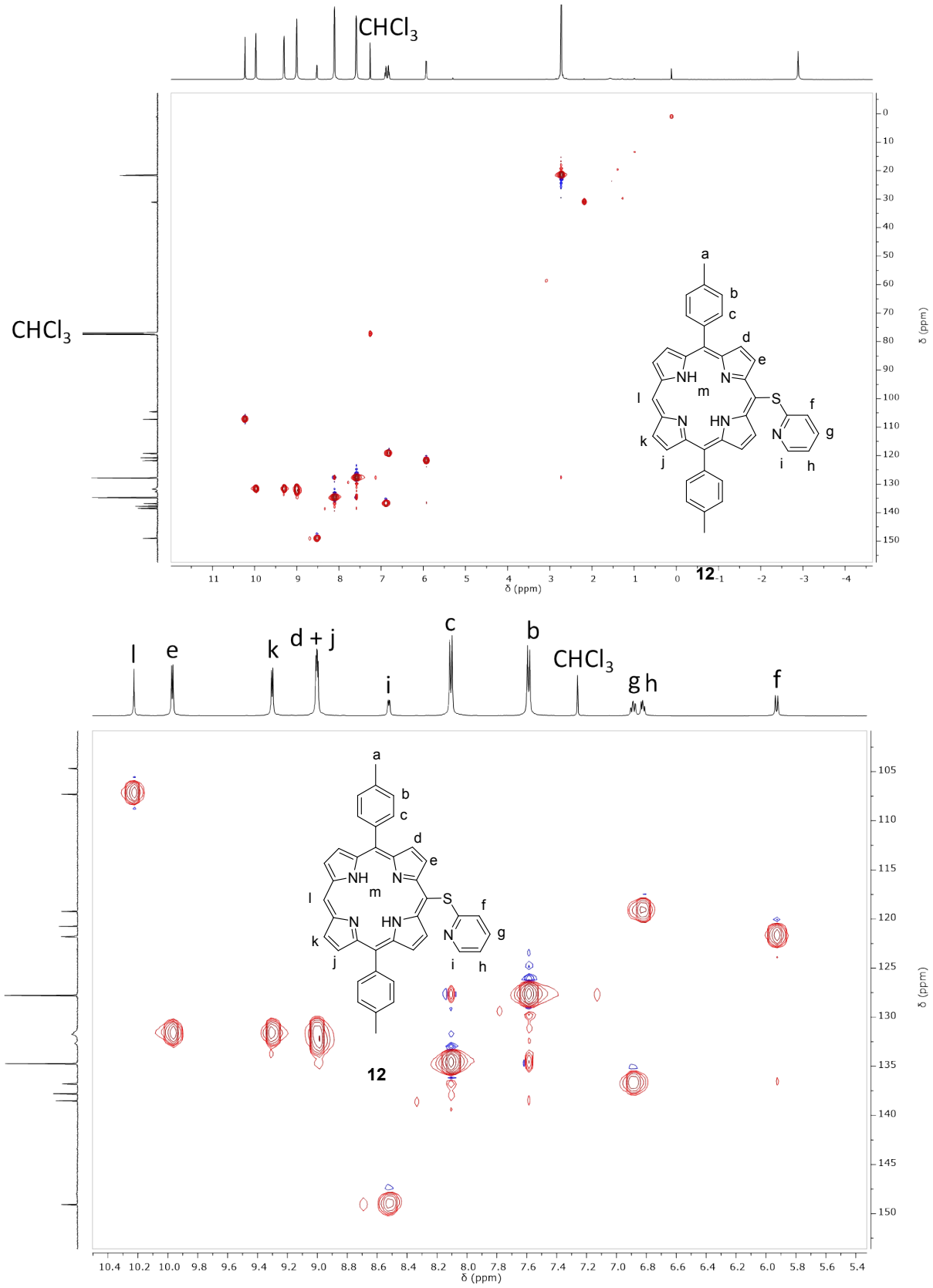

Figure S38. Full range (top) and partial (bottom) ^{1}H-^{13}C HSQC NMR spectra of **12** in $CDCl_3$, 500 MHz, 298 K.

C:\Xcalibur\...\MB\18mb_4_01_fractionD_1 1/4/2018 10:47:46 AM
dcm/meoh
18mb 4 01 fractionD 1 #1-20 RT: 0.01-0.30 AV: 20 NL: 1.33E7
T: FTMS + p ESI Full ms [100.00-2000.00]

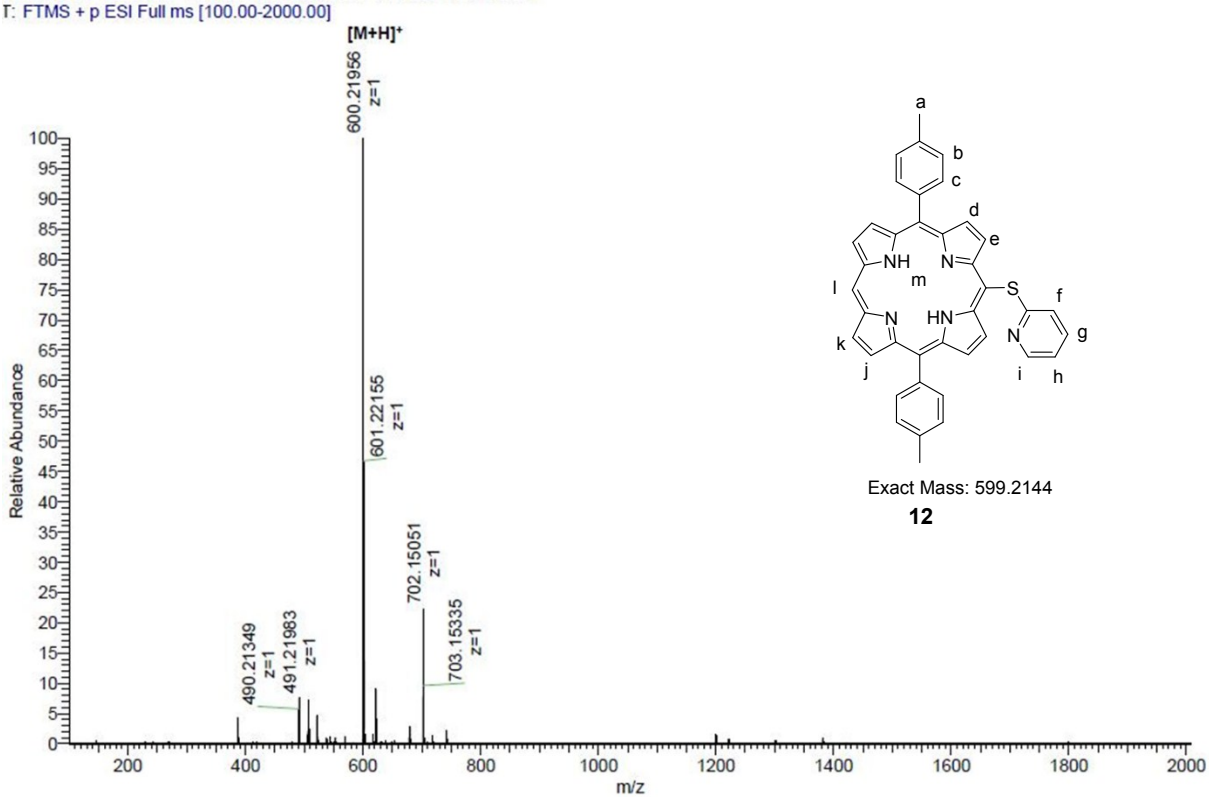

Exact Mass: 599.2144

12

C:\Xcalibur\...\MB\18mb_4_01_fractionD_1 1/4/2018 10:47:46 AM
dcm/meoh
18mb 4 01 fractionD 1 #1-20 RT: 0.01-0.30 AV: 20 NL: 1.33E7
T: FTMS + p ESI Full ms [100.00-2000.00]

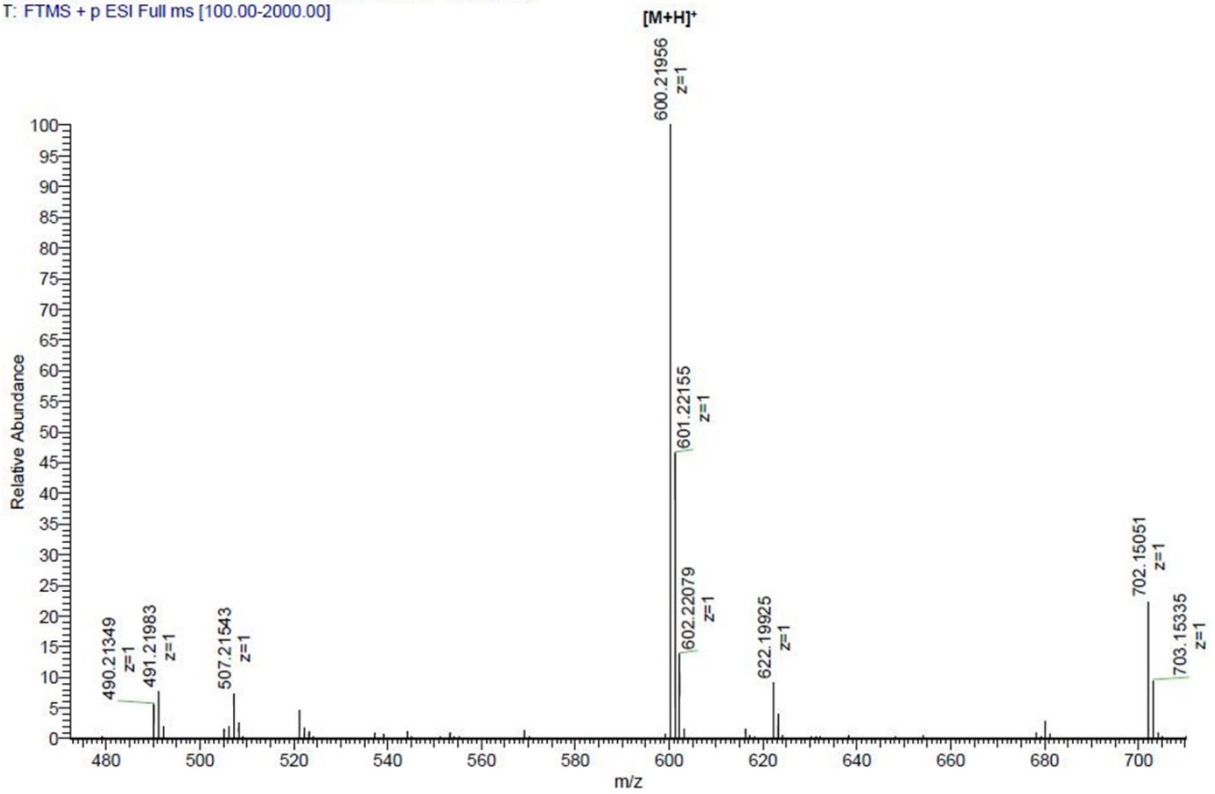

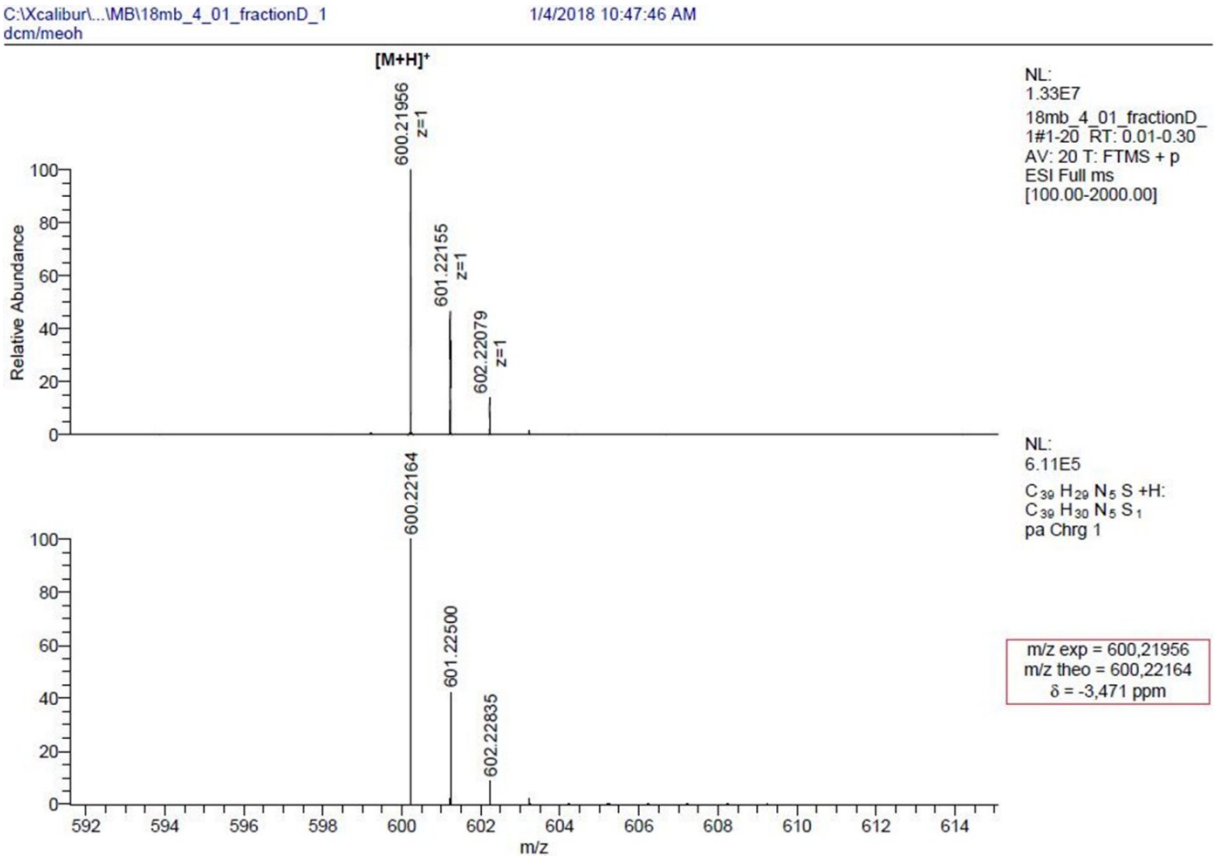

Figure S39.. High resolution ESI mass spectra of **12** and simulation of its isotopic pattern.

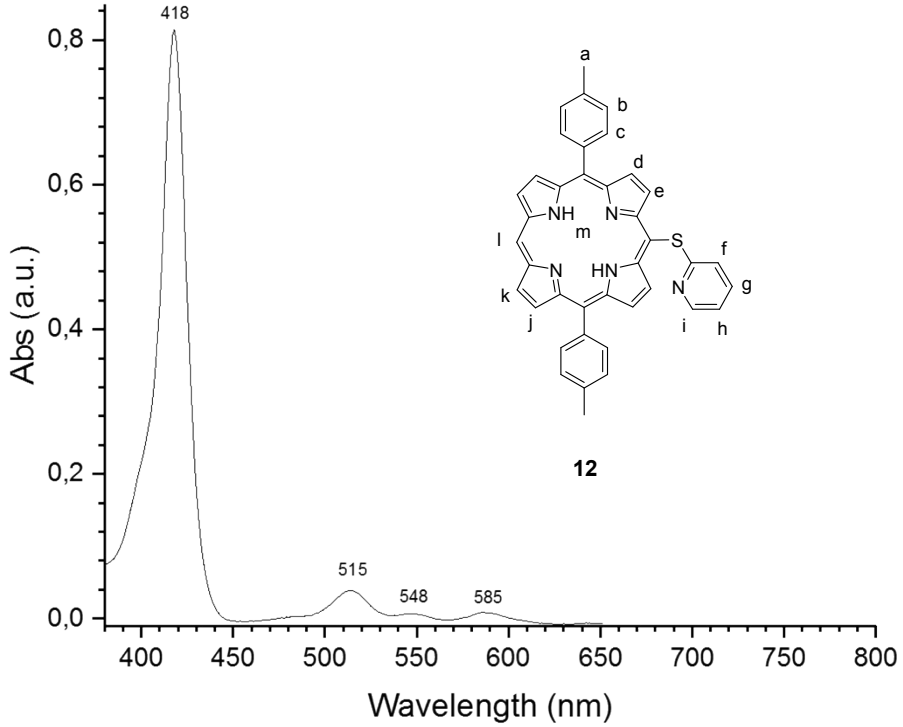

Figure S40. UV-Vis. absorption spectrum of **12** in CH_2Cl_2.

Compound 2

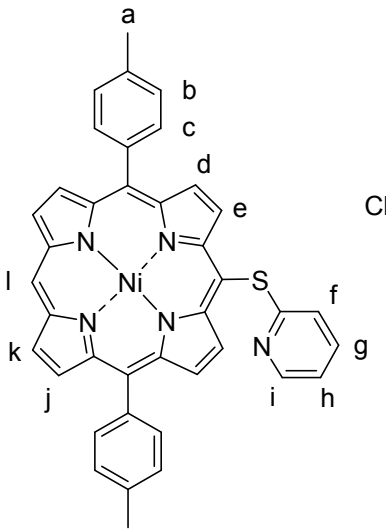

2

Chemical Formula: $C_{39}H_{27}N_5NiS$
Exact Mass: 655.1341
Molecular Weight: 656.4334

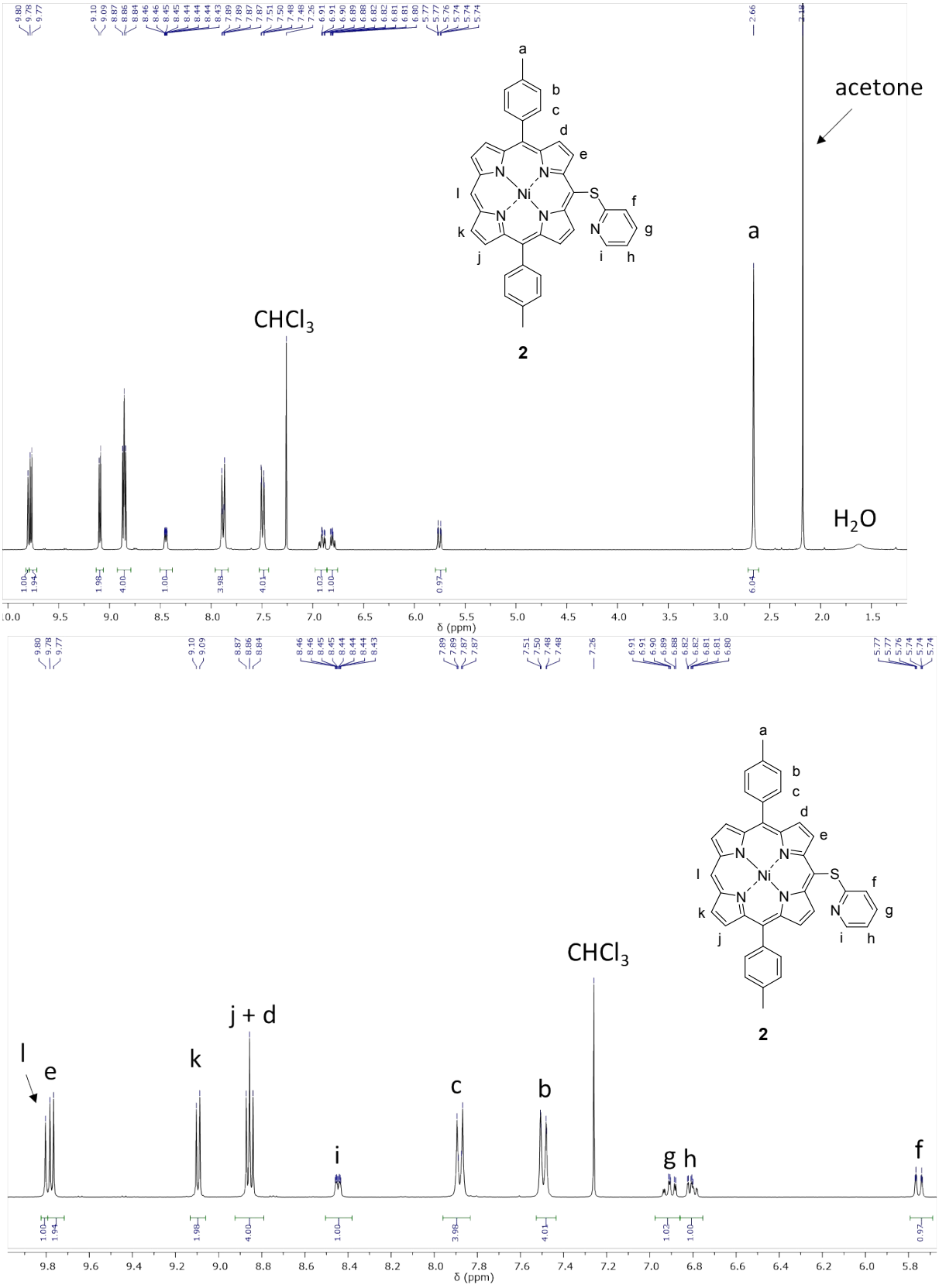

Figure S41. Full range (top) and partial (bottom) ^{1}H NMR spectra of **2** in $CDCl_3$, 300 MHz, 295 K.

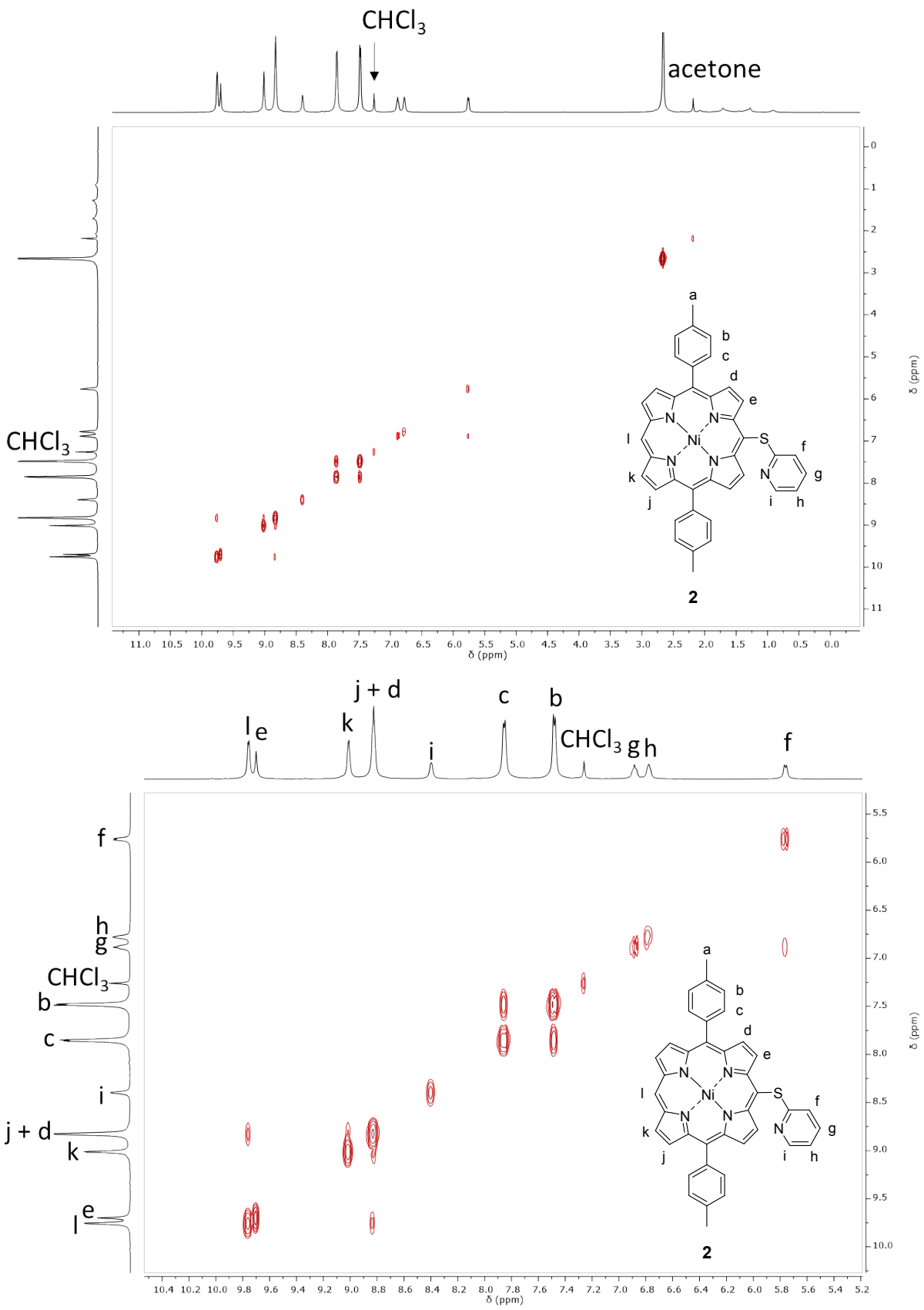

Figure S42. Full range (top) and partial (bottom) ^{1}H-^{1}H COSY NMR spectra of **2** in $CDCl_3$, 500 MHz, 298 K.

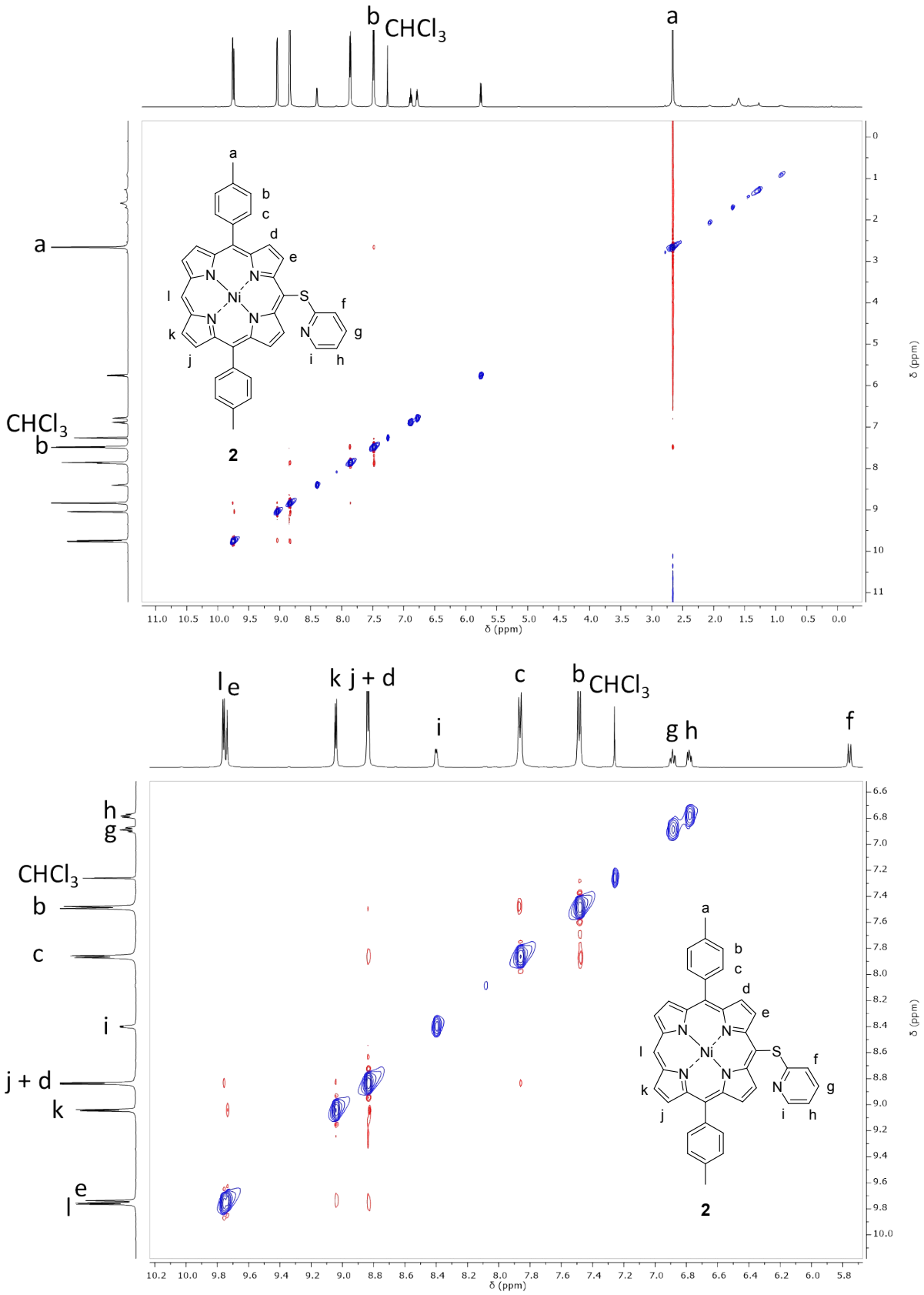

Figure S43. Full range (top) and partial (bottom) ^{1}H-^{1}H NOESY NMR spectra of **2** in $CDCl_3$, 500 MHz, 298 K.

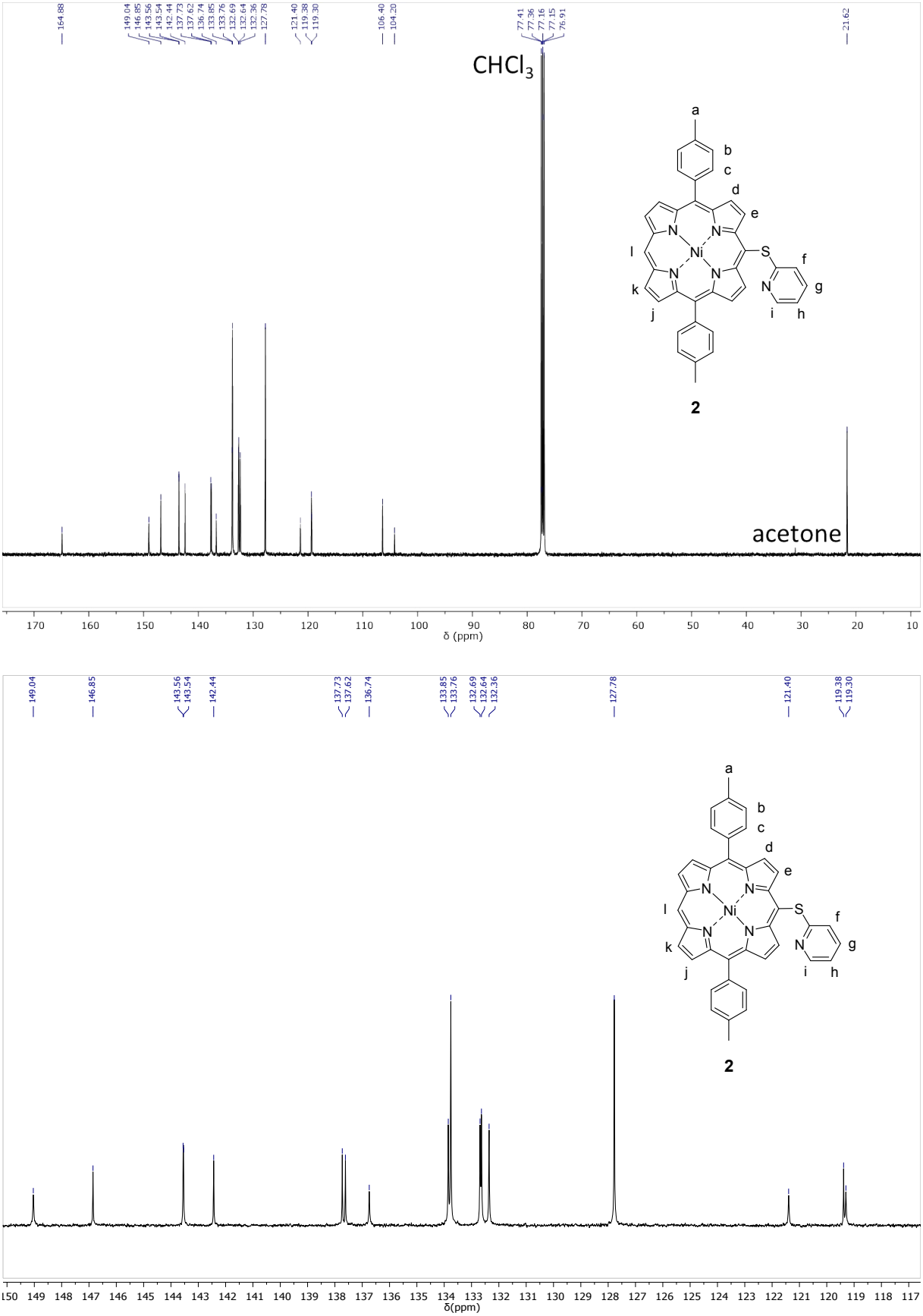

Figure S44. Full range (top) and partial (bottom) $^{13}C\{^{1}H\}$ NMR spectra of **2** in $CDCl_3$, 126 MHz, 298 K.

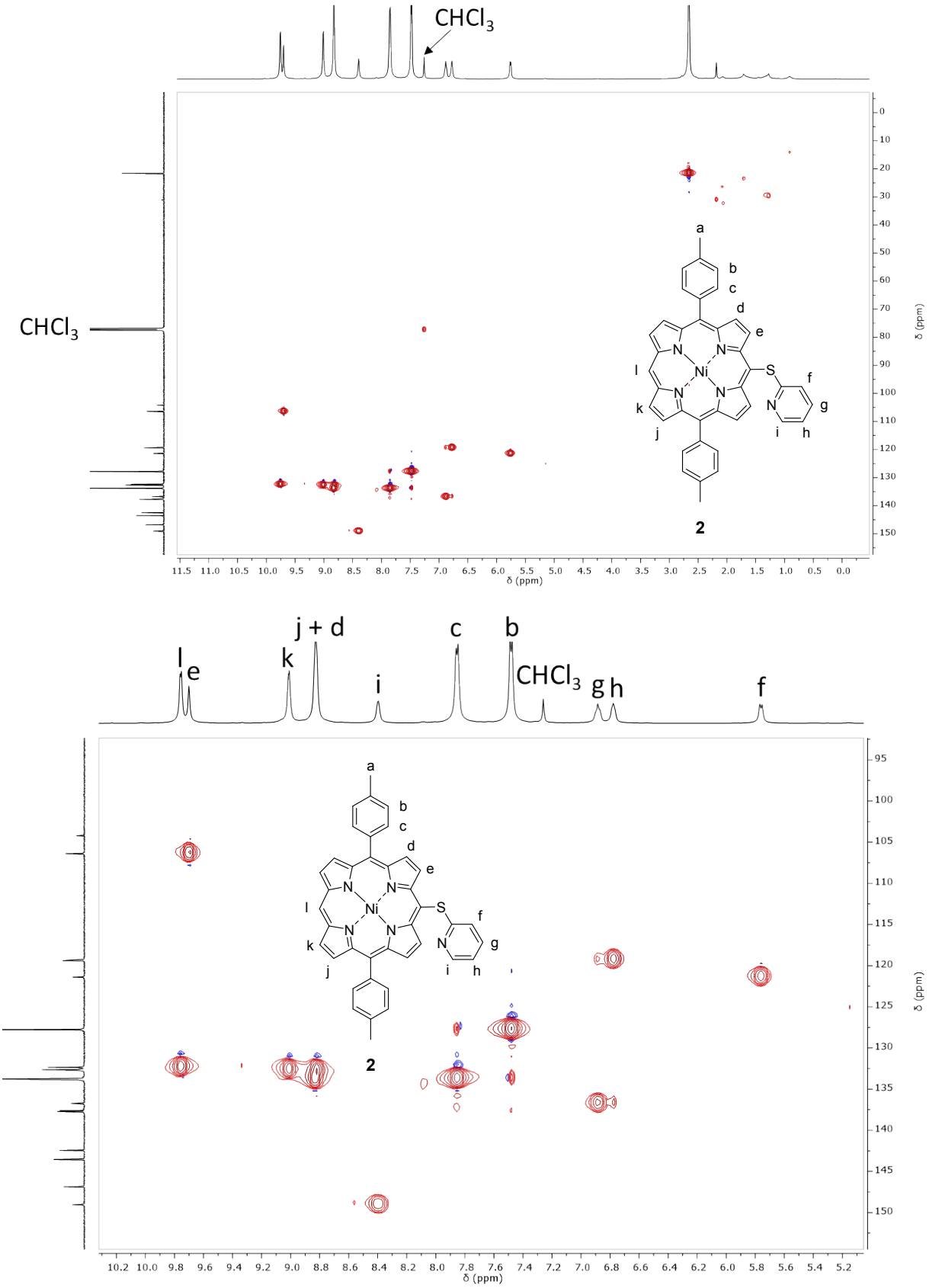

Figure S45. Full range ^{1}H-^{13}C HSQC NMR spectrum of **2** in $CDCl_3$, 500 MHz, 298 K.

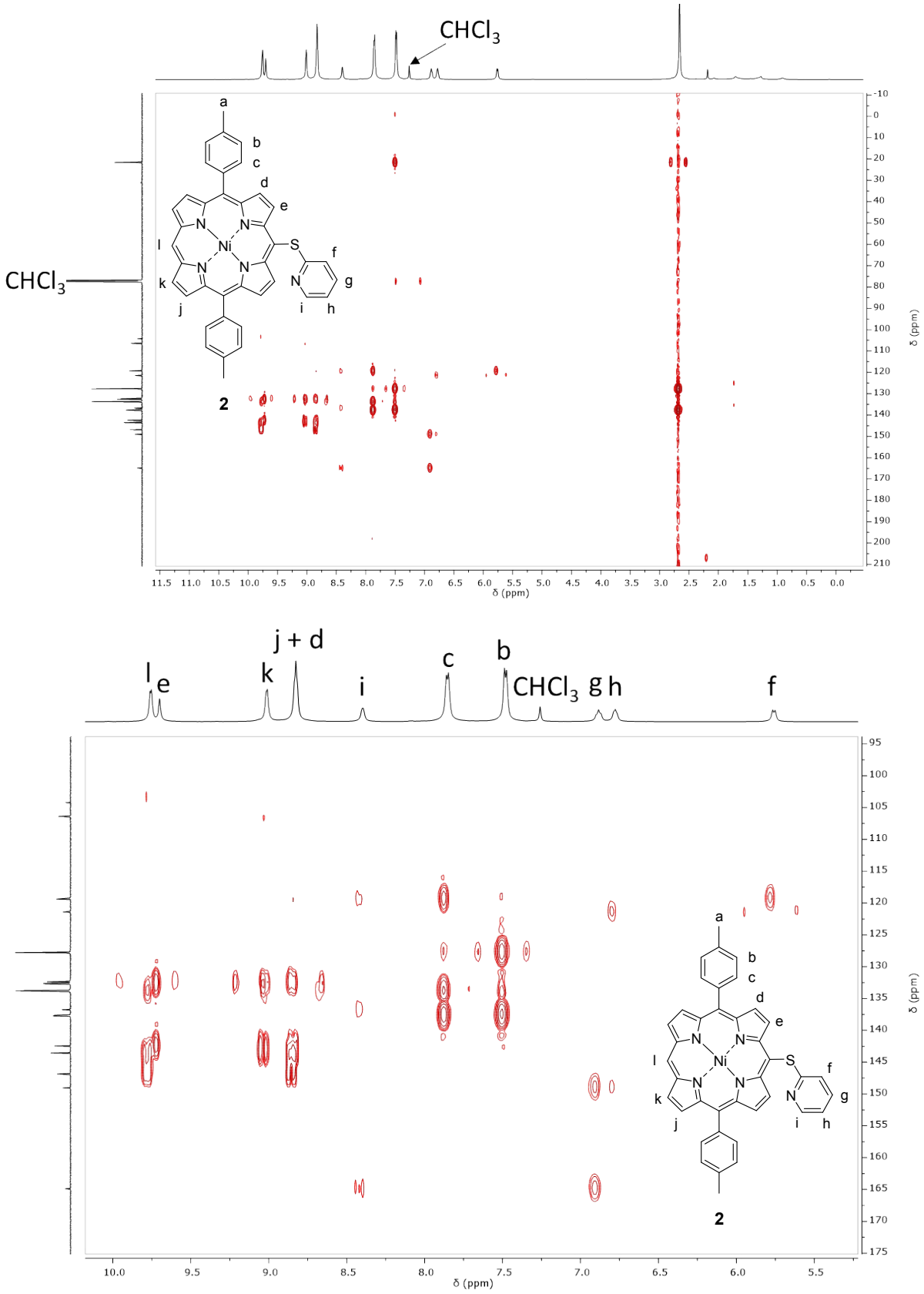

Figure S46. Full range ^{1}H-^{13}C HMBC NMR spectrum of **2** in $CDCl_3$, 500 MHz, 298 K.

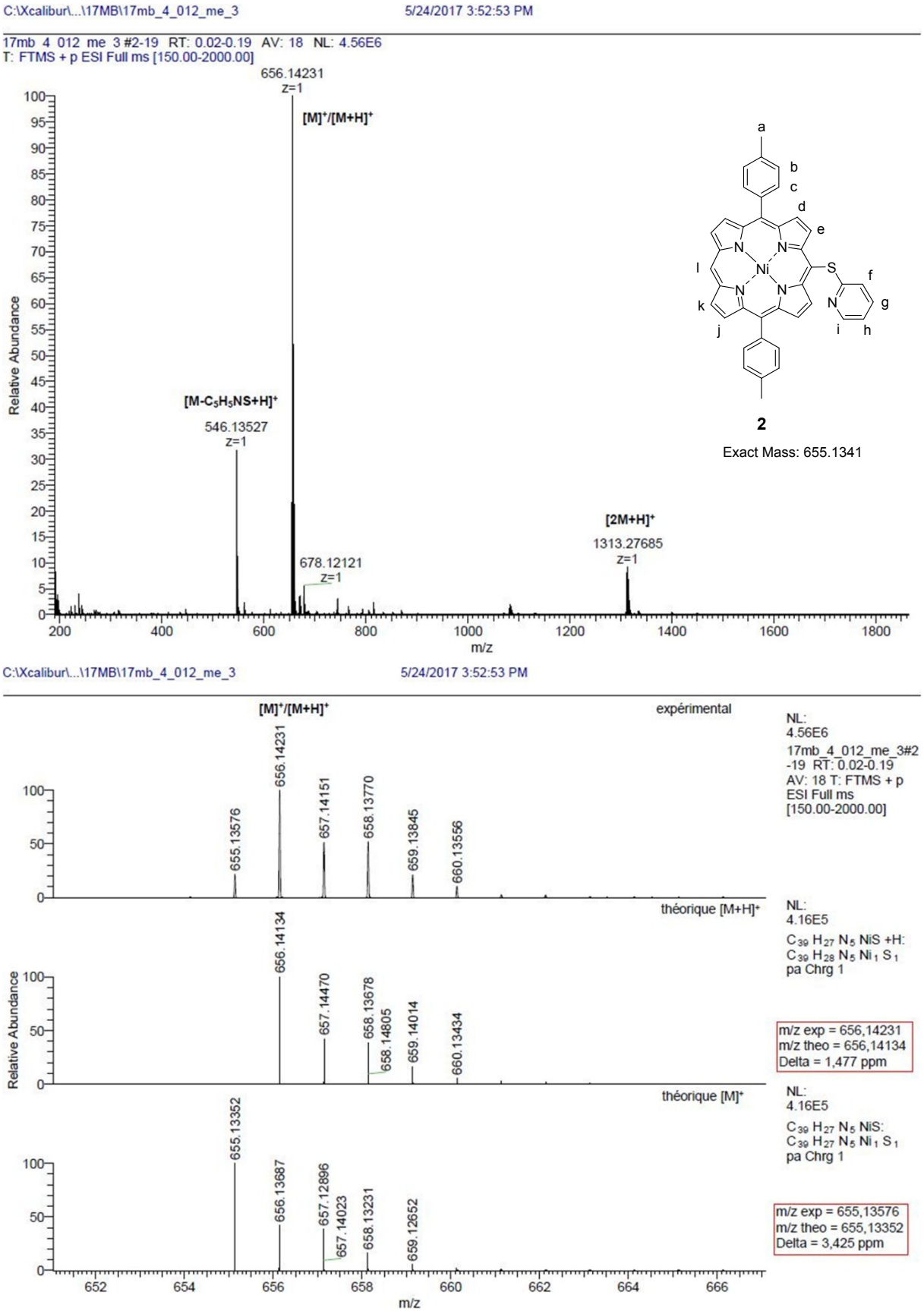

Figure S47. High resolution ESI mass spectrum of **2** and simulation of its isotopic pattern.

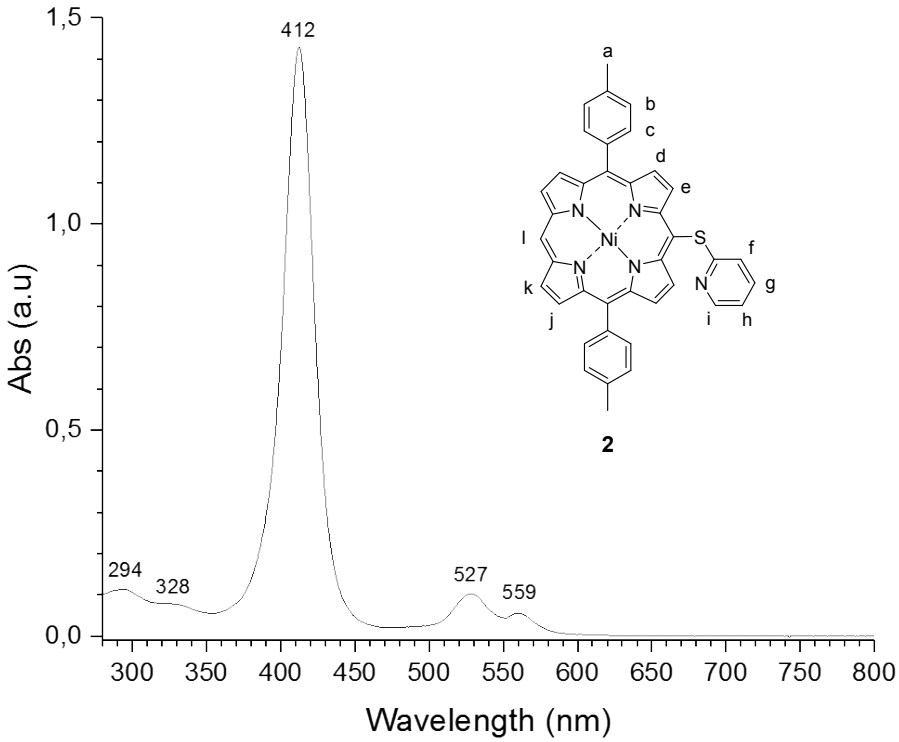

Figure S48. UV-Vis. absorption spectrum of **2** in CH_2Cl_2.

Compound 2^{+},PF_6^{-}

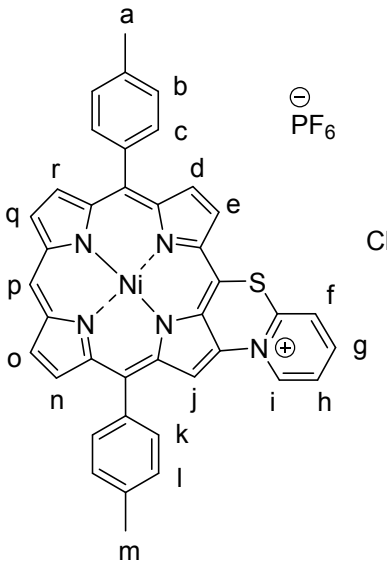

2^{+},PF_6^{-}

Chemical Formula: $C_{39}H_{26}F_6N_5NiPS$
Molecular Weight: 800.3896

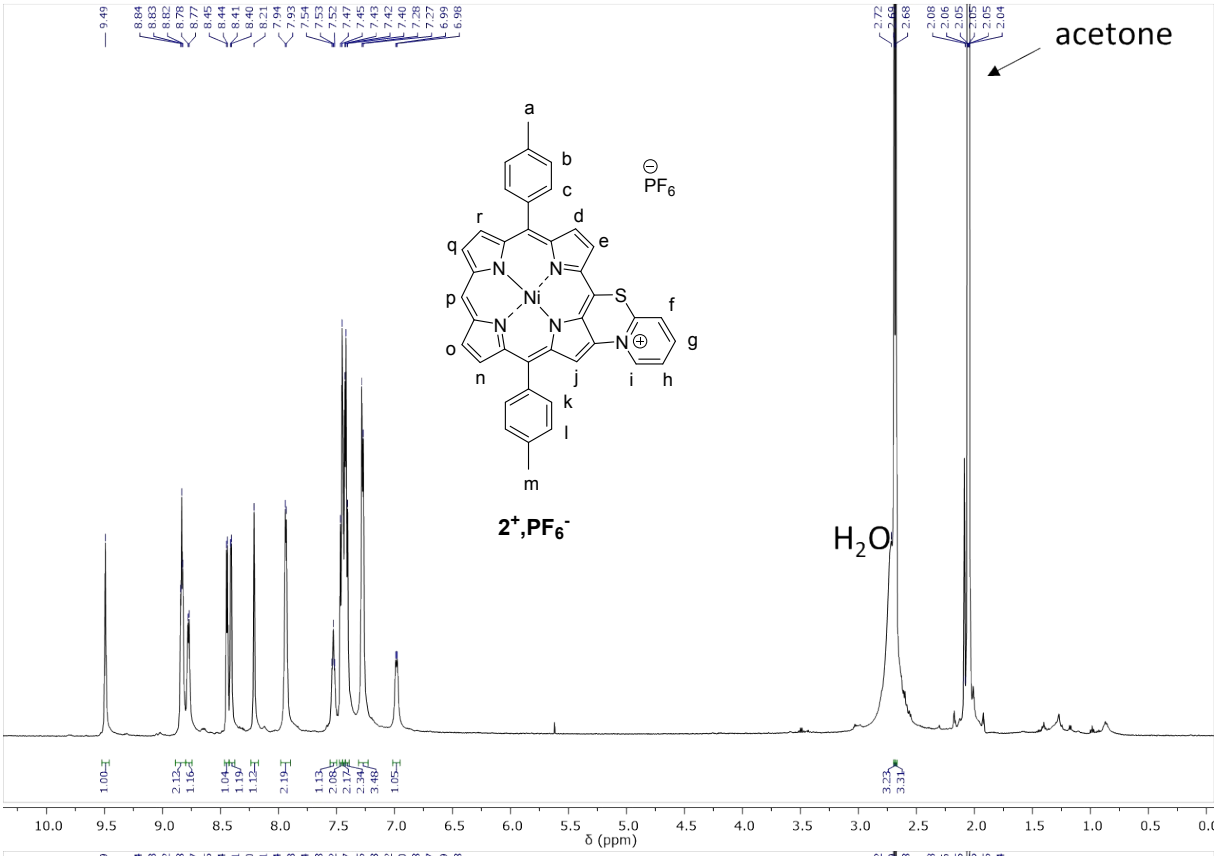

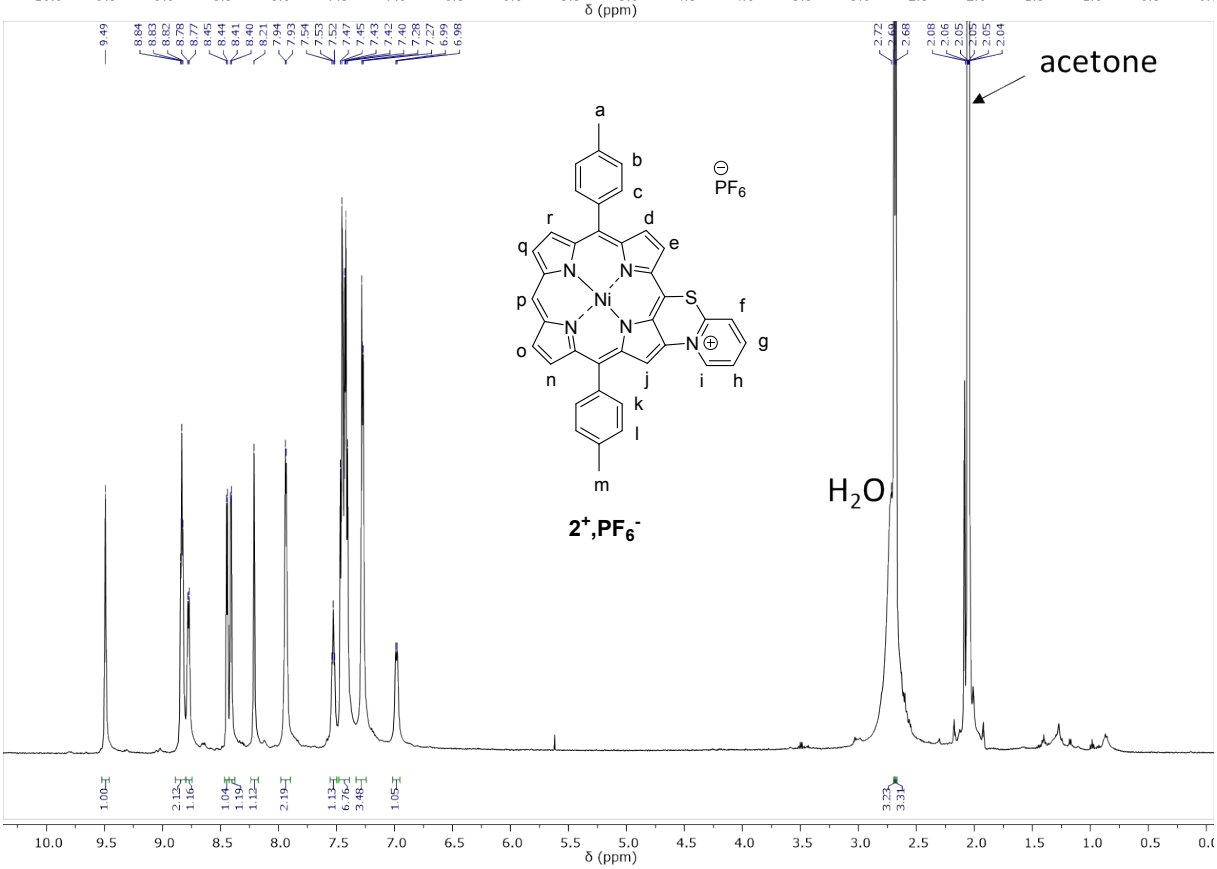

Figure S49. Full range ^{1}H NMR spectra of **2$^+$,PF$_6^-$** in CD_3COCD_3, 500 MHz, 298 K.

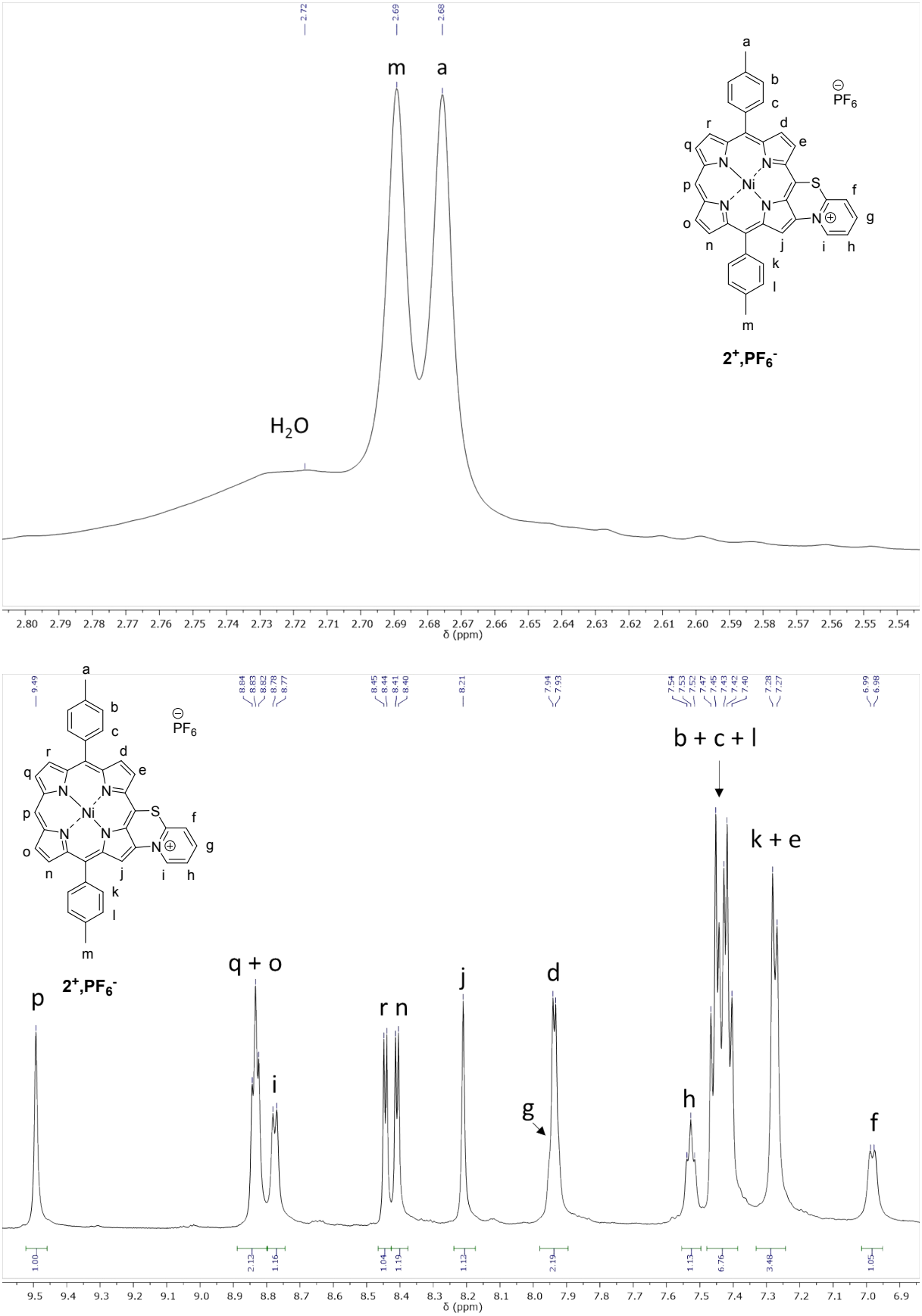

Figure S50. Partial ^{1}H NMR spectra of **2$^+$,PF$_6^-$** in CD_3COCD_3, 500 MHz, 298 K.

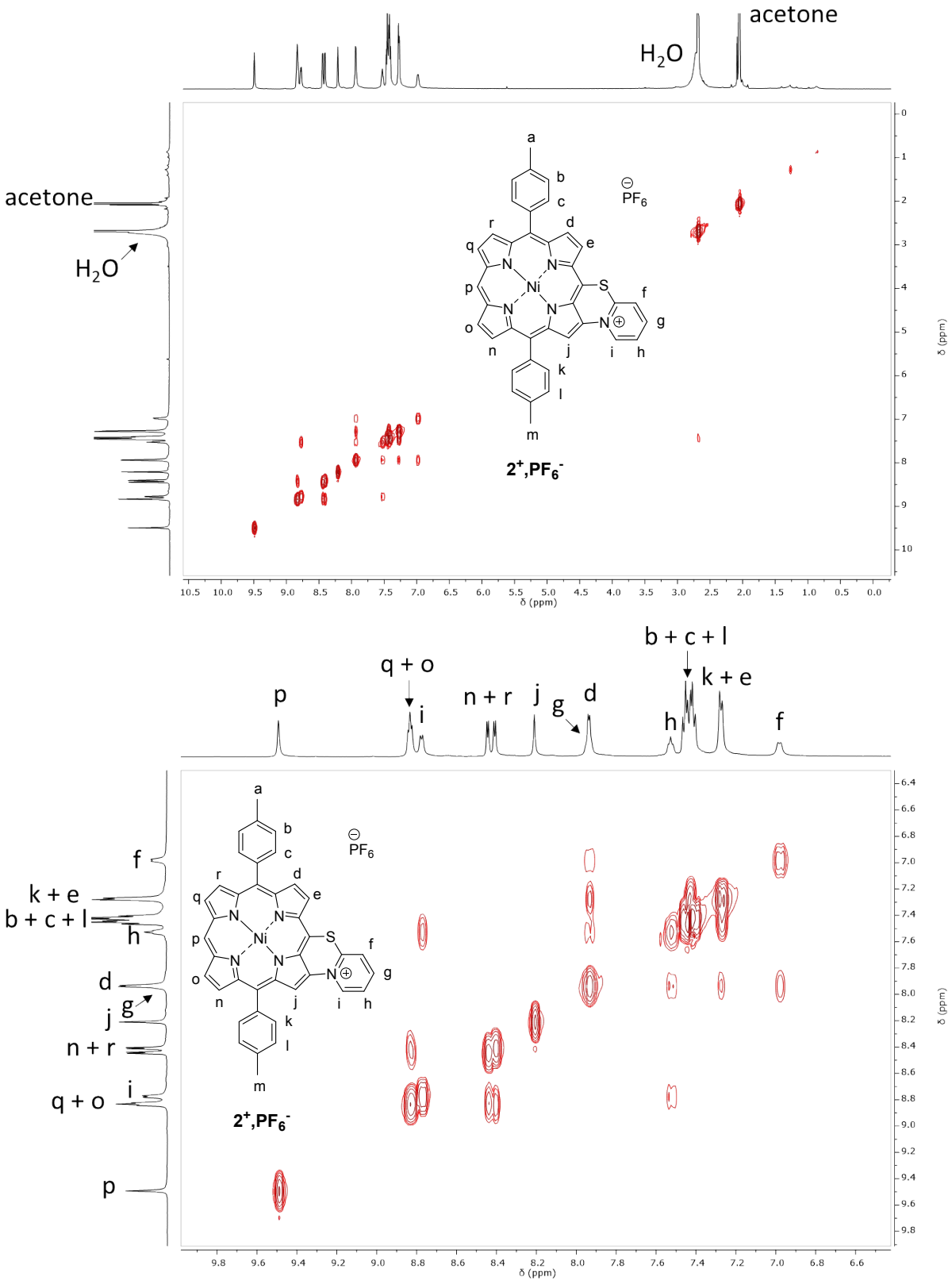

Figure S51. Full range (top) and partial (bottom) ^{1}H-^{1}H COSY NMR spectra of **2**$^{+}$,**PF**$_{6}^{-}$ in CD_3COCD_3, 500 MHz, 298 K.

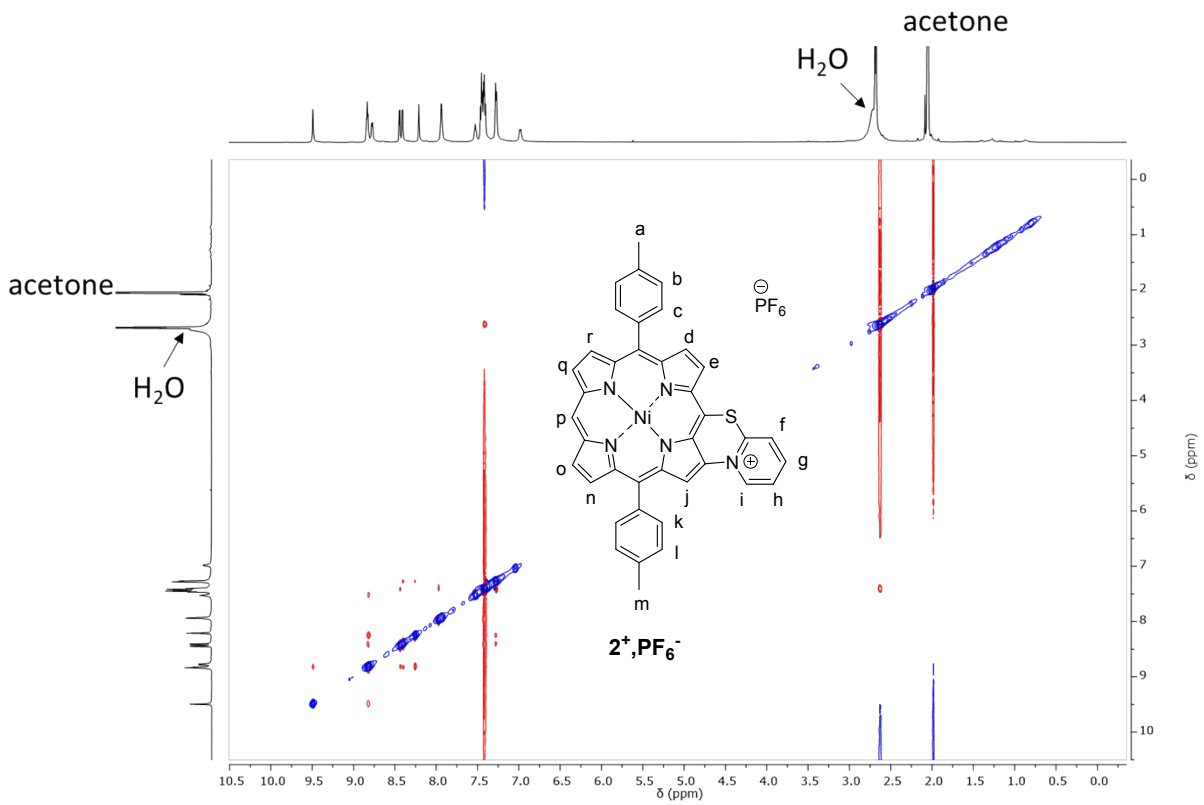

Figure S52. Full range ^{1}H-^{1}H ROESY NMR spectra of **2**$^{+}$,**PF**$_6^-$ in CD_3COCD_3, 500 MHz, 298 K.

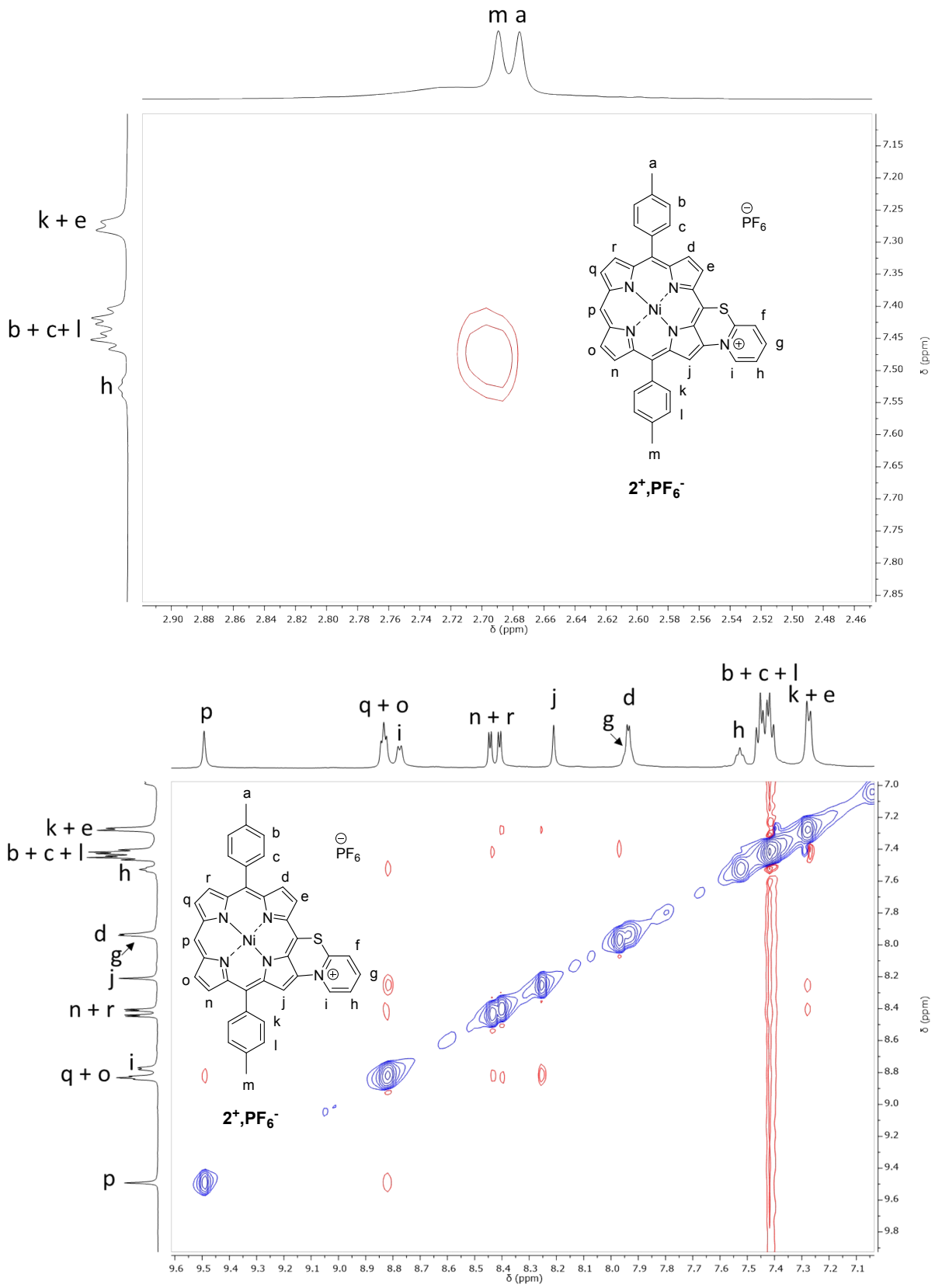

Figure S53. Full range (top) and partial (bottom) ^{1}H-^{1}H NOESY NMR spectra of **2^{+},PF$_{6}^{-}$** in CD_3COCD_3, 500 MHz, 298 K.

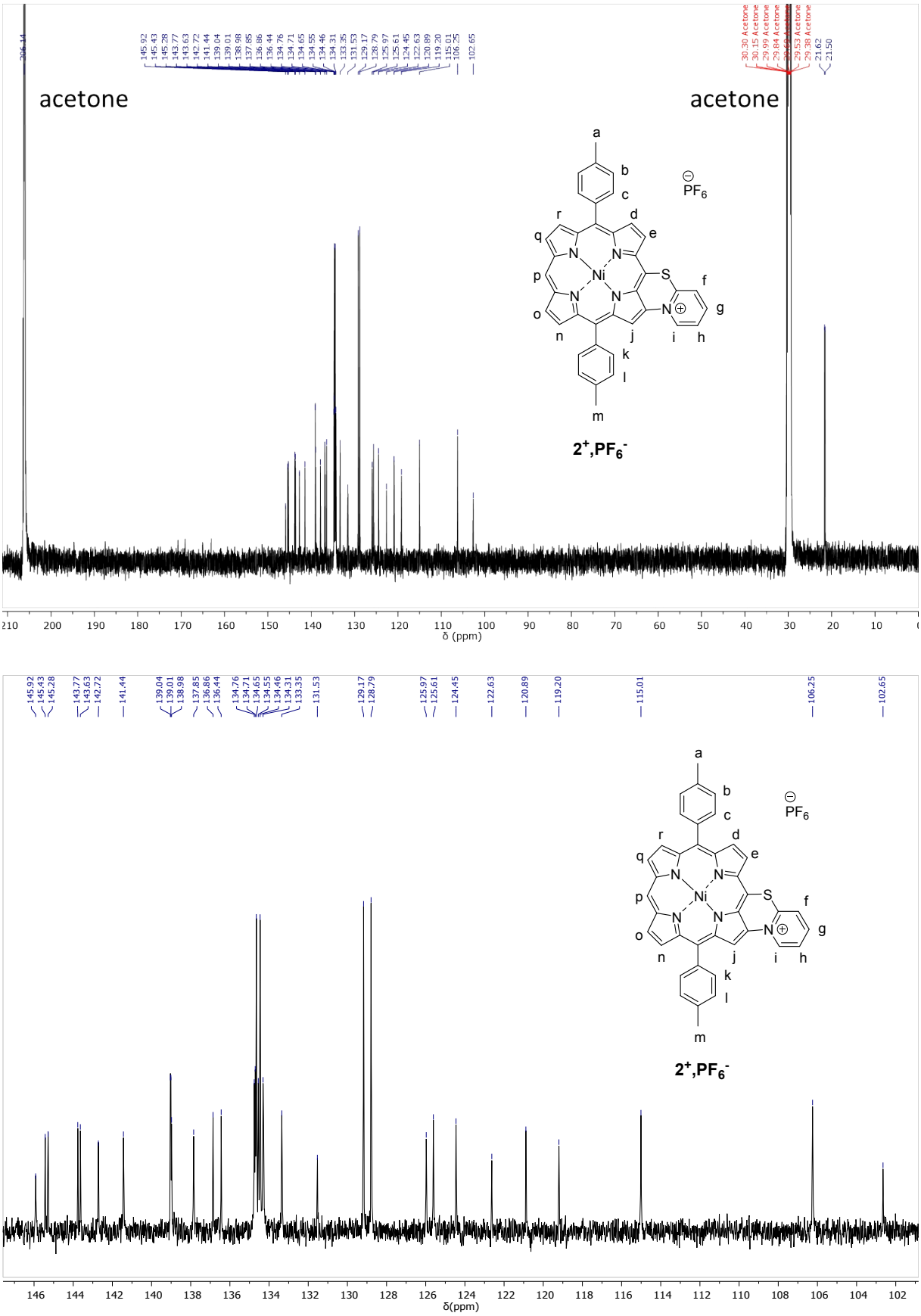

Figure S54. Full range (top) and partial (bottom) $^{13}C\{^{1}H\}$ NMR spectra of **2**$^{+}$,**PF**$_{6}^{-}$ in CD_3COCD_3, 126 MHz, 298 K.

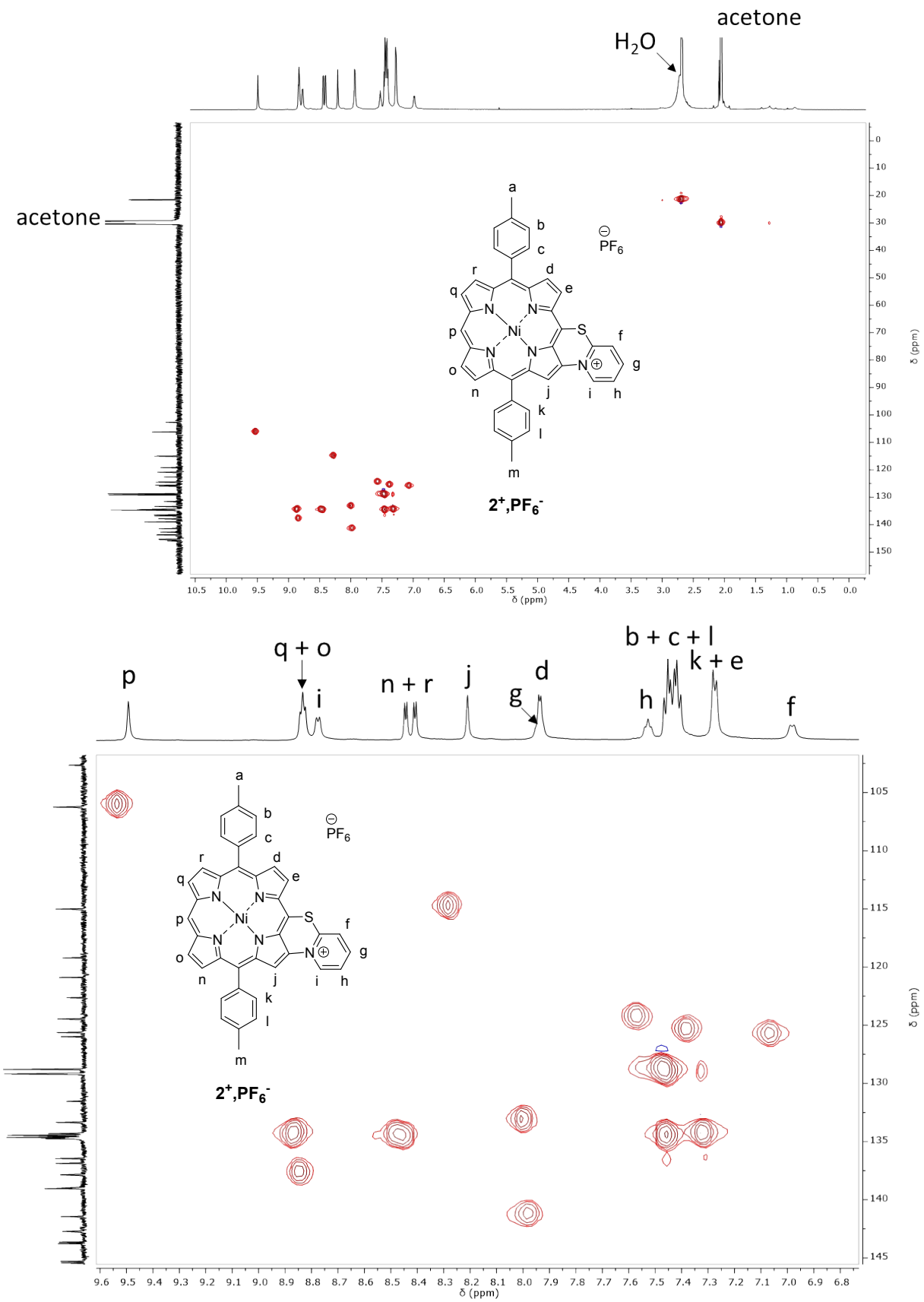

Figure S55. Full range (top) and partial (bottom) ^{1}H-^{13}C HSQC NMR spectra of **2**$^{+}$,**PF**$_6^{-}$ in CD_3COCD_3, 500 MHz, 298 K.

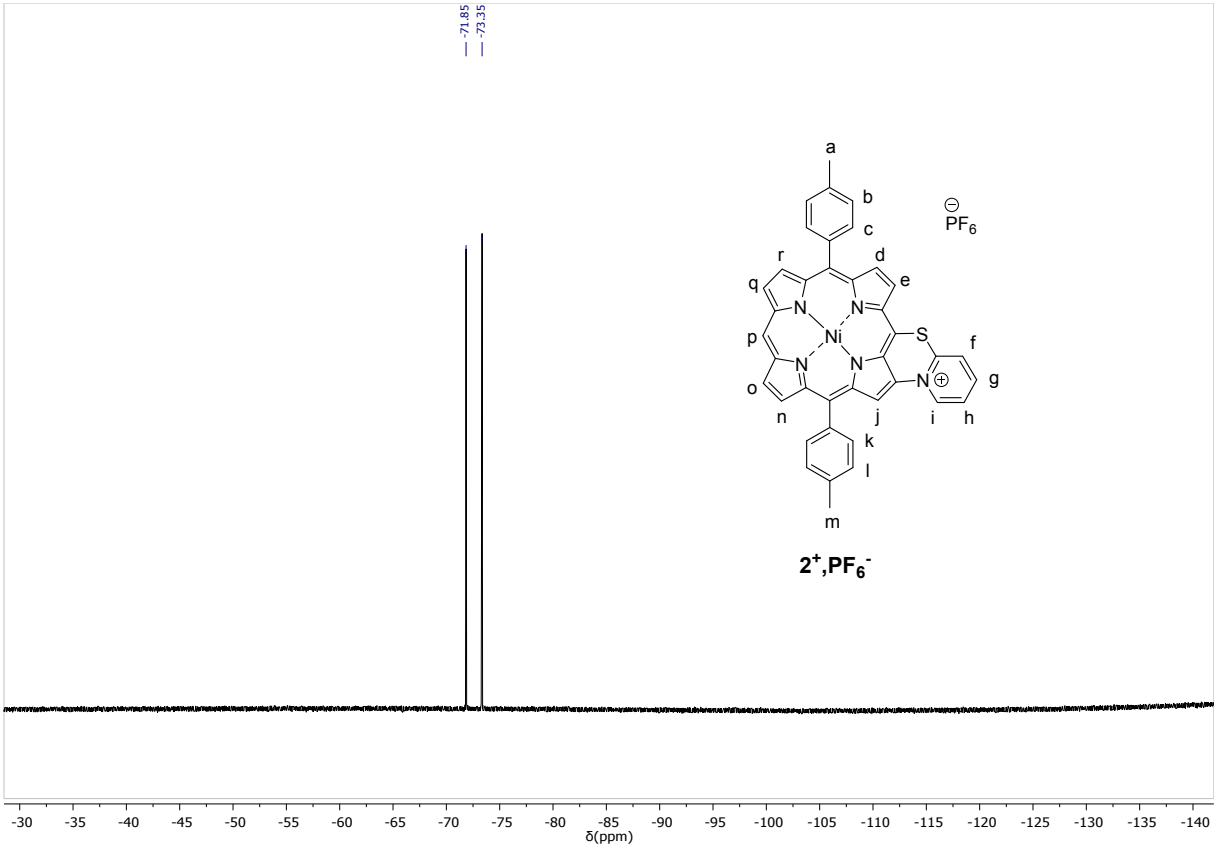

Figure S56. ^{19}F NMR spectrum of $\mathbf{2^{+}{,}PF_6^{-}}$ in CD_3COCD_3, 470 MHz, 298 K.

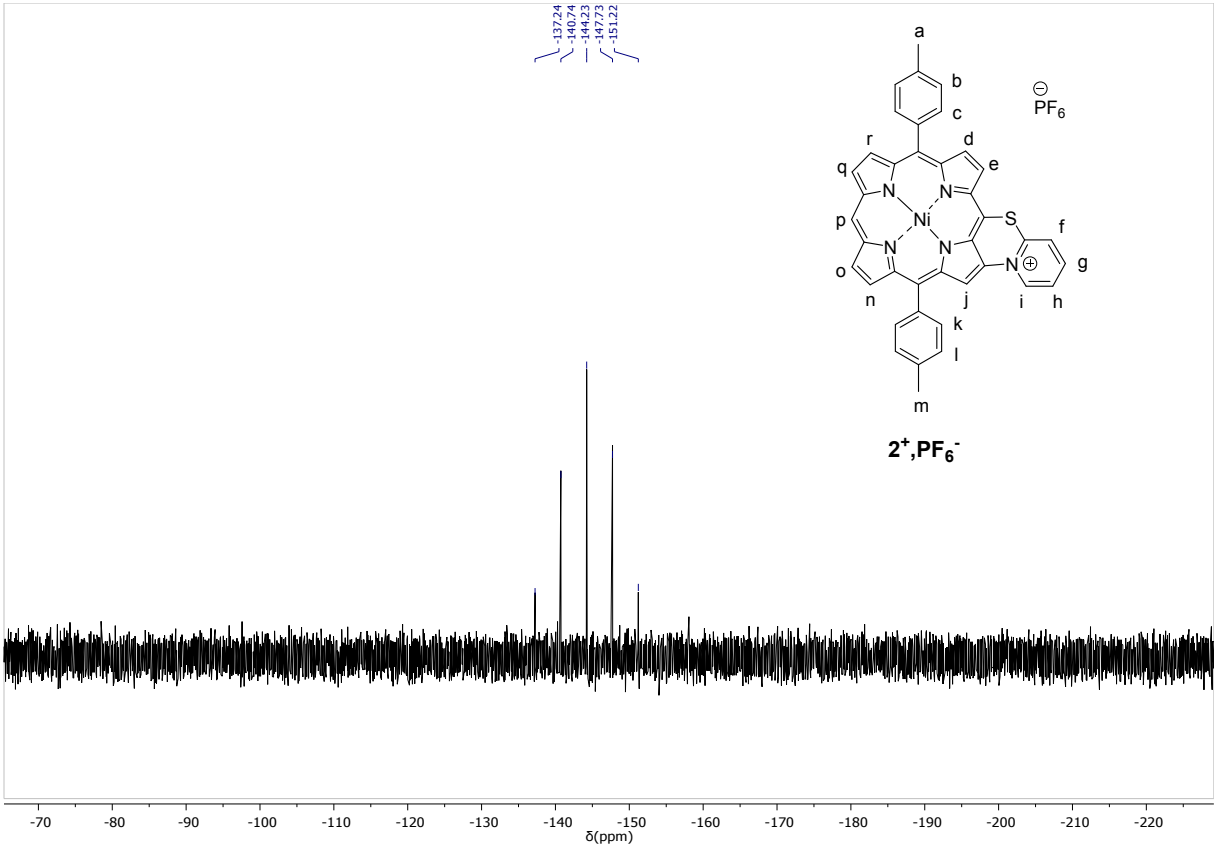

Figure S57. ^{31}P NMR spectrum of $\mathbf{2^{+}{,}PF_6^{-}}$ in CD_3COCD_3, 202 MHz, 298 K.

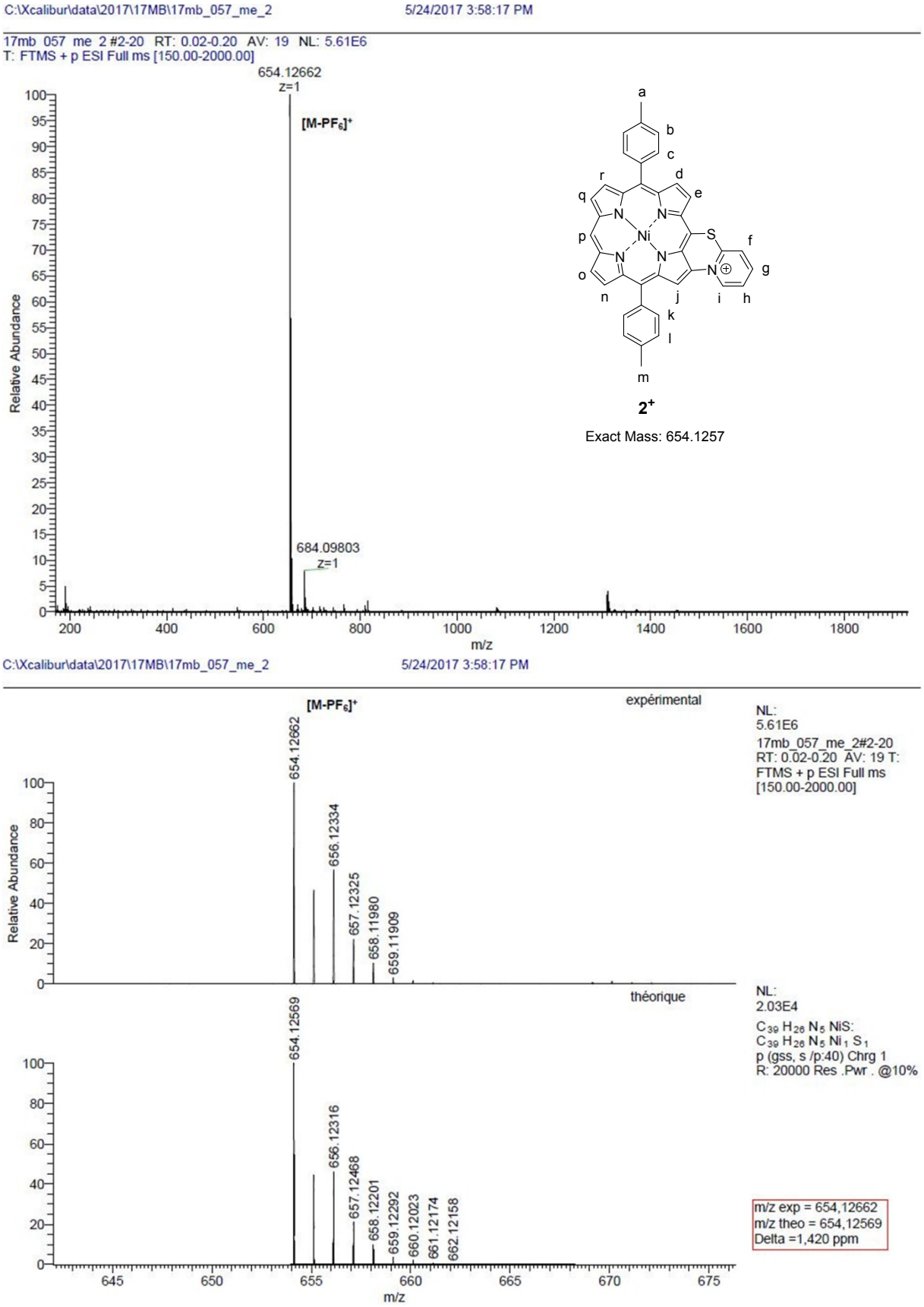

Figure S58. High resolution ESI mass spectrum of $\mathbf{2}^{+}$,$\mathbf{PF_6}^{-}$ and simulation of its isotopic pattern.

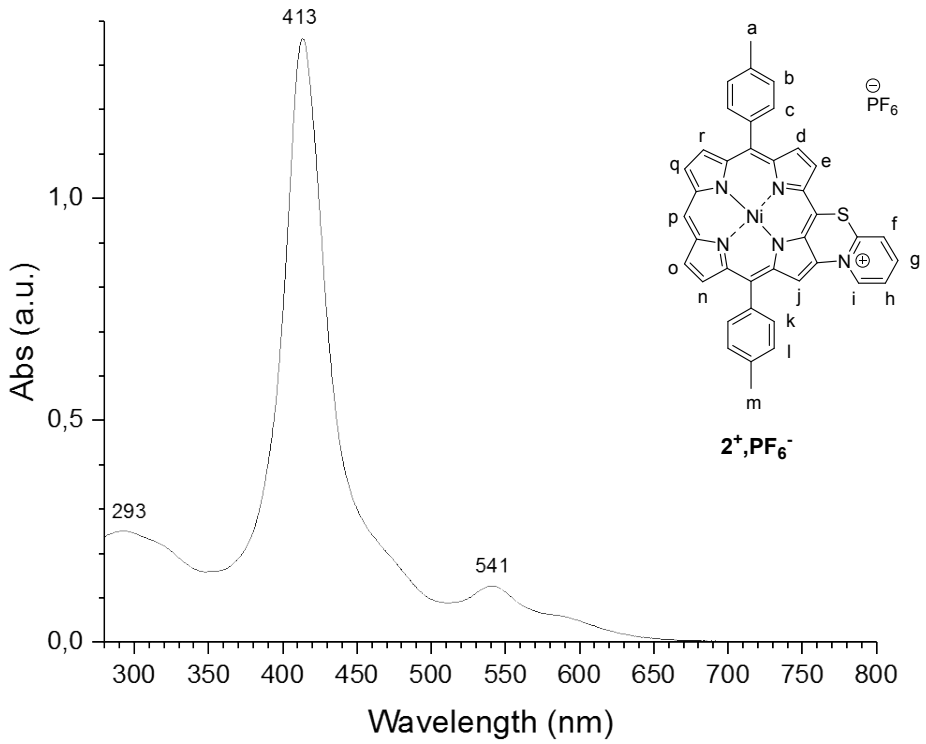

Figure S59. UV-Vis. absorption spectrum of $\mathbf{2^{+},PF_6^{-}}$ in CH_2Cl_2.

Compound 13

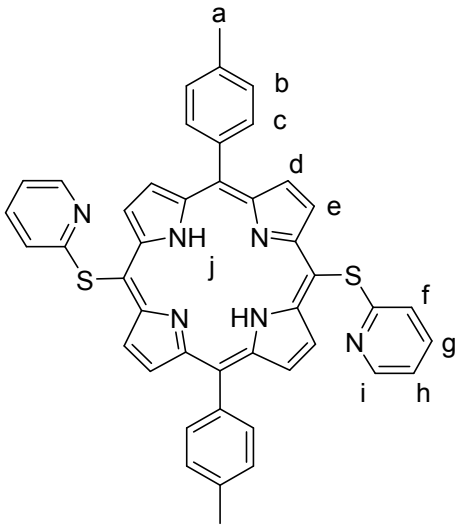

13

Chemical Formula: $C_{44}H_{32}N_6S_2$
Exact Mass: 708.2130
Molecular Weight: 708.9020

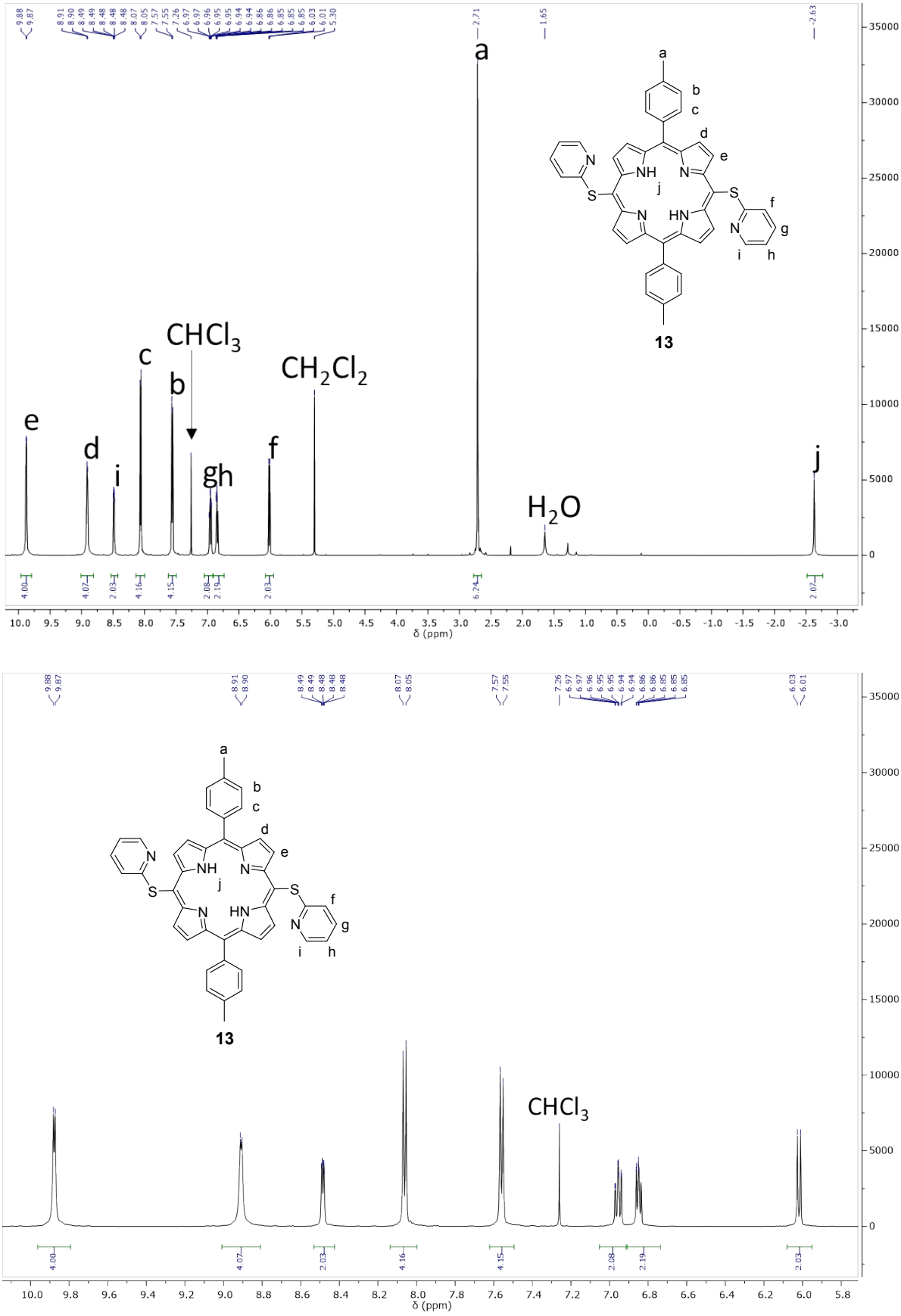

Figure S60. Full range (top) and partial (bottom) ^{1}H NMR spectra of **13** in $CDCl_3$, 500 MHz, 298 K.

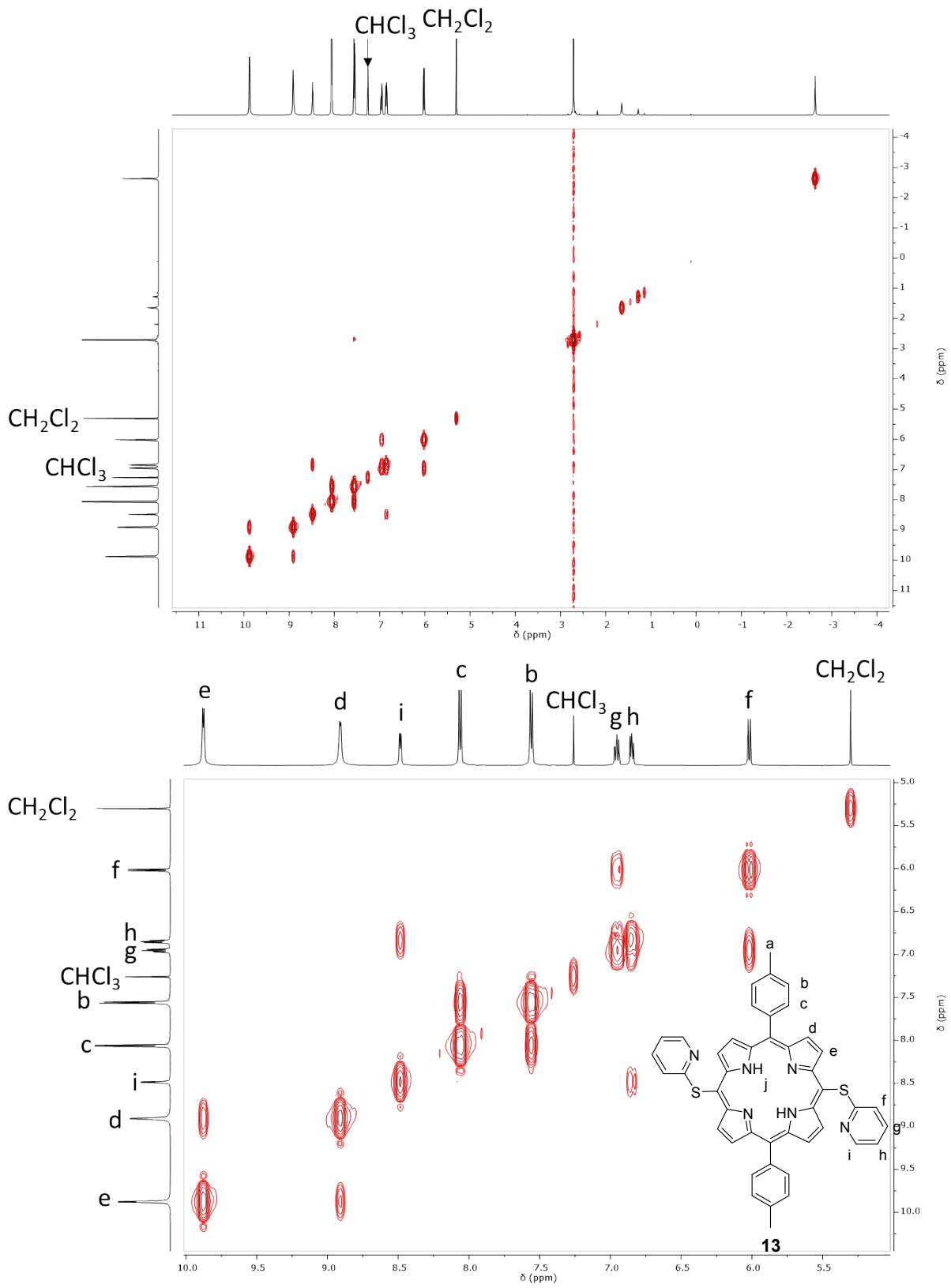

Figure S61. Full range (top) and partial (bottom) ^{1}H-^{1}H COSY NMR spectra of **13** in $CDCl_3$, 500 MHz, 298 K.

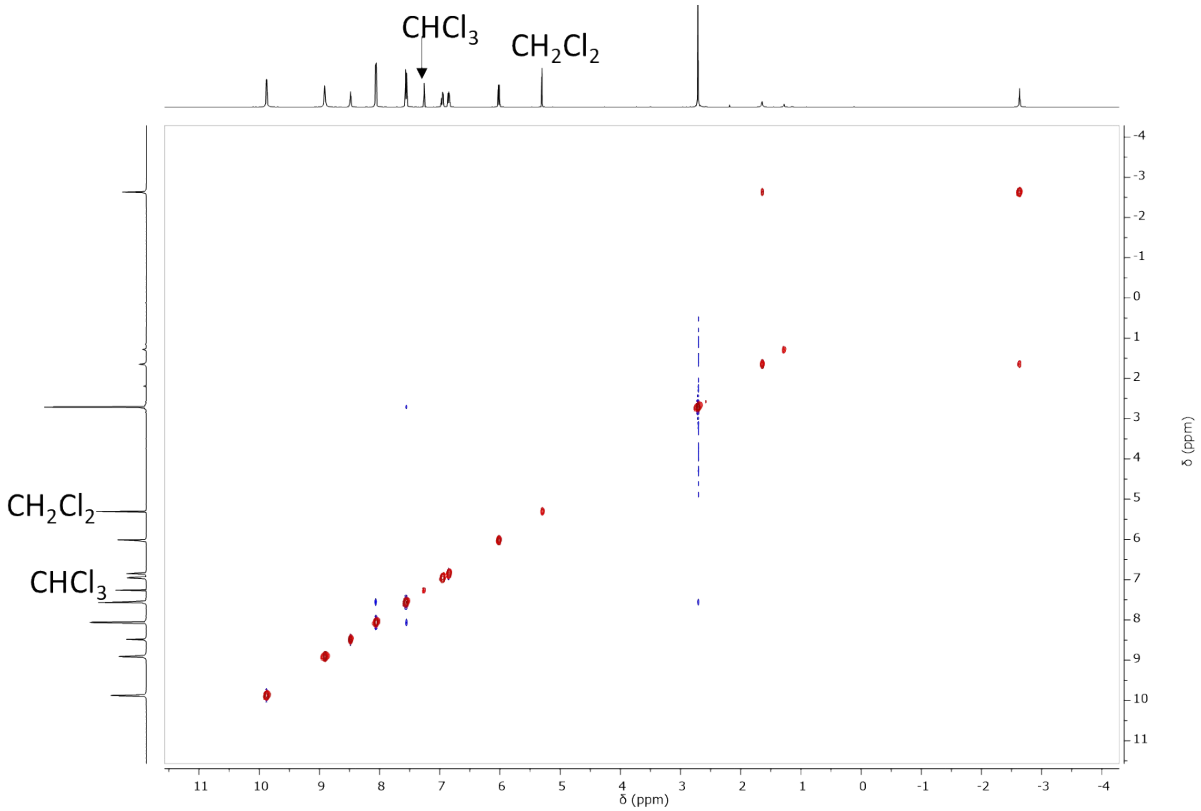

Figure S62. Full range ^{1}H-^{1}H NOESY NMR spectrum of **13** in $CDCl_3$, 500 MHz, 298 K.

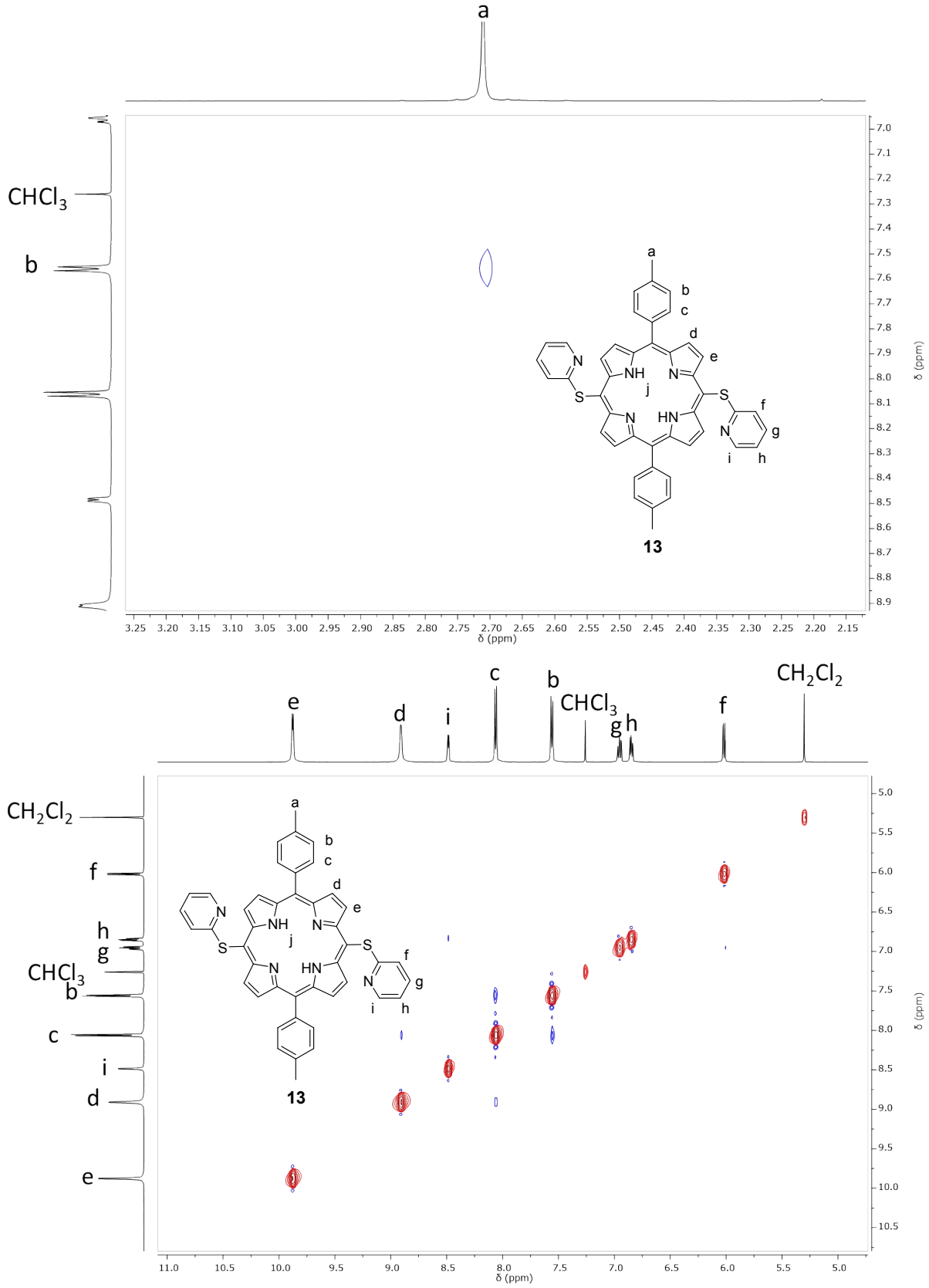

Figure S63. Partial ^{1}H-^{1}H NOESY NMR spectra of **13** in $CDCl_3$, 500 MHz, 298 K.

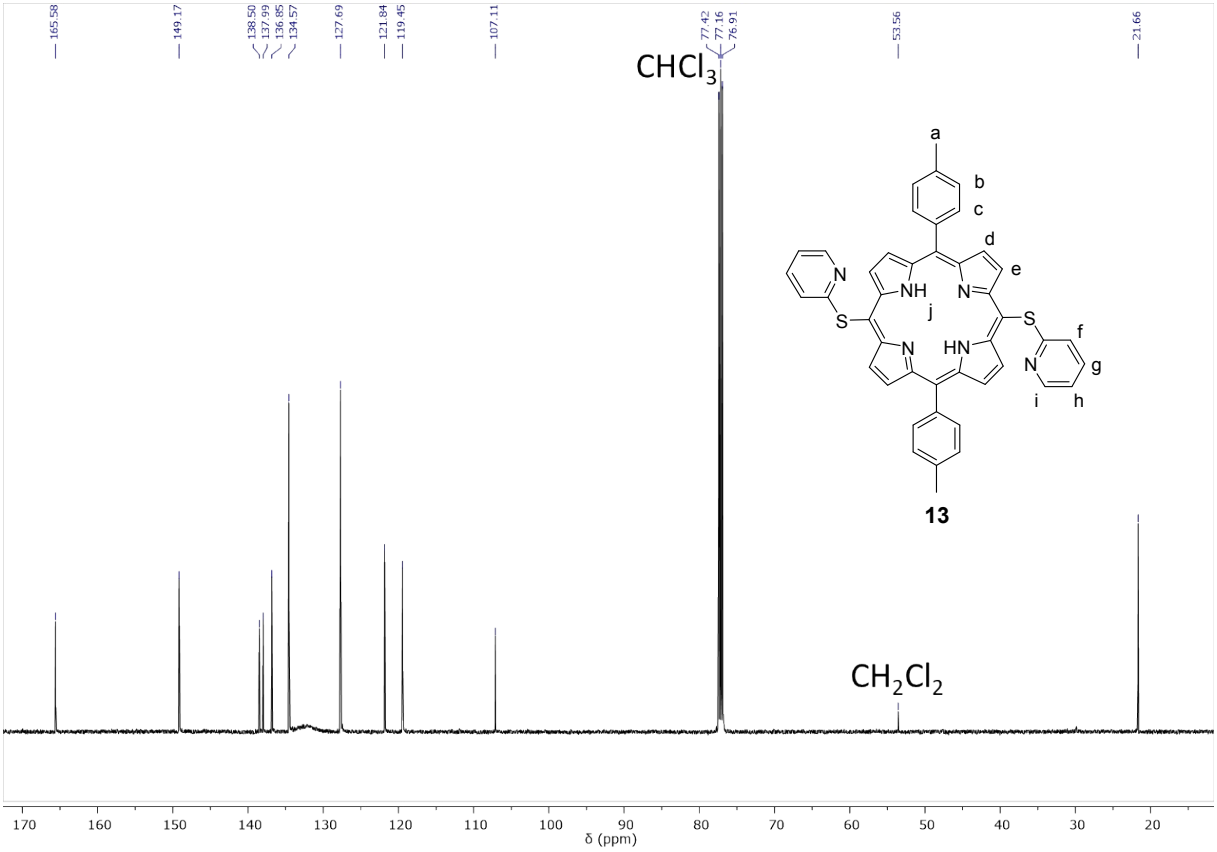

Figure S64. Full range $^{13}C\{^{1}H\}$ NMR spectrum of **13** in $CDCl_3$, 126 MHz, 300 K.

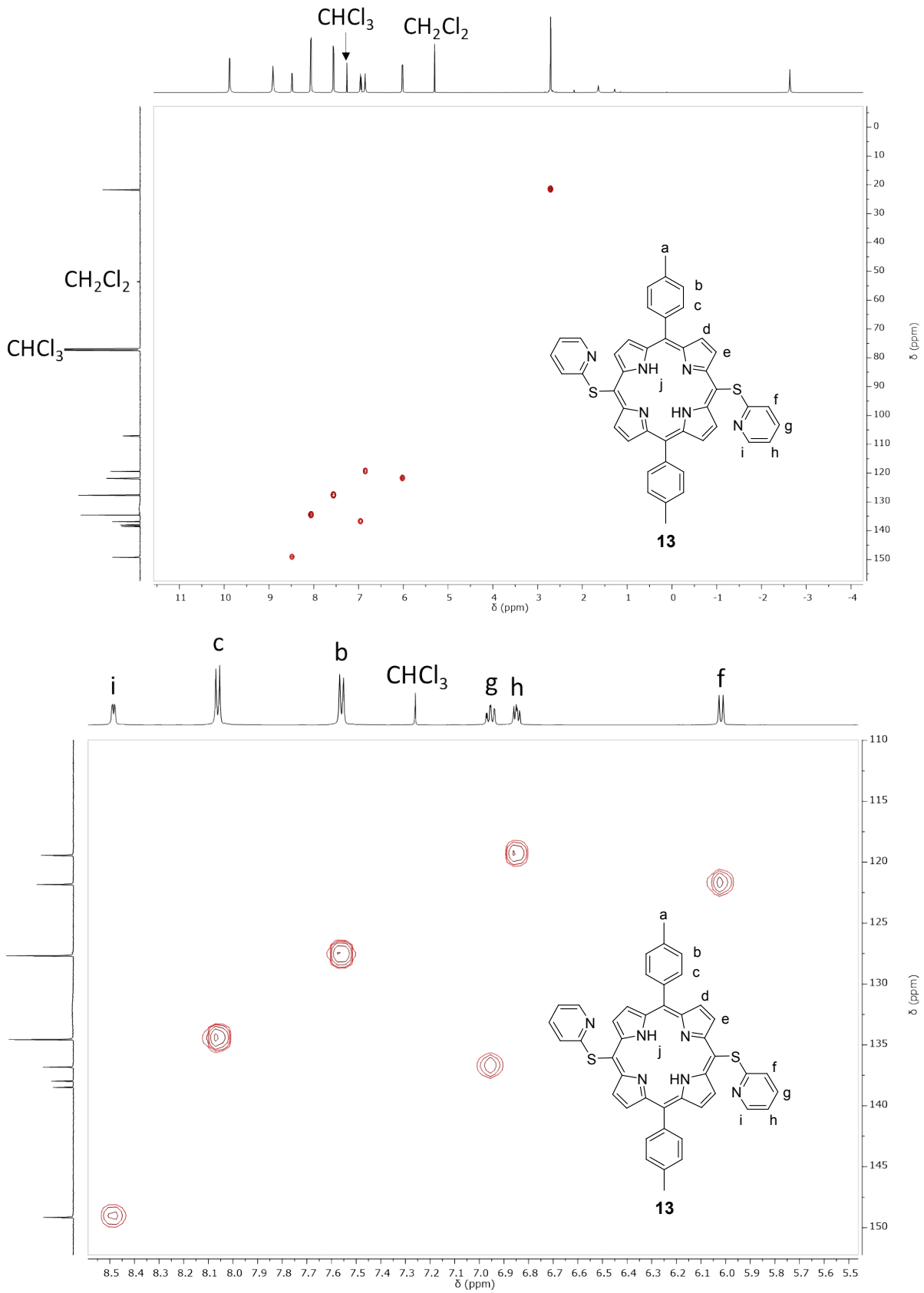

Figure S65. Full range ^{1}H-^{13}C HSQC NMR spectrum of **13** in $CDCl_3$, 500 MHz, 298 K.

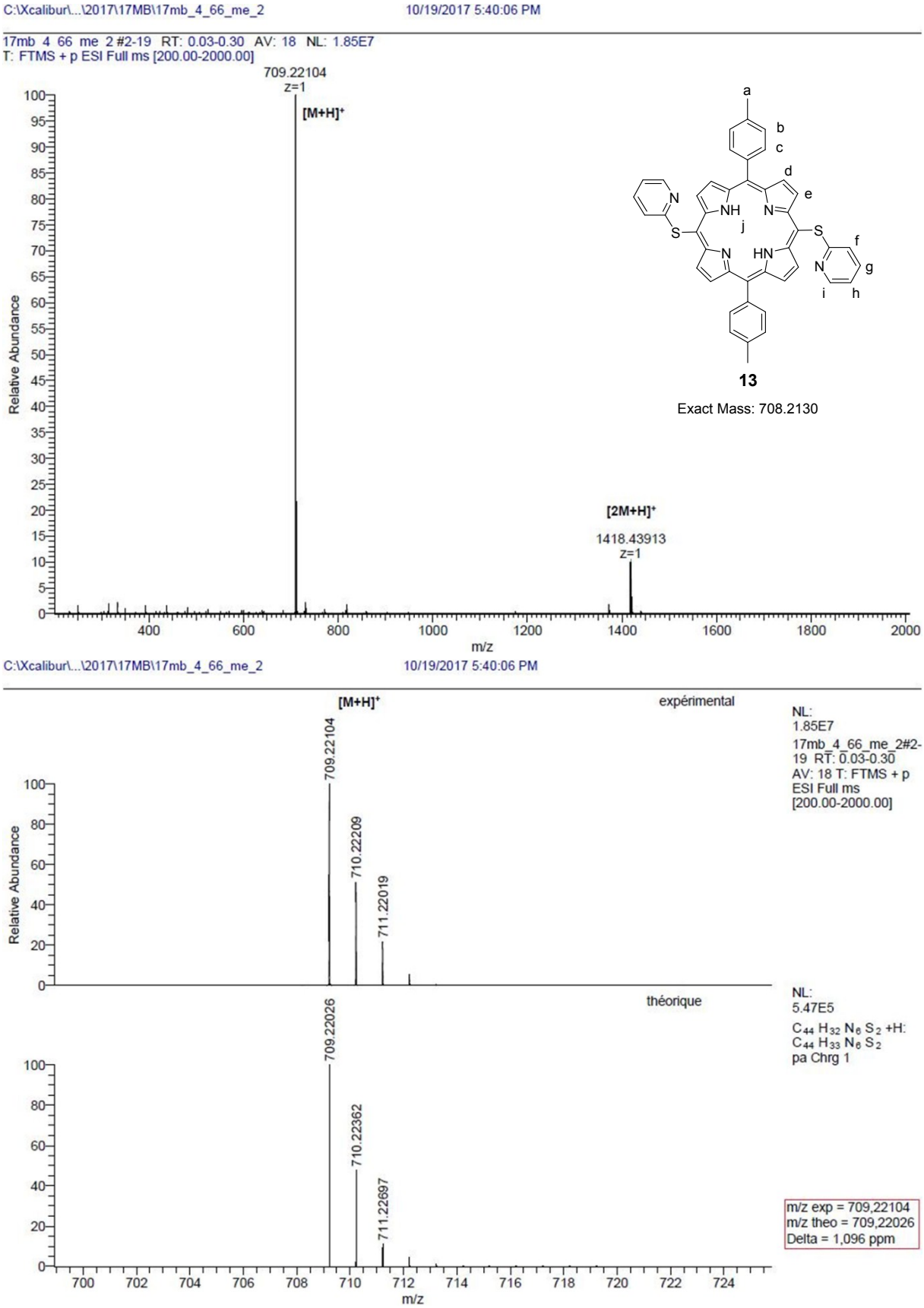

Figure S66. High resolution ESI mass spectrum of **13** and simulation of its isotopic pattern.

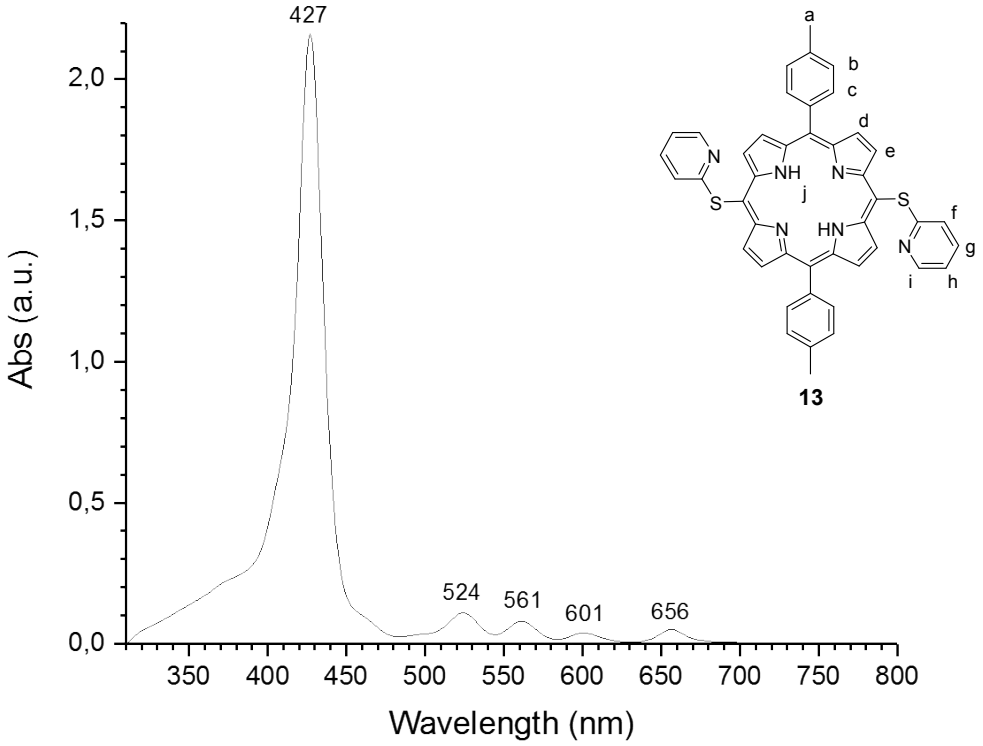

Figure S67. UV-Vis. absorption spectrum of **13** in CH_2Cl_2.

Compound 3

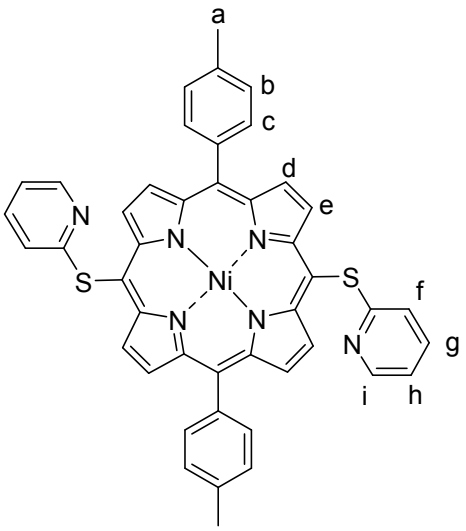

3

Chemical Formula: $C_{44}H_{30}N_6NiS_2$
Exact Mass: 764,13
Molecular Weight: 765,58

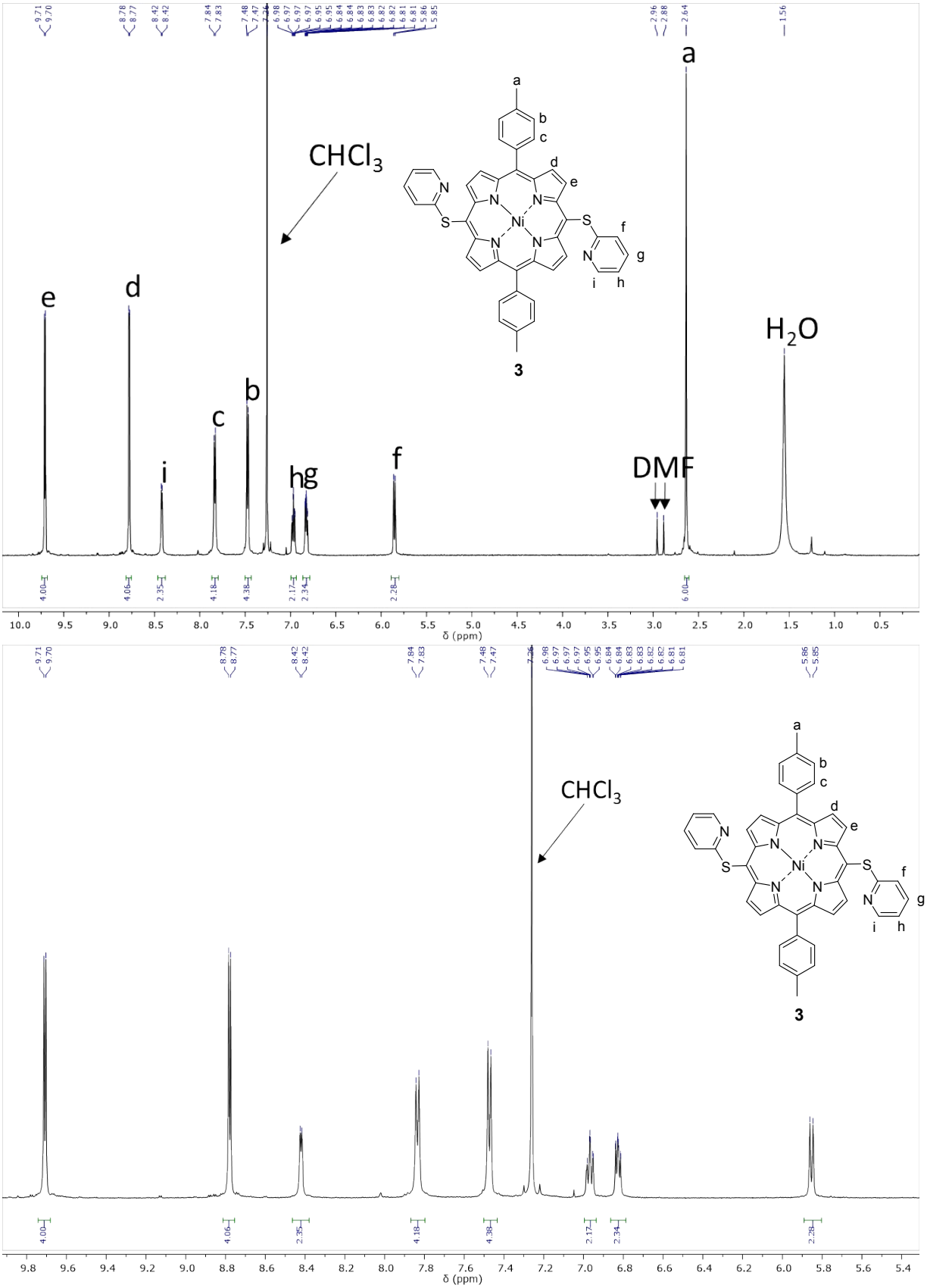

Figure S68. Full range (top) and partial (bottom) ^{1}H NMR spectra of **3** in $CDCl_3$, 500 MHz, 297 K.

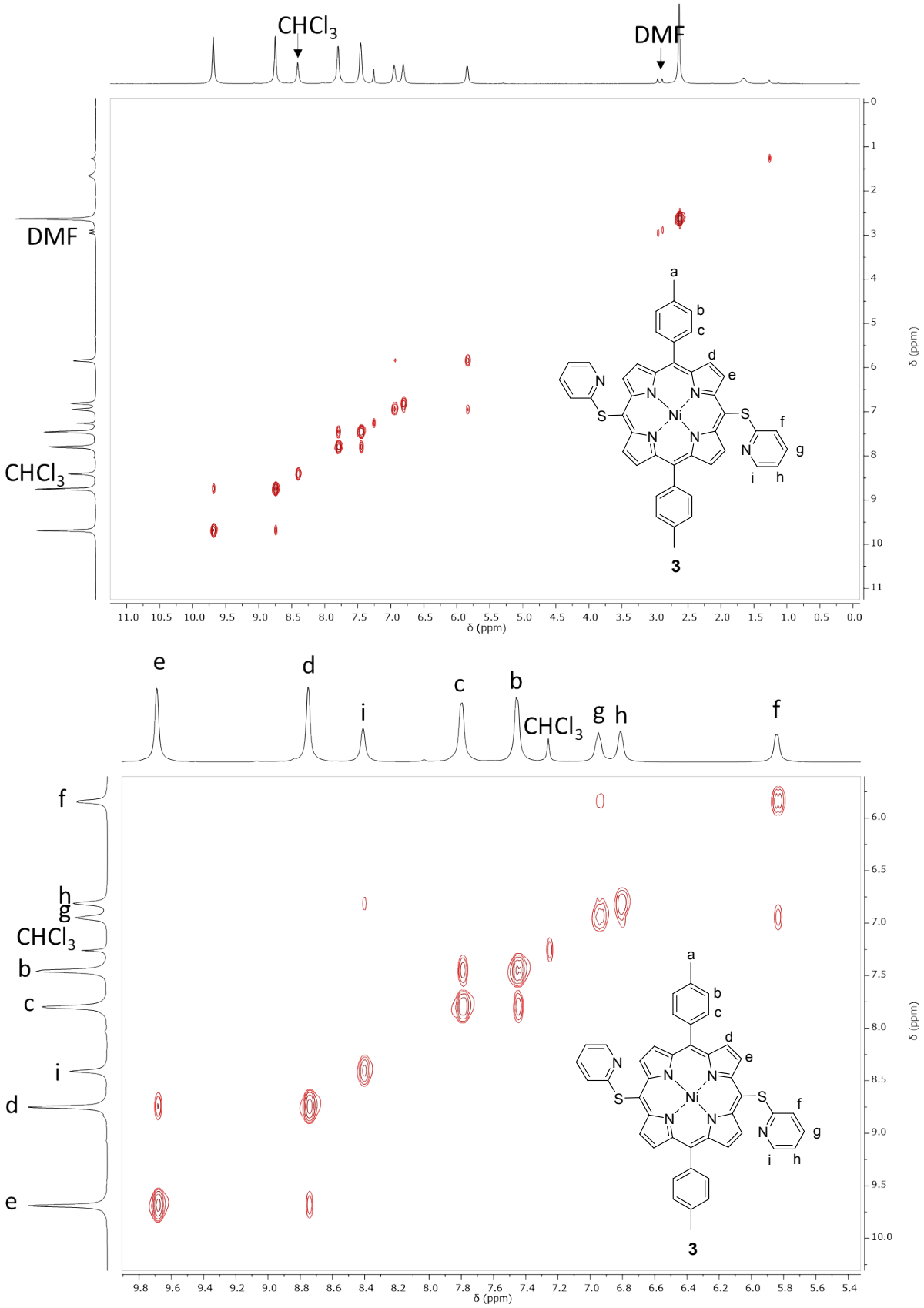

Figure S69. Full range (top) and partial (bottom) ^{1}H-^{1}H COSY NMR spectra of **3** in $CDCl_3$, 500 MHz, 298 K.

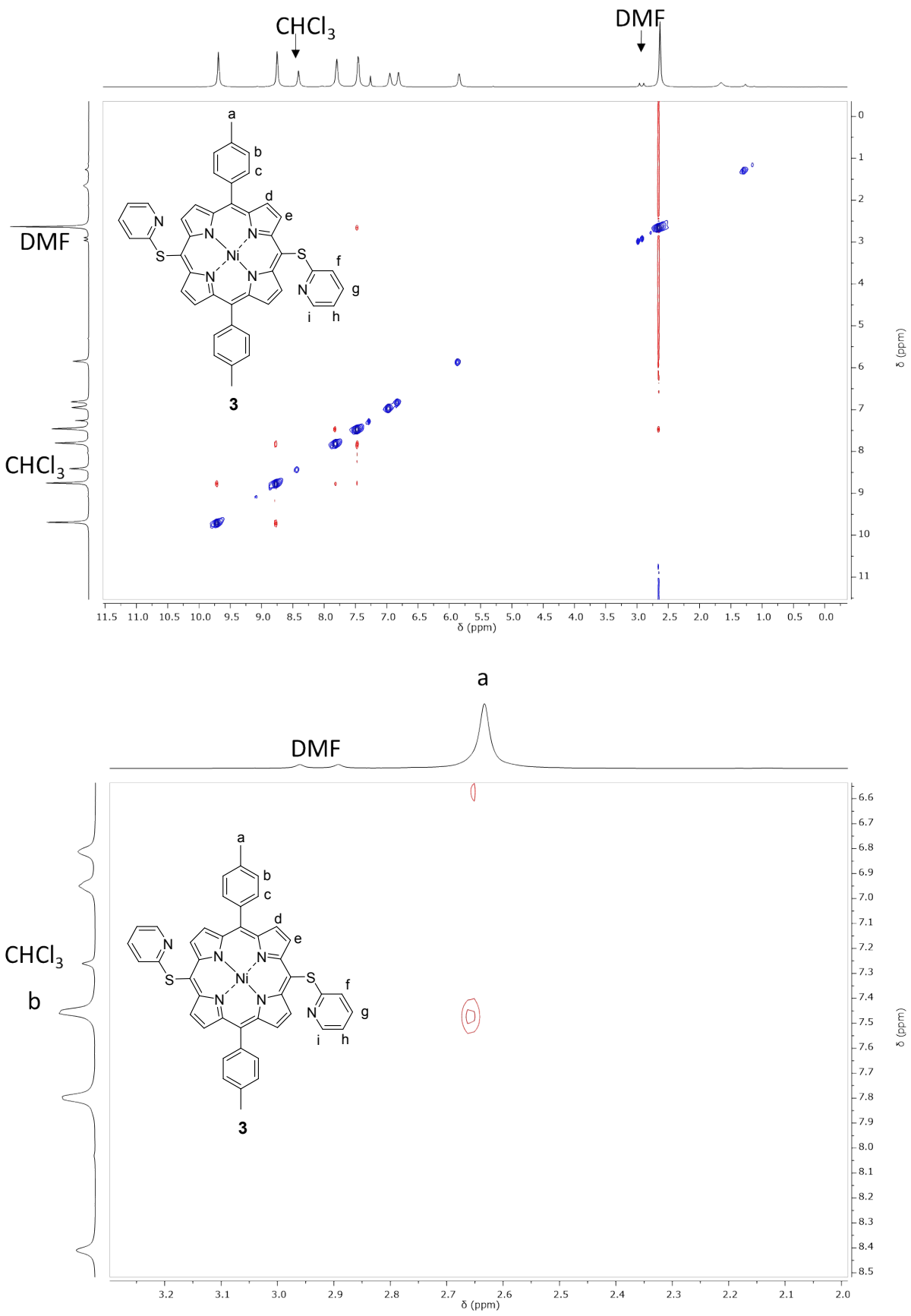

Figure S70. Full range (top) and partial (bottom) ^{1}H-^{1}H NOESY NMR spectra of **3** in $CDCl_3$, 500 MHz, 298 K.

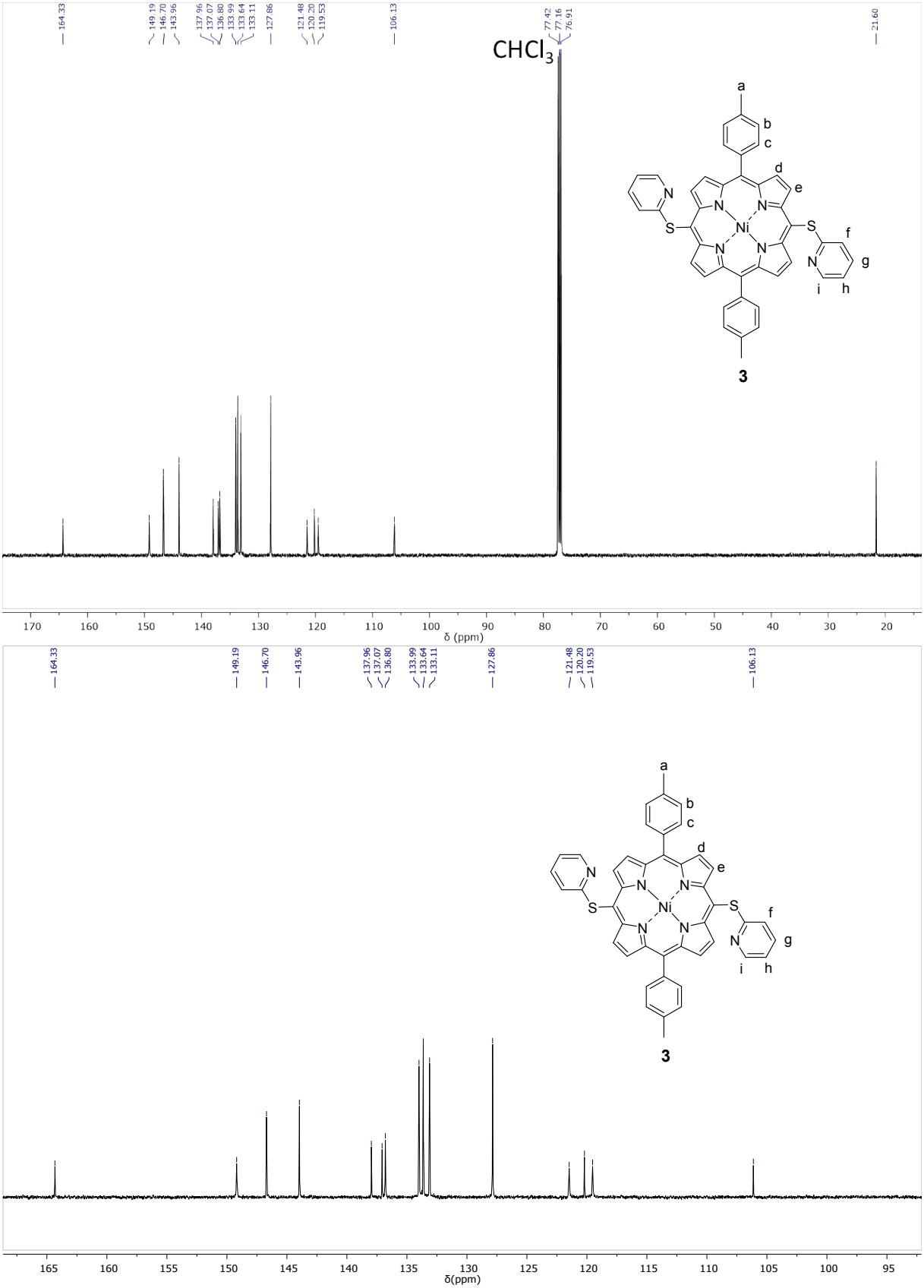

Figure S71. Full range (top) and partial (bottom) $^{13}C\{^{1}H\}$ NMR spectra of **3** in $CDCl_3$, 126 MHz, 298 K.

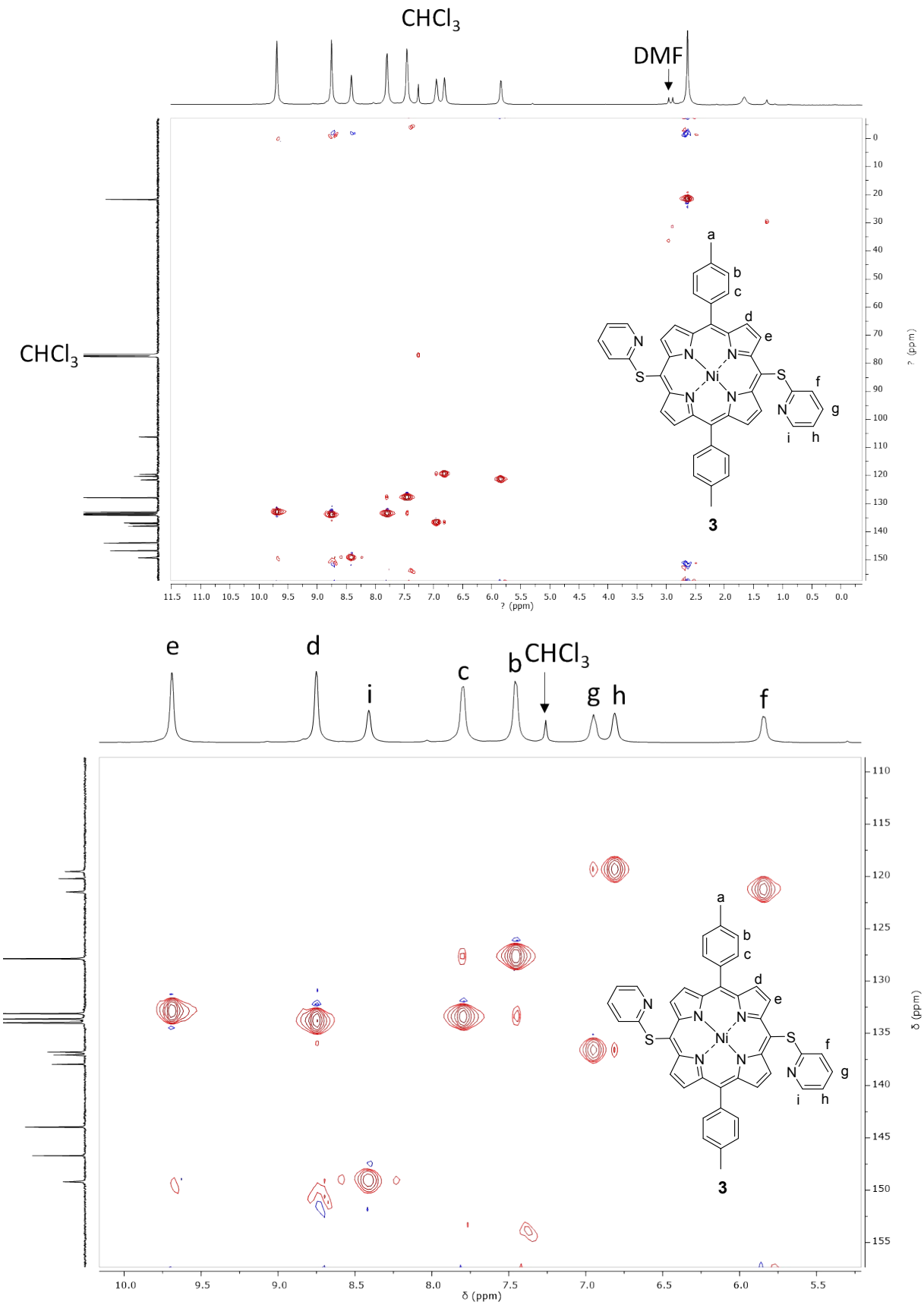

Figure S72. Full range (top) and partial (bottom) ^{1}H-^{13}C HSQC NMR spectra of **3** in $CDCl_3$, 500 MHz, 298 K.

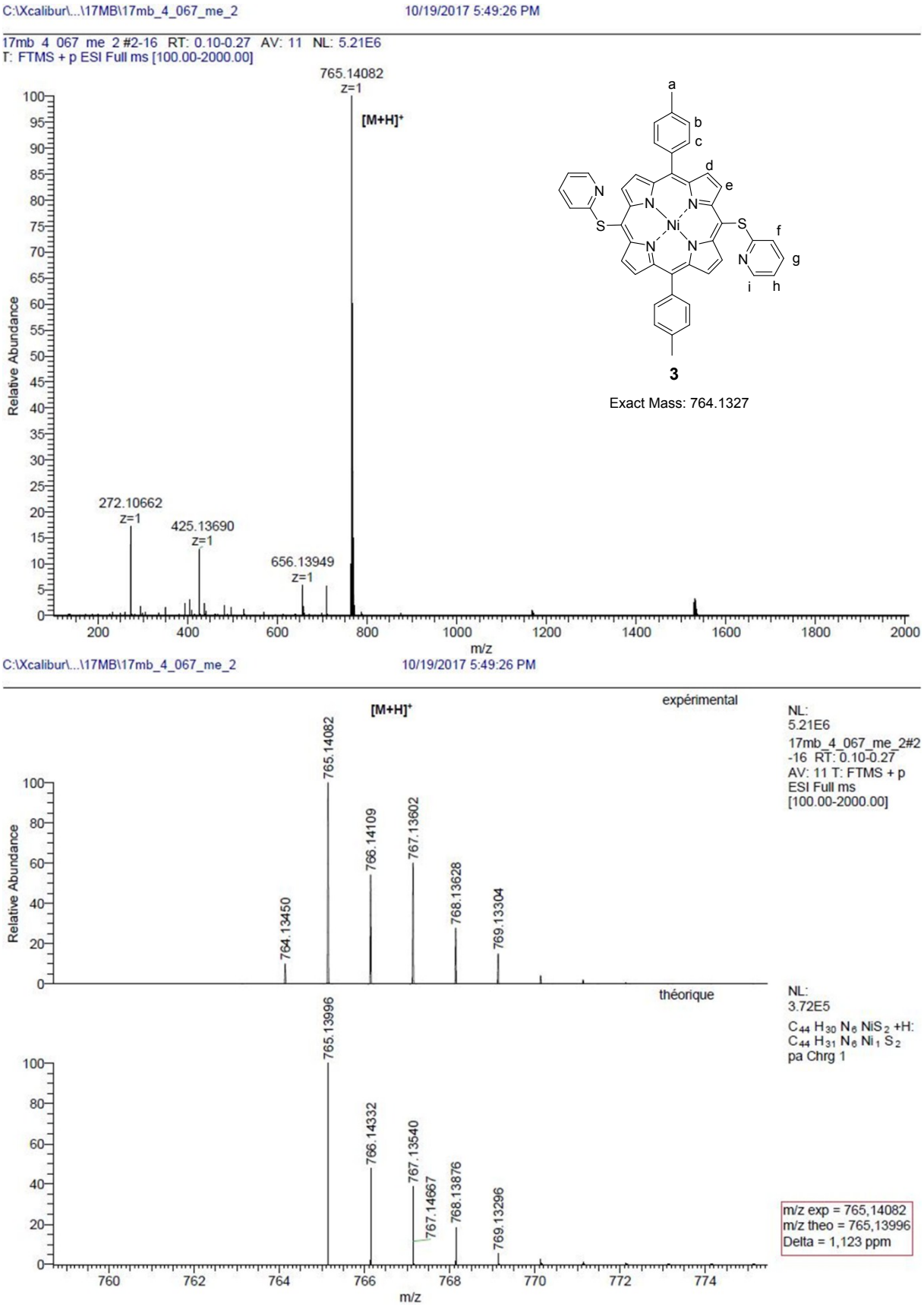

Figure S73. High resolution ESI mass spectrum of **3** and simulation of its isotopic pattern.

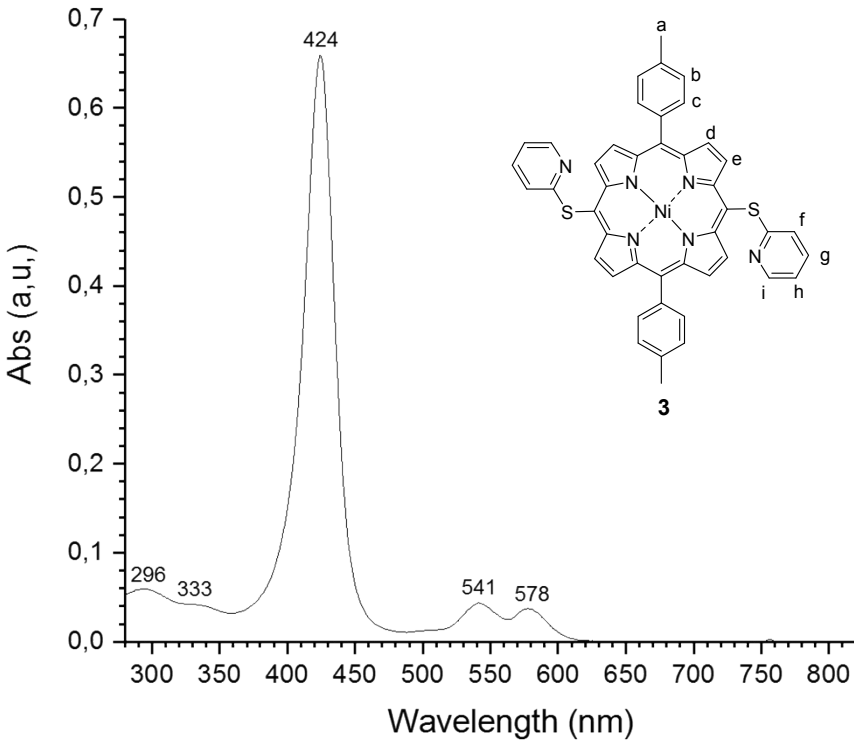

Figure S74. UV-Vis. absorption spectrum of **3** in CH_2Cl_2.

Compound 3^{+},PF_6^{-}

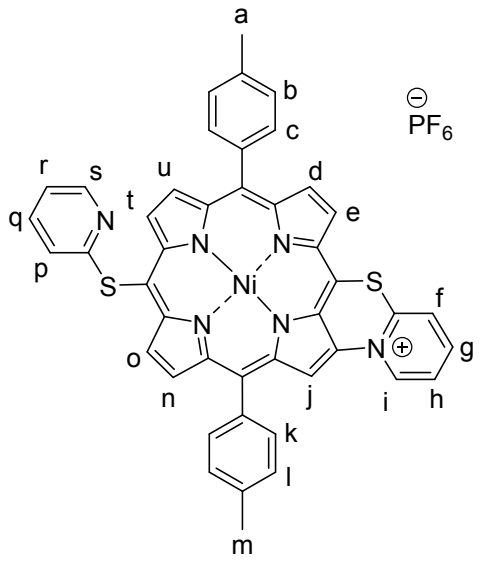

3^{+},PF_6^{-}

Chemical Formula: $C_{44}H_{29}F_6N_6NiPS_2$
Molecular Weight: 909.5356

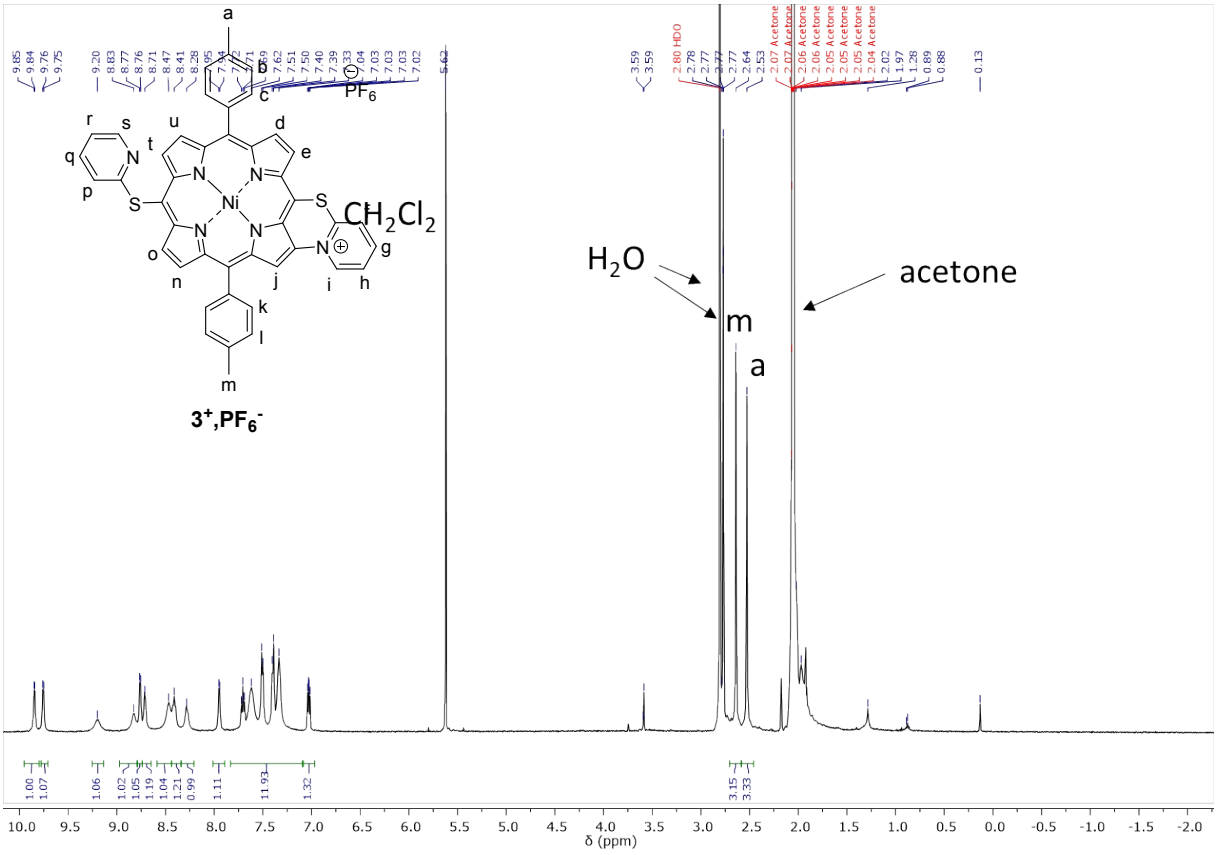

Figure S75. Full range ^{1}H NMR spectra of $\mathbf{3^+,PF_6^-}$ in CD_3COCD_3, 500 MHz, 298 K.

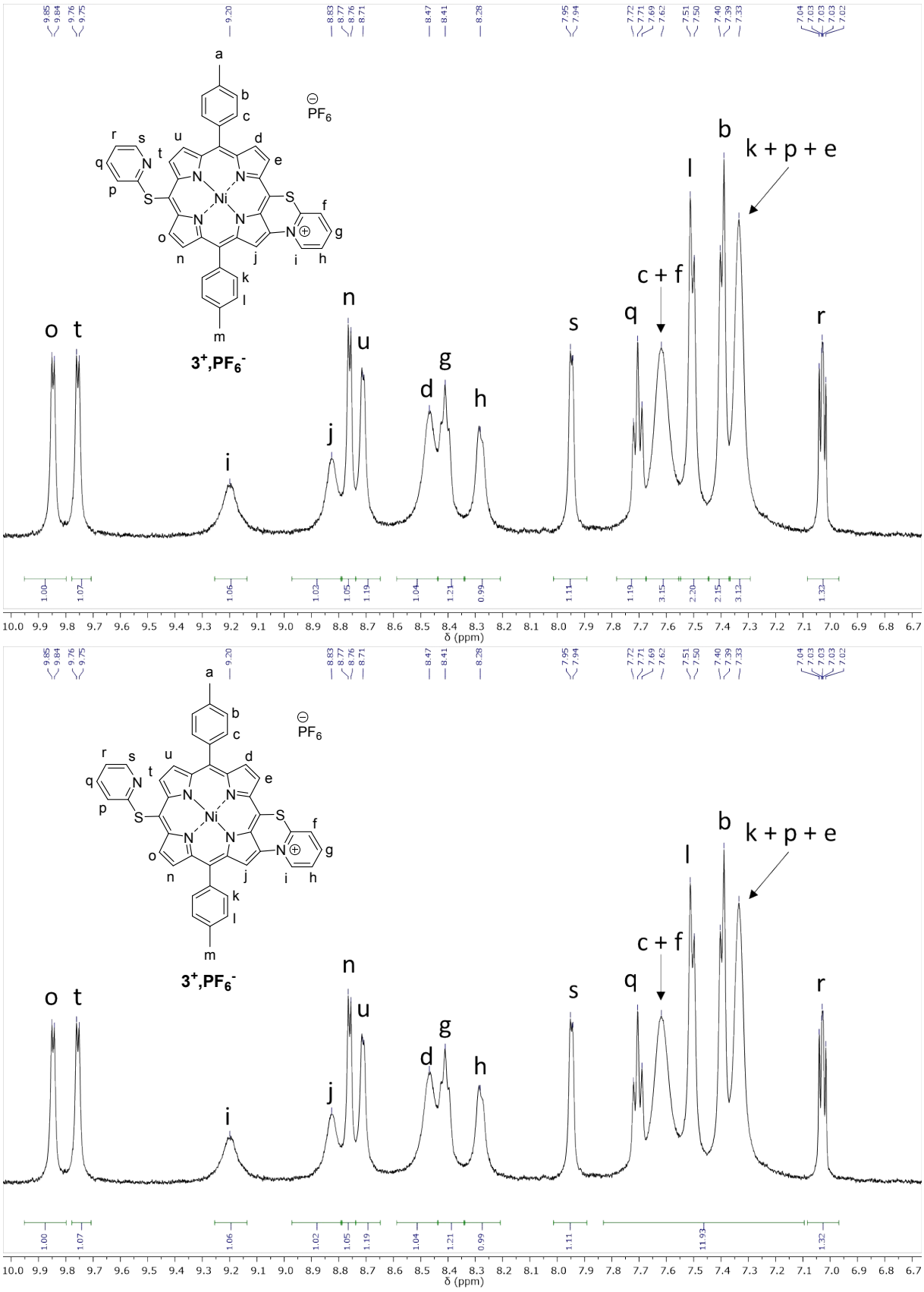

Figure S76. Partial ^{1}H NMR spectra of **3**$^+$,**PF**$_6^-$ in CD_3COCD_3, 500 MHz, 298 K.

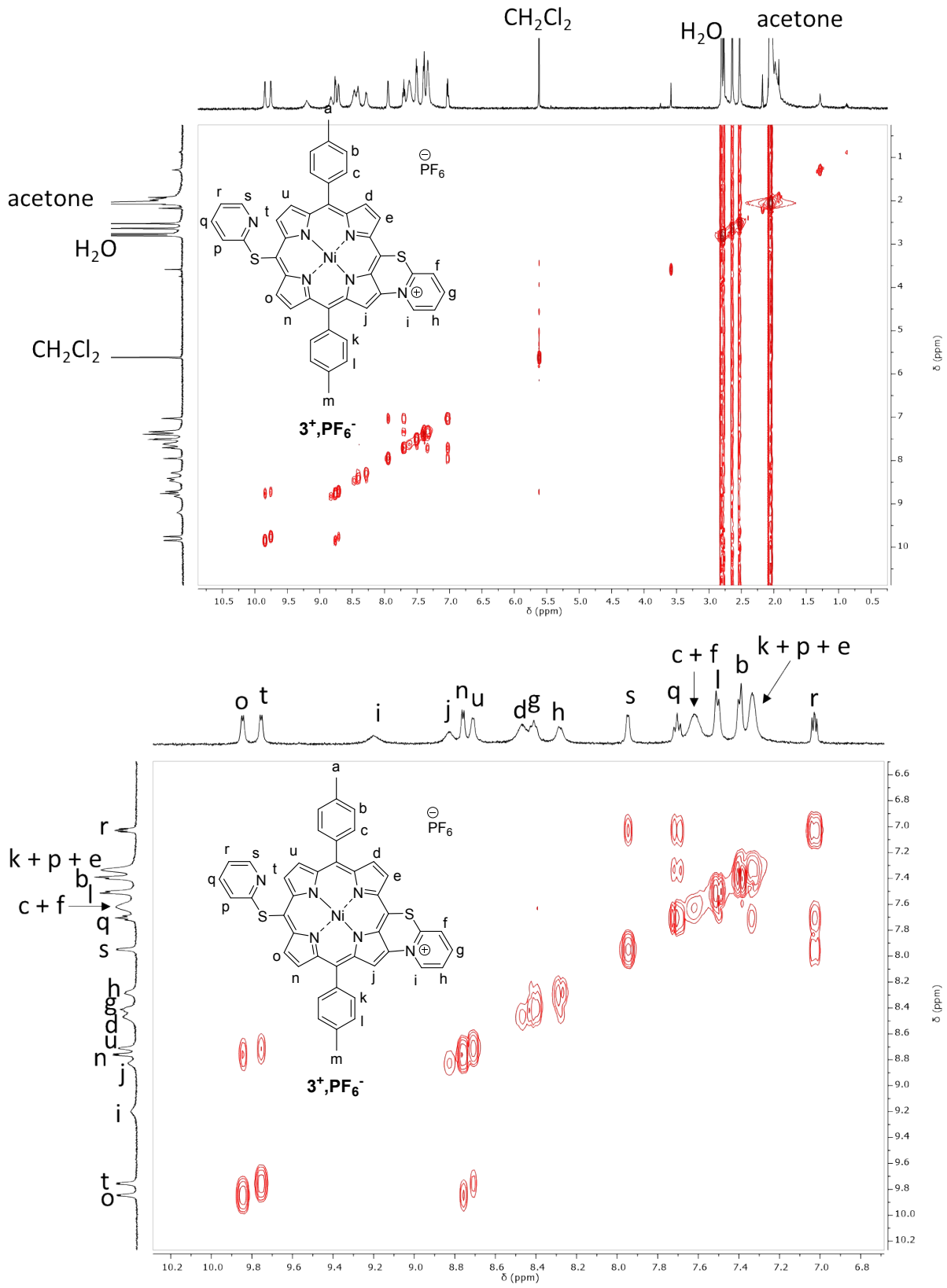

Figure S77. Full range (top) and partial (bottom) ^{1}H-^{1}H COSY NMR spectra of **3**$^{+}$,**PF**$_{6}^{-}$ in CD_3COCD_3, 500 MHz, 298 K.

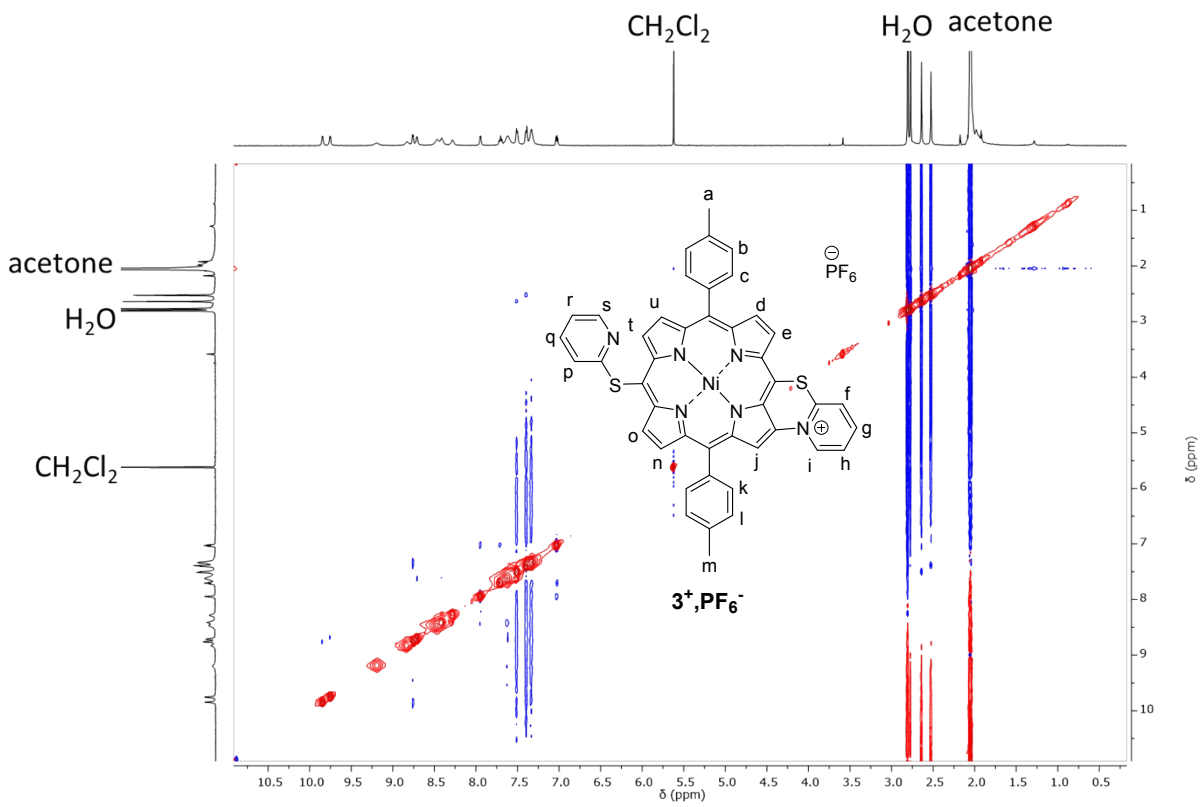

Figure S78. Full ^{1}H-^{1}H NOESY NMR spectra of **3**$^{+}$**,PF**$_{6}^{-}$ in CD_3COCD_3, 500 MHz, 298 K.

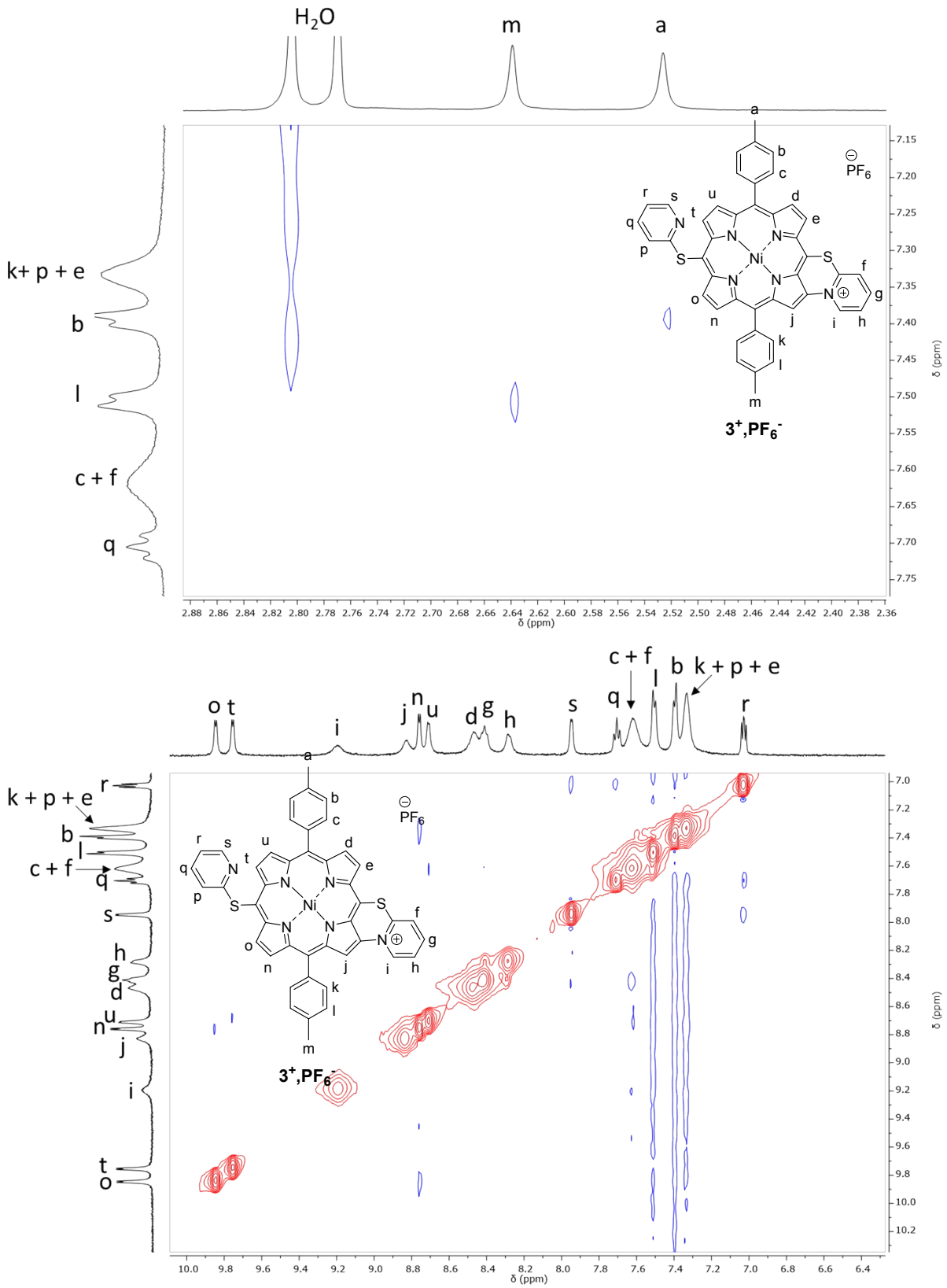

Figure S79. Partial ^{1}H-^{1}H NOESY NMR spectra of **3**$^{+}$,**PF**$_{6}^{-}$ in CD_3COCD_3, 500 MHz, 298 K.

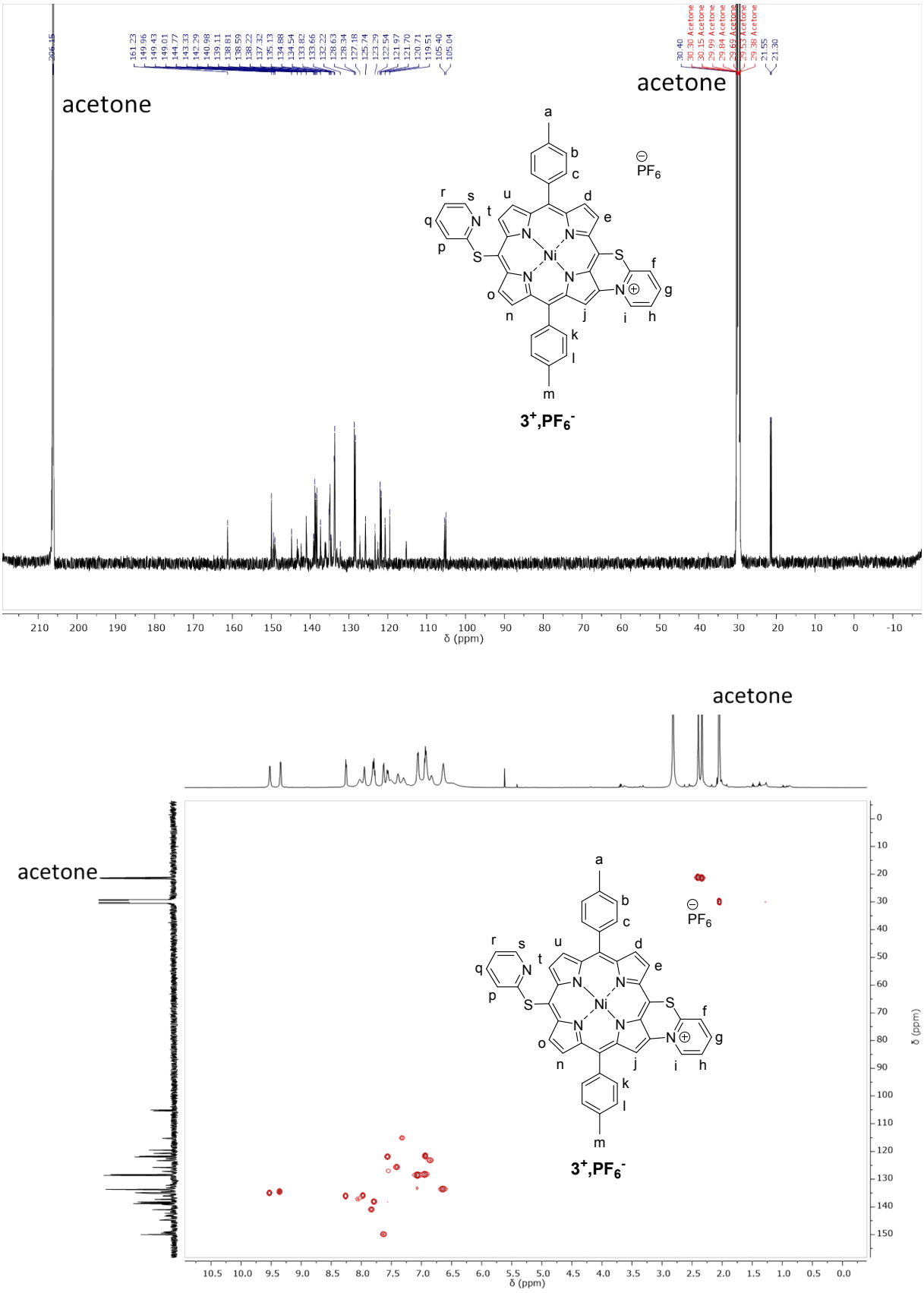

Figure S80. Full range (top) and partial (bottom) $^{13}C\{^{1}H\}$NMR spectrum of **3**$^{+}$,**PF**$_{6}^{-}$ in CD_3COCD_3, 126 MHz, 298 K.

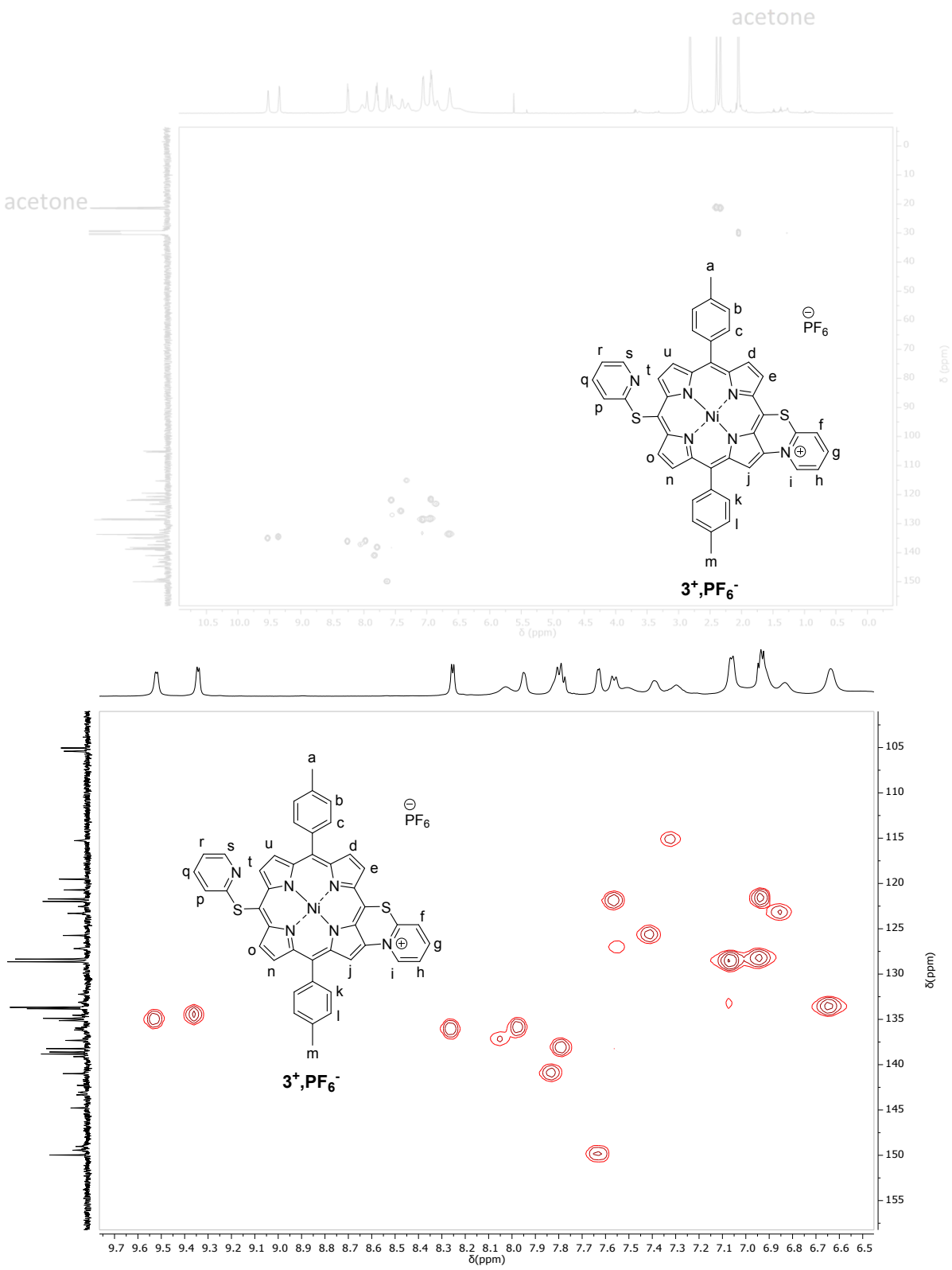

Figure S81. Full range (top) and partial (bottom) ^{1}H-^{13}C HSQC NMR spectra of **3⁺,PF₆⁻** in CD_3COCD_3, 500 MHz, 298 K.

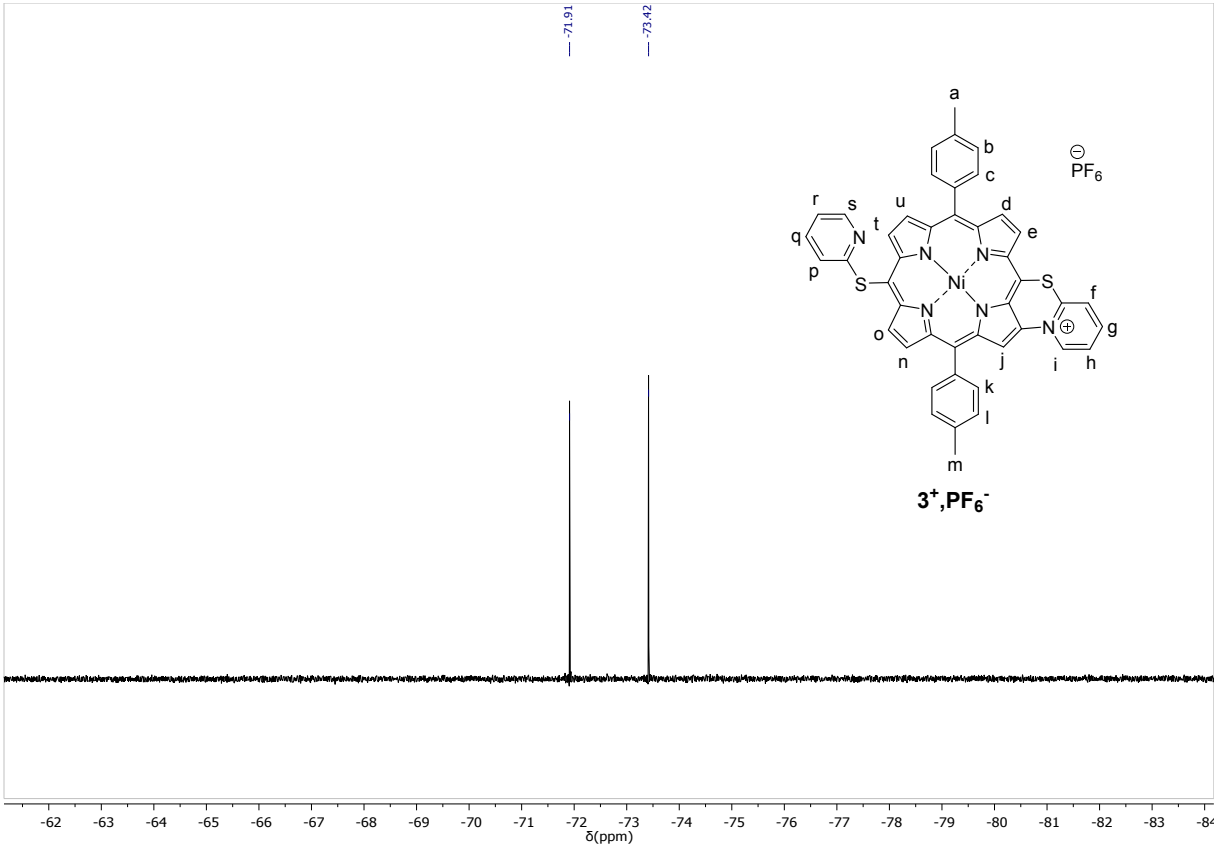

Figure S82. ^{19}F NMR spectrum of **3**$^{+}$**,PF**$_6^{-}$ in CD_3COCD_3, 470 MHz, 298 K.

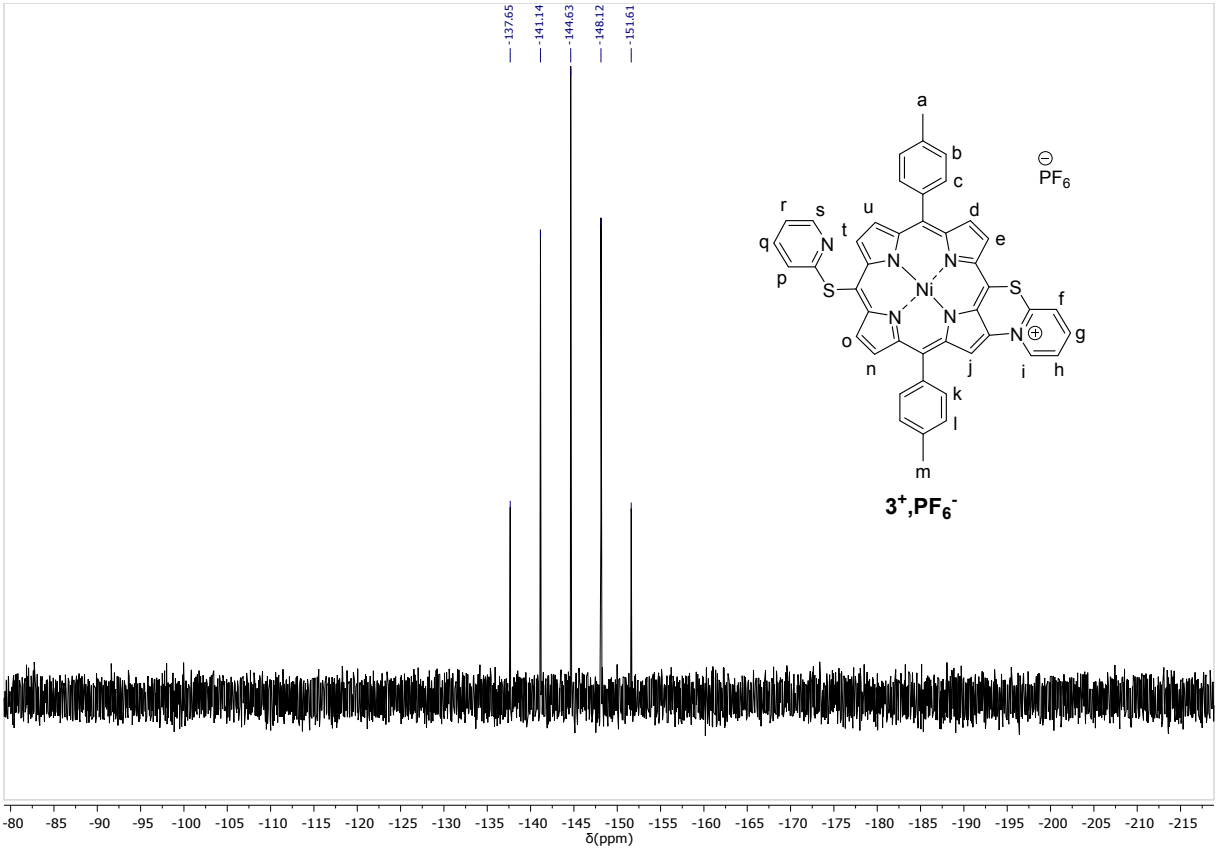

Figure S83. ^{31}P NMR spectrum of **3**$^{+}$**,PF**$_6^{-}$ in CD_3COCD_3, 202 MHz, 298 K.

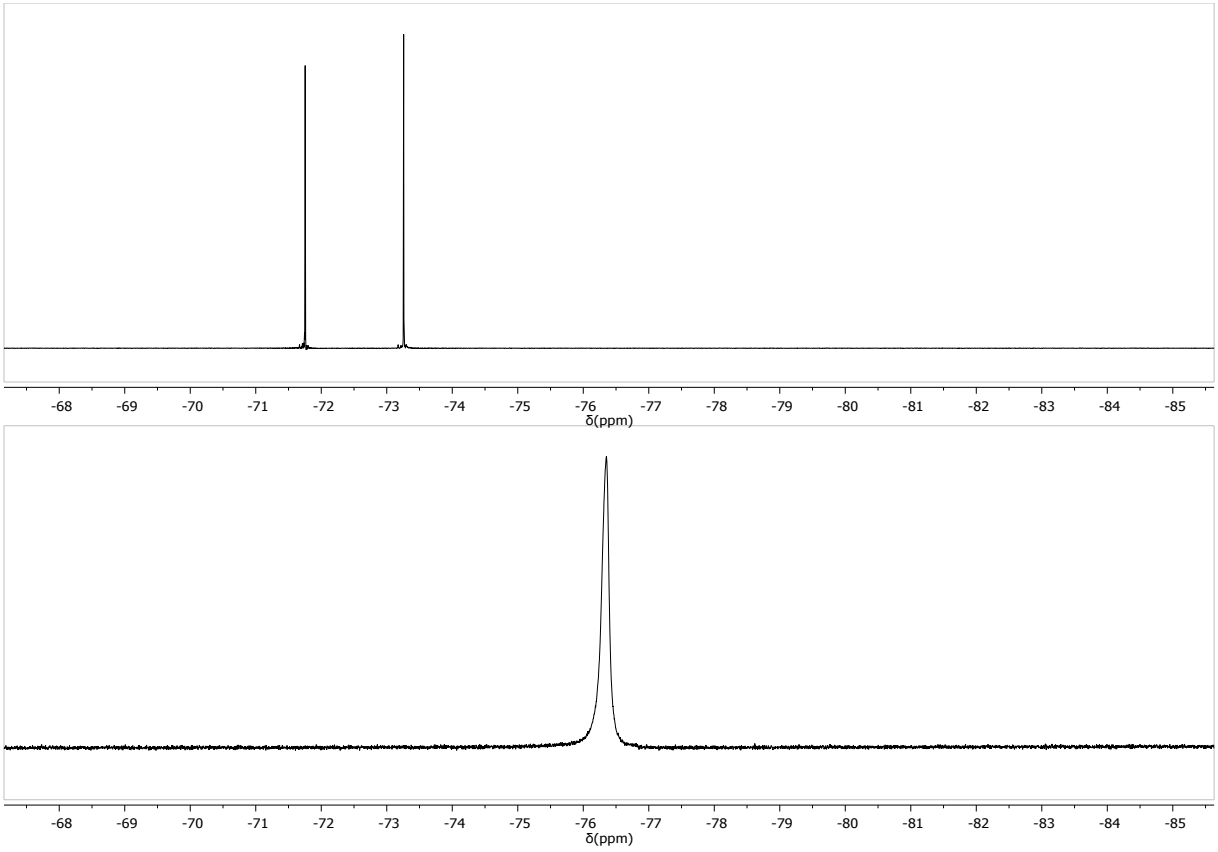

Figure S84. ^{19}F NMR before (**3**$^{+}$**,CF$_3$COO**$^{-}$ obtained from **3** using chemical oxidation with PIFA, bottom) and after (**3**$^{+}$**,PF$_6$**$^{-}$, top) ion exchange resin (CD_3COCD_3, 470 MHz, 298 K.).

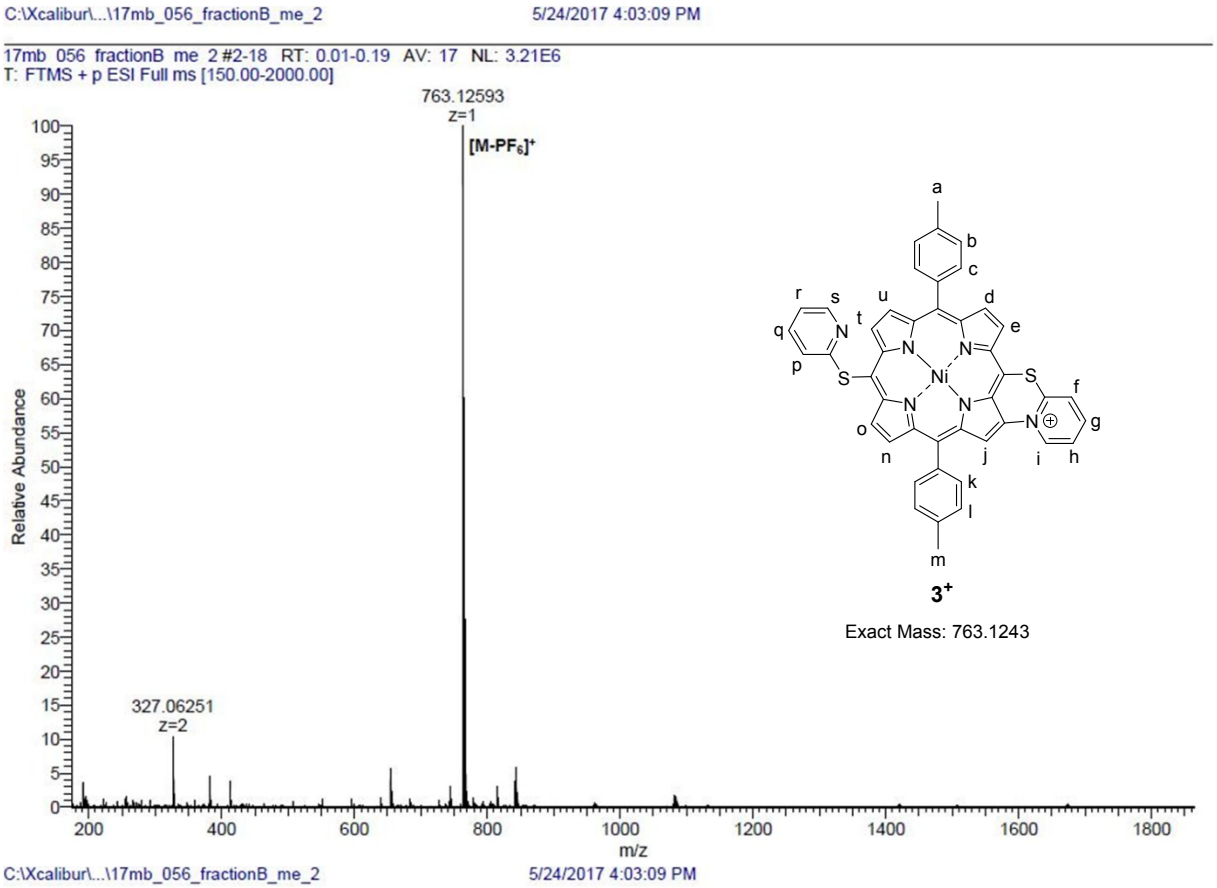

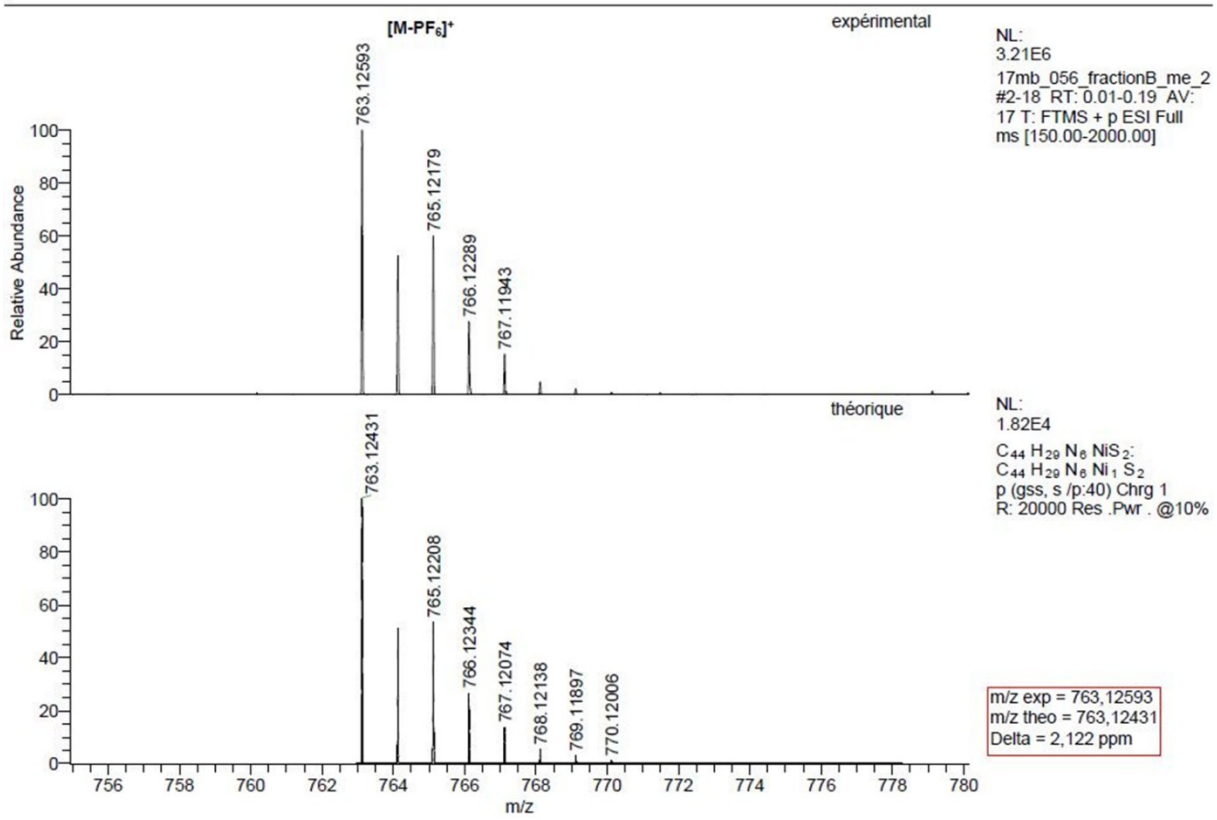

Figure S85. High resolution ESI mass spectrum of **3**$^{+}$,**PF**$_6^{-}$ and simulation of its isotopic pattern.

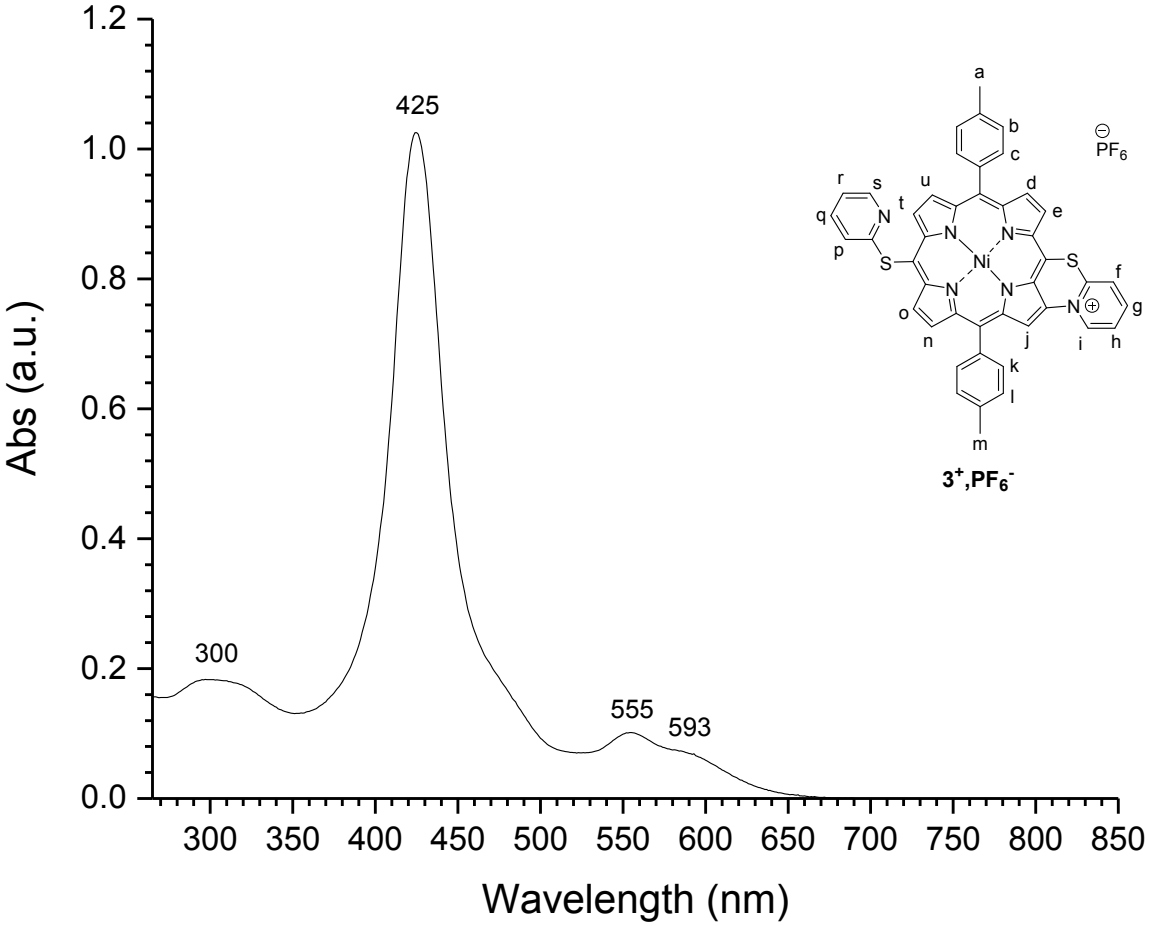

Figure S86. UV-Vis. absorption spectrum of $\mathbf{3^{+}}$,$\mathbf{PF_6^{-}}$ in CH_2Cl_2.

Compound anti-3^{2+},$(PF_6^-)_2$

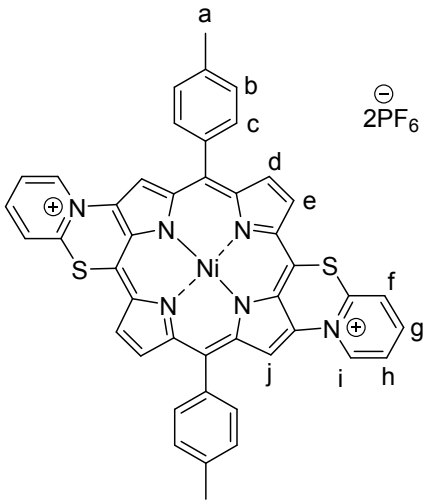

Chemical Formula: $C_{44}H_{28}F_{12}N_6NiP_2S_2$
Molecular Weight: 1053.4918

***anti*-3^{2+},$(PF_6^-)_2$**

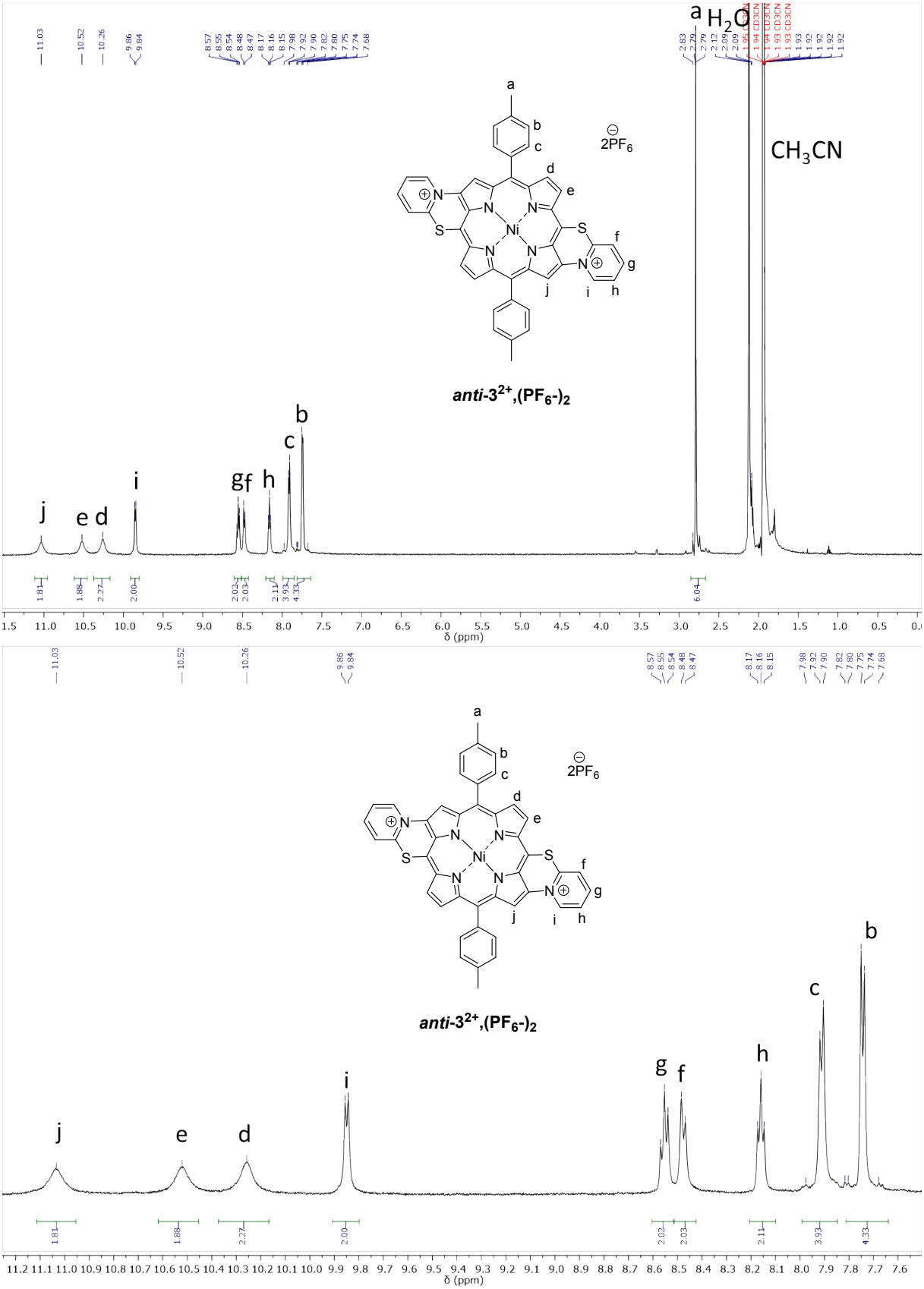

Figure S87. Full range (top) and partial (bottom) ^{1}H NMR spectra of ***anti*-3^{2+},(PF$_6^-$)$_2$**, in CD_3CN, 500 MHz, 298 K.

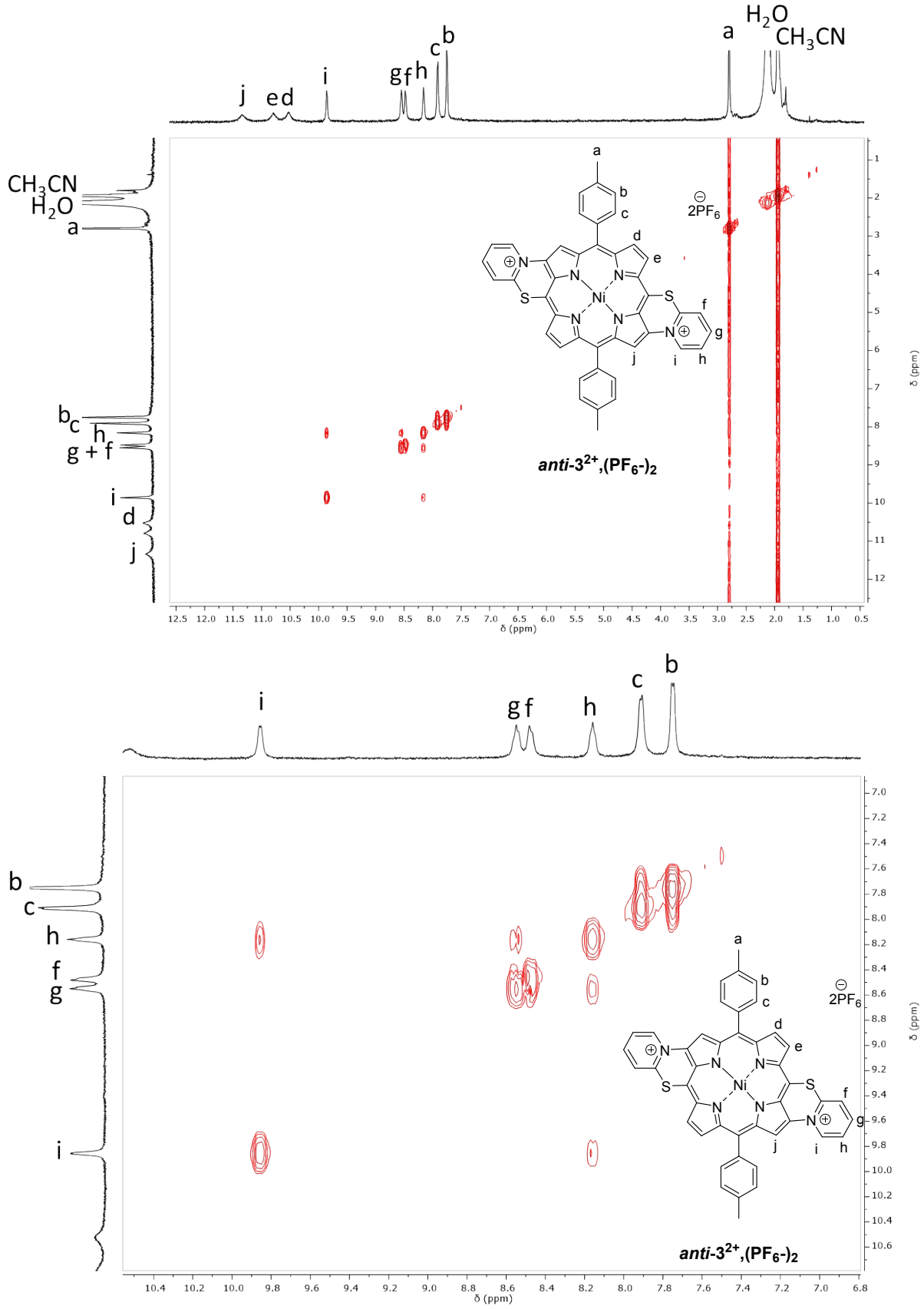

Figure S88. Full range (top) and partial (bottom) ^{1}H-^{1}H COSY NMR spectra of ***anti*-3^{2+},(PF$_6^-$)$_2$,** in CD$_3$CN, 500 MHz, 298 K.

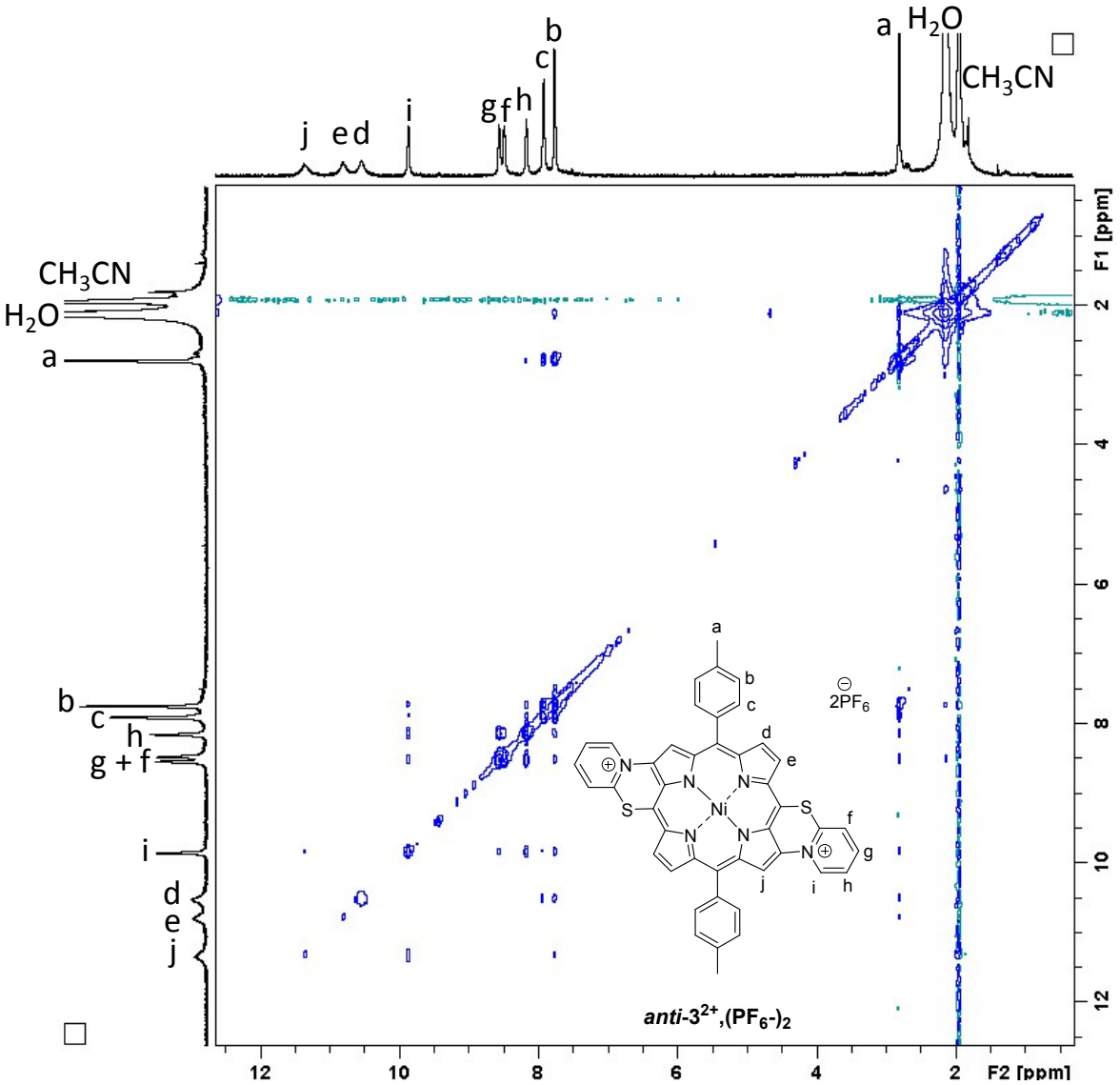

Figure S89. Full range ^{1}H-^{1}H NOESY NMR spectra of ***anti*-3^{2+},(PF$_6^-$)$_2$**, in CD_3CN, 500 MHz, 298 K.

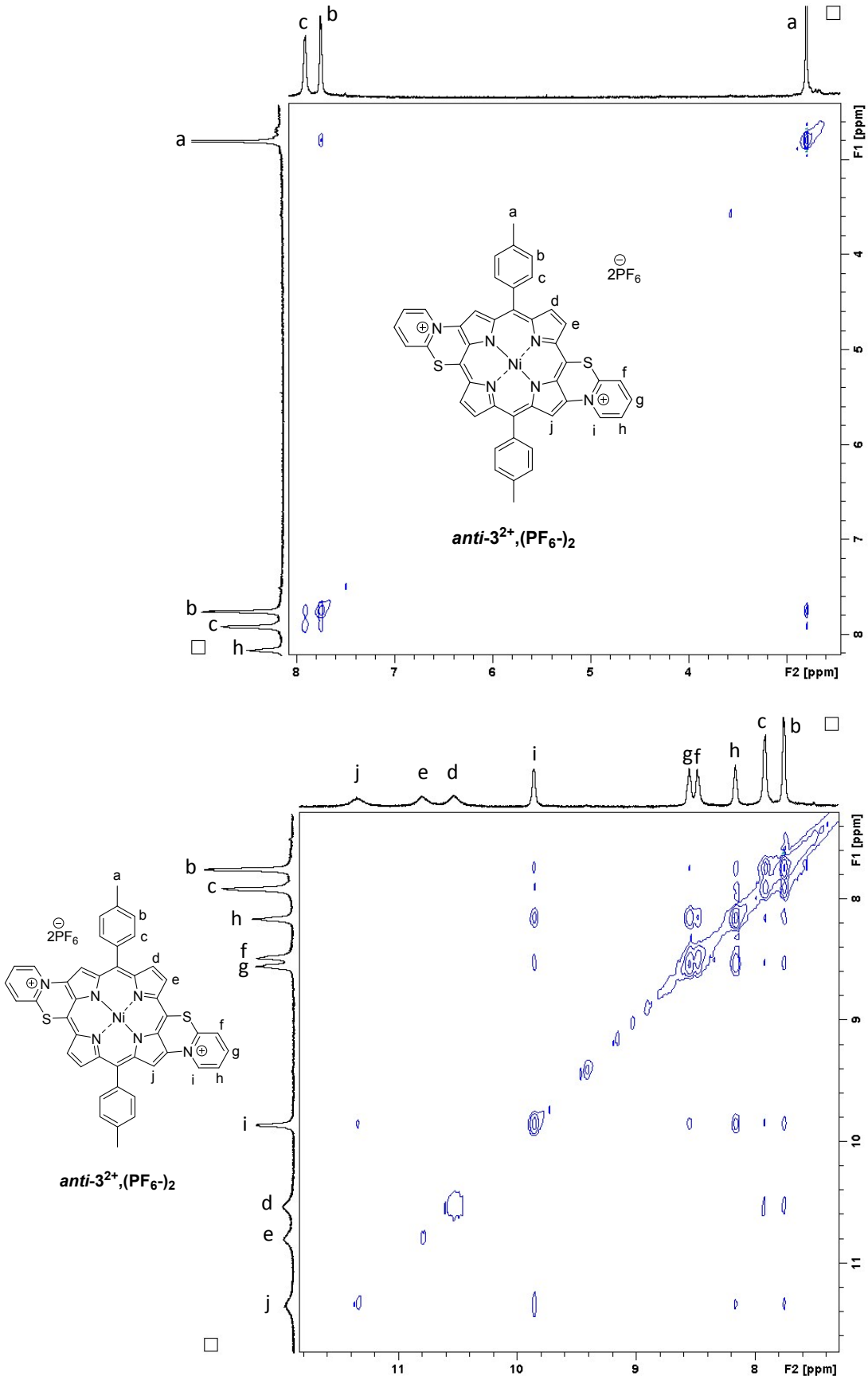

Figure S 90. Partial ^{1}H-^{1}H NOESY NMR spectra of ***anti*-3^{2+},(PF$_6^-$)$_2$**, in CD_3CN, 500 MHz, 298 K.

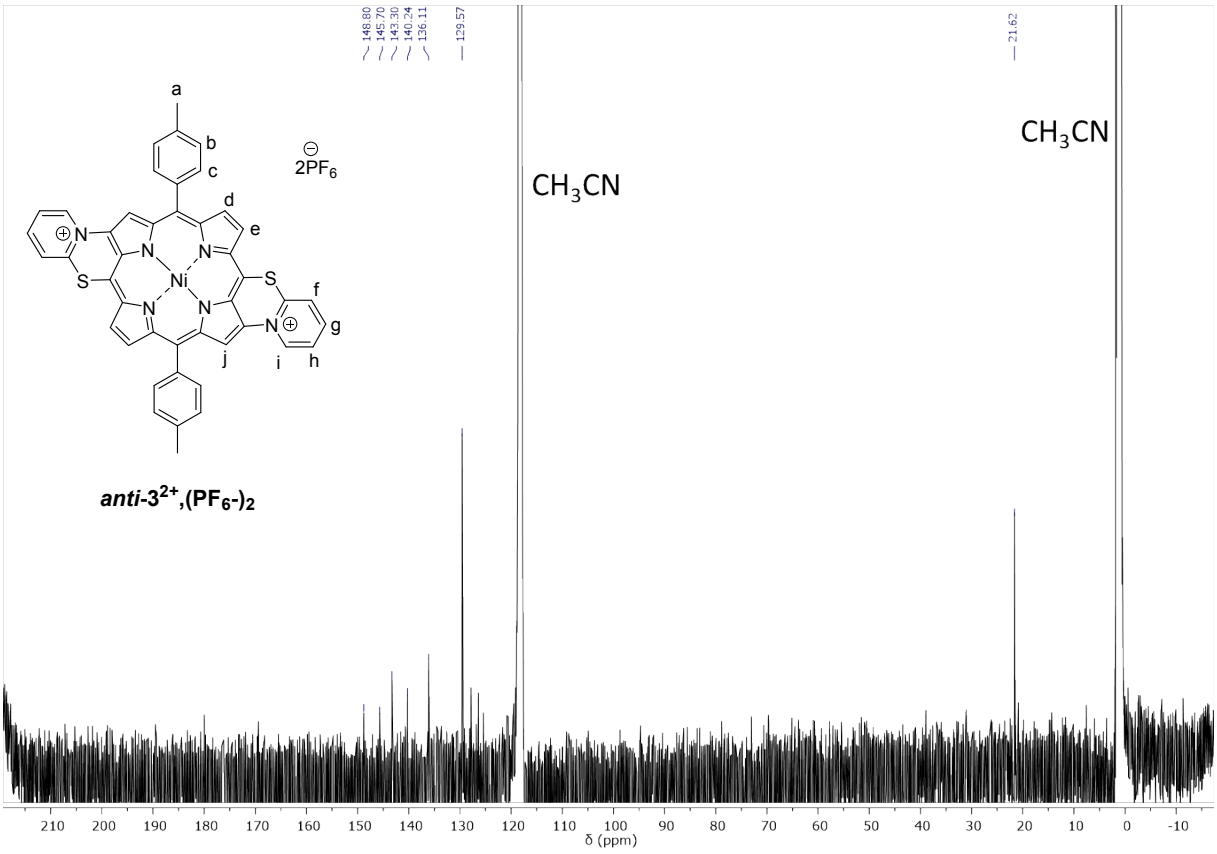

Figure S91. Full range ^{13}C NMR spectrum of ***anti*-3^{2+},(PF$_6^-$)$_2$**, in CD_3CN, 126 MHz, 298 K.

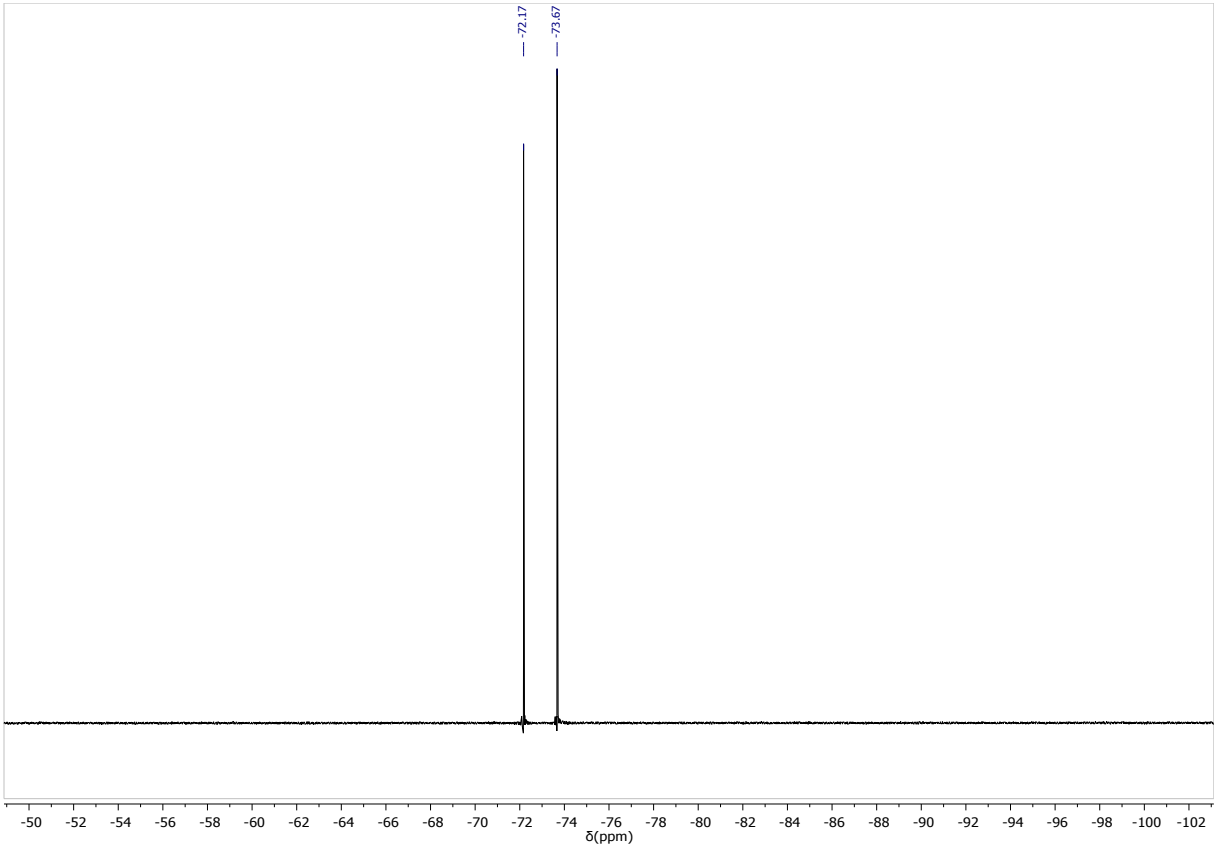

Figure S92. ^{19}F NMR spectrum of ***anti*-3^{2+},(PF$_6^-$)$_2$**, in CD_3CN, 470 MHz, 298 K.

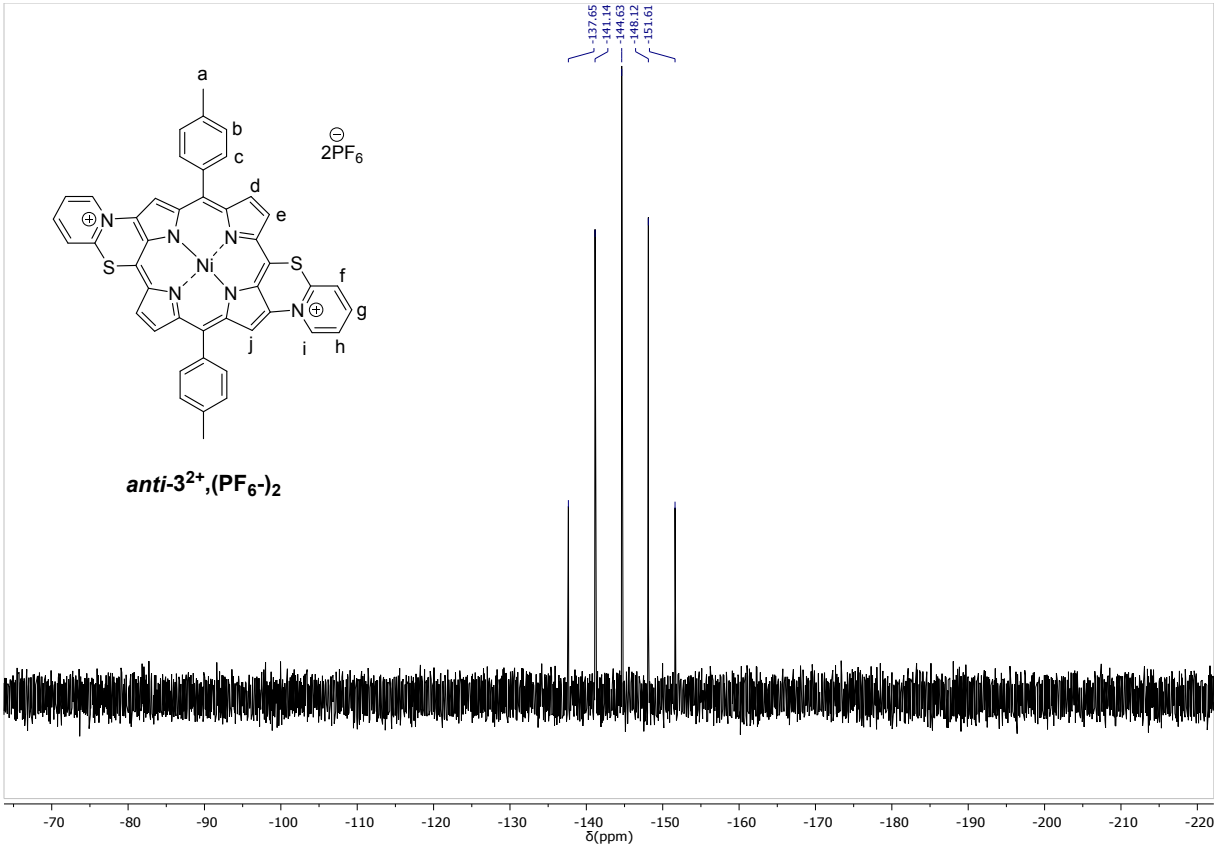

Figure S93. ^{31}P NMR spectrum of ***anti*-3^{2+},(PF$_6^-$)$_2$**, in CD_3CN, 202 MHz, 298 K.

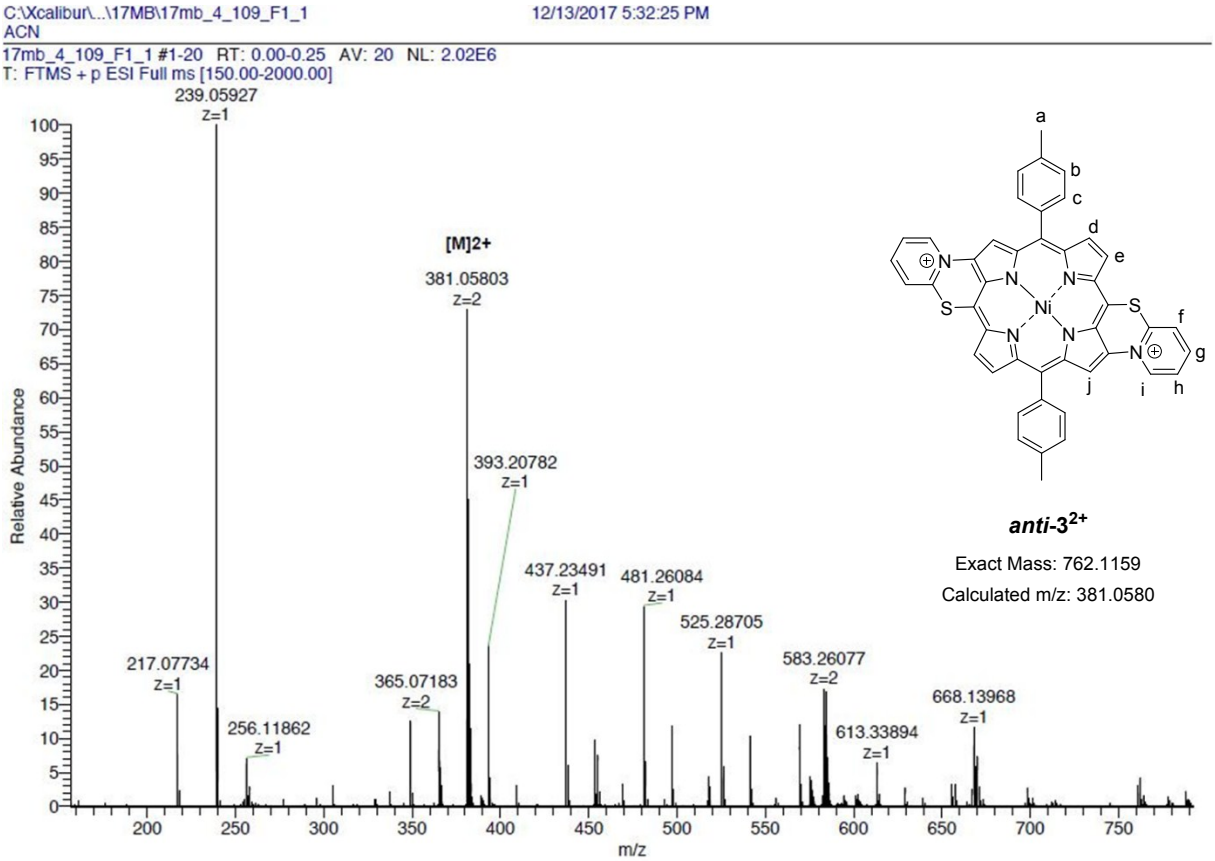
C:\Xcalibur\...\17MB\17mb_4_109_F1_1
12/13/2017 5:32:25 PM
ACN
17mb_4_109_F1_1 #1-20 RT: 0.00-0.25 AV: 20 NL: 2.02E6
T: FTMS + p ESI Full ms [150.00-2000.00]
239.05927 z=1
[M]2+
381.05803 z=2
393.20782 z=1
437.23491 z=1
481.26084 z=1
525.28705 z=1
583.26077 z=2
668.13968 z=1
613.33894 z=1
217.07734 z=1
256.11862 z=1
365.07183 z=2
Relative Abundance
m/z
anti-3²⁺
Exact Mass: 762.1159
Calculated m/z: 381.0580

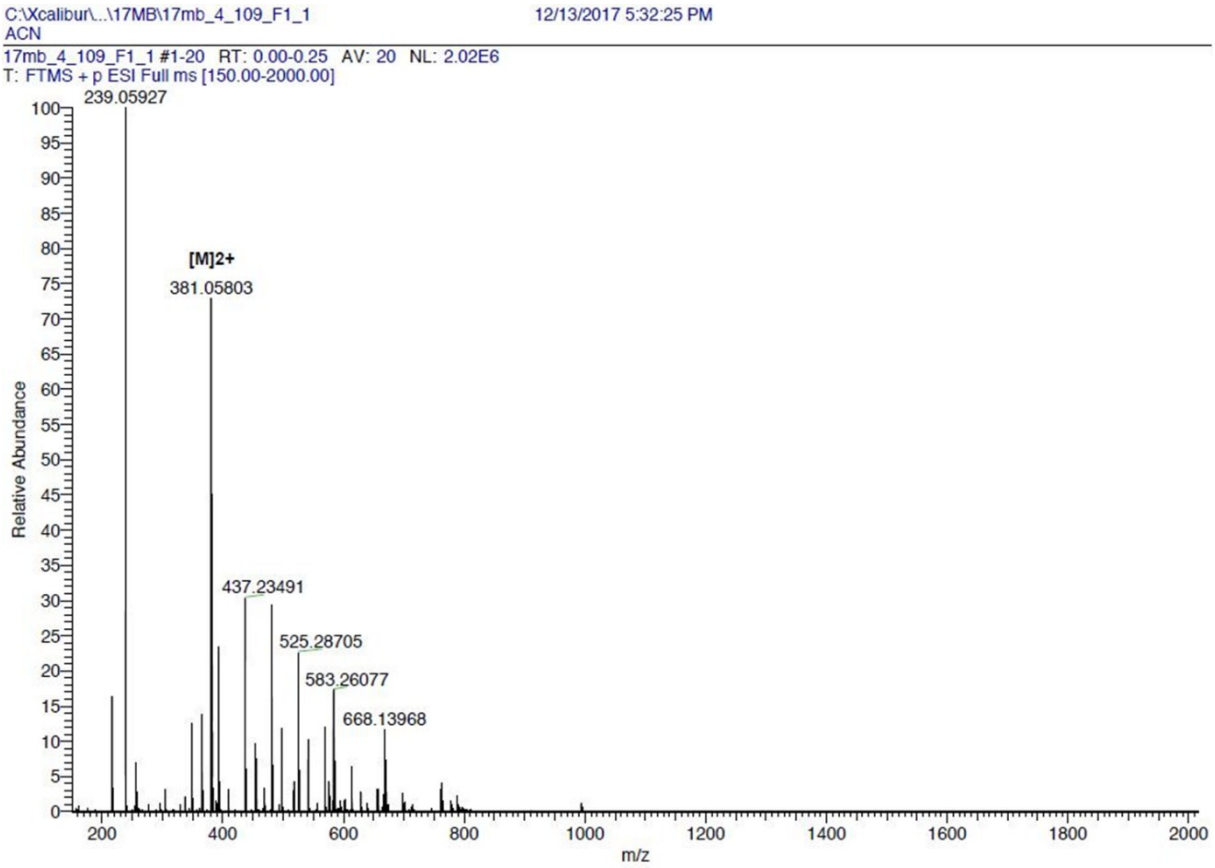
C:\Xcalibur\...\17MB\17mb_4_109_F1_1
12/13/2017 5:32:25 PM
ACN
17mb_4_109_F1_1 #1-20 RT: 0.00-0.25 AV: 20 NL: 2.02E6
T: FTMS + p ESI Full ms [150.00-2000.00]
239.05927
[M]2+
381.05803
437.23491
525.28705
583.26077
668.13968
Relative Abundance
m/z

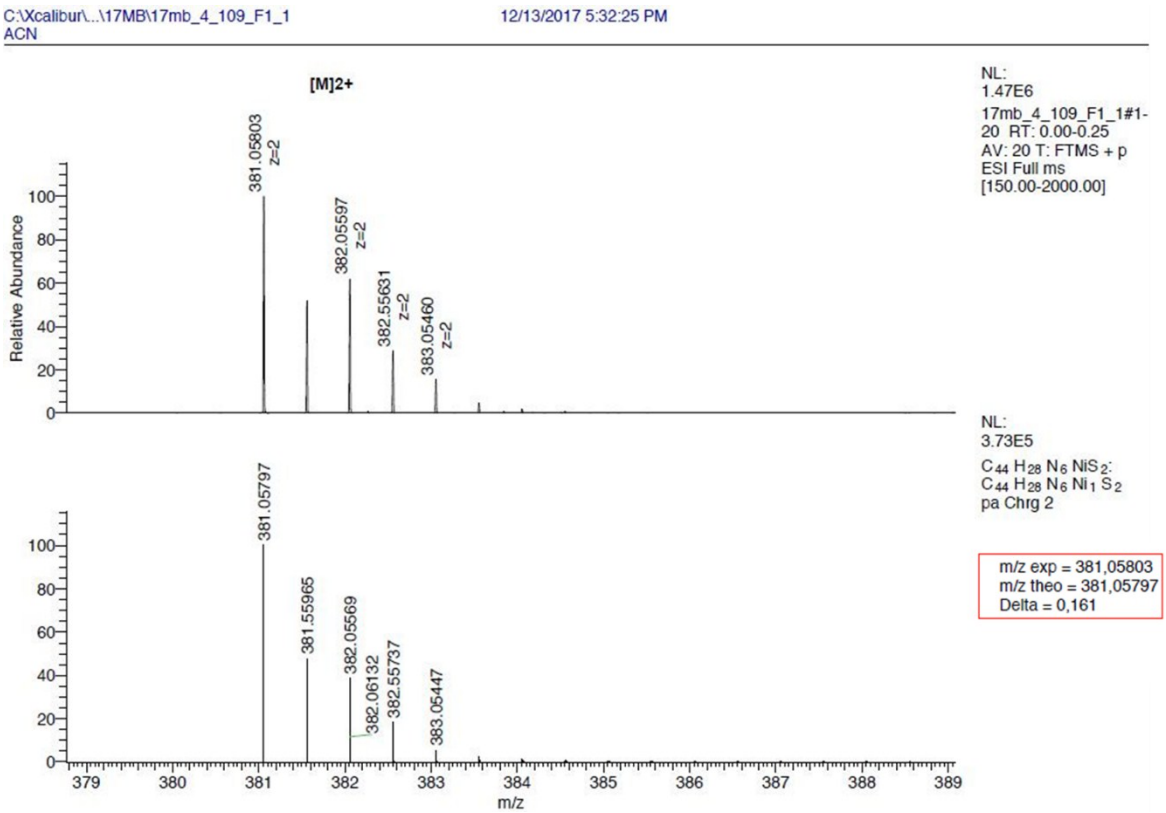

Figure S94. High resolution ESI mass spectra of ***anti*-3^{2+},(PF$_6^-$)$_2$** and simulation of its isotopic pattern.

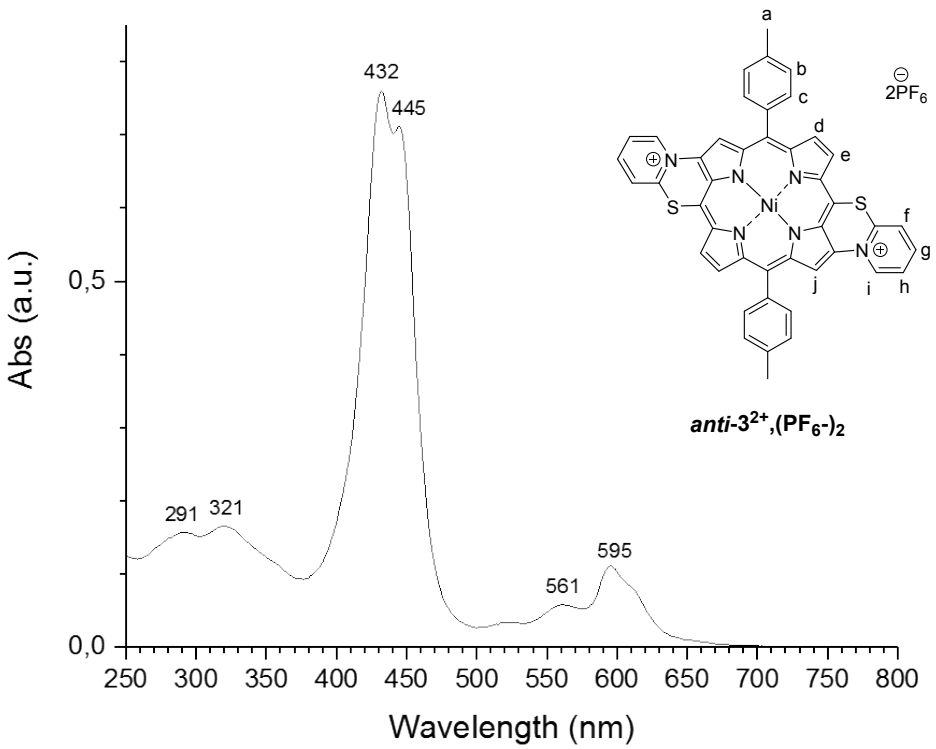

Figure S95. UV-Visible absorption spectrum of ***anti*-3^{2+},(PF$_6^-$)$_2$**, in CH_3CN.

Crystallographic data for 1, 2 and 1_{fus}^{+},PF_6^{-}

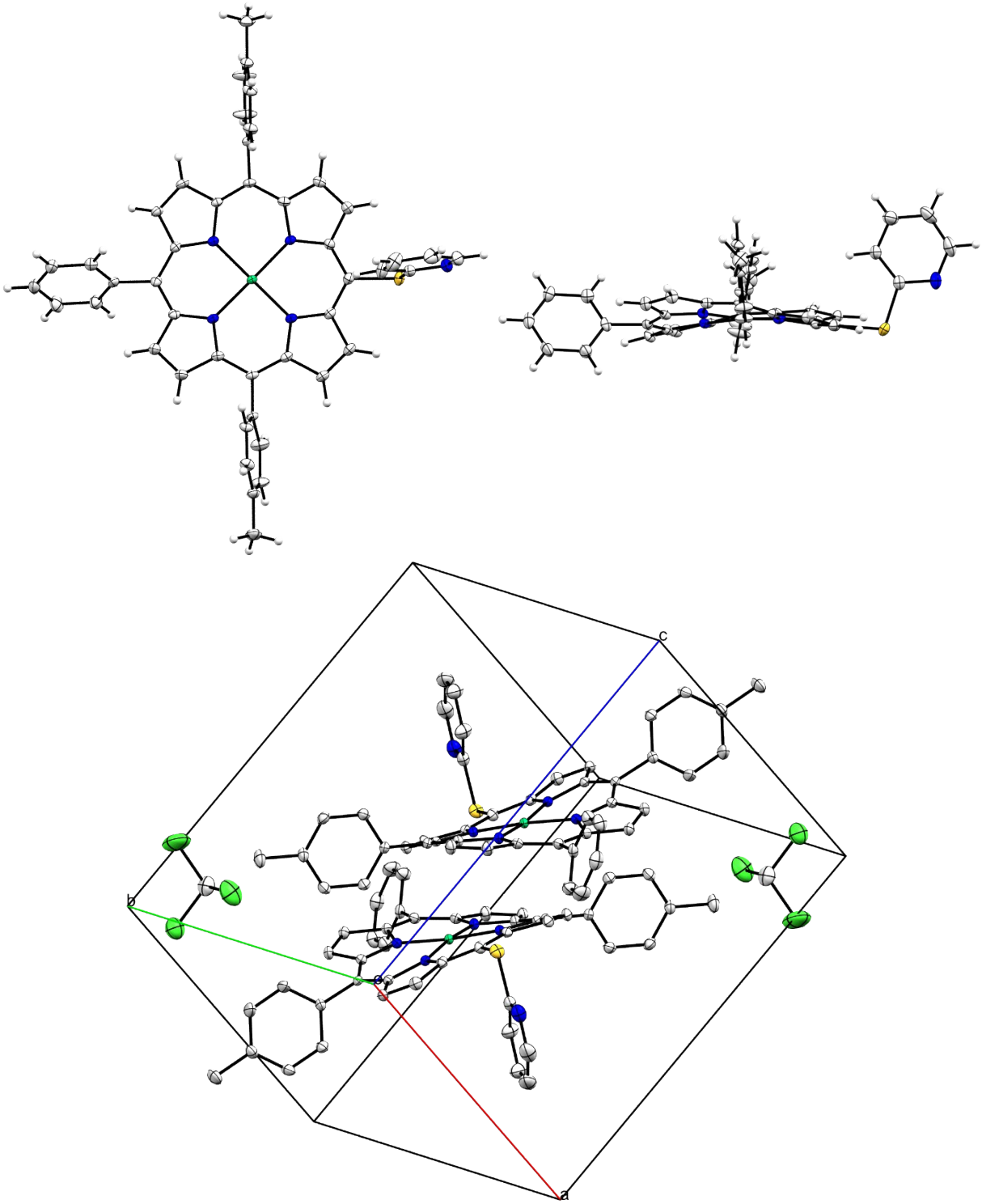

Figure S96. Front, side (top) and packing (bottom) Mercury views of **1**. In the packing view, H atoms are omitted for clarity. Thermal ellipsoids are scaled to the 50% probability level.

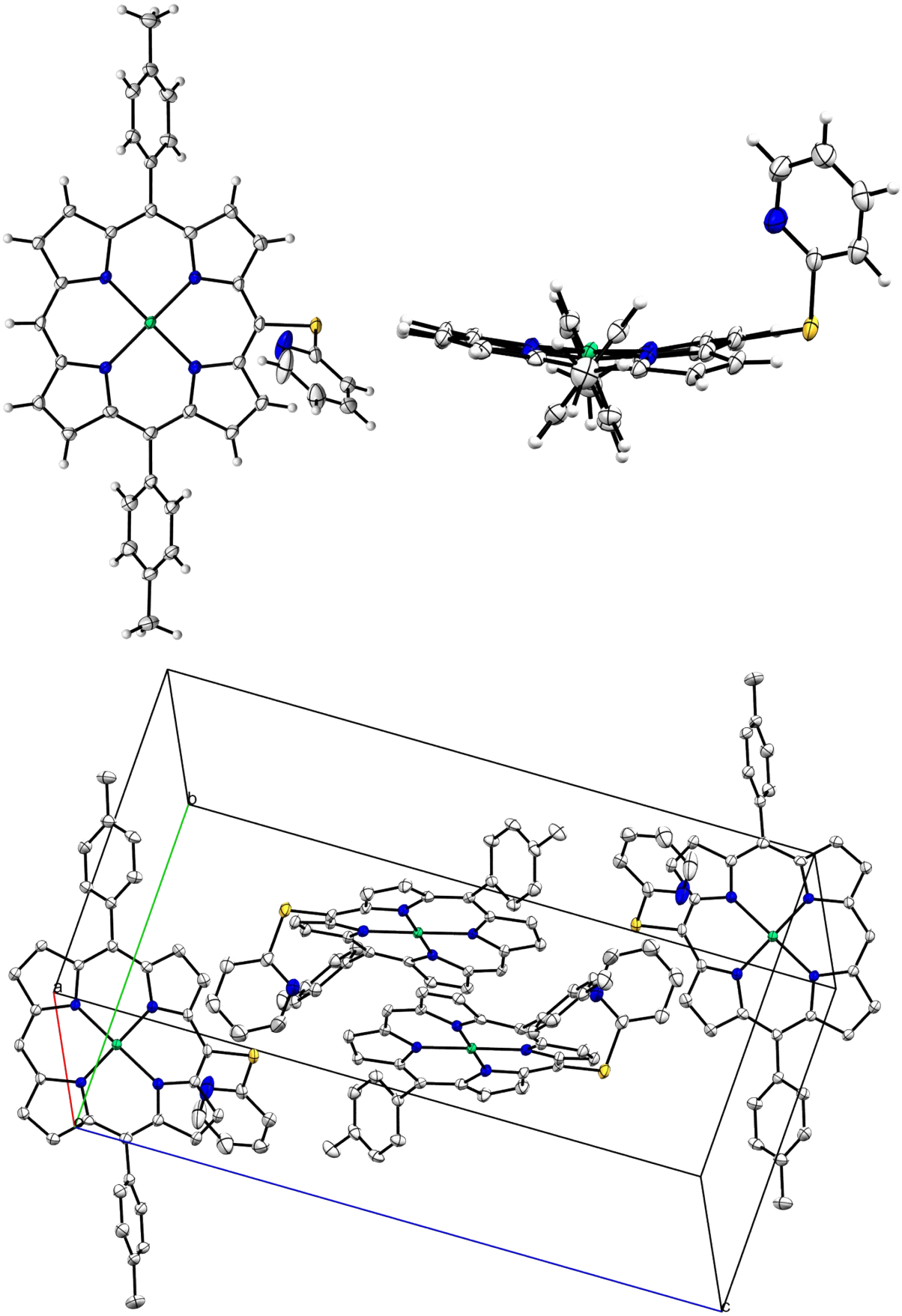

Figure S97. Front, side (top) and packing (bottom) Mercury views of **2**. In the packing view, H atoms are omitted for clarity. Thermal ellipsoids are scaled to the 50% probability level.

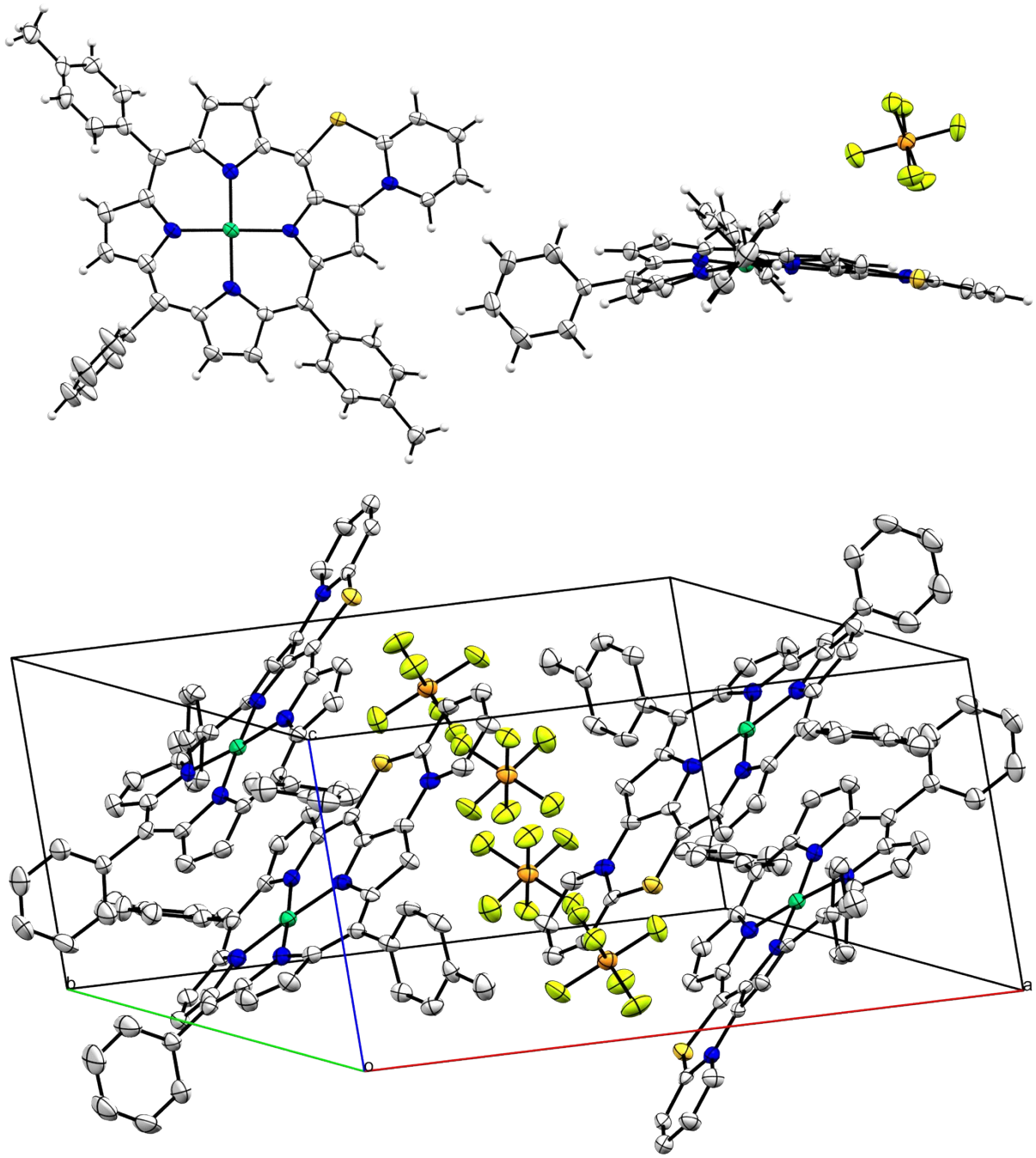

Figure S98. Front, side (top) and packing (bottom) Mercury views of $\mathbf{1_{fus}^{+}}$**,**$\mathbf{PF_6^{-}}$ (top). In the packing view, H atoms are omitted for clarity. Thermal ellipsoids are scaled to the 50% probability level.

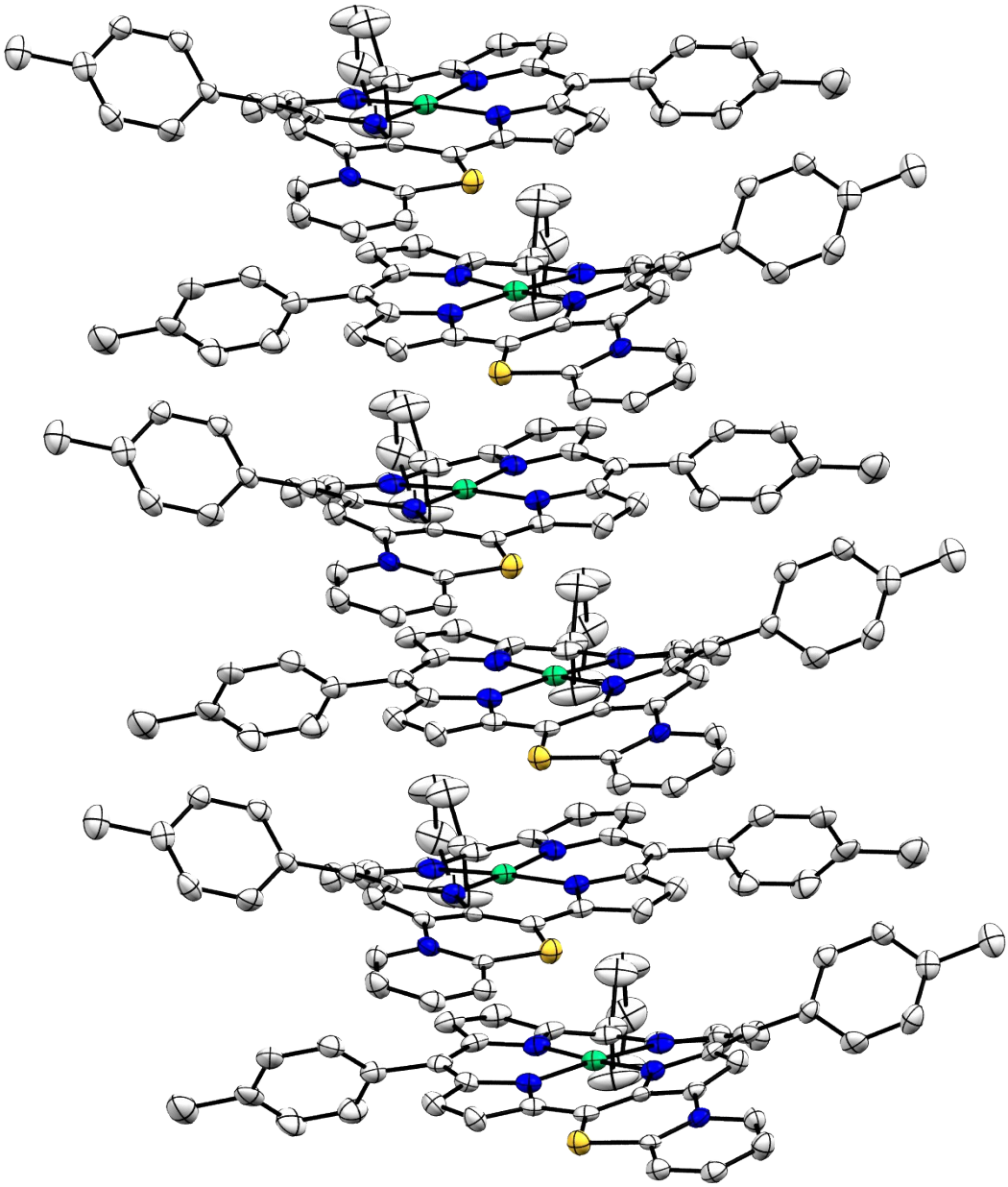

Figure S99. Mercury view of the infinite 1D network formed by π-stacked $\mathbf{1}_{fus}^{+}$,$\mathbf{PF_6}^{-}$ molecules. Hydrogen atoms were omitted for clarity. Thermal ellipsoids are scaled to the 50% probability level.

CCDC	**1557313** (compound **1**)	**1557314** (compound **2**)	**1813003** (compound $\mathbf{1_{fus}^{+}}$,$\mathbf{PF_6^{-}}$)
Formula	$C_{46}H_{32}Cl_3N_5NiS$	$C_{39}H_{27}N_5NiS$	$C_{45}H_{30}F_6N_5NiPS$
$D_{calc.}$/ g cm^{-3}	1.485	1.370	1.557
μ/mm^{-1}	0.817	0.712	0.691
Formula Weight	851.88	656.42	876.48
Colour	red	dark violet	red
Shape	needle	needle	prism
Size/mm^3	0.35×0.28×0.10	0.30×0.20×0.08	0.43×0.38×0.08
T/K	100	100	150
Crystal System	triclinic	monoclinic	monoclinic
Space Group	P-1	$P2_1/c$	$P2_1/c$
a/Å	10.2159(6)	10.9758(9)	19.386(3)
b/Å	14.3590(8)	12.6253(10)	20.956(3)
c/Å	15.0898(8)	23.0050(18)	9.2559(16)
α/°	113.223(2)	90	90
β/°	103.443(2)	93.015(2)	96.226(5)
γ/°	98.599(2)	90	90
V/Å^3	1905.05(19)	3183.5(4)	3738.0(11)
Z	2	4	4
Z'	1	1	1
Wavelength/Å	0.71073	0.71073	0.71073
Radiation type	MoK$_\alpha$	MoK$_\alpha$	MoK$_\alpha$
Θ_{min}/°	2.872	2.976	3.048
Θ_{max}/°	27.702	27.592	25.055
Measured Refl.	98012	54545	30651
Independent Refl.	8844	7337	6587
Reflections Used	7197	5506	3492
R_{int}	0.0556	0.0713	0.1438
Parameters	544	417	534
Restraints	36	0	0
Largest Peak	1.501	0.603	0.793
Deepest Hole	-0.711	-0.500	-0.559
GooF	1.041	1.049	0.995
wR_2 (all data)	0.1134	0.1249	0.1297
wR_2	0.1022	0.1119	0.1024
R_1 (all data)	0.0627	0.0825	0.1451
R_1	0.0443	0.0540	0.0566

Table S2. Crystal data and structure refinement

Computational Details

Quantum mechanics calculations were performed with the Gaussian09 software package. [7] Energy and forces were computed by density functional theory with the hybrid B3PW91 exchange-correlation functional. The solvent effects were modelled using a polarizable continuum model[8] (PCM) as implemented in Gaussian09 to describe the bulk medium. Transition states were localized using the string theory as implemented in Opt'n Path.[9] Geometries were optimized and characterized with the 6-31+G(d,p) basis sets for all atoms. Frequency calculations were performed to ensure the absence of any imaginary frequencies on local minima, and the presence of only one imaginary frequency on transition states. Gibbs free energies were computed at 298K, 1 atm. using the electronic energies and frequencies computed at the 6-31+G(d,p) level.
The transition state energy for the intramolecular nucleophilic addition in **1** was recomputed at the B3PW91/6-311++G(2df,2p) level on the B3PW91/6-31+G(d,p) geometry to get an accurate free energy barrier.

The standard redox potential were estimated in two steps. First, they were computed using the thermodynamic relationship :

$$\Delta_r G^\circ = -nFE^\circ$$

in which n is the number of exchanged electron, F is the Faraday (=96485.3 C), $\Delta_r G^\circ$ is the standard Gibbs free energy and E° is the standard redox potential. This leads to an absolute redox potential that should then be corrected by the redox potential of the reference electrode.[10] However, we discovered that this procedure lead to an overestimation of the O_3 and O_4 redox steps. This might be due to our approximate way of taking into account the solvent effects, or to the fact that the link between the computed standard potential and the peak potential deviates from the usual 59/n mV shift, or to the charge accumulations on the molecules generated by these oxidation.
As we are mostly interested in estimating the 'hidden' oxidation steps O_A and O_B we decided to fit the theoretical values onto the measured pic potentials, and to use this fit to evaluate the values for the hidden oxidation potentials.

Oxidation of 1

Two mechanisms for the fusion and oxidation of the fused compound were studied, as depicted on Scheme S1. In the first one, the intramolecular nucleophilic addition proceeds directly on the cation radical $\mathbf{1}^{+\bullet}$ which is then oxidized into $\mathbf{1}_{\mathbf{fus}}^{2+}$. On the other hand, the cation radical $\mathbf{1}^{+\bullet}$ could be also be oxidized first into the dication $\mathbf{1}^{2+}$ which gives the fused $\mathbf{1}_{\mathbf{fus}}^{2+}$ molecule by an intramolecular nucleophilic addition.

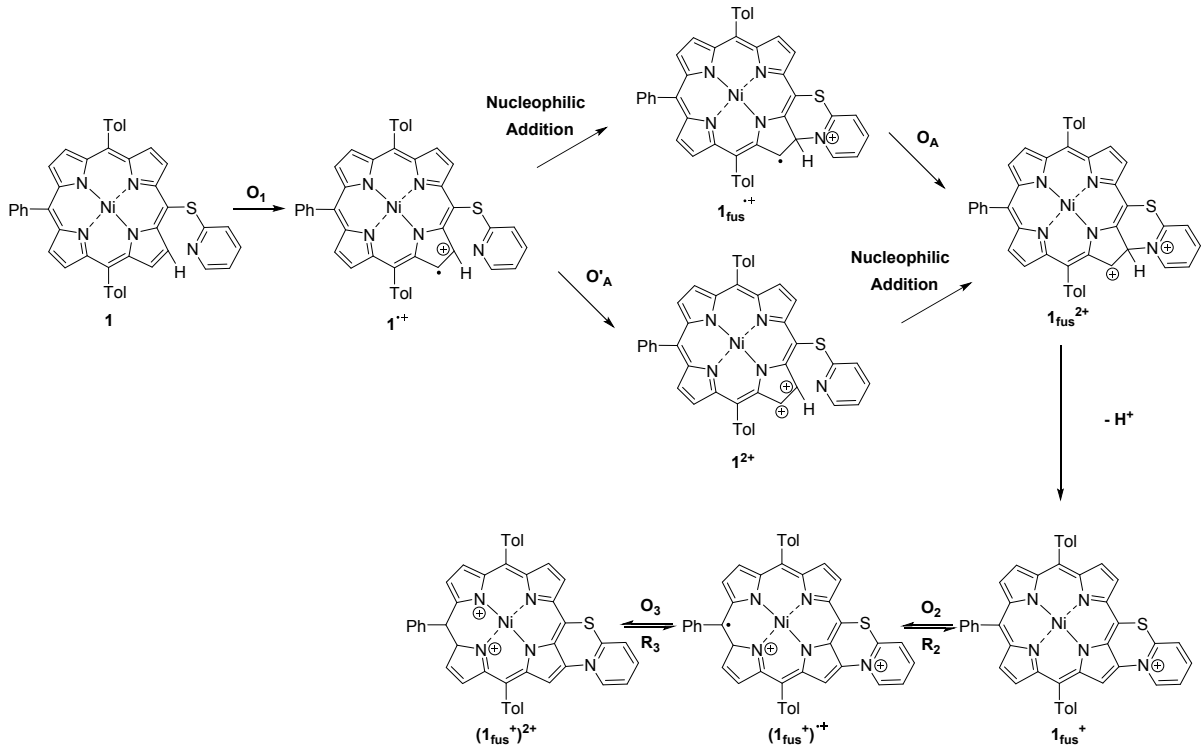

Scheme S1. Two possible paths for the oxidation and fusion of **1**.

The experimental values, raw theoretical values and adjusted theoretical values for the redox potentials are given in Table S3.

Table S3. Experimental, raw theoretical and adjusted redox potentials starting from **1**. (a) in V (b) Fit equation: $E_{pa}^{th} = 0.519 \times E(\text{B3PW91/6 - 31 + G(d,p)}) - 1.844_{\text{V}}$.

	$O_{1(a)}$	$O_{2(a)}$	$O_{3(a)}$	$O_{A(a)}$	$O'_{A(a)}$
Experiment (*vs.* SCE)	1.03	1.19	1.40	-	-
raw B3PW91 6-31+G(d,p)	5.56	5.81	6.71	5.39	5.83
Adjusted B3PW91 6-31+G(d, p) (*vs.* SCE)	1.04[(b)]	1.17	1.41	0.96	1.18

According to these theoretical redox potentials, the second path is unlikely, as it would proceed through an oxidation peak around $E_{pa}^{th}(O'_A) = 1.18$V that could be experimentally measured between O_2 and O_3. On the contrary, the intermediate oxidation O_A is hidden as it occurs at a potential lower than O_1: $E_{pa}^{th}(O_A) = 0.96$V *vs.* $E_{pa}^{th}(O_1) = 1.04$V.

To further confirm this, we have computed activation free energy for the nucleophilic addition from $\mathbf{1}^{+\bullet}$ to $\mathbf{1_{fus}}^{+\bullet}$: $\Delta_r G^{\#} = 12.8$ kcal/mol, corresponding to a kinetic constant k=2529.1 mol^{-1} L s^{-1}, in fair agreement with the ECEC mechanism.

Structure of the transition state is given in Figure S100.

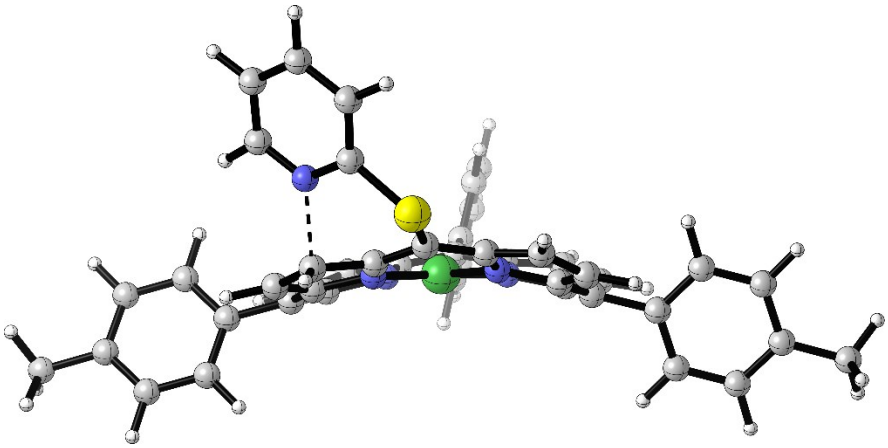

Figure S100. Structure of the intramolecular nucleophilic addition transition state from $\mathbf{1}^{+\bullet}$ to $\mathbf{1}_{\mathbf{fus}}^{+\bullet}$.

Oxidation of 2

The mechanism for the oxidation and fusion of **2** is depicted in Scheme S2. Experimental and computed redox potentials are gathered in **Erreur ! Source du renvoi introuvable.**.

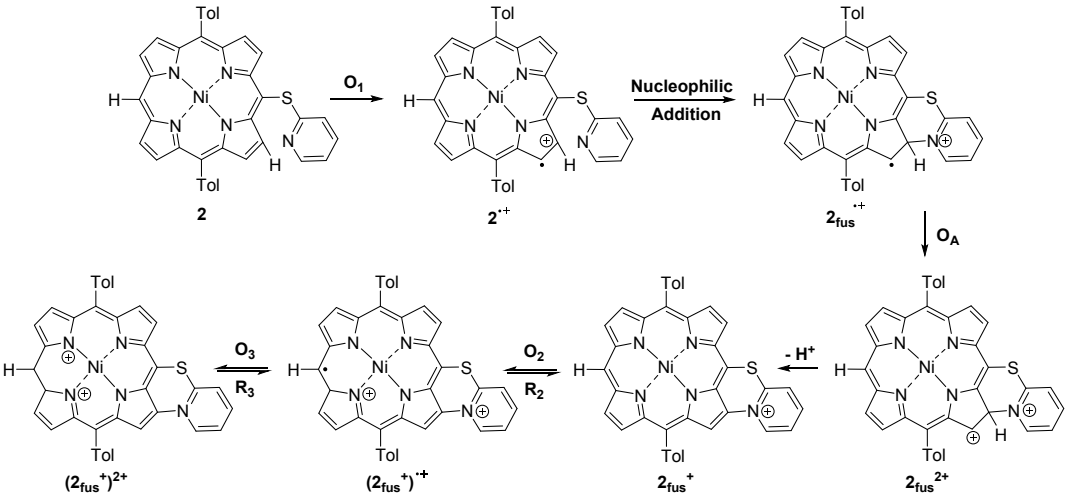

Scheme S2. Mechanism for the oxidation and fusion of **2**.

Table S4. Experimental, raw theoretical and adjusted redox potentials starting from **2**. (a) in V (b) Fit equation: $E_{pa}^{th} = 0.378 \times E(\text{B3PW91/6 - 31 + G(d,p)}) - 1.047_{\text{V}}$.

	$O_{1(a)}$	$O_{2(a)}$	$O_{3(a)}$	$O_{A(a)}$	$O'_{A(a)}$
Experiment (*vs.* SCE)	1.04	1.20	1.37	-	-
raw B3PW91/6-31+G(d,p)	5.47	5.96	6.44	5.37	5.87
Adjusted B3PW91/6-31+G(d, p) (*vs.* SCE)	1.02[(b)]	1.21	1.39	0.98	1.17

Again, the intermediate oxidation O_A is hidden as it occurs at lower potential than O_1: $E_{pa}^{th}(O_A)$ = 0.98V *vs.* $E_{pa}^{th}(O_1)$ = 1.02V.

Oxidation of 3

The mechanism for the oxidation and fusion of **3** is depicted in Scheme S3. Experimental and computed redox potentials are gathered in **Erreur ! Source du renvoi introuvable.**.

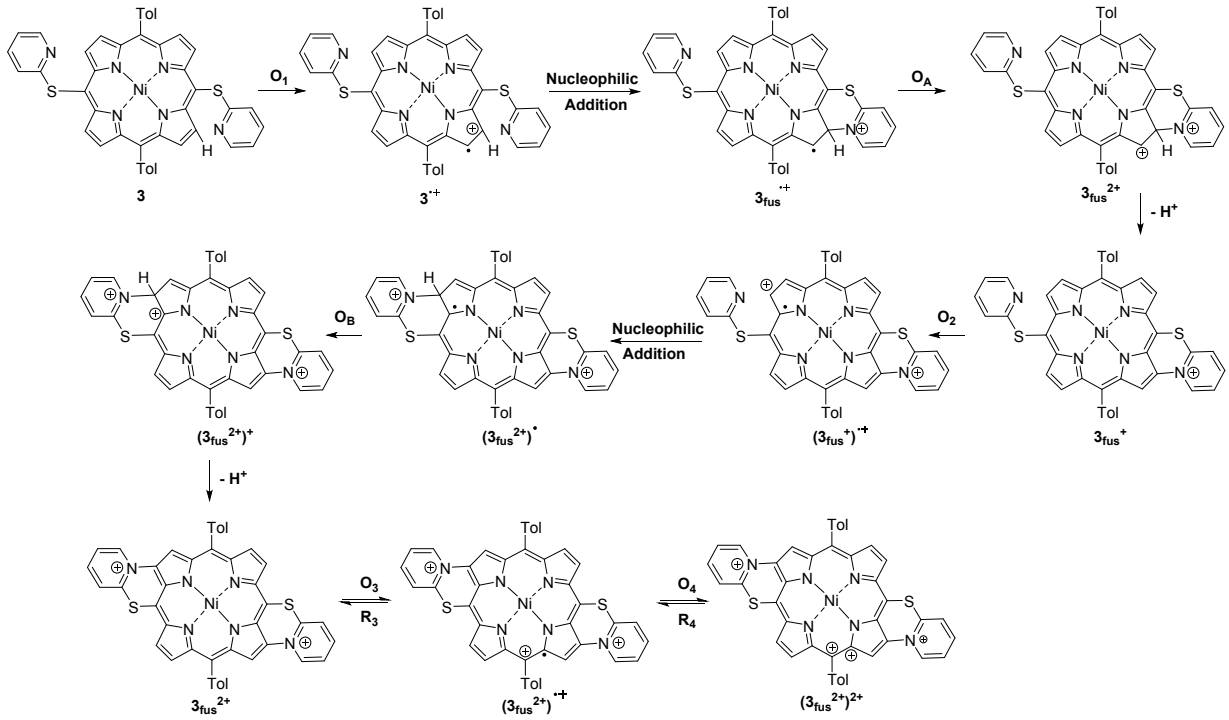

Scheme S3. Mechanism for the oxidation and fusion of **3**.

Table S5. Experimental, raw theoretical and adjusted redox potentials starting from **3**. (a) in V (b) Fit equation: $E_{pa}^{th} = 0.321 \times E(\text{B3PW91/6 - 31 + G(d,p)}) - 0.655_{\text{V}}$.

	$O_{1(a)}$	$O_{2(a)}$	$O_{3(a)}$	$O_{4(a)}$	$O_{A(a)}$	$O_{B(a)}$
Experiment (*vs.* SCE)	1.13	1.24	1.37	1.43	-	-
raw B3PW91/6-31+G(d,p)	5.61	5.95	6.13	6.58	5.37	5.84
Adjusted B3PW91/6-31+G(d, p) (*vs.* SCE)	1.13[(b)]	1.25	1.32	1.47	1.05	1.22

In this case, both O_A and O_B are hidden: $E_{pa}^{th}(O_A) = 1.05$V lower than $E_{pa}^{th}(O_1) = 1.13$V, and $E_{pa}^{th}(O_B) = 1.22$V lower than $E_{pa}^{th}(O_2) = 1.25_{\text{V}}$.

The singly occupied molecular orbital of the cation radical $\mathbf{3_{fus}}^{+\bullet}$ is shown in Figure S101.

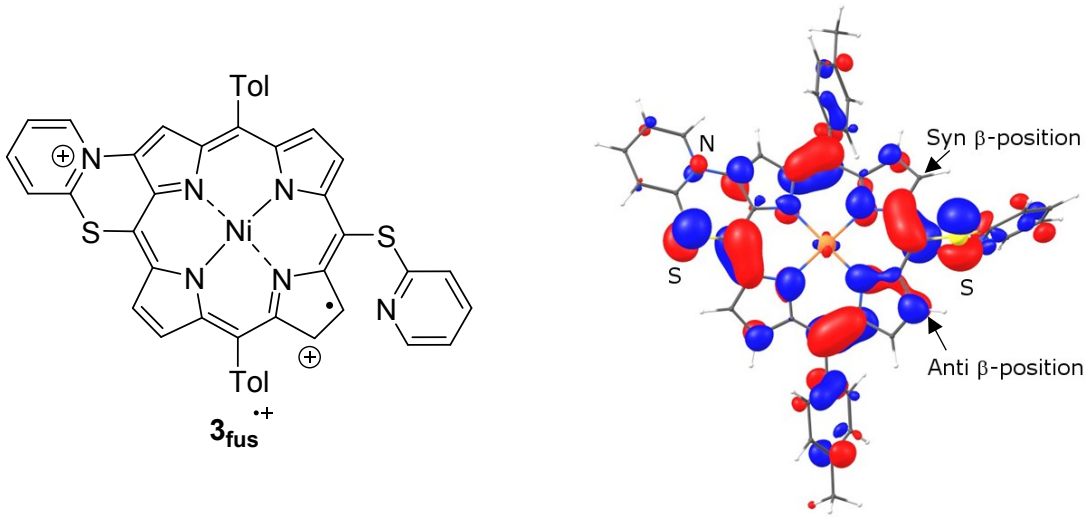

Figure S101. SOMO of the cation radical $\mathbf{3}_{\mathbf{fus}}^{+\bullet}$.

Table S6. Absolute energies and free energies of all compounds

Compound	Electronic Energy (Hartree)	Gibbs Free Energy (Hartree)
1	-3912.970836	-3912.408396
$\mathbf{1}^{+\cdot}$	-3912.766433	-3912.204135
$\mathbf{1}_{fus}^{+\bullet}$	-3912.766829	-3912.199630
$\mathbf{1}_{fus}^{2+}$	-3912.574357	-3912.001388
$\mathbf{1}_{fus}^{+}$	-3912.199330	-3911.641911
$(\mathbf{1}_{fus}^{+})^{+\bullet}$	-3911.988165	-3911.428411
$(\mathbf{1}_{fus}^{+})^{2+}$	-3911.745530	-3911.181725
$\mathbf{1}^{2+}$	-3912.544961	-3911.979802
2	-3681.994880	-3681.508407
$\mathbf{2}^{+\bullet}$	-3681.794843	-3681.307413
$\mathbf{2}^{2+}$	-3681.568746	-3681.077055
$\mathbf{2}_{fus}^{+\bullet}$	-3681.789764	-3681.296878
$\mathbf{2}_{fus}^{2+}$	-3681.596328	-3681.099622
$\mathbf{2}_{fus}^{+}$	-3681.224380	-3680.740093
$(\mathbf{2}_{fus}^{+})^{+\bullet}$	-3681.006618	-3680.521159
$(\mathbf{2}_{fus}^{+})^{2+}$	-3680.749392	-3680.266205
3	-4327.136016	-4326.587535
$\mathbf{3}^{+\cdot}$	-4326.928739	-4326.381281
$\mathbf{3}_{fus}^{+\bullet}$	-4326.931081	-4326.378754
$\mathbf{3}_{fus}^{2+}$	-4326.738205	-4326.181213
$\mathbf{3}_{fus}^{+\bullet}$	-4326.364361	-4325.822009
$(\mathbf{3}_{fus}^{+})^{+\bullet}$	-4326.150752	-4325.606169
$(\mathbf{3}_{fus}^{2+})\bullet$	-4326.151055	-4325.600941
$(\mathbf{3}_{fus}^{2+})^{+}$	-4325.940723	-4325.386160
$\mathbf{3}_{fus}^{2+}$	-4325.584915	-4325.044275
$(\mathbf{3}_{fus}^{2+})^{+\bullet}$	-4325.359228	-4324.818768
$(\mathbf{3}_{fus}^{2+})^{2+}$	-4325.105568	-4324.560677

References

1. J. K. Laha, S. Dhanalekshmi, M. Taniguchi, A. Ambroise and J. S. Lindsey, *Org. Process Res. Dev.*, 2003, **7**, 799;B. Habermeyer, A. Takai, C. P. Gros, M. E. Ojaimi, J.-M. Barbe and S. Fukuzumi, *Chem. Eur. J.*, 2011, **17**, 10670.
2. G. R. Fulmer, A. J. M. Miller, N. H. Sherden, H. E. Gottlieb, A. Nudelman, B. M. Stoltz, J. E. Bercaw and K. I. Goldberg, *Organometallics*, 2010, **29**, 2176.
3. C. H. Devillers, S. Hebié, D. Lucas, H. Cattey, S. Clément and S. Richeter, *J. Org. Chem.*, 2014, **79**, 6424.
4. A. A. Ryan, S. Plunkett, A. Casey, T. McCabe and M. O. Senge, *Chem. Commun.*, 2014, **50**, 353.
5. Y. Y. Enakieva, J. Michalak, I. A. Abdulaeva, M. V. Volostnykh, C. Stern, R. Guilard, A. G. Bessmertnykh-Lemeune, Y. G. Gorbunova, A. Y. Tsivadze and K. M. Kadish, *Eur. J. Org. Chem.*, 2016, **2016**, 4881.
6. H. A. Collins, M. Khurana, E. H. Moriyama, A. Mariampillai, E. Dahlstedt, M. Balaz, M. K. Kuimova, M. Drobizhev, V. X. D. Yang, D. Phillips, A. Rebane, B. C. Wilson and H. L. Anderson, *Nat. Photonics*, 2008, **2**, 420.
7. G. W. T. M. J. Frisch, H. B. Schlegel, G. E. Scuseria, M. A. Robb, J. R. Cheeseman, G. Scalmani, V. Barone, B. Mennucci, G. A. Petersson, H. Nakatsuji, M. Caricato, X. Li, H. P. Hratchian, A. F. Izmaylov, J. Bloino, G. Zheng, J. L. Sonnenberg, M. Hada, M. Ehara, K. Toyota, R. Fukuda, J. Hasegawa, M. Ishida, T. Nakajima, Y. Honda, O. Kitao, H. Nakai, T. Vreven, J. A., Jr. Montgomery, J. E. Peralta, F. Ogliaro, M. Bearpark, J. J. Heyd, E. Brothers, K. N. Kudin, V. N. Staroverov, R. Kobayashi, J. Normand, K. Raghavachari, A. Rendell, J. C. Burant, S. S. Iyengar, J. Tomasi, M. Cossi, N. Rega, N. J. Millam, M. Klene, J. E. Knox, J. B. Cross, V.Bakken, C. Adamo, J. Jaramillo, R. Gomperts, R. E. Stratmann, O. Yazyev, A. J. Austin, R. Cammi, C. Pomelli, J. W. Ochterski, R. L. Martin, K. Morokuma, V. G. Zakrzewski, G. A. Voth, P. Salvador, J. J. Dannenberg, S. Dapprich, A. D. Daniels, Ö. Farkas, J. B. Foresman, J. V. Ortiz, J. Cioslowski, D. J. Fox, *Gaussian 09, Revision D.01, Gaussian, Inc., Wallingford CT, 2009*, (2009).
8. S. Miertuš, E. Scrocco and J. Tomasi, *Chem. Phys.*, 1981, **55**, 117;M. Cossi, B. Mennucci and J. Tomasi, *Chem. Phys. Lett.*, 1994, **228**, 165;B. Mennucci, E. Cancès and J. Tomasi, *J. Phys. Chem. B*, 1997, **101**, 10506.
9. W. E, W. Ren and E. Vanden-Eijnden, *Phys. Rev. B*, 2002, **66**, 052301;P. Fleurat-Lessard and P. Dayal, *Opt'n Path v1.50; Freely available at: http://pfleurat.free.fr/ReactionPath.html*.
10. J. C. Ho, M. L.; Cramer, C. J.; Truhlar, D. G. *Organic Electrochemistry*, 5th ed.; Speiser, B.; Hammerich, O., Eds.; CRC Press: Boca Raton, FL, **2013**.